8 January 2010 | $10

# Science

AAAS

abcam®

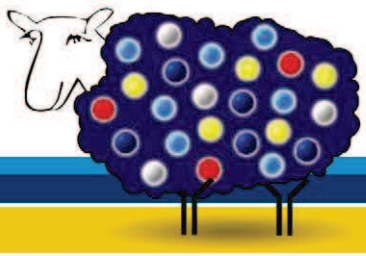

# Active proteins for stem cell differentiation

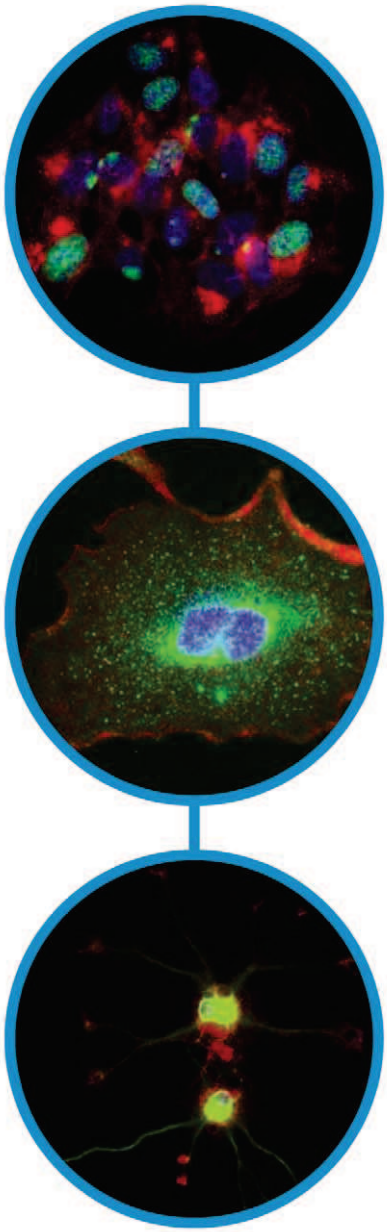

Abcam offer over 10,000 antibodies for stem cells. We also have proteins, lysates and differentiation supplements. We have over 300 proteins for stem cell differentiation in culture including recombinant human, mouse and rat:

## Human Differentiation Cytokines:

| | | | |
|---|---|---|---|
| • BAFF protein | ab50087 | • IL12 | ab73621 |
| • EGF protein | ab9697 | • IL13 | ab73624 |
| • FGF basic | ab73134 | • IL2 | ab73598 |
| • FGF8 protein | ab50128 | • Leptin | ab73583 |
| • Flt3 / CD135 | ab73449 | • MCSF | ab73751 |
| • G-CSF | ab73371 | • Neurotrophin 3 | ab73754 |
| • GM-CSF | ab73121 | • Noggin | ab73756 |
| • GMCSF + IL3 | ab73275 | • Oncostatin M protein | ab9634 |
| • IGF1 | ab73457 | • PDGF AA | ab73226 |
| • IGF2 | ab73495 | • SCF protein | ab9754 |
| • IL1 alpha | ab73567 | • Sonic Hedgehog protein | ab63216 |
| • IL1 beta | ab73577 | • Thrombopoietin protein | ab9719 |
| • IL11 | ab73620 | • VEGF protein | ab50078 |

Exclusive offer for Science readers. Quote **SCIENCES-Y77MW** at checkout to receive 15% off your order on the products listed above. This offer is valid 1/8/2010 – 3/31/2010.

View more of our 300 differentiation supplements at: **www.abcam.com**


**Abcam in the USA**
Abcam Inc
1 Kendall Square, Ste 341
Cambridge, MA 02139-1517
USA

Tel: +1-617-225-2272
Toll free: +1-888-77-ABCAM
Fax: +1-866-739-9884

**Abcam in Europe**
Abcam plc
330 Cambridge Science Park
Milton Road
Cambridge CB4 0FL
UK

Tel: +44-(0)1223-696000
Fax: +44-(0)1223-771600

**Abcam in Japan**
Abcam KK
1-16-8 Nihonbashi
Kakigaracho, Chuo-ku
Tokyo 103-0014
Japan

Tel: +81-(0)3-6231-0940
Fax: +81-(0)3-6231-0941

**Abcam in Hong Kong**
Abcam (Hong Kong) Ltd.
Unit 3328, 33/F
China Merchants Tower
168 Connaught Road Central
Hong Kong

Tel: (852)-3793-3454
Fax: (852)-30161-888

# Call for Papers

# *Science Signaling*

***Science Signaling***, from the publisher of ***Science***, AAAS, features top-notch, peer-reviewed, original research weekly. Submit your manuscripts in the following areas of cellular regulation:

- Biochemistry
- Bioinformatics
- Cell Biology
- Development
- Immunology
- Microbiology
- Molecular Biology
- Neuroscience
- Pharmacology
- Physiology and Medicine
- Systems Biology

***Science Signaling*** is indexed in CrossRef and MEDLINE.




**Submit your research at:**
**www.sciencesignaling.org/about/help/research.dtl**

Subscribing to the weekly ***Science Signaling*** ensures that you and your lab have the latest cell signaling resources. For more information visit **www.ScienceSignaling.org**

Science Signaling
AAAS

GE Healthcare
Life Sciences


# Interesting what a little imagination can do

Imagination has always inspired the scientific mind. At GE Healthcare Life Sciences, the same imagination inspires us to provide the most complete range of products and solutions available. Everything from innovative research system platforms, such as ÄKTA™, Biacore™ and IN Cell Analyzer, to everyday lab essentials from our Whatman™ and Amersham™ brands, to a full range of products for bioprocessing. Scientists around the world rely on these brands to deliver reproducible results, with the highest quality, that ultimately helps improve their productivity.

At GE Healthcare Life Sciences, our focus is on helping scientists achieve even more, faster. It's a commitment we have in our genes. And all this is backed by the service, support and investment for the future that being part of GE can bring.

Want to set your imagination free and do more? Why not talk with us today. Visit **www.gelifesciences.com**

I ÄKTA I Amersham I Biacore I IN Cell Analyzer I Whatman I GE Service I

imagination at work


First published September 2009
GE Healthcare Bio-Sciences AB, Björkgatan 30, 751 84 Uppsala, Sweden
GE15-09

# CONTENTS

Volume 327 Issue 5962



**CONTENTS** continued **>>**

page 134

page 146


## COVER

Corals such as this 150-million-year-old colony of *Thecosmilia trichotoma* (with oyster *Actinostreon* attached) from southern Germany formed reefs during most of the Phanerozoic eon. These reefs harbored tremendous biodiversity that was subsequently exported to non-reef habitats.
See page 196.

***Photo: Antje Dittmann and Carola Radke/Museum für Naturkunde, Berlin***

## DEPARTMENTS

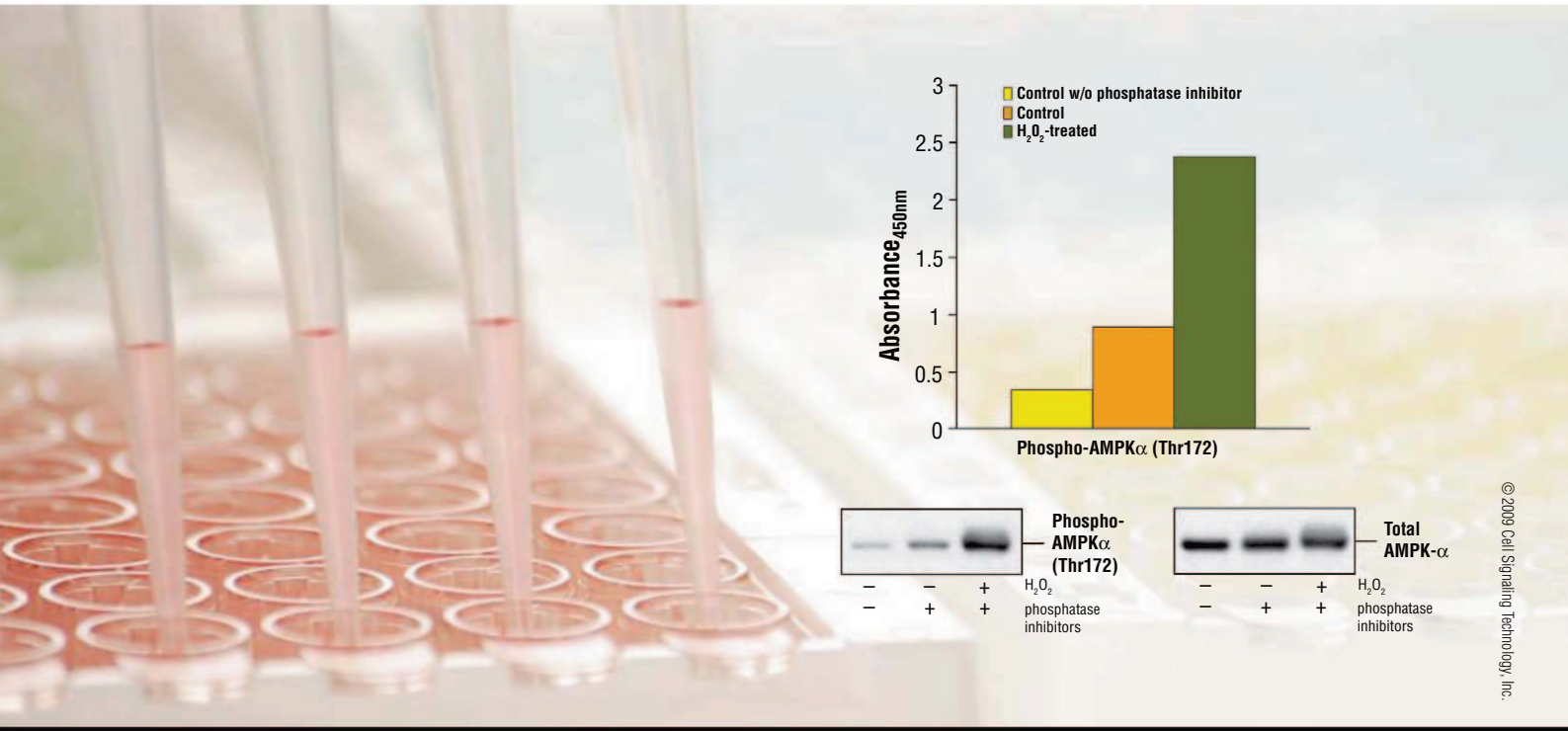




# PathScan® Sandwich ELISA Kits & Antibody Pairs

*from Cell Signaling Technology®*

***Above:*** *Treatment of C2C12 cells with $H_2O_2$ stimulates phosphorylation of AMPKα at Thr172, detected by the* ***PathScan® Phospho-AMPKα (Thr172) Sandwich ELISA Kit #7959****. The absorbance readings at 450 nm are shown in the top figure, while the corresponding western blots using Phospho-AMPKα (Thr172) (D79.5E) XP™ Rabbit mAb #4188 (left panel) or AMPKα (23A3) Rabbit mAb #2603 (right panel) are shown in the bottom figure.*

## Unparalleled product quality, validation and technical support

- Over 140 PathScan® ELISA Kits covering a broad spectrum of signaling pathways
- In-house development, production and validation ensures the highest product quality
- Technical support provided by the same scientists that develop and produce the products
- Matched modification state and total ELISA kits and Antibody Pairs available
- Custom 96- and 384-well formatting available upon request

**New PathScan® Chemiluminescent Kits offer the broadest dynamic range and assay sensitivity while requiring half the sample size due to the use of low volume microplates.**

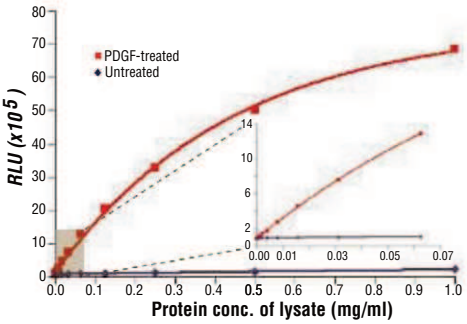


**PathScan® Phospho-Akt1 (Ser473) Chemiluminescent Sandwich ELISA Kit #7134**

for quality products you can trust...

www.cellsignal.com

Cell Signaling TECHNOLOGY®

**Orders** (toll-free) 1-877-616-2355 | **Technical support** (toll-free) 1-877-678-8324 support@cellsignal.com | **Inquiries** info@cellsignal.com | **Environmental Commitment** eco.cellsignal.com

## BREVIA



## RESEARCH ARTICLES



## REPORTS



**CONTENTS** continued >>

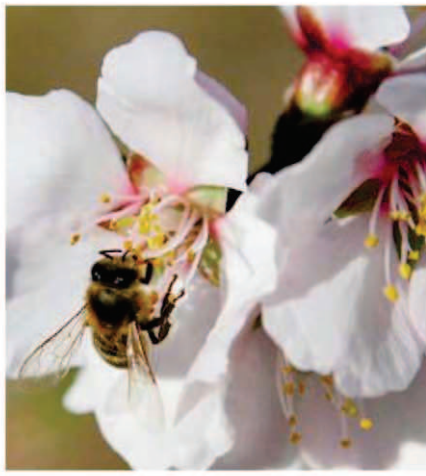

page 152

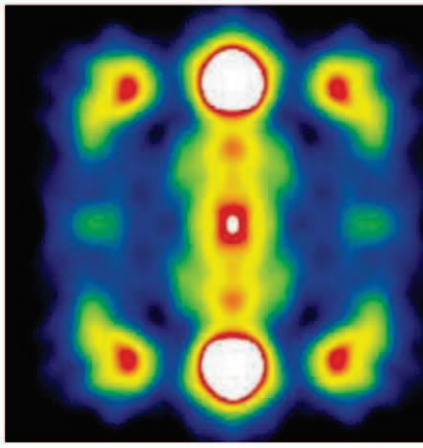

pages 155 & 181

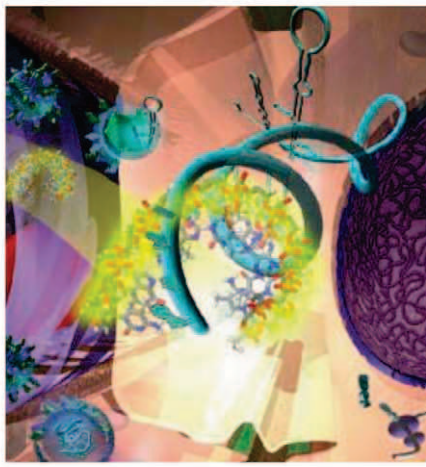

page 198

# SCIENCEONLINE

## SCIENCEXPRESS
www.sciencexpress.org

*Kepler* Planet-Detection Mission: Introduction and First Results
*W. J. Borucki* et al.
Initial observations confirm the existence of planets with densities lower than those predicted for gas giant planets.
10.1126/science.1185402

Gamma-Ray Emission from the Shell of Supernova Remnant W44 Revealed by the Fermi LAT
*A. A. Abdo* et al.
Satellite observations suggest that protons are accelerated in the shell of a supernova remnant.
10.1126/science.1182787

A Composite of Multiple Signals Distinguishes Causal Variants in Regions of Positive Selection
*S. R. Grossman* et al.
Combining statistical methods detects signals of selection with increased sensitivity and a lower false-positive rate.
10.1126/science.1183863

Axon Extension Occurs Independently of Centrosomal Microtubule Nucleation
*M. Stiess* et al.
Neuronal polarization and axon regeneration depend on decentralized microtubule assembly rather than a functional centrosome.
10.1126/science.1182179

## SCIENCENOW
www.sciencenow.org
Highlights From Our Daily News Coverage

Five New Exoplanets Run the Gamut From Styrofoam to Ice
'Fluffy' Jupiters and a Neptune-like world bring astronomers closer to an extrasolar Earth.

Mosquitoes: Love at First Buzz
Insects mate only with those that can sing with them in perfect harmony.

Slideshow: Deep-Sea Spiders Have a Snack
Robot submersible captures rare creatures in the act of devouring sea anemones.

## SCIENCESIGNALING
www.sciencesignaling.org
The Signal Transduction Knowledge Environment

EDITORIAL GUIDE: 2009—Signaling Breakthroughs of the Year
*E. M. Adler*
The signaling breakthroughs of 2009 emphasize the importance of looking beyond linear signaling pathways.

RESEARCH ARTICLE: Impaired $\alpha_{IIb}\beta_3$ Integrin Activation and Shear-Dependent Thrombus Formation in Mice Lacking Phospholipase D1
*M. Elvers* et al.
In the absence of PLD1, platelets do not form stable aggregates under high shear conditions.

PERSPECTIVE: New Endogenous Regulators of Class I Histone Deacetylases
*A. Riccio*
Extracellular stimuli can elicit alterations in gene transcription through regulation of histone deacetylases by sphingosine-1-phosphate.

PODCAST
*M. B. Yaffe and A. M. VanHook*
Chief Scientific Editor Michael Yaffe reviews the year in *Science Signaling*.

## SCIENCECAREERS
www.sciencecareers.org/career_magazine
Free Career Resources for Scientists

Taken for Granted: A Shot at Transforming America's Energy Future
*B. L. Benderly*
A postdoc's new company wins one of the 37 coveted first-round ARPA-E grants.

Generating Science and Public Interest
*E. Pain*
Portuguese cellular biologist Mónica Bettencourt Dias sees promoting science communication as an integral part of her job.

MySciNet: Sell Yourself—Refining the Personal Statement
*B. Rybarczyk*
A career adviser offers tips on writing a critical piece of your graduate school application.

## SCIENCETRANSLATIONAL MEDICINE
www.sciencetranslationalmedicine.org
Integrating Medicine and Science

COMMENTARY: Biotechnology—Delivering on the Promise
*J. C. Greenwood*
Biotechnology offers concrete hope for biomedical innovation.

PERSPECTIVE: Antisense Gets a Grip on miR-122 in Chimpanzees
*A. D. Branch and C. M. Rice*
MicroRNAs may serve as prime targets for new life-saving therapies for patients with liver disease.

RESEARCH ARTICLE: Modeling an Anti-Amyloid Combination Therapy for Alzheimer's Disease
*V. W. Chow* et al.
Simultaneous reduction of two enzymes involved in Alzheimer's disease ameliorates symptoms in aged mice.

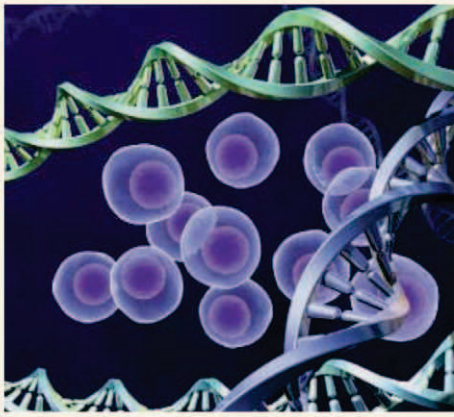

CREDIT: CHRIS BICKEL/AAAS

SCIENCETRANSLATIONAL MEDICINE
Policy changes that buoy biotechnology.

RESEARCH ARTICLE: Elafin Is a Biomarker of Graft Versus Host Disease of the Skin
*S. Paczesny* et al.
Plasma elafin levels correlate with graft versus host disease of the skin and long-term survival.

## SCIENCEPODCAST
www.sciencemag.org/multimedia/podcast
Free Weekly Show
Download the 8 January *Science* Podcast to hear about how cocaine alters gene expression; third-party punishment in fish; and working toward simpler, cheaper particle accelerators.

## ORIGINSBLOG
blogs.sciencemag.org/origins
A History of Beginnings

## SCIENCEINSIDER
blogs.sciencemag.org/scienceinsider
Science Policy News and Analysis

**SCIENCE (ISSN 0036-8075) is published weekly on Friday, except the last week in December, by the American Association for the Advancement of Science, 1200 New York Avenue, NW, Washington, DC 20005.** Periodicals Mail postage (publication No. 484460) paid at Washington, DC, and additional mailing offices.  Domestic individual membership and subscription (51 issues): $146 ($74 allocated to subscription). Domestic institutional subscription (51 issues): $910; Foreign postage extra: Mexico, Caribbean (surface mail) $55; other countries (air assist delivery) $85. First class, airmail, student, and emeritus rates on request. Canadian rates with GST available upon request, GST #1254 88122. Publications Mail Agreement Number 1069624. **Printed in the U.S.A.**

**Change of address:** Allow 4 weeks, giving old and new addresses and 8-digit account number. **Postmaster:** Send change of address to AAAS, P.O. Box 96178, Washington, DC 20090–6178. **Single-copy sales:** $10.00 current issue, $15.00 back issue prepaid includes surface postage; bulk rates on request. **Authorization to photocopy** material for internal or personal use under circumstances not falling within the fair use provisions of the Copyright Act is granted by AAAS to libraries and other users registered with the Copyright Clearance Center (CCC) Transactional Reporting Service, provided that $20.00 per article is paid directly to CCC, 222 Rosewood Drive, Danvers, MA 01923. The identification code for *Science* is 0036-8075. *Science* is indexed in the *Reader's Guide to Periodical Literature* and in several specialized indexes.

AAAS
ADVANCING SCIENCE, SERVING SOCIETY


NORTHROP GRUMMAN
If you're going to reach for the heavens, make sure you're standing on a sturdy ladder.
www.northropgrumman.com/spacescience
SPACE SCIENCE
If you're planning a space mission, make sure you have a reliable and experienced partner. Northrop Grumman has the people and the know-how to be that partner. From our experience teaming with NASA on the Chandra X-Ray Observatory, to our role in building the James Webb Space Telescope and the Lunar CRater Observation and Sensing Satellite, Northrop Grumman is equipped to deliver highly reliable solutions for any and all space science missions.
©2010 Northrop Grumman Corporation
Photo credit: NASA

EDITED BY STELLA HURTLEY

## Cradle of Diversity

Is the biological diversity of reefs a result of attracting species that originated elsewhere, or are they particularly important as cradles of evolution? **Kiessling *et al.*** (p. 196; see the cover) examine a large database of fossil benthic marine organisms dating back to the Cambrian to test these questions. It seems that reefs, even in comparison to other shallow marine environments, were indeed important during the origination of new species, including ones that migrate elsewhere.

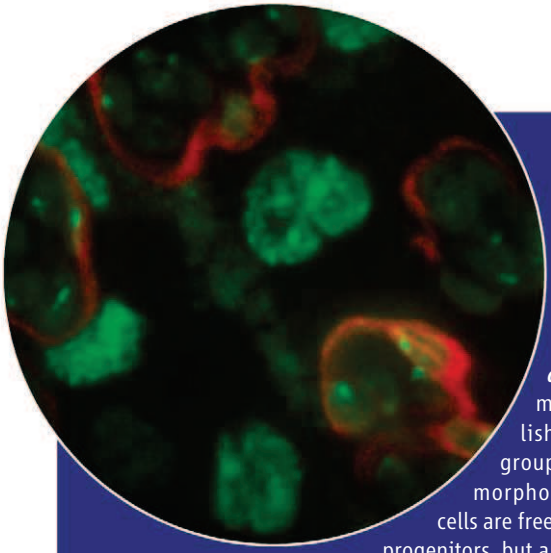

## << Niche Metamorphosis

The gut epithelium is continually renewed by cells generated from intestinal stem cells. In the fruit fly *Drosophila*, cells of the adult gut are derived from cells set aside before metamorphosis. **Mathur *et al.*** (p. 210) now show that an early asymmetric cell division in larval stages establishes a niche that encloses a proliferating group of undifferentiated stem cells. At metamorphosis, the niche breaks down and the stem cells are freed. Most of them differentiate into adult gut progenitors, but a minority takes on the task of establishing a new, adult, stem cell niche with more liberal operating rules.

## Nematic Electronic Order in Iron Superconductors

The properties of many high-temperature superconductors vary strongly as the composition of a doping element changes, and at sufficient under- or overdoping, other phases with different types of electronic ordering can form. Chuang et al. (p. 181; see the Perspective by Fradkin and Kivelson) use scanning tunneling microscopy techniques to probe the electronic structure of an underdoped compound in the iron superconductor family, $Ca(Fe_{1-x}Co_x)_2As_2$. They observed periodic nanostructures oriented along Fe–Fe bonds that exhibit an electronic ordering related to ordering seen in nematic liquid crystals.

## Hidden Symmetry Revealed

It is not often that an exact theory can describe a many-particle quantum-mechanical system, but one of the few exceptions is the behavior of a string of ferromagnets—an Ising chain—at magnetic field strengths that separate different types of ordering. Its excitations were predicted 20 years ago to be governed by the symmetry group E8, one of the most intriguing objects in mathematics. Now, **Coldea *et al.*** (p. 177) report direct experimental confirmation of this result in a quasi-one-dimensional Ising ferromagnet $CoNb_2O_6$, which they probed by neutron scattering. Two of the eight predicted excitations could be observed. Moreover, the ratio of the two lowest excitations is in quantitative agreement with the so-called "golden ratio" predicted by theory.

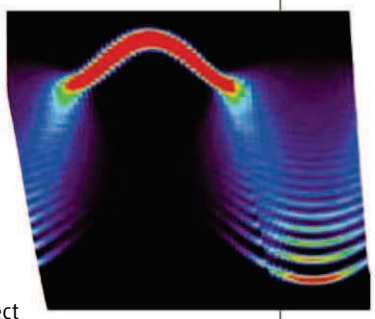

CREDITS (TOP TO BOTTOM): DIVYA MATHUR; COLDEA *ET AL.*

## Stars Going Quietly or with a Bang

Stars with masses seven to ten times the mass of the Sun, which can burn carbon in their cores at their end of their lives, may end up as oxygen-neon core white dwarfs or explode as core-collapse supernovae. The defining line between these two end products of stellar evolution is not well understood. **Gänsicke *et al.*** (p. 188; published online 12 November) identified two white dwarfs whose photospheric oxygen-to-carbon abundance ratio exceeds unity. Their low carbon abundance and their large quantity of oxygen imply that they are oxygen-neon white dwarfs that lost their hydrogen envelopes. As such, they may have evolved from stars at the borderline between stars that explode as supernova and stars that form white dwarfs.

## Smooth Space Pebble

In September 2008, on its way to meet comet 67P/Churyumov-Gerasimenko, the Rosetta spacecraft flew by asteroid Steins, a member of a very rare class of asteroids that had never been observed closely by spacecraft. **Keller *et al.*** (p. 190) analyzed the images to generate a reconstruction of the asteroid's shape. Steins is oblate with an effective spherical diameter of 5.3 kilometers, and it lacks small craters, which may have been erased by surface reshaping. Indeed, Steins's shape resembles that of a body that was spun-up by the YORP effect—a torque produced by incident sunlight, which can alter the rotation rate of a small body—that causes material to slide toward the equator. This effect may have produced Steins's distinctive diamond-like shape.

## CRISPR Defenses

Prokaryotes can be infected by parasites and pathogens and, like eukaryotes, have evolved systems to protect themselves. **Horvath and Barrangou** (p. 167) review a recently discovered prokaryotic "immune system" characterized by CRISPR—clustered regularly interspaced short palindromic repeats—found in most archaeal and many bacterial species. CRISPR loci harbor short sequences captured from viruses and invasive genetic elements. These sequences are transcribed, and the RNA is cleaved into short CRISPR RNAs (crRNAs) by one of a family of CRISPR-associated (cas) proteins. These crRNAs direct other cas family proteins to homologous nucleic acid targets to effect their destruction. Through its ability to impede the spread of specific nucleic acid sequences, the CRISPR/Cas systems might be exploited to block the dissemination of antibiotic-resistance markers.

## Recruiting the Components for Cell Division

A complete chromosome set must be apportioned to each daughter cell during cell division. A number of molecular mechanisms check that chromosome pairs or homologs are cor-

*Continued on page 124*

## This Week in *Science*

*Continued from page 123*

rectly aligned and attached to microtubules just before they separate to the two daughters; their spatial orientation ensures an even inheritance of the genome. One critical component of this system is the protein kinase Bub1. **Kawashima *et al.*** (p. 172, see the Perspective by **Javerzat**; published online 19 November) now show that the main substrate for Bub1 kinase activity in fission yeast is the chromatin protein histone H2A. Phosphorylation of H2A recruits the shugoshin proteins to chromatin, and especially to centromeres, where they also act to ensure correct chromosome segregation. This link between Bub1, histone H2A phosphorylation, and shugoshin is conserved in budding yeast and mammalian cells.

### Anti-MicroRNA Antiviral

MicroRNAs (miRNAs) are small noncoding RNAs found in eukaryotes and viruses. They are critical regulators of a wide range of cellular processes. The highly conserved miRNA miR-122 is required for infection by hepatitis C virus (HCV), a leading cause of liver disease in humans. Present HCV treatment regimes can have serious side effects and are effective in only 50% of cases. In order to try to tackle HCV infection, **Lanford *et al.*** (p. 198, published online 3 December) targeted miR-122 using a complementary locked nucleic acid (LNA) oligonucleotide. Treatment of chimpanzees infected by HCV with the LNA antagonist resulted in a long-term reduction of disease symptoms without the concomitant appearance of resistant strains of the virus.

### Dissecting TFIIB Mechanics

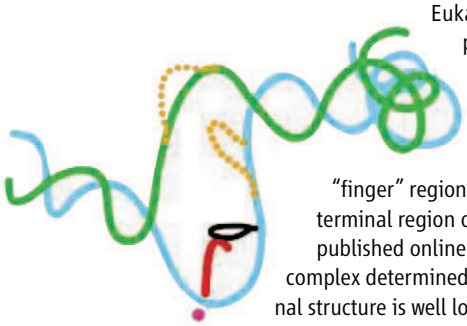

Eukaryotic RNA polymerase II (Pol II) requires five protein cofactors for promoter recognition and initiation of transcription. The factor TFIIB is implicated in start site selection and stabilization of the initial transcript. The co-crystal structure of Pol II and TFIIB showed an N-terminal "finger" region located in the RNA exit channel, but the core C-terminal region of TFIIB was disordered. Now **Liu *et al.*** (p. 206; published online 12 November) present a structure of the same complex determined under different conditions in which the C-terminal structure is well localized but the finger is disordered. Docking DNA into the structure suggests that the C-terminal region stabilizes initial promoter melting. After transcription of a few bases, TFIIB probably switches to the alternate conformation where the C-terminal region is released and the finger region stabilizes the initial transcript.

### RNA Structural Principles Revealed

The thermodynamic principles that link RNA primary and secondary structure are well understood, but the relation to tertiary structure is unclear. To gain insight, **Bailor *et al.*** (p. 202) analyzed all available three-dimensional structures of an important RNA motif, the two-way junction, and found that flanking helices sample only a small percentage of possible interhelical orientations. They identified a set of general rules for the relative orientation of helices as a function of the size of the interconnecting junction. The results also rationalize how ligands stabilize specific conformations. Understanding the topological constraints that define RNA global conformation and dynamic adaptation provides guiding principles for rational manipulation of RNA structure.

### Cocaine Addiction and Histone Methylation

Long-lasting behavioral syndromes associated with chronic cocaine exposure may result from dysregulation of the global transcriptional machinery. **Maze *et al.*** (p. 213) observed that histone lysine methylation in the nucleus accumbens plays a critical role in mediating the regulation of gene expression in response to repeated cocaine self-administration. Chronic cocaine was linked to overall reductions in dimethylation of lysine 9 of histone 3 (H3K9) in this brain region. Repressing H3K9 after chronic cocaine administration facilitated reward-related changes in behavior. The authors identifed the methyltransferase G9a as an essential mediator and an important regulator of dendritic spine plasticity. Downregulation of G9a was linked to the transcription factor ΔFosB.

CREDIT: LIU *ET AL.*

# Spreading the Spirit of EMBO

Maria Leptin is director of the European Molecular Biology Organization and is professor of Genetics, Cologne University, Germany. Her research is focused on cell and developmental biology and the genetics of pathogen resistance. E-mail: maria.leptin@embo.org

THIS MONTH I SUCCEED HERMANN BUJARD AS DIRECTOR OF THE EUROPEAN MOLECULAR BIOLOGY Organization (EMBO). EMBO was founded in 1964 with the goal of promoting cross-border cooperation in molecular biology research in Europe. From the start, it aimed to act as a counterweight to the hierarchical academic structures in the European research and funding culture. Although the organization is funded directly by 27 participating countries, EMBO is guided in its decisions by its members. These are some 1300 distinguished scientists in Europe and abroad, who select the people and programs to be supported based exclusively on merit.

Society looks to science to help find solutions to the problems we face—ill-health, climate change, energy and food shortages—and society provides the money required for scientific research. But the allocation of funds often comes with demands that are not easy to reconcile with creative research. I believe that the vibrant culture of discovery that is essential for the future of Europe will require that scientists, rather than politicians, direct the continent's future financial investments in basic science. The type of top-down control that is prevalent, for example, in the European Framework Programmes, and may be relevant to allocating funds for applied research, is both unnecessary and counterproductive for basic research. Only scientists themselves can effectively control the quality of scientific research, or expose fraudulent findings or errors. And who but scientists can judge the scope of a scientific discovery or recognize genuine novelty in research?

In particular, grants funded by the European Commission (EC) often force the formation of transnational networks, restricting the freedom to concentrate on new topics that are not already being worked on by many research groups. Indeed, science thrives on interactions between researchers, but program or group grants that insist on collaborations can do as much harm as good, depriving researchers of the freedom they need to pursue the kind of highly individual ideas that form the basis for great scientific leaps forward. Some EC grants are awarded as "contracts" with "deliverables." If a scientist has a contract to find out something that is well defined in advance, how can that result in a true discovery of something new?

To gain and maintain public trust, scientists need to be rigorously accountable to the public for money that is spent on their research. Not only do scientists need to publish their findings in scientific journals, they must also be prepared to explain them in widely understandable terms, as well as listen to the concerns of the public. At the same time, accountability should not be imposed in a way that strangles scientific creativity or belies common sense.

If Europe is to place most of its decisions concerning science funding, policies, and organization in the hands of scientists, as it should, scientists must work with politicians to reassure them that scientists can direct resources effectively. We have seen the impact that the voices of scientists can have in the creation of the European Research Council (ERC), the new European funding body that awards large research grants based exclusively on excellence and originality of the proposed projects, judged only by scientific peer review. The ERC was set up with essential input from EMBO, and one of EMBO's important roles will be to support that institution, both through its members serving as reviewers and panel members, and by fighting to secure its continuation. EMBO has occasionally advised national agencies on their local research institutions, always stressing the importance of free and open structures. I look forward to working with my colleagues throughout Europe to advance both EMBO and European science in the same spirit. The large issues before us include changes required in the culture and organization of scientific publishing, as well as strengthening connections with scientific institutions and scientists beyond the borders of Europe.

**–Maria Leptin**

10.1126/science.1185865

CHEMISTRY

## Pass the Salt

As our global freshwater resources continue to be consumed at an unsustainable rate, the demand for new sources of abundant, clean water continues to rise. Desalinated seawater is an attractive option as a complement to natural freshwater sources, but it remains fraught with unresolved problems such as minimizing energy requirements for the process and improving the quality of the product stream. To further understand the latter concern, Agus and Sedlak analyzed the chemical by-products generated by the addition of disinfecting chlorine to seawater under pilot-scale as well as various bench-scale conditions. Although few harmful by-products exceeded the recommended drinking water thresholds, certain patterns emerged that may further improve water quality. Seasonal and geographic increases in seawater-dissolved organic matter correlated with increased levels of potentially toxic by-products such as brominated trihalomethanes. Blending common freshwater sources (e.g., river water) with desalinated seawater could reduce the potential for chlorinated by-product formation; however, because seawater is naturally rich in bromine, nontrivial levels of other harmful by-products, such as dihaloacetonitriles, may be produced. Ultimately, the quality of desalinated seawater should pose little threat to human health or aquatic ecosystems, thus increasing the likelihood that desalination will remain a viable option for meeting our freshwater demands. — NW

*Wat. Res.* 10.1016/j.watres.2009.11.015 (2009).

CHEMISTRY

## Big Steps for Little Feet

Macroscopic robots can already walk—the trouble is getting them to think. At the molecular scale, though, channeling stochastic motion into something resembling a series of purposeful strides is still a great challenge. Von Delius *et al.* now show that carefully designed feet appended to a small hydrocarbon chain can shuffle to and fro along a four-site track under proper chemical stimulation. One foot forms disulfide bonds to two of the track sites, whereas the other forms hydrazone linkages to interspersed sites. By introducing acids or bases that selectively favor these respective reactions, the authors shift the chain's position one step at a time. Replacing the base treatment with a redox protocol asserts some degree of control over the directionality of the stroll. — JSY

*Nat. Chem.* 10.1038/nchem.481 (2009).

EVOLUTION

## Sulfate Supplier

The mitochondrion was kidnapped from the ranks of free-living bacteria, and subsequently coerced in various ways by eukaryotic cells to supply them with energy in the form of ATP synthesized by means of aerobic respiration. Historically, anaerobic cells were thought to lack mitochondria, but this prohibition has been modified somewhat with the discovery of intracellular organelles sporting mitochondrion-like features such as a double membrane, the protein chaperonin 60, and enzymes that assemble iron-sulfur clusters (which are a component of many respiratory enzymes). The hydrogenosome of *Trichomonas* produces hydrogen and ATP, and the mitosome, which produces neither hydrogen nor ATP, is found in *Entamoeba*. Mi-ichi *et al.* have begun to tabulate the protein repertoire of the mitosome, which appears to have been patched together from two proteobacterial sources, as well as a eukaryote. Three of the dominant constituents were ATP sulfurylase, adenylyl-sulfate kinase, and inorganic pyrophosphatase, indicating that one of the functions of this organelle may be the activation of sulfate, quite possibly for incorporation into sulfolipids. — CA

*Proc. Natl. Acad. Sci. U.S.A.* **106**, 21731 (2009).

CLIMATE SCIENCE

## Slow Roast

Of all the wildcards in the climate system, one of the most potentially important is oceanic methane hydrates. Methane hydrates are frozen associations of methane and water found worldwide in marine sediments within a field of stability that extends from near the sediment surface down several hundred meters. Huge quantities of methane are thought to exist in these hydrates, and that is what makes them such a concern to climate scientists—as we warm the world by burning fossil fuels, the ocean eventually may warm enough to destabilize the hydrates and add methane (a potent greenhouse gas) to the atmosphere. Substantial release of this stored methane could accelerate the rate and amount of global warming considerably above current estimates. Sadly, we still understand little about this possibility. Archer *et al.* present initial calculations of the amount of methane contained in the hydrates, as well as estimates of how much might be released in various anthropogenic global warming scenarios. Their calculations show that humankind does have the capacity to cause large methane releases from the sea floor, and correspondingly great additional warming, and that the impact of such release is likely to occur over millennia rather than abruptly over the next century, making the issue a long-term danger rather than an immediate one. — HJS

*Proc. Natl. Acad. Sci. U.S.A.* **106**, 20596 (2009).

www.sciencemag.org

# Science

**1200 New York Avenue, NW**
**Washington, DC 20005**
Editorial: 202-326-6550, FAX 202-289-7562
News: 202-326-6581, FAX 202-371-9227
**Bateman House, 82-88 Hills Road**
**Cambridge, UK CB2 1LQ**
+44 (0) 1223 326500, FAX +44 (0) 1223 326501

**Subscription Services** For change of address, missing issues, new orders and renewals, and payment questions: 866-434-AAAS (2227) or 202-326-6417, FAX 202-842-1065. Mailing addresses: AAAS, P.O. Box 96178, Washington, DC 20090-6178 or AAAS Member Services, 1200 New York Avenue, NW, Washington, DC 20005

**Institutional Site Licenses** please call 202-326-6755 for any questions or information

**Reprints:** Author Inquiries 800-635-7181
Commercial Inquiries 803-359-4578

**Permissions** 202-326-7074, FAX 202-682-0816

**Member Benefits** AAAS/Barnes&Noble.com bookstore www.aaas.org/bn; AAAS Online Store www.apisource.com/aaas/ code MKB6; AAAS Travels: Betchart Expeditions 800-252-4910; Apple Store www.apple.com/eppstore/aaas; Bank of America MasterCard 1-800-833-6262 priority code FAA3YU; Cold Spring Harbor Laboratory Press Publications www.cshlpress.com/affiliates/aaas.htm; GEICO Auto Insurance www.geico.com/landingpage/go51.htm?logo=17624; Hertz 800-654-2200 CDP#343457; Office Depot https://bsd.officedepot.com/portalLogin.do; Seabury & Smith Life Insurance 800-424-9883; Subaru VIP Program 202-326-6417; VIP Moving Services www.vipmayflower.com/domestic/index.html; Other Benefits: AAAS Member Services 202-326-6417 or www.aaasmember.org.

| | |
|---|---|
| science_editors@aaas.org | (for general editorial queries) |
| science_letters@aaas.org | (for queries about letters) |
| science_reviews@aaas.org | (for returning manuscript reviews) |
| science_bookrevs@aaas.org | (for book review queries) |

Published by the American Association for the Advancement of Science (AAAS), *Science* serves its readers as a forum for the presentation and discussion of important issues related to the advancement of science, including the presentation of minority or conflicting points of view, rather than by publishing only material on which a consensus has been reached. Accordingly, all articles published in *Science*—including editorials, news and comment, and book reviews—are signed and reflect the individual views of the authors and not official points of view adopted by AAAS or the institutions with which the authors are affiliated.

AAAS was founded in 1848 and incorporated in 1874. Its mission is to advance science, engineering, and innovation throughout the world for the benefit of all people. The goals of the association are to: enhance communication among scientists, engineers, and the public; promote and defend the integrity of science and its use; strengthen support for the science and technology enterprise; provide a voice for science on societal issues; promote the responsible use of science in public policy; strengthen and diversify the science and technology workforce; foster education in science and technology for everyone; increase public engagement with science and technology; and advance international cooperation in science.

**Information for Authors**
See pages 807 and 808 of the 6 February 2009 issue or access www.sciencemag.org/about/authors

EDITOR-IN-CHIEF **Bruce Alberts**
EXECUTIVE EDITOR **Monica M. Bradford**
NEWS EDITOR **Colin Norman**
MANAGING EDITOR, RESEARCH JOURNALS **Katrina L. Kelner**
DEPUTY EDITORS **R. Brooks Hanson, Barbara R. Jasny, Andrew M. Sugden**

**Editorial senior editors/commentary** Lisa D. Chong, Brad Wible; **senior editors** Gilbert J. Chin, Pamela J. Hines, Paula A. Kiberstis (Boston), Marc S. Lavine (Toronto), Beverly A. Purnell, L. Bryan Ray, Guy Riddihough, H. Jesse Smith, Phillip D. Szuromi (Tennessee), Valda Vinson, Jake S. Yeston; **associate editors** Kristen L. Mueller, Jelena Stajic, Nicholas S. Wigginton, Laura M. Zahn; **research associate** Alexis Wynne Mogul; **online editor** Stewart Wills; **associate online editors** Robert Frederick, Tara S. Marathe; **web content developer** Martyn Green; **book review editor** Sherman J. Suter; **associate letters editor** Jennifer Sills; **editorial manager** Cara Tate; **senior copy editors** Jeffrey E. Cook, Cynthia Howe, Harry Jach, Barbara P. Ordway, Trista Wagoner; **copy editors** Chris Filiatreau, Lauren Kmec; **editorial coordinators** Carolyn Kyle, Beverly Shields; **publications assistants** Ramatoulaye Diop, Joi S. Granger, Jeffrey Hearn, Lisa Johnson, Scott Miller, Jerry Richardson, Jennifer A. Seibert, Brian White, Anita Wynn; **editorial assistants** Emily Guise, Michael Hicks, Patricia M. Moore, Miriam Weinberg; **executive assistant** Sylvia S. Kihara; **administrative support** Maryrose Madrid; **editorial fellow** Melissa R. McCartney

**News deputy news editors** Robert Coontz, Eliot Marshall, Jeffrey Mervis, Leslie Roberts; **contributing editors** Elizabeth Culotta, Polly Shulman; **news writers** Yudhijit Bhattacharjee, Adrian Cho, Jennifer Couzin, David Grimm, Constance Holden, Jocelyn Kaiser, Sam Kean, Richard A. Kerr, Eli Kintisch, Andrew Lawler (New England), Greg Miller, Elizabeth Pennisi, Robert F. Service (Pacific NW), Erik Stokstad; **interns** Michael Torrice, Jue Wang; **contributing correspondents** Jon Cohen (San Diego, CA), Daniel Ferber, Ann Gibbons, Robert Koenig, Mitch Leslie, Charles C. Mann, Virginia Morell, Gary Taubes; **copy editors** Linda B. Felaco, Melvin Gatling, Melissa Raimondi; **administrative support** Scherraine Mack, Fannie Groom; **bureaus** New England: 207-549-7755; San Diego, CA: 760-942-3252, FAX 760-942-4979; Pacific Northwest: 503-963-1940

**Production director** James Landry; **senior manager** Wendy K. Shank; **assistant manager** Rebecca Doshi; **senior specialists** Steve Forrester, Chris Redwood; **specialist** Anthony Rosen; **Preflight director** David M. Tompkins; **manager** Marcus Spiegler; **specialist** Jason Hillman

**Art director** Yael Kats; **associate art director** Laura Creveling; **senior illustrators** Chris Bickel, Katharine Sutliff; **illustrator** Yana Greenman; **senior art associates** Holly Bishop, Preston Huey, Nayomi Kevitiyagala; **art associates** Jessica Newfield, Matthew Twombly; **photo editor** Leslie Blizard

***Science* International**

**Europe** (science@science-int.co.uk) **editorial: international managing editor** Andrew M. Sugden; **senior editor/commentary** Julia Fahrenkamp-Uppenbrink; **senior editors** Caroline Ash, Stella M. Hurtley, Ian S. Osborne, Peter Stern; **associate editor** Maria Cruz; **locum editor** Helen Pickersgill; **editorial support** Deborah Dennison, Rachel Roberts, Alice Whaley; **administrative support** John Cannell, Janet Clements, Louise Moore; **news: europe news editor** John Travis; **deputy news editor** Daniel Clery; **contributing correspondents** Michael Balter (Paris), John Bohannon (Vienna), Martin Enserink (Amsterdam and Paris), Gretchen Vogel (Berlin)

**Latin America contributing correspondent** Antonio Regalado

**Asia** Japan Office: Asca Corporation, Tomoko Furusawa, Rustic Bldg. 7F, 77 Tenjin-cho, Shinjuku-ku, Tokyo 162-0808, Japan; +81 3 6802 4616, FAX +81 3 6802 4615, inquiry@sciencemag.jp; **asia news editor** Richard Stone (Beijing: rstone@aaas.org); **contributing correspondents** Dennis Normile [Japan: +81 (0) 3 3391 0630, FAX +81 (0) 3 5936 3531; dnormile@gol.com]; Hao Xin [China: +86 (0) 10 6307 4439 or 6307 3676, FAX +86 (0) 10 6307 4358; cindyhao@gmail.com]; Pallava Bagla [South Asia: +91 (0) 11 2271 2896; pbagla@vsnl.com]

EXECUTIVE PUBLISHER **Alan I. Leshner**
PUBLISHER **Beth Rosner**

**Fulfillment Systems and Operations** (membership@aaas.org); **director** Waylon Butler; **senior systems analyst** Nomuna Nyamaa; **customer service supervisor** Pat Butler; **specialists** Latoya Casteel, LaVonda Crawford, Vicki Linton, April Marshall; **data entry supervisor** Cynthia Johnson; **specialists** Shirlene Hall, Tarrika Hill, William Jones

**Business Operations and Administration director** Deborah Rivera-Wienhold; **assistant director, business operations** Randy Yi; **manager, business analysis** Eric Knott; **manager, business operations** Jessica Tierney; **financial analysts** Priti Pamnani, Celeste Troxler; **rights and permissions: administrator** Emilie David; **associate** Elizabeth Sandler; **marketing director** Ian King; **marketing managers** Allison Pritchard, Alison Chandler, Julianne Wielga; **marketing associates** Aimee Aponte, Mary Ellen Crowley, Adrian Parham, Wendy Wise; **marketing executive** Jennifer Reeves; **director, site licensing** Tom Ryan; **director, corporate relations** Eileen Bernadette Moran; **publisher relations, eresources specialist** Kiki Forsythe; **senior publisher relations specialist** Catherine Holland; **publisher relations, east coast** Phillip Smith; **publisher relations, west coast** Philip Tsolakidis; **fulfillment supervisor** Iquo Edim; **fulfillment coordinator** Carrie MacDonald; **marketing manager** Christina Schlecht; **marketing associate** Mary Lagnaoui; **electronic media: manager** Lizabeth Harman; **project manager** Trista Snyder; **assistant manager** Lisa Stanford; **senior production specialists** Ryan Atkins, Christopher Coleman, Walter Jones; **production specialists** Nichele Johnston, Kimberly Oster; **director, web and new media** Will Collins

**advertising director, worldwide ad sales** Bill Moran
**commercial editor** Sean Sanders: 202-326-6430
**project director, outreach** Brianna Blaser

**Product** (science_advertising@aaas.org); **midwest/west coast/w. canada** Rick Bongiovanni: 330-405-7080, FAX 330-405-7081; **east coast/e. canada** Laurie Faraday: 508-747-9395, FAX 617-507-8189; **uk/europe/asia** Roger Goncalves: TEL/FAX +41 43 243 1358; **japan** ASCA Corporation, Nanako Ide +81 (0) 3 6802 4616, FAX +81 (0) 3 6802 4615; ads@sciencemag.jp; **senior traffic associate** Deiandra Simms

**worldwide associate director of *Science* Careers** Tracy Holmes: +44 (0) 1223 326525, FAX +44 (0) 1223 326532

**Classified** (advertise@sciencecareers.org); **u.s.: sales manager** Daryl Anderson: 202-326-6543; **midwest** Tina Burks: 202-326-6577; **east coast** Alexis Fleming: 202-326-6578; **west/south central** Nicholas Hintibidze: 202-326-6533; **sales coordinators** Rohan Edmonson, Shirley Young; **sales** Susanne Kharraz, Dan Pennington, Alex Palmer; **sales assistant** Lisa Patterson; **japan** ASCA Corporation, Jie Chin +81 (0) 3 6802 4616, FAX +81 (0) 3 6802 4615; careerads@sciencemag.jp; **advertising support manager** Karen Foote: 202-326-6740; **advertising production operations manager** Deborah Tompkins; **senior production specialist/graphic designer** Amy Hardcastle; **senior production specialist** Robert Buck; **senior traffic associate** Christine Hall

## Iraqi Artifacts Go Online

Internet giant Google has announced that it is photographing thousands of artifacts at the Iraq Museum in Baghdad and will post the images online early this year. The museum houses artifacts dating back to the Stone Age, including items made by the Sumerians, Assyrians, and other civilizations that have inhabited the region throughout the millennia. Looters stole thousands of objects in the chaos following the U.S.-led invasion that toppled the regime of Saddam Hussein (*Science*, 1 August 2003, p. 582). Museum officials now estimate that about a third of the roughly 15,000 looted objects have been returned, and the museum reopened in February 2009 (although so far, tourist traffic has been light). Google plans to post about 14,000 images, which should help make the collections more accessible to people around the world.

## Learning With Style

Are you a visual learner? Verbal? Auditory? Kinesthetic? Creative? Practical? Analytical? Divergent? Assimilative? Accommodating?

There's a huge industry out there on "learning styles." It's based on the theory that people learn best when taught in a manner compatible with their style. But now a team of psychologists argues that the literature offers no evidence that such "matching" improves learning.

The authors, headed by Harold Pashler of the University of California, San Diego, set a rigorous standard: For any experiment to be valid, it must randomly assign students to two different teaching conditions on a particular subject, then give them all the same test. The theory is supported if students who prefer teaching style "A" do better than students who prefer style "B" when style "A" is used—and that the reverse is true with teaching style "B." Pashler's team reports that very few studies used this design and concludes that if a teaching technique is good, it's better for everyone regardless of learning style. The lack of hard evidence suggests that "people out there are selling tests and packages and workshops without having any remote idea whether the methods they promote provide any real educational benefits," says Pashler. The report appeared in the December issue of *Psychological Science in the Public Interest*.

Psychologist Robert Sternberg of Tufts University in Medford, Massachusetts, says the paper "does not even begin to be a serious review of the field. … [In] limiting themselves to random-assignment studies, they ignored almost the entire literature." Just so, says Pashler—most of it is "weak."

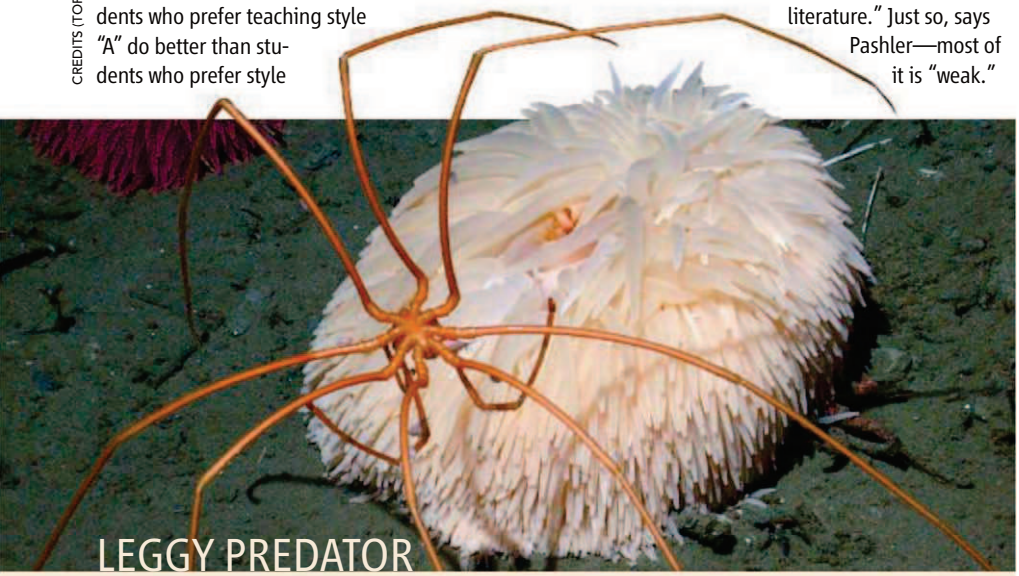

## LEGGY PREDATOR

A remotely operated vehicle has captured never-before-seen images of deep-sea spiders feeding in a canyon off the central California coast. This pycnogonid hovers over a pom-pom anemone, inserts its proboscis into a tentacle, and sucks out the contents. The team, led by evolutionary biologist Robert C. Vrijenhoek of the Monterey Bay Aquarium Research Institute, reported the findings in the fall issue of the *Journal of Invertebrate Biology*.

CREDITS (TOP TO BOTTOM): GOOGLE; J. BOHANNON, *SCIENCE*; © 2005 MBARI

## THREE Q'S >>

The buzz from President Barack Obama's visit in June still hasn't worn off for Egypt's scientists. Among the promises Obama made was "a new fund" and "centers of scientific excellence" for science and technology development in the Middle East. Last month, Obama named Egyptian Nobel Prize–winning physicist Ahmed Zewail—now at the California Institute of Technology in Pasadena—as the United States's "scientific envoy" to the Middle East. *Science* spoke with **Tareq Hussein**, a particle physicist and president of the Egyptian Academy of Scientific Research and Technology, about the developments.

**Q: Do Egyptian scientists have ideas for the new U.S. funds?**

Zewail was here 2 weeks ago to discuss the ideas. One idea is to give real funding to [Jordan's research synchrotron] SESAME. It needs about $100 million. Another area of interest is solar energy. We are talking with Italy and Spain about building a prototype electrical grid, linking to Europe with cables under the Mediterranean. But an even higher priority than energy is food security. We are working very hard on agricultural biotechnology. We really need crops that are drought-resistant, even growing when irrigated with salty water.

**Q: Are you worried that the Egyptian public might reject genetically modified food?**

I'm confident it will not be a problem. People in the Middle East are more worried about poverty and hunger.

**Q: Obama's vision is for science to promote peace in the region. Will that include Israel?**

Egypt is going to wait until Israel finds a peaceful solution with the Palestinians before directly collaborating in science.

PUBLIC HEALTH

# U.S. Panel Favors Wider Use Of Preventive Drug Treatment

If regulators agree, the pool of people in the United States eligible for cholesterol-lowering drugs could soon expand dramatically to include as many as 6 million people whose cholesterol levels fall within a normal range. The potential boon to drugmakers and preventive health care came from an advisory committee to the U.S. Food and Drug Administration (FDA). The panel last month endorsed a wider use for Crestor, a statin manufactured by AstraZeneca. The decision, which could affect other statins too, raises tough questions: Who should get potentially risky medications to cut the chance of a deadly disease? And how many healthy people is it reasonable to treat to avoid one heart attack?

Statins, which have been around since 1987, bring down cholesterol and lower the risk of heart attack and stroke. They are already taken by millions with no overt disease but with high LDL cholesterol. The definition of "high LDL" has been trending downward in recent years, however, and scientists are considering new groups for whom the benefits of statins might outweigh the risks.

A clinical trial highlighted one of these groups in late 2008. Called JUPITER, it enrolled 17,800 middle-aged men and women whose LDL cholesterol levels were healthy by current standards but who had high blood levels of a marker for inflammation called c-reactive protein (CRP). Benefits appeared quickly in a very modest percentage of those treated: After less than 2 years on Crestor, 142 people, or 1.6%, who got the drug had had a cardiac event, such as a heart attack, stroke, or hospitalization for angina, compared with 251, or 2.8%, who received a placebo (*Science*, 14 November 2008, p. 1039). Although the number directly helped was small, last month an FDA advisory committee voted 12 to 4 to offer Crestor to anyone who fits the JUPITER risk profile.

Extrapolating JUPITER's results to a wider population could be tricky. Like other statins, Crestor can have side effects, including muscle weakness and liver toxicity. (It's also expensive at more than $3 a day.) And although JUPITER's results could prompt a wider use of all statins, no one knows whether the benefits conferred in the JUPITER trial would translate to other cholesterol drugs.


**On the rise.** 18 million U.S. residents use statins, including Crestor.

In prevention circles, physicians often talk of the "number needed to treat" (NNT): how many people must receive a preventive therapy for one case to be avoided. The NNT in the JUPITER trial matches up favorably with NNTs in other cohorts treated to prevent cardiovascular disease. JUPITER's researchers, led by cardiologist Paul Ridker of Brigham and Women's Hospital in Boston, estimated that treating 29 people for 5 years would prevent one cardiovascular event. That's somewhat more impressive than the NNT for people with slightly elevated cholesterol who already take statins and, Ridker points out, for those who take blood pressure drugs to prevent heart problems. Furthermore, any NNT drops over time: As a cohort sticks with statins for many years, the number of heart attacks prevented climbs (as does the number of people coping with drug side effects).

**Avoidable?** Heart attack is something statins can prevent.

But attitudes are changing with the push for personalized medicine; many say that NNTs now deemed acceptable are too high, with too many people taking drugs who won't be helped by them directly. "We should be able to do much better" at predicting who's most likely to fall ill and treating that narrower cohort, says Eric Topol, a cardiologist and director of the Scripps Translational Science Institute in San Diego, California.

CRP, for example, is a crude measure that's not tightly linked to inflammation of the arteries: It can also rise in someone with gingivitis or an inflamed joint. Cardiologists hope to find more refined markers. One possibility was reported on 24 December in a paper in *The New England Journal of Medicine*, in which researchers discussed two new genetic variants associated with the lipoprotein Lp(a), which appear to substantially raise the risk of coronary disease.

Whether guided by CRP or something else, proposals for widespread statin use are intensely debated these days. Some see the benefits as undeniable. Preventive cardiologist Daniel Rader of the University of Pennsylvania points out that even average-risk individuals in middle age, looking ahead 30 years, have a relatively high chance of heart disease—as much as 30% or even higher. It's not pertinent to focus solely on NNT, he argues, which is "more of an economic issue" than a health consideration. Although "I don't think I'm quite ready to say that when you turn a certain age, start your statin," says Rader, he did just that himself when he hit 50 last year. But given that statins have side effects, many cardiologists are leery of modifying guidelines without hard evidence.

Another reason for caution is that some past efforts to expand preventive care have not stood the test of time. For example, says Steven Nissen, chair of cardiovascular medicine at the Cleveland Clinic in Ohio, "millions of Americans [were] told to take an aspirin a day" to prevent heart attacks. But several years ago, an FDA advisory panel on which Nissen sat "overwhelmingly" agreed that for

CREDITS: (TABLE SOURCES) S. WOLOSHIN *ET AL.*, *JOURNAL OF GENERAL INTERNAL MEDICINE* **22**, 2 (FEBRUARY 2007); FDA; (BOTTOM, PHOTO) SHOUT/ALAMY

The virtual world of archaeology
140

EMMA's coming debut
142

those at low risk, the hazards of aspirin, such as bleeding, outweigh its benefits. "A therapy became established in very low-risk individuals when, on further reflection, there's evidence it's the wrong thing to do," Nissen says. Some cardiologists don't want to chance a repeat with the statins, and because of that possibility, stress that any extension of statin use be considered only for people like those in JUPITER, with high CRP.

If history is any guide, approving Crestor for a much wider audience could result in many takers. Statins are already enormously popular, and physicians working in prevention in other fields have been intrigued by the number of people who willingly take them for years. In breast and prostate cancer, on the other hand, for which drugs exist that can cut 5-year risk of those cancers by as much as half, relatively few opt for them. "We apply a different standard when it comes to cancer risk reduction" than when slashing cardiovascular risks, says Victor Vogel, national vice president for research at the American Cancer Society in Atlanta. In cancer, "there was a lot of criticism that drugs used for prevention have to be absolutely safe," a standard Vogel considers unrealistic—and one that doesn't apply to statins, either.

FDA hasn't made its final determination yet but usually follows its advisory committees' recommendations. It's expected to rule later this year. **–JENNIFER COUZIN-FRANKEL**

JAPAN

# 2010 Science Budget Not Apocalyptic, as Feared

**TOKYO—**For weeks, Japan's scientific community agonized over spending cuts recommended by a government task force. Now researchers are breathing a sigh of relief: Although some projects will absorb big hits, the new administration's first budget, approved by the Cabinet at the end of December, calls for relatively minor changes in science priorities.

Figures for total S&T expenditures won't be known until bureaucrats comb through individual ministry and agency budgets. But "the overall total has probably not decreased," says Koichi Kitazawa, president of the Japan Science and Technology Agency, which administers government grants. The budget now goes to the legislature, which is expected to make few changes, and will take effect on 1 April.

A handful of high-profile projects will suffer in 2010. Among the losers is the $1.3 billion Next-Generation Supercomputer project, slated for completion in 2012. The previous administration had earmarked $290 million for the effort; the new government will allot $230 million. "We had been hoping to complete the system early, but those plans have to be pushed back," says Tadashi Watanabe, who heads the project for RIKEN, a network of national labs headquartered near Tokyo. The SPring-8 synchrotron near Kobe will have to get by on 2% less in fiscal 2010, or about $93 million. "It's not a big cut, but it will have some effect," says Koki Sorimachi, head of planning for the RIKEN Harima Institute, which operates SPring-8.

Meanwhile, the Japan Agency for Marine-Earth Science and Technology (JAMSTEC) is facing a 6% cut to its annual budget of roughly $400 million. Because of high fixed costs, "reductions will come out of pure research-related money," says Asahiko Taira, an executive director of JAMSTEC. His organization aims to minimize the impact on the drill ship *Chikyu*, Japan's contribution to the International Ocean Drilling Program.

Increased support for emerging fields should compensate for areas being cut, says Kitazawa. Gaining ground, for example, are green technology programs; money for initiatives under the education ministry will nearly triple this year to $107 million.


**Staying afloat.** JAMSTEC hopes to keep the drill ship *Chikyu* operating despite a 6% budget cut.

CREDIT: JAMSTEC/IODP

Funding for universities and academic research is essentially flat. The budget for grants-in-aid for scientific research, the bread-and-butter support for university researchers, will stay at $2.1 billion, matching a public plea last month by a group of university research officers. "More would have been better, but at least it's in line with our request," says Masafumi Akahira, a vice president of the University of Tsukuba. But base funding for national universities is being squeezed 1% to $12.5 billion.

At one point, scientists feared much worse. When the Democratic Party took power last August, it announced it would rewrite the rules for preparing budgets, starting with the fiscal 2010 budget proposed by the long-ruling Liberal Democratic Party just 2 days before its historic electoral defeat. In November, a task force set up to identify fat in the budget recommended freezing spending on the supercomputer, pending a review, and deep cuts to JAMSTEC and SPring-8 (*Science*, 20 November 2009, p. 1046). The ensuing storm of protests from scientists—including most of Japan's living Nobel laureates—got much of the funding restored.

Managers are already worrying about next year. "We're really afraid this trend may continue. If the economy continues downward, we could face more budget cuts," says Taira. In the past, bureaucrats worked out funding details for each program and institution and then totaled the numbers for each budget category. This time, the Cabinet set funding for broad categories. "If scientists can't explain their work to policymakers, they are going to see their budgets go down," warns Kitazawa. With the new party bypassing the bureaucrats, Taira says scientists need to find new ways to influence policy. "Exactly how we're going to do that, we don't know yet," he says. **–DENNIS NORMILE**

CHINA

# After Long March, Scientists Create 'Chinese NIH'

**BEIJING**—Scientists here rang in the New Year with the debut of China's first biomedical research fund. Last week, the National Natural Science Foundation of China (NSFC) launched a medical department that expects to disburse about 1 billion renminbi ($150 million) in government grants in 2010.

The department should be a shot in the arm for unraveling disease mechanisms, modernizing traditional Chinese medicine, and moving results from bench to bedside. "It will promote a speedy transition of basic research into clinical application," says Pei Duanqing, director general of the Guangzhou Institute of Biomedicine and Health of the Chinese Academy of Sciences.

For backers of basic biomedical research, the new department is a decisive victory in a decade-long ideological struggle. In 2001, when NSFC first declared its intention to create a medical department, "some people believed that there was no basic research in medical science," says NSFC President Chen Yiyu. That unfavorable climate compelled many scientists to work abroad. In the early 1990s, says Ma Yue, a "poor atmosphere" and a shortage of grants made it "hard to do medical research." Ma left for the United States in 1994 and returned here in 2006 to conduct stem cell research at the Institute of Biophysics of the Chinese Academy of Sciences.

The prevailing winds shifted in 2008, when hematologist Chen Zhu was appointed health minister. He has campaigned vigorously for creation of an agency akin to the U.S. National Institutes of Health (NIH) (*Science*, 28 March 2008, p. 1748). Although Chen Zhu has not forsaken that goal, he threw his weight behind NSFC's effort. The health minister was "instrumental" in helping to get the medical department off the ground, says Chen Yiyu.

Unlike NIH, NSFC's medical department will not have an intramural research program. Nevertheless, says Stephen Roper, a biophysicist at the University of Miami in Florida, "the target of NSFC and NIH is the same: apply basic research to solving ongoing human disease problems."

Chen Yiyu has tapped Wang Hong-Yang, an expert on hepatitis-induced liver cancer, as the medical department's first director. Wang, director of the International Cooperation Laboratory on Signal Transduction at the Second Military Medical University in Shanghai, will spend a third of her time here overseeing the new department. "My job is to clarify the research directions and make sure the best medical scientists get funded," she says.

That's music to the ears of Huang Liquan of the Monell Chemical Senses Center in Philadelphia, Pennsylvania. The medical department's initial budget "is an excellent start," says Huang, who believes the new entity will usher in a much wider range of opportunities for cooperation between Chinese and U.S. scientists on basic biomedical research. **–LI JIAO**

Li Jiao is a writer in Beijing. With reporting by Richard Stone.

ECOLOGY

# Europe's Bats Resist Fungal Scourge of North America

The same fungus that has devastated bat colonies in the northeastern United States has been identified for the first time in Europe—in a healthy bat. "The astonishing thing is that [the fungus] affects North American bats so devastatingly, but that European bats can get along with it," says Christian Voigt, a bat physiologist at the Leibniz Institute for Zoo and Wildlife Research (IZW) in Berlin.

**Survivor.** This French bat was not killed by fungus on its nose (arrow).

White-nose syndrome was first identified in a cave in upstate New York in 2006. Since then, it has spread across nine states and caused unprecedented mortalities. Affected bats emerge from hibernation too frequently and lose body fat, and many starve to death. Last year, a group led by microbiologist David Blehert of the U.S. Geological Survey in Madison, identified the fungus associated with the syndrome as *Geomyces destructans*, but many puzzles remain about the nature of the disease, such as whether the bats' immune systems were compromised (*Science*, 29 May 2009, p. 1134).

European researchers watched the U.S. outbreak with alarm. "I thought, 'Oh my God, we've got a huge nightmare on our hands,' " recalls Kate Jones of the Zoological Society of London. So far, no mass casualties have been detected among Europe's species, but researchers did find anecdotal reports of bats with white fungus that no one had paid attention to previously.

On 12 March, Sébastien Puechmaille of University College Dublin (UCD) spotted a mouse-eared bat (*Myotis myotis*) covered with fungus in a cave 130 kilometers northeast of Bordeaux, France. Microscopic examination of the spores and two molecular markers showed that it was *G. destructans*, the team reported online 29 December in *Emerging Infectious Diseases*. Another group, led by Gudrun Wibbelt of IZW, has also identified the fungus in bats from three other European countries, none reporting bat deaths. Their results have been submitted to the same journal.

Now the challenge is to figure out why most European bats are not infected and why those that are remain healthy—and whether that knowledge can be used to help ailing bat populations in the United States. One scenario is that *G. destructans* has been present in Europe for a long time, and European bat species have evolved immunity, says Emma Teeling of UCD, the senior author of the December paper. Or perhaps the fungus evolved greater virulence after arriving in North America, a possibility that could be investigated with further sequencing.

Whatever the explanation, the European reports are "great news," says Alan Hicks, a mammal specialist with New York's Department of Environmental Conservation in Albany, who has charted the decline of the state's once-massive bat colonies. Eventually, an understanding of these differences could help lead to the development of a vaccine or treatments for endangered bats, Blehert says. Meanwhile, researchers are beginning once again to survey hibernating bats in the Northeast United States. Hicks says the signs so far are that deaths are continuing. **–ERIK STOKSTAD**

CREDIT: PASCAL VERDEYROUX, *EMERGING INFECTIOUS DISEASES* (ADVANCED ONLINE EDITION, 2010)

INDIA

# Fatal Fire and Tritium Poisoning Leave Nuclear Labs Searching for Answers

**THIRUVANANTHAPURAM, INDIA**—A pair of mishaps has left India's nuclear establishment on edge. On 28 December, two biochemistry Ph.D. students burned to death in a mysterious fire in the country's main nuclear laboratory, the Bhabha Atomic Research Centre (BARC) in Mumbai. A month earlier, dozens of workers at a nuclear plant in Kaiga were exposed to tritium in an apparent case of attempted poisoning.

The incidents—both unsolved as *Science* went to press—raise the specter of "terrorist elements checking the vulnerability of India's nuclear establishment before a bigger and more deadly attack is mounted," argues former BARC director A. N. Prasad. Others discount that possibility. "I don't believe [that's the case]," materials scientist Srikumar Banerjee, chair of India's Atomic Energy Commission (AEC), told *Science* on the sidelines of the India Science Congress here this week. "These are two isolated events."

**Seeking clues.** Last month's fire at the Bhabha Atomic Research Centre in Mumbai has put AEC "on a war footing," says commission chair Srikumar Banerjee.

Even before the twin incidents, the Department of Atomic Energy (DAE) was on heightened alert. After U.S. terror suspect David C. Headley was arrested in Chicago last October in possession of photos of BARC, DAE ordered a security audit for all nuclear facilities. Now the department has ordered an additional safety review. "We have been doing this on a war footing," says Banerjee.

The fatal fire last week was the worst accident in BARC's 55-year history. The facility is home to India's nuclear weapons program—but the fire was "in no way related to the strategic program," Banerjee says. A DAE spokesperson adds that "no reactor, radioactivity, or radiation was involved in the accident." However, says Prithviraj Chavan, India's science minister and an AEC member, "we have not yet been able to exactly pinpoint what … caused the fire."

The fire apparently was set off by a midday explosion that shook the third floor of BARC's Radiation and Photochemistry Division. Firefighters quickly doused the flames. They recovered from an analytical chemistry lab—the only area that suffered damage—two bodies that had been charred beyond recognition. The victims were later identified as Umang Singh, 25, and Partha Pratim Bag, 24.

The fire "is baffling," says Tulsi Mukherjee, director of BARC's chemistry group. The chemistry lab where the fire broke out was "not functional," as it was being refurbished and had been painted a few days earlier. "There was just not enough incendiary material in the lab to have caused this devastating fire," Mukherjee says. The lab, he says, housed a spectrophotometer that was turned off, two computers, a nitrogen cylinder—intact after the accident—a laminar flow hood, and small quantities of solvents. "No one heard any screams or shouts of help," Mukherjee says. Singh and Bag were preparing to study the possible use of herbal extracts for radiation protection, he says, and usually worked with "harmless chemicals."

A more bizarre incident occurred on 24 November at the 220-MW pressurized heavy water reactor in Kaiga, some 700 km south of Mumbai. That day, as many as 92 workers drank from a water cooler tainted with tritium-laced heavy water. "It was perhaps the work of some disgruntled employee" who spiked the water cooler, says Chavan. "The area was a security area; no question of anybody from outside coming in." No workers were harmed by the slight exposures to radioactivity, and all have since returned to work. No arrest has been made so far.

Like Banerjee, Chavan dismisses a terrorist threat but sees an urgent need for stricter measures at labs across India. For starters, Prasad suggests that authorities conduct more rigorous background checks on personnel.

–PALLAVA BAGLA

CREDITS: PALLAVA BAGLA/CORBIS; (INSET) P. BAGLA

## ScienceNOW.org

### From *Science*'s Online Daily News Site

**Five New Exoplanets Discovered**
Those hoping that the opening plenary talk of the American Astronomical Society meeting would deliver a stunning revelation probably came away disappointed. NASA's Kepler mission has added five new planets to a growing roster of more than 400 beyond our solar system—and none of the newbies is remotely hospitable to life. But there's still plenty to chew on. One of the planets, for example, is as light as Styrofoam—and that has astronomers scratching their heads. http://bit.ly/keplerplanets

**Mosquitoes: Love at First Buzz**
How do you mate with the right person if everyone looks exactly the same? That's a problem that faces the *Anopheles gambiae* complex of mosquitoes, a group that comprises six identical-looking species. The solution, according to a new study, is to find a partner who can sing in perfect harmony with you. http://bit.ly/mosquitoharmony

Read the full postings, comments, and more on **sciencenow.sciencemag.org**.

## ScienceInsider

**Planes, Boats, and Greenhouse Gas**
A new report lays out the challenges of reducing greenhouse gas emissions from the airplane and boat transportation sectors. Those sectors make up roughly 3% of global greenhouse gas emissions, but their contribution could increase by 10 times by 2050. Recent moves by the airline industry to study biofuels and even hydrogen-powered airplanes might mitigate such carbon pollution, however. http://bit.ly/7mQWQk

**Deadline Looms for Earth-Sensing Satellites** Congress is demanding that the three agencies that run the National Polar-orbiting Operational Environmental Satellite System provide plans to overhaul the management structure for the troubled system. As of press time, NASA, NOAA, and the Pentagon had yet to file a report lawmakers wanted by 4 January on the costs and management options for the $15 billion system. http://bit.ly/6ackwr

For the full postings and more, go to **blogs.sciencemag.org/scienceinsider.**

# From Medfly to Moth: Raising a Buzz of Dissent

**Twenty years after California's Medfly wars, a vocal critic of government eradication policies is back in a battle over a new invader**

**Indiscriminate eater.** The light brown apple moth, an invader in California, feeds on more than 2000 plant species.

CREDIT: USDA

**JAMES CAREY IS AT IT AGAIN. IN THE EARLY** 1990s, as a scientific adviser in California's unpopular pesticide-spraying war against the Mediterranean fruit fly, the entomologist vocally charged that the state's program was fundamentally flawed. Bucking conventional wisdom, Carey claimed that the Medfly was already established, defying the eradication attempts.

Carey, a professor at the University of California (UC), Davis, then largely vanished from the invasion-biology research scene, gaining prominence instead as an innovative biodemographer who has elucidated universal principles of aging by tracking mortality and reproduction rates in huge populations of insects. He currently directs a $3.4 million federally funded program to investigate the ecology, evolution, and mechanisms of life span and aging.

Then in February 2007, a voracious new invasive pest—the light brown apple moth from Australia, dubbed LBAM—was identified in Berkeley. The insect's larvae feed on more than 2000 plant species, from apples, grapes, and berries to cypress trees. The California Department of Food and Agriculture (CDFA) kicked into crisis mode to get rid of the moth in northern California, launching a program of aerially spraying a pheromone to disrupt the insect's mating. But those efforts prompted a red-hot public ruckus, forcing the state to shift to a plan to release zillions of sterile moths to achieve the same ends. And once again, Carey has surfaced as a relentless voice of dissent.

His core argument is essentially the same. Contrary to the agriculture agencies' view that the moth is a new and vanquishable arrival, he thinks it was established long ago and is too widespread to wipe out. The idea of a long-standing invasion can't be discounted, yet it is hard to prove or disprove. But it is Carey's take-no-prisoners style, as much as his bold scientific interpretations, that has riled agriculture officials from Sacramento to Washington, D.C.

Carey calls the moth-eradication program "a travesty" driven by politics where instead rigorous science should be brought to bear. He says that as a scientist at a public university, he feels a responsibility to render his candid expertise, especially when other entomologists may be reluctant to criticize the agriculture agencies that provide research funding. "I'm not an environmentalist per se, but it just looked like something that was completely wrongheaded," he says of the LBAM plan. Evidence doesn't support that eradication is feasible—or even needed, he says, because it's unclear that the moth is indeed a major crop pest.

Carey's admirers say his contrarian views have a place and that he has raised important issues in the invasive-species debates. Others say his insistent criticism has helped derail the state's efforts to deal with the apple moth, resulting in more harm than good. Officials at CDFA and the U.S. Department of Agriculture (USDA) declined to answer any questions from *Science* about Carey or his scientific critiques.

### Taking a stand in the Medfly wars

When an exotic pest first pops up on the radar, the great worry is that it may wreak havoc as it outcompetes or devours an area's native species. Agricultural agencies, as well as some ecologists, traditionally have regarded the discovery of a foreign species as a new infiltration. But with the Medfly and LBAM, some invasion biologists like Carey have viewed the new detection as sightings of a population that actually came and settled in earlier.

It is Carey's radical take, however, that this invasion process may unfold over not months or years but decades to a century, like the slow, long latency growth of a stealthy cancer; most of the doublings of a new exotic pest population remain invisible, at still-tiny numbers that elude trapping surveys. By the time the established population is diagnosed, it's often metastatic and can at best be controlled, not cured.

Carey came to this model 2 decades ago, after plotting by pencil the locations of every Medfly the state had ever caught on a series of maps—949 flies in 106 cities, with some detections popping up in the same exact neighborhoods, years apart, in a peculiar pattern. It was 1990; near-yearly infestations of the devastating crop pest were plaguing the Los Angeles basin despite aerial malathion sprayings. Carey, who'd been conducting demography studies of the fly, was on CDFA's Medfly science advisory panel.

CDFA and USDA officials explained the recurrences as new introductions of flies hitchhiking on fruit brought in from abroad. But in testimony before the California Legislature, Carey presented his dissenting view that the state's eradication efforts were failing to fully eliminate a long-resident Medfly population; a rethinking of how to fight the insect was needed. He published his hypothesis in *Science* in 1991.

Carey's role in the Medfly debate "was akin to pointing out that the emperor has no clothes," says Daniel Simberloff, an invasion biologist at the University of Tennessee, Knoxville, laughing. Simberloff's perspective is that Carey "was probably right, in general." But the agencies rejected Carey's theory, which carried enormous economic repercussions: If the state declared it couldn't eradicate the Medfly, California's multi-billion-dollar-a-year farming industry would be embargoed from shipping produce

to other countries or would be required to implement costly control measures.

The agencies also noted that trapping arrays had failed to spot any Medflies after each eradication. Carey insisted that a low-level population was lurking below the radar, but "you can't prove a negative," says retired USDA entomologist Derrell Chambers, then a colleague on the advisory panel.

Which theory was right? In 2001 and 2002, genetic analyses of Medflies captured in the '90s found evidence for several separate introductions *and* for the existence of populations that persisted from one year to the next. "Both things happened, and we need to accept that and learn from it," says David Haymer, a University of Hawaii, Manoa, geneticist and co-author of one of the studies. Yet, consensus remains elusive on whether those persisting flies represented small, incipient populations or an established one. Carey is sticking to his guns. And CDFA press releases still claim that the state has successfully eradicated every Medfly introduction since 1975.

### Into the moth maelstrom

For those who followed the Medfly wars, the LBAM debate seems like déjà vu. Upon learning that the Davis biodemographer was involved, "I thought, Oh, my God, there's Carey again," recalls Simberloff, who last summer sat on a National Research Council (NRC) panel that reviewed certain aspects of the controversy at USDA's request (see sidebar, p. 136).

In late 2007, Carey received an e-mail from a citizens group that was filing a lawsuit to stop the state from spraying pheromone over Monterey and Santa Cruz. Would Carey weigh in on the matter? Given that soon after the moth's discovery, infestations were spotted in nine counties—an area of more than 20,000 square kilometers—Carey believed the invasion was old and too far gone. "There was absolutely no way in the world that they were going to have any chance to eradicate this thing," he recalls; pheromone spraying and other tools were too weak to do the job.

He submitted an affidavit to that effect—and thereby leaped into the biggest, most bitterly divisive battle over an invasive species in the Golden State in 2 decades. Any way one slices it, the $89.5 million moth-eradication plan has been a public relations disaster. Besieged by lawsuits and a fierce backlash from a public fearful of anything resembling a pesticide—as well as a mounting debate over just how dangerous a pest the moth really is (see box, right)—CDFA tabled the aerial pheromone treatments after several sprayings. CDFA and USDA believe LBAM arrived recently and was shuffled around via the nursery-plant trade, because prior to 2007, the state's network of moth-luring traps failed to pick up the insect.

But LBAM is tricky to distinguish from many other nondescript little brown moths, and Carey has said all along that the trapping network was inadequate for detecting this pest's presence. (He also disputes the conventional wisdom that the increased movement of invasive species via trade or human traffic can explain the sudden, widespread appearance of a pest like the moth. If so, the insect should be cropping up in Arizona or other states too, he says.) The NRC panel independently reached the same conclusion after reviewing trapping protocols and data from the state and other sources.

Carey goes so far as to claim that the moth has been in California for 30 to 50 years. "I'm not kidding," he says—the invasion process is chronic, insidious, and long undetectable. His estimate is roughly extrapolated from the case of the exotic gypsy moth, which took 4 decades to spread 25,000 square kilometers in the Northeast.

USDA and CDFA have noted that there are no hard data to support Carey's calculation. There is no way to verify or disprove the estimate, says Ring Cardé, an insect pheromone researcher at UC Riverside and an adviser on CDFA's technical working group on the moth.

But regardless of whether the invasion started 3 or 50 years ago, others concur with Carey's central point: The insect is too far-flung to eliminate. NRC panel member Simberloff raises his eyebrows at Carey's half-century guesstimate but nonetheless thinks that the moth's sprawling distribution and numbers suggest "it's been here awhile" and was beyond hope of eradication in 2007.

Despite such criticisms, CDFA and USDA are moving forward on the expensive sterile-insect technique (SIT). USDA has been breeding and sterilizing moths for release as a contraceptive to the insect's reproduction; field testing in Napa and Sonoma vineyards began last November and will continue through late 2011. Carey says the effort, like the pheromone spraying, is "throwing money down a rat hole"; he thinks the state should instead shift to areawide pest management of the moth.

It will take a couple of years to develop a robust SIT program. By then, even CDFA science adviser Cardé admits that it is uncertain the tool could push back the moth population's boundaries, although it could still help manage low-density infestations or eradicate small outlying pockets. Cardé and the technical working group maintain that had the state been able to carry out the pheromone-spraying program to reduce the moth's population prior to SIT, there was a chance of eliminating it. But now, if the invasion keeps spreading, eradication becomes more and more of a long shot, Cardé says.

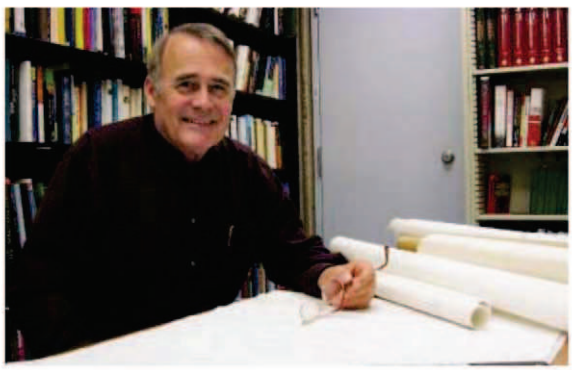

**Pesky dissenter.** Jim Carey, here with his old Medfly plotting maps, wants more data and less politics in California's invasive-pest policymaking.

CREDITS (TOP TO BOTTOM): ADAPTED FROM USDA ANIMAL AND PLANT HEALTH INSPECTION SERVICE; INGFEI CHEN

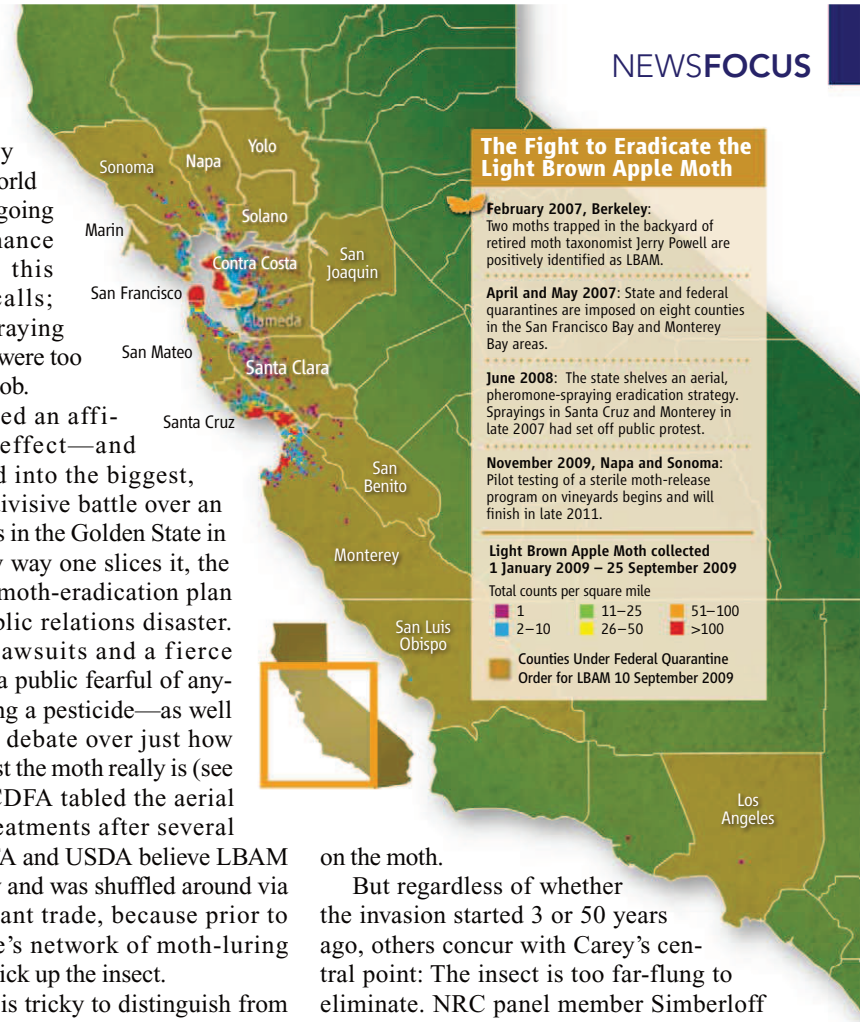

**Not so bad after all?** Scientists are debating whether the light brown apple moth truly poses a major threat to California crops.

## Gaps in Moth Logic

When the Australian light brown apple moth was identified in Berkeley in 2007—its first sighting in North America—the California Department of Food and Agriculture (CDFA) and U.S. Department of Agriculture (USDA) rushed into action to eradicate it. They saw a grave emergency for California agriculture, and justifiably so, given the insect's reputation as a voracious, indiscriminate eater with a liking for many of the state's most valuable crop species. USDA, which had long ranked the moth a high-risk pest that required quarantines to prevent its spread, warned that it could be one of the most destructive invaders ever.

But nearly 3 years later, the insect hasn't lived up to that reputation. More than 257,907 moths have been trapped in 18 counties from Napa to Los Angeles, but they haven't yet made substantial inroads into the prime agricultural Central Valley. Major crop damage hasn't materialized.

Entomologists Frank Zalom and James Carey of the University of California, Davis, along with former UC Santa Cruz arboretum director Daniel Harder, believe that the state's farmers can learn to live with the exotic invader—perhaps with the same control tools they already use to manage other moths in the same leafroller family. Along those lines, two groups of citizens, including Harder, have petitioned USDA's Animal and Plant Health Inspection Service (APHIS) to reclassify the insect as a minor pest so that costly quarantine measures can be lifted; forget eradication, they say. However, USDA and CDFA maintain that without an eradication plan, or if the pest's status were downgraded, trading partners (and other states) would likely permanently ban or slap restrictions on California produce. (Canada and Mexico have already enacted some restrictions.) Whether USDA can negotiate around such barriers is an issue of debate.

APHIS drafted a denial to the petitioners' request but also asked the National Academy of Sciences to evaluate the response. In a report last August, a committee of the academy's National Research Council determined that APHIS has the regulatory authority to continue classifying the moth as high-risk. But the panel found that the agency's rationale for that rating—which, others note, is the basis for justifying the state's moth-eradication program—wasn't grounded in sound, rigorous science.

Specifically, USDA's model predicting a dramatic spread of the insect throughout the southern United States relied upon "questionable" assumptions, says May Berenbaum, a University of Illinois, Urbana-Champaign, entomologist who chaired the review. That geographic projection was then plugged into assessments of potential national economic damages that used "inconsistent and sometimes incomprehensible analytic techniques," the reviewers wrote. In an extreme scenario, the USDA analysis estimated $9 billion in yearly losses from global trade restrictions.

Berenbaum says USDA was "between a rock and a hard place" in navigating trade laws and making rapid decisions when little is known about how the moth will behave here. It is to APHIS's credit, she adds, that it asked for the academy's feedback and made some revisions in its response, which has not yet been finalized. An APHIS spokesperson wrote in an e-mail that the agency continues to seek the best predictive models. **–I.C.**

Cardé concedes that Carey's questions about the age of the invasion and whether it can be eradicated are reasonable. But questions that lack definitive answers can sometimes be used by advocates to "completely scotch" agency programs from moving forward—as has happened with LBAM, he says.

Furthermore, others point out that the agencies typically don't have the luxury of an academic debate when they have to make quick political and financial decisions with billions of dollars in trade at stake. (Even without major moth-inflicted crop damage, the potential for huge trade losses is, again, driving the state's eradication push.)

Agency officials are now concerned that the moth case may hurt their ability to eradicate future exotic pest invasions that may be far more dangerous to agriculture, Cardé says; opponents may try to employ the same counterarguments. "It's *very* worrisome," he says.

Carey bristles at Cardé's criticism. Scientists have a responsibility to push back and "not to simply go along, get along" with a flawed eradication plan that will waste tens to hundreds of millions of dollars, he says.

**Pilot project.** USDA light brown apple moth program coordinator Gregory Simmons releases thousands of sterile moths into a Napa vineyard last November.

And in no case has a pest like the apple moth—so widespread and with so many plant hosts—ever been eradicated, he says.

Others applaud Carey's efforts to inject more science into agency decisions. "His actions represent science at its best as a pursuit of understanding reality, not just fitting a preconceived agenda," writes Hawaii's Haymer in an e-mail.

### Rethinking the future

To Carey, the apple moth episode epitomizes a system badly broken. "This pest-invasion paradigm has got to be revisited in a big way," he says. With new exotic species flooding the state and public opposition to any chemical spraying, eradication isn't always technically or politically possible. The relatively new concept of areawide control, implemented through "pest-free" zones of trade, should be tried instead, he says.

At UC Davis, the chair of Carey's entomology department, Michael Parrella, is organizing a conference for this spring to reexamine the invasive species–policy paradigm from top to bottom. The goal is an open dialogue with major stakeholders, including USDA and CDFA administrators. Will they come? Parrella acknowledges that Carey's forceful style can be a deterrent. Says Parrella: "It would be nice to think we could sit down and discuss things. It's not us versus them."

**–INGFEI CHEN**

Ingfei Chen is a writer in Santa Cruz, California

CREDITS (TOP TO BOTTOM): USDA; J. L. SOUSA/NAPA VALLEY REGISTER/ZUMA PRESS

RESEARCH INSTITUTIONS

# Plan to Merge Texas Schools Runs Into Faculty Opposition

**Baylor College of Medicine, seeking financial security, is considering joining with Rice; but Rice faculty members have challenged the plan**

On the congenial campus of Rice University in Houston, Texas, faculty members in departments such as bioengineering and physics have lately found themselves facing off in a bitter public dispute. The issue: whether Rice, a small research university with deep pockets, should merge with nearby Baylor College of Medicine (BCM), which needs money. Proponents say it is a natural to add a top medical school to Rice's strengths in physical and life sciences. But critics at Rice say that pairing up with BCM is not worth the financial risks.

BCM, the only private medical school in the U.S. Southwest, is part of a huge complex called the Texas Medical Center that includes a dozen or so hospitals and the M. D. Anderson Cancer Center. Across the street from the complex is Rice, which has about 3300 undergraduates and 2300 graduate students. The two schools already have joint research and education programs, and many Rice undergrads go on to medical school at BCM.

Officials floated the merger idea 15 months ago as Baylor was seeking to overcome a financial crisis that began in 2004 when it split from the Methodist Hospital System, a key source of clinical income. (The college continues to have teaching partnerships with other hospitals.) Baylor started to build its own hospital but froze construction last March after the project went over budget. Rice administrators argue that Baylor would gain a measure of financial stability by joining the university. The joint operation, they say, would be highly competitive for federal research funding, especially as biology and the physical sciences increasingly overlap. "To us, it is very, very compelling," says Rice Provost Eugene Levy. Rice officials note that acquiring BCM's more than $210 million in National Institutes of Health support would elevate Rice from 130th to 23rd in the country in federal research funding.

Last summer, a joint Rice-BCM committee came up with a list of "research synergies" that could be pursued. They included creating a neuroscience major and a personalized medicine initiative involving Baylor's NIH-funded human genome–sequencing center. "From our side of the road, it offers great opportunities for collaboration on what is really the future of biomedical research," says committee member and BCM neuroscientist Michael Friedlander, speaking for himself. (Baylor is granting no official interviews.)

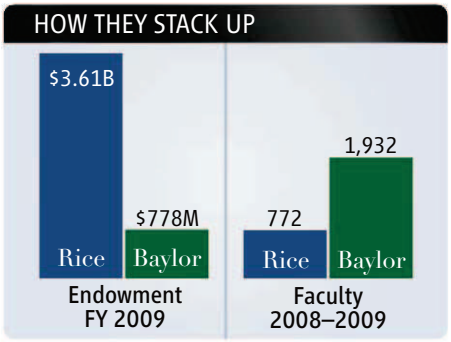


A Rice-only faculty committee, however, was more cautious about the possible merger, noting that it will require "a substantial one-time investment" from Rice. This panel said the merger should take place only if certain conditions are met, including putting Baylor on a "credible path" to eliminating its deficit, partnering with general-care hospitals, and raising $250 million for Rice programs.

In November, a public debate on the merger erupted in a series of op-eds and letters to the editor from Rice faculty, some pro, others against. "The costs have been underestimated, and the academic benefits have been hyped," says Moshe Y. Vardi, a Rice computer science professor who has been a vocal opponent. Others worry that the Rice administration's attention will shift away from physical sciences and humanities. "We could become a very unbalanced institution," says chemical and biomolecular engineering professor Matteo Pasquali.

In early December, a group of Rice faculty met and voted 61–59 against a resolution opposing the merger—defeating the faculty opponents only because four administrators exercised their right to vote. A recent survey of Rice's roughly 700 faculty found a similar split: 50% oppose the merger, 39% support it, and 11% are undecided, according to a Rice faculty member with a copy of the results.

Levy responds that faculty opinion is actually "more nuanced." He says that if financial concerns can be resolved, there is "substantial support." Indeed, 53% of faculty would support the merger and 39% oppose it if specific conditions listed by the Rice administration are satisfied, the survey reportedly says.

Observers expect the Rice board to make a decision before a memorandum of understanding between the two schools expires on 31 January. Vardi, who has pored over an audit of Baylor's books, points out that the document states that without a merger agreement, creditors will soon require the medical school to hire a manager to oversee a cost-cutting reorganization. Baylor faculty seem confident that the college will persevere and build stronger hospital partnerships even without a merger. "It's not a do-or-die thing," says Friedlander.

**–JOCELYN KAISER**

**Marriage proposal.** Rice (*foreground*) has offered to tie the knot with nearby Baylor College of Medicine.

SOURCES: RICE *THRESHER*; RICE UNIVERSITY

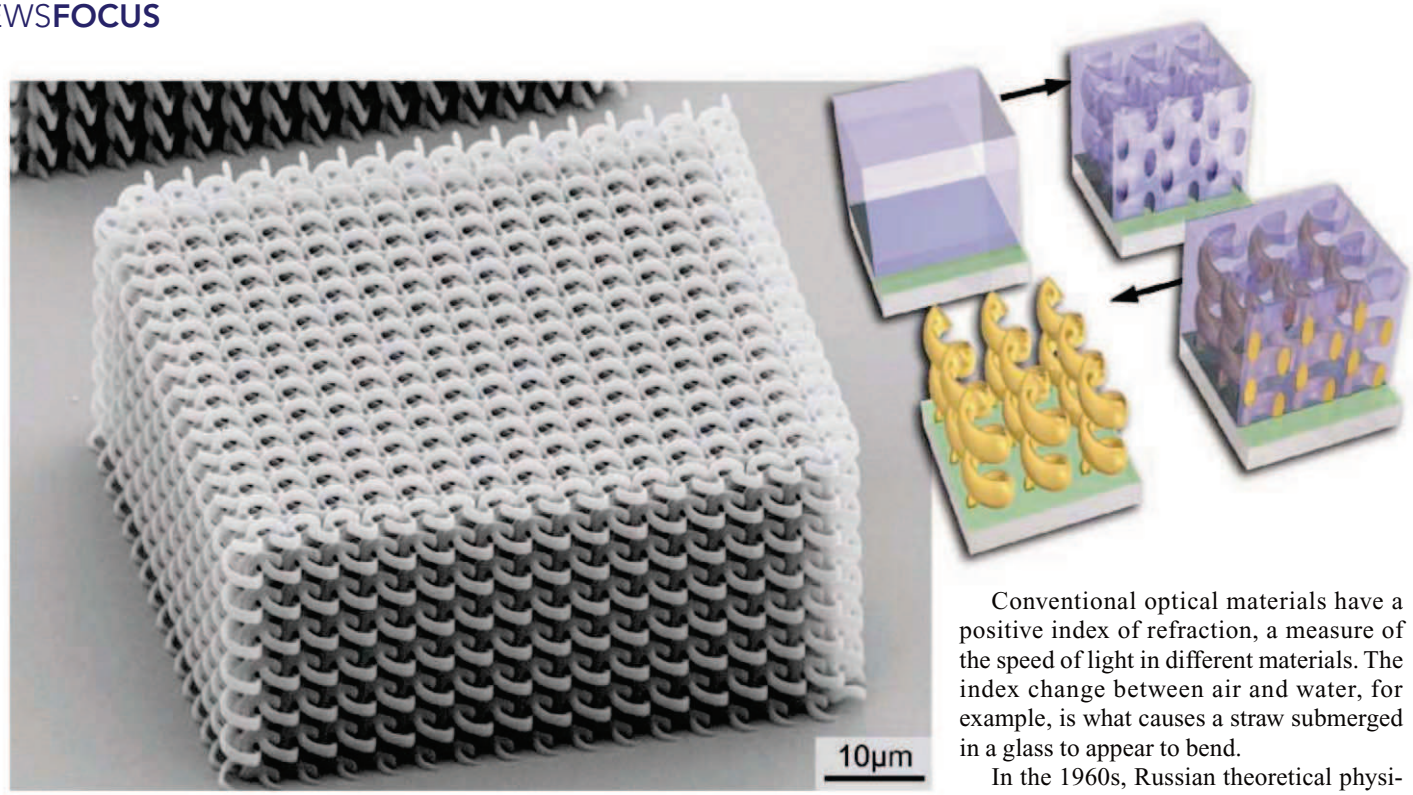


MATERIALS SCIENCE

# Next Wave of Metamaterials Hopes to Fuel the Revolution

**Designing invisibility cloaks may be fun. But for more practical applications of metamaterials, scientists need to find ways to have less of the light absorbed**

In 2001, researchers in the United States and the United Kingdom pulled off a trick with light that few thought possible: They bent it backward. To be more precise, they altered the refraction pattern by shining microwaves at material made from a circuit board topped with an array of rings and wires. The feat forced physicists everywhere to rethink what they thought they knew about manipulating light.

The concoction was the first to demonstrate this odd light-bending trick. And its negative index of refraction made it one of the original "metamaterials." Metamaterials are composites engineered to manipulate electromagnetic waves in new ways. Researchers have designed everything from invisibility cloaks and lenses that focus light to a point smaller than the diffraction limit—the tightest focus possible by conventional optics—to materials that mimic the light-trapping ability of black holes. "There have been tremendous developments in metamaterials over the last 10 years," says Xiang Zhang, a physicist and metamaterials expert at the University of California (UC), Berkeley.

But the field faces sizable challenges as well. Despite the researchers' successes in manipulating electromagnetic waves, the fact that most metamaterials are strong light absorbers and ultrathin has hampered their real-world uses. "Conceptually, there has already been a revolution," says Martin Wegener, a physicist at the University of Karlsruhe in Germany. "Whether it will lead to revolutionary products remains to be seen." The challenge, Wegener and others say, is to come up with better ways to create complex, three-dimensional patterns in thick materials and limit their tendency to absorb light.

## Active materials

Centuries ago, glassmakers realized that they could focus light by precisely cutting, grinding, and polishing glass. That discovery led to everything from eyeglasses to telescopes. More recently, fiber optics has made possible modern communications. All of these devices manipulate light based on the chemical composition of the matter through which light travels.

Conventional optical materials have a positive index of refraction, a measure of the speed of light in different materials. The index change between air and water, for example, is what causes a straw submerged in a glass to appear to bend.

In the 1960s, Russian theoretical physicist Victor Veselago realized that if materials could be properly engineered, their index of refraction could be negative. If water's refractive index were negative, for example, a straw entering it would appear not just to bend but actually to stick out of the water's surface. Veselago's work implied that flat metamaterials could act like lenses and produce other counterintuitive phenomena, such as a reverse Doppler effect and negative refraction.

It took more than 30 years, but in 2001, researchers led by John Pendry, a theoretical physicist at Imperial College London, and David Smith, now at Duke University in Durham, North Carolina, made just such a material. They began with an assembly of metal wires and rings, the latter having had a thin slice removed (*Science*, 6 April 2001, p. 77). When Pendry and his colleagues then shined microwaves on their metamaterial, the microwaves excited electrons in the metal rings, causing them to slosh back and forth. That sloshing produced a resonant magnetic field that affected the propagation of subsequent microwaves, producing a negative index of refraction. It also spurred a tide of related innovations.

Since then, physicists and materials scientists have had little trouble designing metamaterials that work with radio waves, microwaves, and terahertz waves, all forms of electromagnetic radiation with long wavelengths. That's because the individual components of metamaterials must be smaller than the wavelength of the light they are trying to manipulate. For instance,

**Going vertical.** Carving intricate structures in polymers (*far left*) is the first step in creating metamaterials with metallic features (*left*) that can manipulate light.

for microwaves that means in the centimeter range.

But to manipulate shorter wavelength light, such as infrared or visible rays, researchers must design metamaterials with features on the micrometer or nano scale. That's certainly possible with conventional microchip patterning techniques. But in many cases the patterns that metamaterials makers are trying to make are more complex than microchip patterning can handle.

Absorption is another big problem. Metamaterials work because incoming light triggers electrons to flow in ways that create a standing magnetic field that affects the propagation of the light waves that follow. Researchers typically use metals, which are good electrical conductors, to make the portions of their metamaterials that carry electron current. But metals are also strong absorbers of visible and infrared light.

Researchers have partly sidestepped the problem for metamaterials that work in the visible and infrared ranges by using just single ultrathin layers of metals. "The losses are so high right now, so we can only use thin films for metamaterials applications," says Costas Soukoulis, a condensed-matter physicist at Iowa State University in Ames. But the light must propagate through thicker samples for scientists to be able to observe many unique properties of metamaterials, such as a negative refractive index.

## Going 3D

Metamaterials designers have tried a number of approaches to counteract the losses from absorption. Foremost among them are novel, complex 3D metamaterial designs that manipulate the spacing of features in the material. If the geometry can be tailored precisely enough, it can prevent light of certain frequencies from being absorbed. Reporting in the 18 September 2009 issue of *Science* (p. 1513), for example, Wegener and his colleagues used a method called direct laser writing to cut into a polymer slab an array of intricate helices that turned either clockwise or counterclockwise. They then filled those helical vacancies with gold and removed the polymer to create a 3D array of gold helices.

When they shined infrared light along the long axis of the helices, the arrays acted like a filter for polarized light, allowing light with certain polarizations to go through while blocking others. There are already polarization filters that work with conventional optics. But the metamaterial version is able to work over a much broader range of frequencies.

Groups are making progress in designing bulk metamaterials that work with visible light as well. In the 18 September 2008 issue of *Nature*, for example, Zhang and his UC Berkeley colleagues described a bulk-fishnet structure that had a negative refractive index for near-infrared light. They made the material by stacking alternating layers of silver and magnesium fluoride and used a focused ion beam to cut a fishnet pattern of holes into the stack, leaving behind structures that control the movement of electrons.

The pairs of conducting and nonconducting layers form a circuit. And the series of circuits created by stacking the layers generate a resonant magnetic field that causes incoming infrared light to have a negative index of refraction. In the 15 August 2008 issue of *Science* (p. 930), Zhang's group reported achieving a related effect with red light by using an arrangement of vertically aligned silver nanowires grown inside a sheet of porous aluminum oxide.

But fishnets, helical structures, and most other metamaterials typically work only when the light hitting them comes from a particular direction, or within a narrow range. At a recent meeting,* Michael Sinclair reported that he and his colleagues at Sandia National Laboratories in Albuquerque, New Mexico, are developing a technique to produce metamaterials that work with infrared light coming from virtually any direction. Instead of depositing magnetic features on a flat surface, the researchers evaporate gold through thin slits in a membrane onto curved polymer surfaces. In theory, this should allow them to craft resonant structures with any orientation they choose. The technique has already proven capable of creating gold structures that resonate at a particular frequency, says Sandia team member Bruce Burckel. The next step is to layer the structures to produce the collective behavior needed for a metamaterial.

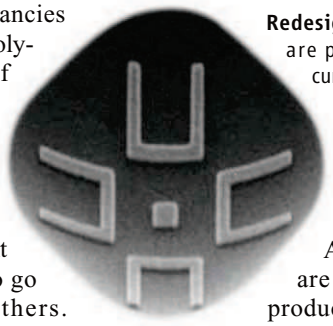

**Redesigned rings.** Sandia researchers are patterning gold split rings on curved polymer surfaces to manipulate incoming infrared light.

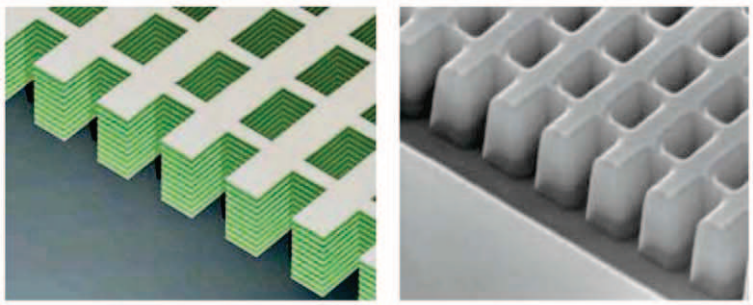

**Better in bulk.** These 15-layer "fishnet" structures produce a negative refractive index—but only when the light hits them from above.

## Gaining ground

Other researchers have taken a different approach to overcoming absorption losses. The idea is to create structures that generate additional photons when they are hit with light at a particular frequency, akin to the way lasers produce a swell of photons at a single frequency. In the past few years, several groups have looked into adding metal nanoparticles and other materials to the insulating portion of a metamaterial that surrounds the metallic portions. The goal is to compensate for some of the light absorbed by the metals. For example, in the 9 June 2009 issue of *Physical Review B*, researchers led by Soukoulis and Wegener reported on a simulation in which tiny metallic particles incorporated in the gaps in split ring resonators produced gains that compensated for metamaterials losses. But to date, they and others have not managed to show the effect experimentally.

"This doesn't work well yet, but this is a big area of progress," says Soukoulis. Much the same could be said for the entire field. "It's a pretty rich tool set," says Sinclair. "People are still exploring what you can do."

**–ROBERT F. SERVICE**

*Materials Research Society, Boston, 30 November–4 December 2009.

CREDITS (TOP TO BOTTOM): COURTESY OF SANDIA; JASON VALENTINE *ET AL.*, *NATURE* **455** (18 SEPTEMBER 2008)

**Palace tour.** Video game technology lets researchers virtually stroll Nimrud's palace.

ARCHAEOLOGY

# Virtual Archaeologists Recreate Parts of Ancient Worlds

**Using techniques borrowed from the entertainment industry, more and more archaeologists are boosting their imaginations and insights with virtual worlds**

Back in the late 1990s, archaeologist Sam Paley of the University at Buffalo in New York was frustrated in his study of the throne room of the 9th century B.C.E. Northwest Palace at Nimrud, the storied Assyrian capital in what is now Iraq. The room was embellished by paintings and bas reliefs aimed at impressing visitors, but the artwork and inscriptions were dispersed in bits and pieces in 60 museums around the globe, and Paley was having trouble picturing the layout. Then at a conference he heard a presentation by Donald Sanders, a leading proponent of using interactive 3D computer graphics in archaeology, and enlisted Sanders's help.

The pair spent many years getting photographs from museums and building a virtual 3D model. Finally, they were able to imagine and test detailed hypotheses about the throne room's layout. For example, had there been enough light to see the artwork in the presumed windowless room? Sanders assumed that the Assyrians used oil torches. Different oils produce light in different ranges of the spectrum, and certain types of light accentuate certain colors, so he simulated various types of oils in strategically situated torches. Sanders concluded that the torches could have been fueled by several types of fish oil and positioned to enhance the art so people could have seen it. Today, "you can walk in the palace of a virtual-reality model," says Paley. A 3D rendering of the model is now on display at the Metropolitan Museum of Art in New York City, and Sanders is at work on a reconstruction of the whole palace.

The throne room is a classic example of the growth of virtual archaeology, in which archaeologists use computers to recreate the environment and conditions of the past, including objects, buildings, and landscapes with human actors, such as ancient battles. The field is a natural evolution of archaeology in the digital age, says archaeologist Maurizio Forte of the University of California, Merced, who spent 3 years recreating the landscape of Rome in the second century C.E. And although virtual archaeology arose in the mid-1990s, it is only now going mainstream, as archaeologists realize the benefits of using computers to make the most of their necessarily incomplete data.

As costs go down, virtual archaeology "definitely is on the rise," says Sanders, with several hundred projects worldwide and plans for a new multimedia journal in the works. Sanders, who has his own company, Learning Sites Inc. in Williamstown, Massachusetts, argues that virtual worlds offer archaeologists the best way to "test complex spatial, behavioral, or temporal hypotheses."

### Recreating the Four Corners

As the field continues to develop, a virtual expert "is now a standard member of the archaeological team" in many countries, says Bernard Frischer, an archaeologist and art historian at the University of Virginia, Charlottesville. Sanders says this is partly due to the decreasing cost of the tools of the virtual trade, such as laser scanners. (Sanders's projects cost anywhere from a few thousand to $100,000.) The field also gets a boost from the entertainment industry: The technology is the same as that used in video games and movie special effects, and many universities have recently added 3D modeling programs. "Once [universities] invest in the technology, they have to look for excuses to use it," says Sanders. Many recent archaeology grads are familiar with virtual techniques, although older archaeologists may not understand the technology as well, says Sanders, leading to "a digital divide."

Despite such frivolous roots, virtual experts are setting their sights on some of archaeology's thorniest scientific problems. For example, one of the enduring mysteries of American archaeology is why the Ancestral Puebloan peoples, or Anasazi, abandoned the Four Corners region of the Southwestern United States some 700 years ago, leaving striking cliff dwellings behind. Decades of study have yielded answers including conflict and climate change.

Researchers with the Village Ecodynamics Project (VEP), led by Tim Kohler of Washington State University, Pullman, and Ziad Kobti of the University of Windsor in Canada, took a different tack to solving the mystery: They virtually recreated a prehistoric world, including everything from landscape to climate to human behavior. They were intent on solving several puzzles, including a cycle of population growth and decline from 920 to 1280 C.E., by which time the Pueblo peoples had left the area. Using archaeological data for variables such as numbers of households, ethnographic data on behaviors such as food sharing, and tree ring and soil data for

climate clues, the researchers meticulously recreated part of the Ancestral Puebloans homeland—an 1827-square-kilometer area in southwest Colorado.

Then they put 200 virtual Pueblo households on the landscape and let them respond to various real-life scenarios, choosing how much corn to grow, how many animals to kill, and so on; their work will be described in a forthcoming book from the University of California Press.

"A part of the simulation is looking at the economic structure of these societies," explains Mark Varien, a VEP archaeologist with Crow Canyon Archaeological Center in Dolores, Colorado. If a household couldn't grow enough corn to survive, the simulation shows how they might have coped, for example, by trading with another household or spending more time hunting game. The simulation is not 3D, but the team did put representations of "agents" onto a two-dimensional landscape. "Spatial relationships are really important," says Kohler, because location was key to determining how a household obtained food, water, and wood. Such simulations "let you look at the interaction between humans and their environment" in a way that traditional archaeology can't," says Varien.

One key result: Households resorted to overhunting deer by 900 C.E. Regardless of the variables incorporated in the simulation, households begin "to seriously deplete deer populations" at that time, says Kohler.

The simulation also suggests, and archaeological evidence confirms, that turkeys were domesticated at about this time, perhaps because deer were scarce. Another notable result was extensive deforestation, which wasn't clearly seen in the archaeological record. "Without the simulation, you couldn't calculate the effect of people collecting wood every day," says Kohler.

Kohler believes that many small social units of the Ancestral Puebloans merged into a single large unit that was less-resilient. The production of maize, the primary food for both people and turkeys, declined sharply around 1270 C.E. due to changes in climate that included drought and cooler summers. This, along with conflict and environmental degradation, led to the exodus.

Around 1250 C.E., archaeological evidence suggests movement into defensible settings around springs; this is when the cliff dwellings of Mesa Verde National Park were built. The suggestion that the move "might have been due to competition or conflict is strengthened by the simulation results," says Kohler. The simulations expanded on the existing evidence, revealing details of the unfortunate tale of "lots of people, organized in a way that was highly tuned to competition, heavily dependent on just one resource, and having to cope with widespread violence," says Kohler. "Things fell apart."

The work is an innovative example of what simulations can achieve, says Thomas J. Baerwald of the National Science Foundation, who directs the program that funds VEP. By examining both human activities and the environment, the VEP team has helped reveal the relationship between them, Baerwald says.

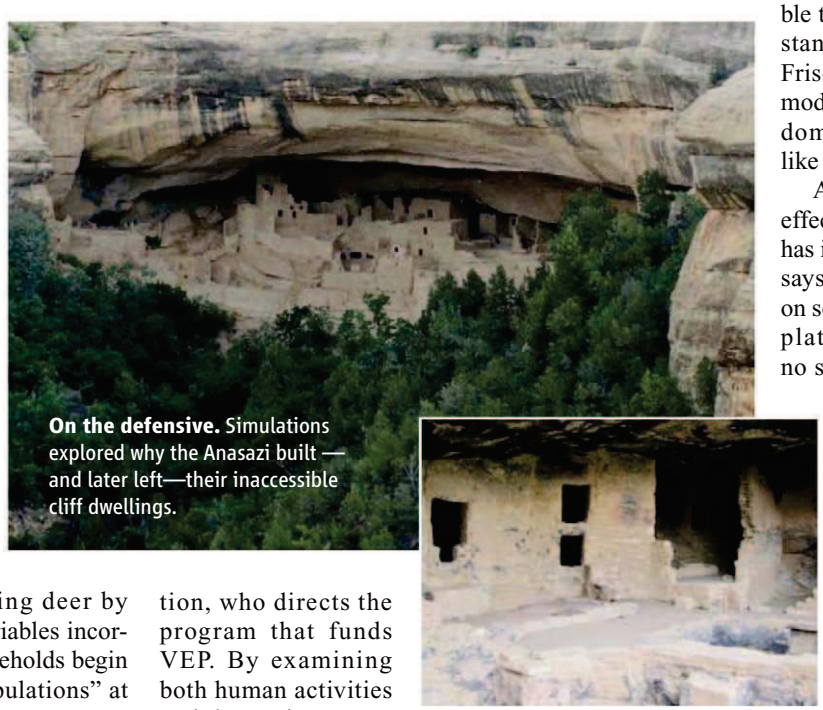

**On the defensive.** Simulations explored why the Anasazi built—and later left—their inaccessible cliff dwellings.

CREDITS: TIM KOHLER

### Traveling in time

In addition to recreating ancient buildings and cultures, virtual archaeologists can go back in time to test hypotheses. For example, many archaeologists believe that the Inka, who fashioned a vast empire during the 15th and 16th centuries in western South America, built large stone pillars to record the sun's location on the horizon during the solstices. Researchers posited that two Inka towers on the Island of the Sun in Lake Titicaca in Bolivia served as markers of the sun's position on the winter solstice at sunset (*Science*, 9 October 1998, p. 227). But other scholars speculated instead that the towers were used as tombs.

The solstice hypothesis could be empirically tested only during sunset on or near the June solstice, and the towers are only partially preserved, making verification difficult. So Frischer and colleague Chris Johanson of the University of California, Los Angeles, devised a virtual-empirical test that eliminates the constraints of time and space. They built a 3D model of the topography of the island and the sanctuary. Using astronomical data, they reconstructed the apparent course of the sun at sunset on dates surrounding the winter solstice in the year 1500 C.E. Their model confirmed the solstice hypothesis, Frischer and Johnson wrote in a book chapter last year, by showing that the "solar pillars would have been visible to the masses of devotees standing to the south," says Frischer. "Once we have the model, we can explore at random," he says. "We can be like time travelers."

Although it can be highly effective, virtual archaeology has its problems, too. Sanders says virtual models are built on so many different software platforms that "there are no standards," which makes viewing them difficult. Given how easy it is to manipulate a virtual model, there is also the matter of trusting its accuracy. He says researchers should make sure that viewers know the evidence and assumptions behind each model.

"Virtual archaeology's number-one problem is how to collect, peer-review, and publish all the 3D digital models that scientists are making in increasing numbers each year," Frischer says. "At the moment, very few of these models, which must number over 1000 by now, are available online. Most—after having been used once for a specific purpose—are sitting in storage on old CD-ROMs and hard disks."

Frischer hopes to remedy this problem next year by launching SAVE, a peer-reviewed online journal for virtual models, though he still needs more funds for the venture. He adds that it would be highly ironic if archaeologists, charged with recording and publishing on the world's cultural heritage, left no record of their own virtual work.

**–MICHAEL BAWAYA**

Michael Bawaya is the editor of *American Archaeology*.

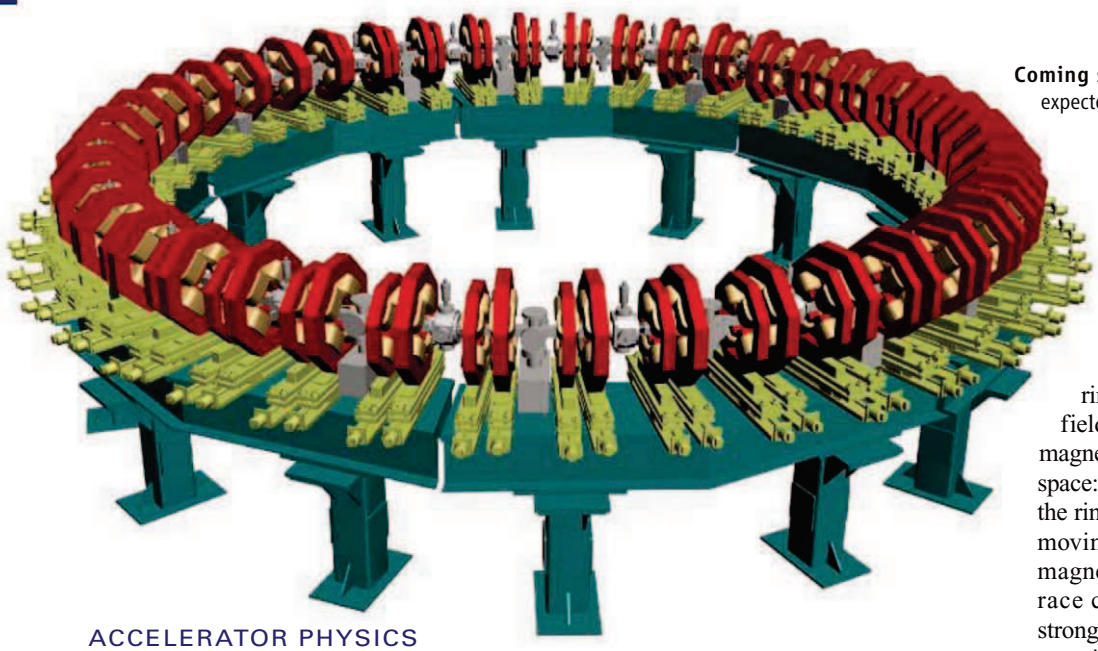

**Coming soon.** The EMMA prototype accelerator is expected to carry its first beam in March.

ACCELERATOR PHYSICS

# The Next Big Beam?

**A long-neglected accelerator technology is making a comeback bid, as its proponents point to possible applications in experimental physics, medicine, and even nuclear power**

If there's one thing you can be sure about with particle accelerators, it's that they're expensive to build. The €3 billion Large Hadron Collider at CERN is the most extreme example. But even at the other end of the scale, a hospital that wants an accelerator for proton beam therapy for cancer patients will likely have to fork out more than $100 million, and neither of the two most common existing technologies—cyclotrons and synchrotrons—is well-suited to the task. Now a handful of accelerator physicists are experimenting with a new type of machine—a cross between a cyclotron and a synchrotron—that avoids many of the shortcomings of both and is simpler and cheaper to build.

Proponents of these machines, known as fixed-field alternating-gradient (FFAG) accelerators, say they would be ideal for applications such as proton therapy, inspecting the contents of cargo containers, and accelerating muons for a muon collider or neutrino factory. FFAGs may even revive the fortunes of a novel type of nuclear reactor called an energy amplifier, which needs a particle accelerator to drive it. After a modest start in Japan about 10 years ago, the field is "kind of exploding," says Carol Johnstone of the Fermi National Accelerator Laboratory (Fermilab) in Batavia, Illinois.

Over the next few months, FFAG fans everywhere will be eagerly awaiting the first beams to whiz around the Electron Model for Many Applications (EMMA), a prototype of a variation on traditional FFAGs that promises to be even simpler and cheaper. A successful demonstration of this so-called nonscaling FFAG, which is under construction at the Daresbury Laboratory in the United Kingdom, could open the floodgates for the application of this technology. "It'll be beautiful if they work," says Roger Barlow of the University of Manchester in the United Kingdom.

FFAGs were first proposed in the 1950s, and several electron accelerators were built in the United States. But FFAGs require large, complex magnets to keep particles on track, and the technology lost out to the rival synchrotron, which emerged at about the same time. Most earlier accelerators had been cyclotrons—machines that use a fixed, uniform magnetic field to steer beams of fast-moving particles in a circle. Particles are injected into the middle of the disk-shaped device and once or more per circuit are given a "kick" with an electric field to speed them up. As they accelerate, they spiral outward until they reach the outer edge of the magnetic field and leave the machine. Hence cyclotrons can produce beams of only a single energy, which is limited by the size and strength of their magnets.

Online
**sciencemag.org**
Podcast interview with author Daniel Clery.

Synchrotrons take a different approach, using a number of variable electromagnets arranged in a ring and ramping up the magnetic fields as the speed of the particles increases. But once you start ramping up the energy, you can't inject more lower-energy particles at the same time. So synchrotrons can reach a higher energy but not a high particle current.

FFAGs marry the synchrotron's ring of magnets with the steady magnetic fields of a cyclotron. Although an FFAG's magnetic field is fixed in time, it changes in space: as you move farther from the center of the ring the field increases, preventing faster moving particles from spiraling out of the magnets, much as a banked track does for race cars. As long as the field increases strongly enough, an FFAG can achieve higher energies than a cyclotron. And with its fixed fields, you can keep injecting more low-energy particles while higher energy ones are still being accelerated, leading to a higher current than a synchrotron.

In the 1990s, with improved magnet technology and computer modeling, researchers at the KEK particle physics lab near Tokyo, led by Yoshiharu Mori, began rethinking FFAGs. In 2000 they built a proof-of-principle device with a beam energy of 1 million electronvolts, followed by a 150-MeV machine in 2003. Other researchers took note, and today another six FFAGs have been built, accelerating protons, electrons, and alpha particles. Three others are under construction, and about 20 designs are in development.

Now there are also variations on the original design. In the late 1990s, researchers in the United Kingdom and the United States began looking at an FFAG for accelerating muons, short-lived particles that need to be brought up to speed very quickly. The rapid acceleration, they figured, would also make possible a radical simplification. In a traditional FFAG magnet, the field increases by a power of the radius as you move away from the center of the ring. This formula keeps the shape of the beam path constant as the beam gains energy and moves outward—the path "scales" with the radius. This scaling suppresses resonances that can throw the beam off line. But this requires very complex magnets. The KEK machines "looked the same as the [1950s] U.S. ones, very dense with big chunky magnets," says Ken Peach, director of the John Adams Institute for Accelerator Science in the United Kingdom.

The muon collider team realized that if the beam accelerates quickly enough, the resonance wouldn't have time to build up. Hence

CREDIT: BASROC CONFORM

they could build magnets that vary linearly with radius and don't scale. Such magnets would be smaller and simpler to make. As a proof of principle, researchers in the United Kingdom and elsewhere designed an electron accelerator based on a nonscaling FFAG. By the time they finished the design in 2005, however, no money was available for their long-sought muon collider.

They had more success when they teamed up with some oncologists who saw the FFAG as an ideal machine for proton therapy. Cyclotrons are the standard machines for such treatment, but FFAGs would be cheaper. They could also easily vary the beam energy to penetrate more deeply into tissue, enabling clinicians to scan across tumors in 3D to destroy all cancer cells. "We were convinced there is a role for FFAGs in clinical oncology," says Peach.

With this real-world application in prospect, the team won £16 million from the U.K. research councils for a 4-year project known as CONFORM, which will construct EMMA, design a prototype nonscaling proton FFAG for cancer treatment, dubbed PAMELA, and look for other applications. Now well into the project's third year, four of EMMA's seven segments are complete, and researchers expect the machine to carry its first beam on 1 March. Accelerator physicists across the world have high expectations for nonscaling FFAGs, so a lot is riding on EMMA's success.

Meanwhile, work has been progressing on the design for PAMELA. PAMELA will be able to accelerate both protons and carbon ions, which some studies suggest may be even better than protons for cancer treatment. "It turned out that moving from an electron to a carbon FFAG is not so simple," says Peach. As a result, PAMELA may end up somewhere between a scaling and a nonscaling FFAG, with magnetic fields that don't vary linearly with radius but that are still simpler than in a traditional FFAG.

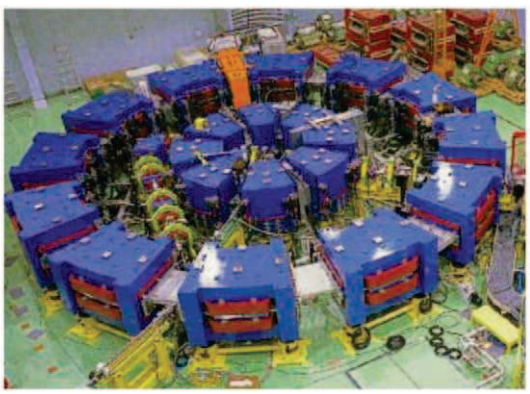

CREDITS (TOP TO BOTTOM): ADAPTED FROM M. K. CRADDOCK/UNIVERSITY OF BRITISH COLUMBIA AND TRIUMF; KEK

**Japan weighs in.** Experimental FFAG at Kyoto University is used in "energy amplifier" research.

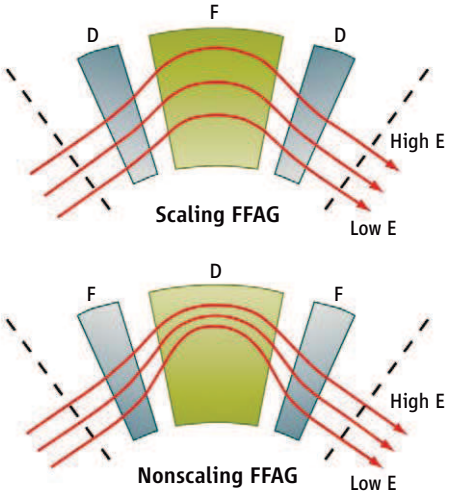


**Quick fix.** In scaling FFAGs, particles take same-shaped paths to avoid beam instabilities. Newer FFAGs accelerate particles faster than such trouble can arise.

Barlow says the United Kingdom's National Health Service is about to call for bids to build two proton-therapy centers. FFAGs won't be ready in time for those jobs, but he thinks they could form a second generation. "I'm increasingly positive about proton therapy," he says. But Johnstone cautions that medical administrators are conservative and reluctant to back new technologies. "It's hard to break into that market," she says.

Johnstone is, however, working on another application that may come to fruition sooner. In collaboration with the company Passport Systems Inc. based near Boston, she has designed ultracompact electron FFAGs whose beams will be used to generate x-rays for scanning cargo containers for explosives, nuclear materials, or other contraband. A prototype scaling FFAG has already been built, and a nonscaling version is in the cards for 2010. "There's nothing like this on the market," she says. "You can throw them in the back of a truck."

The CONFORM project has discussed a more ambitious application: the accelerator-driven subcritical reactor (ADSR), otherwise known as an energy amplifier. This technology, first proposed by Nobel physicist Carlo Rubbia in 1993, starts with a reactor containing slightly too little nuclear fuel to sustain a chain reaction. Instead, nuclear reactions are helped along by an external source of neutrons: a powerful particle accelerator that fires protons into a heavy metal target, knocking out neutrons. An ADSR would produce less high-level waste than a conventional reactor does. It is also inherently safe: Nuclear reactions can't keep going without the external neutrons, so to turn off the reactor you just turn off the beam.

The biggest question mark is the accelerator. Those built so far have been one-off research machines: too expensive, temperamental, and low-powered to keep a nuclear reactor running. The planned accelerator for the European Spallation Source will likely cost €400 million and produce a 5-megawatt (MW) beam. An ADSR would need twice that power. The CONFORM researchers realized that PAMELA's design could be adapted to meet the requirements of an ADSR. "As soon as we looked at the ADSR, it looked like a goer," says Robert Cywinski of the University of Huddersfield in the United Kingdom.

Meanwhile, Japanese researchers were already thinking along similar lines. Over the past few years, the KEK team has put together the world's first ADSR experiment. Using the Kyoto University Critical Assembly (KUCA) as their reactor, they assembled a cascade of three FFAGs boosting a proton beam first to 2.5 MeV, then to 20 MeV, and finally to 100 MeV. The researchers made KUCA subcritical by lowering control rods into the uranium core; then, on 4 March 2009, they fired neutrons into the reactor. Measurements clearly indicated that the neutron beams were triggering sustainable nuclear reactions. Mori says that FFAGs show potential for being able to drive an ADSR, but "it would be necessary to overcome many problems and difficulties, such as beam losses, operational efficiency, reliability, safety, and so on."

The U.K. researchers are taking a different tack with plans to fuel their reactor with thorium. Thorium is more abundant in the earth than uranium is, and its fuel cycle doesn't produce material that could be diverted into nuclear bombs. The team has made a case for a £300 million, partly publicly funded project to develop the ADSR technology over 5 years and is waiting for the government's response. Just over half the money will pay for a series of prototype FFAGs to demonstrate that they are powerful, reliable, and affordable enough to be practical in an ADSR. The rest of the funding will cover materials research and simulation of the proposed reactor. If that government investment is followed by up to £2 billion from industry, Cywinski says the project could produce a working 600-MW prototype by 2025. "It could create for the U.K. a new nuclear export industry. You could sell these to all those countries you can't sell conventional nuclear," says Cywinski.

Even in the early days of the FFAG's revival, researchers are thinking big. But for the moment, all eyes are on EMMA.

**–DANIEL CLERY**



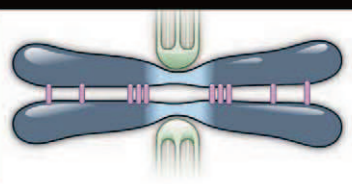



# LETTERS

*edited by Jennifer Sills*

## Editorial Expression of Concern

IN THE 9 OCTOBER 2009 ISSUE, *SCIENCE* PUBLISHED THE RESEARCH Article "Reactome array: Forging a link between metabolome and genome" by A. Beloqui *et al*. (*1*). *Science* is publishing this Editorial Expression of Concern to alert our readers to the fact that serious questions have been raised about the methods and data presented in this article. The questions focus in particular on the synthesis of the dye-labeled metabolites that are central to the microarray technique. In addition, the spectroscopic data the authors cite in support of their claim were not posted to the Bangor University School of Biological Sciences Web site at the time of publication, despite the authors' indication in the Supporting Online Material that the data would be so posted. In response to inquiries from *Science*, the authors have provided new descriptions of the synthetic methods that differ substantially from those in their published article. Based on our original concerns and the authors' response, *Science* has requested evaluation of the original data and records by officials at the authors' institutions: These officials have agreed to undertake this task.

**BRUCE ALBERTS**
Editor-in-Chief

**Reference**

1. A. Beloqui *et al*., *Science* **326**, 252 (2009).

## Financial Conflicts of Interest Worth Knowing

IN HIS LETTER "THE ANTIDOTE TO BIAS IN research" (23 October 2009, p. 522), D. B. Allison argues against the need to disclose sources of funding when publishing scientific research. He claims that "disclosure does nothing to buttress the validity of the scientific information and conclusions produced." The methods of science, Allison claims, are "the antidote to the poison of bias in research."

Allison is deeply mistaken about disclosure. As J. R. Brown (*1*) reports, when a published study "is funded by one of the pharmaceutical companies, the sponsor's drug invariably does better." Brown cites evidence from a variety of studies, including Davidson (*2*), Friedberg *et al*. (*3*), and Stelfox *et al*. (*4*). Davidson, for example, reports that "of 107 published papers that compared rival drugs, the drug produced by the sponsor of the research was found to be superior in every single case" (*1*).

Given the data reported by Brown, researchers ought to report what organizations support their research. Doing so serves the knowledge-seeking goals of science. The aim of the scientific method is to aid scientists in drawing the appropriate conclusions from the data they have gathered. The data Brown presents suggest that in order to properly assess the research results that others publish, it is essential that a researcher know who financed the research. Furthermore, not regularly disclosing such information would prevent us from developing a better understanding of how conflicts of interest affect our pursuit of scientific knowledge.

**K. BRAD WRAY**

Department of Philosophy, State University of New York, Oswego, Oswego, NY 13126, USA. E-mail: kwray@oswego.edu

**References**

1. J. R. Brown, in *The Challenges of the Social and the Pressure of Practice: Science and Values Revisited*, M. Carrier *et al*., Eds. (Univ. of Pittsburgh Press, Pittsburgh, PA, 2008).
2. R. Davidson, *J. Gen. Intern. Med*. **12**, 155 (1986).
3. M. Friedberg *et al*., *JAMA* **282**, 1453 (1999).
4. H. T. Stelfox *et al*., *N. Engl. J. Med*. **338**, 101 (1998).

## Honing the Geoengineering Strategy

IN THEIR PERSPECTIVE ("RISKS OF CLIMATE engineering," 21 August 2009, p. 955), G. C. Hegerl and S. Solomon note that geoengineering strategies intended to reduce global warming may have unintended consequences on broader climate systems (such as rainfall patterns). We are particularly concerned by geoengineering strategies that do not reduce the concentration of atmospheric $CO_2$, but rather attempt to reduce warming; such actions treat the symptoms, not the cause, and ignore potentially catastrophic effects of $CO_2$ on natural systems. For example, there is increasing evidence that ocean acidification caused by absorption of $CO_2$ may drive immense ecosystem shifts and loss in ecosystem services (*1*, *2*), yet plans to rapidly cool the atmosphere will do nothing to reduce the effects of $CO_2$ in the world's oceans.

The overwhelming danger with the discourse on geoengineering strategies centers on the false sense of security that they create. Geoengineering strategies may be useful as an interim measure to reduce the effects of atmospheric $CO_2$, but are likely to be effective only in the short term, even when combined with other actions to increase resilience in natural systems [such as removal of nutrient

### Letters to the Editor

Letters (~300 words) discuss material published in *Science* in the previous 3 months or issues of general interest. They can be submitted through the Web (www.submit2science.org) or by regular mail (1200 New York Ave., NW, Washington, DC 20005, USA). Letters are not acknowledged upon receipt, nor are authors generally consulted before publication. Whether published in full or in part, letters are subject to editing for clarity and space.

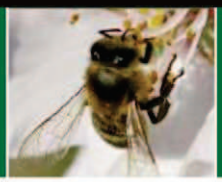

What's killing honey bees?

152

Declines of common species

154

pollution (*3*) or maintaining herbivore density (*4*)]. Ultimately, the only way to combat the plethora of changes driven by increasing atmospheric (and oceanic) $CO_2$ concentrations is to reduce our reliance on carbon-based sources of energy.

**BAYDEN D. RUSSELL* AND SEAN D. CONNELL**

Southern Seas Ecology Laboratories, School of Earth and Environmental Sciences, University of Adelaide, South Australia 5005, Australia.

*To whom correspondence should be addressed. E-mail: bayden.russell@adelaide.edu.au

**References**

1. E. S. Poloczanska *et al.*, *Oceanogr. Mar. Biol.* **45**, 407 (2007).
2. S. R. Cooley, S. C. Doney, *Environ. Res. Lett.* **4**, 024007 (2009).
3. B. D. Russell, J. I. Thompson, L. J. Falkenberg, S. D. Connell, *Glob. Change Biol.* **15**, 2153 (2009).
4. T. P. Hughes *et al.*, *Curr. Biol.* **17**, 360 (2007).

## Incentives: Encouraging Adventurous Ideas

IN HIS EDITORIAL "ON INCENTIVES FOR INNOvation" (27 November 2009, p. 1163), B. Alberts raises an important matter. Incentives for innovation have also been addressed recently by Cancer Council Victoria (CCV) through its Venture Grant Scheme (*1*). This scheme complements Australia's conventional funding programs by funding "adventurous" ideas typically lacking preliminary data.

In 2006, CCV advertised that its Venture Grants Scheme would support creative projects that could not expect funding through conventional grant schemes—high-risk, high-gain research proposals with the potential to revolutionize cancer research and treatment. Of the initial 37 applications, 5 were selected for funding. Typical budgets ranged from $450K to $600K over 3 years. The projects were diverse, including drug discovery, genomic screens for novel tumor suppressors, and synchrotron-based radiation therapy. A panel of mentors negotiated with the successful applicants to reach an agreed set of applicant-determined "milestones" for each project. Continued funding was on the basis of a review every 6 months to determine whether milestones were being achieved. As might be expected, applicants often requested reasonable adjustments to their milestones.

As a funding agency, CCV's strategy was to use these creative projects to solicit donations that they would not otherwise receive. CCV predicted that entrepreneurial supporters would accept moderate risk provided their funds were directed to high-quality innovative research. We contend that the staged release of funds according to the progress against the self-imposed "milestones" is not only sound business practice, but allows the researchers to share risk. Everyone understood that fundraising would commence after the selection process—that is, when specific projects could be offered to donors. Pleasingly, fundraising stayed ahead of projected research expenditure.

Four of five projects continue to meet their adjusted milestones, and two of the projects have already achieved longer-term funding through conventional sources. The panel of mentors has been delighted with the excellence of the science and the flexibility of the new process.

**JOSEPH A. TRAPANI,[1]* ANTONY W. BURGESS,[2] DAVID J. HILL[3]**

[1]Cancer Immunology Program, Peter MacCallum Cancer Centre, East Melbourne, Victoria 3002, Australia. [2]Epithelial Biology, Ludwig Institute for Cancer Research, Melbourne Branch, Parkville, Victoria 3050, Australia. [3]Cancer Council Victoria, Carlton, Victoria 3053, Australia.

*To whom correspondence should be addressed. E-mail: Joe.Trapani@petermac.org

**Reference**

1. Cancer Council Victoria, Biomedical Research (www.cancervic.org.au/about-our-research/biomedical_research).

## Incentives: Stimulus Missed an Opportunity

THE NEWS FOCUS STORY "SCIENCE AND THE stimulus" (J. Mervis, 27 November 2009, p. 1176) asks whether the $18 billion science stimulus is "being spent wisely." B. Alberts answers this question 13 pages earlier in the same issue ("On incentives for innovation," Editorial, p. 1163). He gently points to one of the greatest missed opportunities in U.S. science policy-making. The structure of the stimulus funds will not foster innovation; rather, it will lead to more organizations such as the National Science Foundation, National Institutes of Health, and Department of Energy, which have evolved into sturdy and steady guaranteed support of incremental science. We all support the tiny, labyrinthine, agency efforts at "transformative" research, but the Administration's plans are egregiously misapplied to science. Even block grants to states with some guidelines to emphasize innovation would have achieved more innovation, and they would have served as a useful experiment.

As the major Asian nations surpass the United States in equipment and quality, our advantage must remain the U.S. agility and daring style. The usual agency nanosteps are simply unequal to the opportunity.

I suggest two innovation incentives: (i) Require every principal investigator with tenure to spend one-third of each grant pursuing an area as far outside the funded proposal as possible, and base the renewal of the grant partly on that effort. (ii) Explicitly set aside 5% of every agency's budget for modest grants that any applicant—young or old, from academia or industry—can use to work in any area that involves genuinely new unexplained facts with the potential to be of value. This would encourage the revival of the highly successful Bell Labs motto: "applications-driven basic research."

**RUSTUM ROY**

Materials Research Institute, The Pennsylvania State University, University Park, PA 16802, USA. E-mail: rroy@psu.edu

PERFORMING ARTS

# Scientific Tide on New Wave Stages?

**Stuart Firestein**

Three new theatrical events that cropped up on New York stages late this past fall all had at least a nod to science for their themes. The Public Theater in lower Manhattan offered *Idiot Savant*, a play by avant-garde theater pioneer Richard Foreman. *Inside Out*, a circus performance, and minimalist composer Philip Glass's latest opera, *Kepler*, were presented as parts of the New Wave Festival at the Brooklyn Academy of Music. Although the plural of anecdote is not data, the three events at least suggest that science is becoming a theme of greater interest to writers, directors, and players in the performing arts.

The term "idiot savant" is no longer in scientific use, at least in part because of its pejorative nature, but its oxymoronic property still seems poetically acceptable and interesting. Foreman has been producing intensely personal theater pieces that are nonetheless riveting events for public audiences for more than 40 years. It is remarkable that someone who has passed the 70-year mark is relentlessly more avant-garde (in the literal meaning of the phrase) than many half his age who consider themselves experimental artists. That he has turned even ever-so-slightly toward science for the starting point for his latest play is perhaps an indication that art and science are not so far apart as we tend to believe. This is certainly to be welcomed, because science forms such a critical part of culture that ignoring it is, well, like being an idiot savant.

That said, Foreman's *Idiot Savant* does not so much explore the science of savantism as evoke the idea that to know is to be an idiot—at least in someone's eyes. Willem Dafoe, in what might loosely be called the lead role, is confronted with statements that seem deeply philosophical but whose meanings evaporate the moment he grasps them. The play is perhaps best characterized as a metaphysical comedy: In one of many bizarre scenes, Giant Duck, a puppet character, plays a game of interspecies golf; in another, the poor savant is trailed around the stage by "butlers" who are aiming bows and arrows at his head while he tries to utter sensible phrases (I thought, "They could be reviewers"). *Idiot Savant* is not about science nor does it really use science. It does, however, somehow brush up against science by wondering deeply about knowing and knowledge.

**Idiot Savant.** Elina Lowensohn, Willem Dafoe, Alenka Kraigher, and the company.

**Idiot Savant**

***written and directed by Richard Foreman***

Public Theater, New York.
27 October–20 December 2009.
www.publictheater.org

*Inside Out*, by Cirkus Cirkör, is the literal as well as figurative title of a circus event that attempts to bring the inside of you to the outside. Using the notion that the circus is a means of facing and superceding fears of the physical kind (heights, falls, dangerous animals, and other risky acts of bravura), the performance asks whether we can face down our inner fears, those that have to do with death, meaning, love, and personal identity—pretty heavy going for a circus. In spite of that, the night remains a brilliant spectacle of high and low comedy, a kind of intellectual acrobatics to go with the physical feats that challenge belief.

A comparison with Cirque du Soleil seems almost inescapable, but that would not be fair. Cirkus Cirkör is circus with intellect. Its performance is funny (and occasionally dumb), has a brilliant clown who also serves as a sort of master of ceremonies, and, although lacking a real narrative like one would find in a play, moves through a series of scenes in which the heart is explored—literally. A huge red shiny set piece with valves, arteries, and chambers is tugged about by the central character, a woman named Stephanie, who seems at first to have been plucked from the audience. This heart also serves as a springboard for all sorts of remarkable acrobatics, dances, and illusions. For most of the performance, it sits out on the stage, waiting to be investigated, dissected, and diagnosed.

One of the acrobats performs a wonderful routine with a large metal hoop, a few inches taller than him, which he controls with perfect movements. He spins in unimaginable ways while caught inside this hoop like a three-dimensional kinetic version of Leonardo da Vinci's famous anatomical human in a circle. There are in fact anatomical graphics in the style of da Vinci spread across the backdrop and the floor of the stage.

The troupe makes their home in Stockholm, and director Tilde Björfors gives credit to friends and mentors at the Karolinska Institutet for consulting on the science and even for opening them up to scientific ideas. Once again, there isn't really that much science in the show. But then again, when have you ever seen a circus that has gigantic red blood cells rolling around the stage? Or an acrobatic number that uses an elastic replica of the neurons and connections in a brain that stretches from floor to ceiling and across the entire stage—making neural plasticity (elasticity might be an even better description) as literal as I've ever seen it portrayed? In addition, the "dub-punk-new wave-electro-inspired" band even uses a theremin to produce all those eerie sounds that you may remember from 1950s science fiction movies with social themes.

On the whole, *Inside Out* may involve as much physics as biology, but it is intuitive physics, the kind practiced by acrobats and high-wire performers who know more about gravity than any of us mere mortals. Indeed, for amazing moments gravity seems to just disappear from the stage. This all reminded me of a story about Richard Feynman, a consummate educator and showman, from his legendary Introduction to Physics course at Caltech. For the first class, held in a large lecture hall, he had a heavy bowling ball suspended by a wire from the ceiling in the center of the room. To begin the lecture he held the ball right up to his face and then let it go. It sailed across the room, over the heads of the enraptured students, reached the end of its arc, and began speeding back toward Feynman's head. Feynman didn't budge as the ball came to within the predicted millimeter or so

Department of Biological Sciences, Columbia University, New York, NY 10027, USA. E-mail: sjf24@columbia.edu

CREDIT: JOAN MARCUS/COURTESY THE PUBLIC THEATER

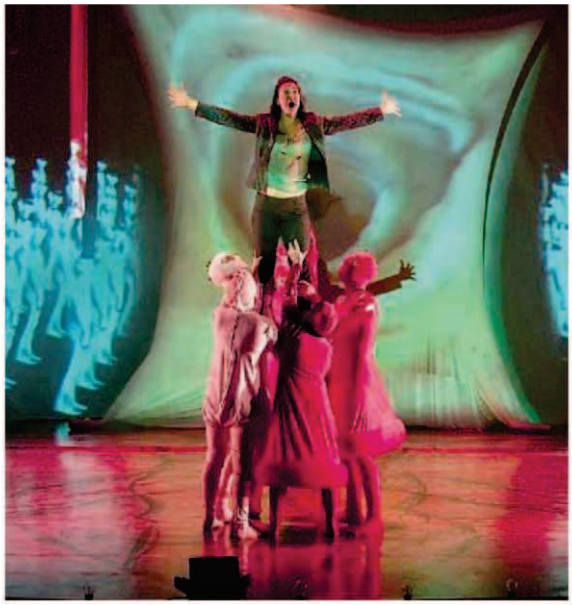

**Inside Out.** Stephanie is about to begin her journey to the Inside, through that giant blood vessel at the back of the stage.

**Inside Out**

***Cirkus Cirkör***
***Music by Irya's Playground***
***Tilde Björfors, director***

Brooklyn Academy of Music, New York. 12–15 November 2009. Next Wave Festival. www.bam.org/view.aspx?pid=1269

of the tip of his nose before receding away in its pendulum swing. Feynman never flinched, saying, "If we want them to listen to us, we have to show them that we believe in this stuff." Cirkus Cirkör believes.

We can look forward to more science in the circus's future shows. Director Björfors has told me that this is an area the group has become deeply interested in as a source for inspiration.

Unquestionably, though, the most successful of the trio of pieces is the concert staging of Glass's *Kepler*. The work was commissioned by the Upper Austrian State Theatre of Linz, the city where Kepler lived and worked from 1612 to 1627. Its premier in 2009 was quite appropriate, as the International Year of Astronomy marked (among other things) the 400th anniversary of the publication of Kepler's *Astronomia Nova* (in which he presented his laws of planetary motion). As the first bars of the opera are taken up by the Bruckner Orchester Linz, one senses—from the repetitive but exhilarating chords that echo from the strings to the brass to the percussion to gorgeous choral voices—that something big is afoot, that big ideas are on their way. Martina Winkel's libretto, pieced together from various texts in Latin and German (and presented through projected English translations), begins with the epitaph Kepler wrote for his own grave—"I measured the skies, now the shadows I measure"—and goes on to explore his astronomical and philosophical meditations.

At one point, I thought to myself, wouldn't it be wonderful to have a score for my next seminar? Wouldn't music help get my points across? In some ways, it seems ironic that science, the very icon of modernity, should find such persuasive expression in a form as traditional as opera. But it is the combination of orchestral music, drama, the human voice, and a poetic libretto that provides the heft to explore the big questions in science. Glass and Winkel take full advantage of the opportunity. Where else might you hear a libretto graced with words such as "icosahedron" and with musical phrases that make the overworked idea of the "music of the spheres" really become the music of the spheres? Kepler himself wrote that the "heavenly motions are nothing but a continuous song for several voices" (*1*).

Although it is not quite equations that are being sung, the interplay between the musical and poetic statements summons Kepler's evolving belief that the universe and its mysteries are to be understood by measuring and counting and calculating. The connections between music and mathematics have been frequently remarked upon, and music's relations to space and the cosmos popularly realized through works by composers such as John Williams and the pairing of vintage Carl Sagan descriptions of the boundless universe with grand Bach concertos on numerous television shows. But Glass goes further. His score explores the confusion of Kepler's mind as Kepler works out the mathematics of the Copernican model, and it takes wing as we share the exhilaration of the great astronomer's sudden perception of the heavens as mathematically precise and comprehendible. The music helps us to inhabit the medieval mind looking into the heavens and seeing the discordance of stability and chaos, divinity and mystery, puzzles and solutions, meaning and void. No wonder that 17th-century philosophy was still a blend of empiricism and deism. And then we ponder, how much are we still in the dark? Will there be, for example, an opera about dark matter in 100 years that portrays our myopic 21st-century views?

**Kepler**

***Philip Glass, composer***
***Libretto by Martina Winkel***

Brooklyn Academy of Music, New York. 18–21 November 2009. Next Wave Festival. www.bam.org/view.aspx?pid=1271

One crucial and contemporary theme in the opera is the tension between science and religion. Kepler was a religious man, but he never felt that his science was in any way heretical. In a particularly telling moment in the libretto, Kepler takes his contemporary churchmen to task for what he sees as their debasing the Bible by taking it as a literal text. For him, there was no split between religion and science except the one created by the foolish—he would even say blasphemous—reading of the Bible as a literal tract, as a book of optics and astronomy when it is really about meaning and life. The stakes may be higher today—although at least we don't burn people at the stake, a threat that hung constantly over Kepler's head—but much of the friction between religion and science we see today stems indeed from literalist readings of the Bible that cannot be reconciled with science. A dose of Kepler may be needed. Was he perhaps correct that literal interpretations of the Bible debase it and that those who insist on doing so are the blasphemers?

**Kepler.** The Bruckner Orchester Linz and a chorus drawn from the Upper Austrian State Theatre, under the direction of conductor Dennis Russell Davies.

*Kepler* does not end in musical triumph, but with a whispered chord on the cello followed by a blackout. That exquisite moment serves as a perfect metaphor for science, then and now. Much has been discovered; more remains to be understood. Science can certainly use a metaphor or two that connect with the public, and it is heartening to see the likes of Philip Glass turning to science for inspiration.

**References and Notes**

1. This quote appears in Kate Daloz's informative program notes, which were funded by the Sloan Foundation's program for arts and science.

10.1126/science.1186012

SCIENCE AND REGULATION

# Mountaintop Mining Consequences

Damage to ecosystems and threats to human health and the lack of effective mitigation require new approaches to mining regulation.

M. A. Palmer,[1,2] E. S. Bernhardt,[3] W. H. Schlesinger,[4] K. N. Eshleman,[1] E. Foufoula-Georgiou,[5] M. S. Hendryx,[6] A. D. Lemly,[7] G. E. Likens,[4] O. L. Loucks,[8] M. E. Power,[9] P. S. White,[10] P. R. Wilcock[11]

There has been a global, 30-year increase in surface mining (*1*), which is now the dominant driver of land-use change in the central Appalachian ecoregion of the United States (*2*). One major form of such mining, mountaintop mining with valley fills (MTM/VF) (*3*), is widespread throughout eastern Kentucky, West Virginia (WV), and southwestern Virginia. Upper elevation forests are cleared and stripped of topsoil, and explosives are used to break up rocks to access buried coal (fig. S1). Excess rock (mine "spoil") is pushed into adjacent valleys, where it buries existing streams.

Despite much debate in the United States (*4*), surprisingly little attention has been given to the growing scientific evidence of the negative impacts of MTM/VF. Our analyses of current peer-reviewed studies and of new water-quality data from WV streams revealed serious environmental impacts that mitigation practices cannot successfully address. Published studies also show a high potential for human health impacts.

### Ecological Losses, Downstream Impacts

The extensive tracts of deciduous forests destroyed by MTM/VF support some of the highest biodiversity in North America, including several endangered species. Burial of headwater streams by valley fills causes permanent loss of ecosystems that play critical roles in ecological processes such as nutrient cycling and production of organic matter for downstream food webs; these small Appalachian streams also support abundant aquatic organisms, including many endemic species (*5*). Many studies show that when more than 5 to 10% of a watershed's area is affected by anthropogenic activities, stream biodiversity and water quality suffer (*6*, *7*). Multiple watersheds in WV already have more than 10% of their total area disturbed by surface mining (table S1).

Hydrologic flow paths in Appalachian forests are predominantly through permeable soil layers. However, in mined sites, removal of vegetation, alterations in topography, loss of topsoil, and soil compaction from use of heavy machinery reduce infiltration capacity and promote runoff by overland flow (*8*). This leads to greater storm runoff and increased frequency and magnitude of downstream flooding (*9*, *10*).

Water emerges from the base of valley fills containing a variety of solutes toxic or damaging to biota (*11*). Declines in stream biodiversity have been linked to the level of mining disturbance in WV watersheds (*12*). Below valley fills in the central Appalachians, streams are characterized by increases in pH, electrical conductivity, and total dissolved solids due to elevated concentrations of sulfate ($SO_4$), calcium, magnesium, and bicarbonate ions (*13*). The ions are released as coal-generated sulfuric acid weathers carbonate rocks. Stream water $SO_4$ concentrations are closely linked to the extent of mining in these watersheds (*11*, *14*). We found that significant linear increases in the concentrations of metals, as well as decreases in multiple measures of biological health, were associated with increases in stream water $SO_4$ in streams below mined sites (see the chart on page 149). Recovery of biodiversity in mining waste-impacted streams has not been documented, and $SO_4$ pollution is known to persist long after mining ceases (*14*).

Conductivity, and concentrations of $SO_4$ and other pollutants associated with mine runoff, can directly cause environmental degradation, including disruption of water and ion balance in aquatic biota (*12*). Elevated $SO_4$ can exacerbate nutrient pollution of downstream rivers and reservoirs by increasing nitrogen and phosphorus availability through internal eutrophication (*15*, *16*). Elevated $SO_4$ can also increase microbial production of hydrogen sulfide, a toxin for many aquatic plants and organisms (*17*). Mn, Fe, Al, and Se can become further concentrated in stream sediments, and Se bioaccumulates in organisms (*11*) (figs. S1 and S2).

A survey of 78 MTM/VF streams found that 73 had Se water concentrations greater than the 2.0 μg/liter threshold for toxic bioaccumulation (*18*). Se levels exceed this in many WV streams (see the chart on page 149). In some freshwater food webs, Se has bioaccumulated to four times the toxic level; this can cause teratogenic deformities in larval fish (fig. S2) (*19*), leave fish with Se concentrations above the threshold for reproductive failure (4 ppm), and expose birds to reproductive failure when they eat fish with Se >7 ppm (*19*, *20*). Biota may be exposed to concentrations higher than in the water since many feed on streambed algae that can bioconcentrate Se as much as 800 to 2000 times that in water concentrations (*21*).

### Potential for Human Health Impacts

Even after mine-site reclamation (attempts to return a site to premined conditions), groundwater samples from domestic supply wells have higher levels of mine-derived chemical constituents than well water from unmined areas (*22*). Human health impacts may come from contact with streams or exposure to airborne toxins and dust. State advisories are in effect for excessive human consumption of Se in fish from MTM/VF affected waters. Elevated levels of airborne, hazardous dust have been documented around surface mining operations (*23*). Adult hospitalizations for chronic pulmonary disorders and hypertension are elevated as a function of county-level coal production, as are rates of mortality; lung cancer; and chronic heart, lung, and kidney disease (*24*). Health problems are for women and men, so effects are not simply a result of direct occupational exposure of predominantly male coal miners (*24*).

### Mitigation Effects

Reclamation of MTM/VF sites historically has involved planting a few grass and herb species (*20*, *25*). Compared with unmined

CREDIT: VIVIAN STOCKMAN

[1]University of Maryland Center for Environmental Science, Cambridge, MD 21613, USA. [2]University of Maryland, College Park, MD 20742, USA. [3]Duke University, Durham, NC 27708, USA. [4]Cary Institute of Ecosystem Studies, Millbrook, NY 12545, USA. [5]University of Minnesota, Minneapolis, MN 55414, USA. [6]West Virginia University, Morgantown, WV 26506, USA. [7]Wake Forest University, Winston-Salem, NC 27109, USA. [8]Miami University, Oxford, OH 45056, USA. [9]University of California at Berkeley, Berkeley, CA 94720, USA. [10]University of North Carolina at Chapel Hill, Chapel Hill, NC 27599, USA. [11]Johns Hopkins University, Baltimore, MD 21218, USA.

*Author for correspondence. E-mail: mpalmer@umd.edu

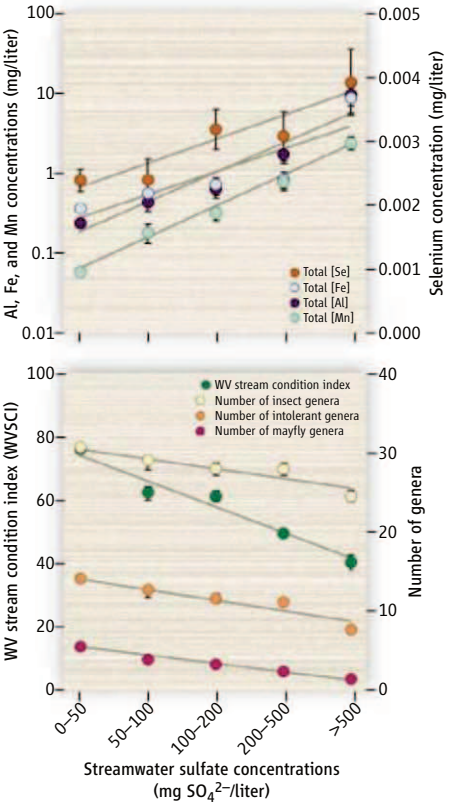


**Mining effects on stream chemistry and biota.** Sulfate concentrations reflect amount of mining in watershed. (**Top**) Average concentrations of manganese, iron, aluminum, and selenium. (**Bottom**) Stream invertebrate community metrics in relation to sulfate concentrations for 1058 WV streams (methods in table S2). Regressions all statistically significant (table S3).

sites, reclaimed soils characteristically have higher bulk density, lower organic content, low water-infiltration rates, and low nutrient content (*8*, *25*). Many reclaimed areas show little or no regrowth of woody vegetation and minimal carbon (C) storage even after 15 years (*26*). Decreased forest productivity may be related to the type of surface material (e.g., brown versus gray sandstone) used in the reclamation (*27*). In reclaimed forests, projected C sequestration after 60 years is only about 77% of that in undisturbed vegetation in the same region (*28*). Mined areas planted to grassland sequester much less. Since reclamation areas encompass >15% of the land surface in some regions (*29*) (table S1), significant potential for terrestrial C storage is lost.

Mitigation plans generally propose creation of intermittently flowing streams on mining sites and enhancement of streams offsite. Stream creation typically involves building channels with morphologies similar to unaffected streams; however, because they are on or near valley fills, the surrounding topography, vegetation, soils, hydrology, and water chemistry are fundamentally altered from the premining state. U.S. rules have considered stream creation a valid form of mitigation while acknowledging the lack of science documenting its efficacy (*30*). Senior officials of the U.S. Army Corps of Engineers (ACOE) have testified that they do not know of a successful stream creation project in conjunction with MTM/VF (*31*).

### A Failure of Policy and Enforcement

The U.S. Clean Water Act and its implementing regulations state that burying streams with materials discharged from mining should be avoided. Mitigation must render nonsignificant the impacts that mining activities have on the structure and function of aquatic ecosystems. The Surface Mining Control and Reclamation Act imposes requirements to minimize impacts on the land and on natural channels, such as requiring that water discharged from mines will not degrade stream water quality below established standards.

Yet mine-related contaminants persist in streams well below valley fills, forests are destroyed, headwater streams are lost, and biodiversity is reduced; all of these demonstrate that MTM/VF causes significant environmental damage despite regulatory requirements to minimize impacts. Current mitigation strategies are meant to compensate for lost stream habitat and functions but do not; water-quality degradation caused by mining activities is neither prevented nor corrected during reclamation or mitigation.

Clearly, current attempts to regulate MTM/VF practices are inadequate. Mining permits are being issued despite the preponderance of scientific evidence that impacts are pervasive and irreversible and that mitigation cannot compensate for losses. Considering environmental impacts of MTM/VF, in combination with evidence that the health of people living in surface-mining regions of the central Appalachians is compromised by mining activities, we conclude that MTM/VF permits should not be granted unless new methods can be subjected to rigorous peer review and shown to remedy these problems. Regulators should no longer ignore rigorous science. The United States should take leadership on these issues, particularly since surface mining in many developing countries is expected to grow extensively (*32*).

### References and Notes


1. World Coal Institute, www.worldcoal.org.
2. K. L. Saylor, *Land Cover Trends: Central Appalachians* [U.S. Department of the Interior, U.S. Geological Survey (USGS), Washington, DC, 2008]; http://landcovertrends.usgs.gov/east/eco69Report.html.
3. MTM/VF refers to surface mining operations that remove coal seams running through a mountain, ridge, or hill; it may also refer more broadly to large-scale surface mining, including area or contour mining in steep terrain that disposes of excess rock in heads of hollows or valleys with streams.
4. Debates are conspicuous because of recent high-profile federal court cases [e.g., (*33*)], widely publicized exchanges between the U.S. Environmental Protection Agency (EPA) and the ACOE over permitting decisions, advocacy by nongovernmental organizations, and protests by miners.
5. J. L. Meyer *et al.*, *J. Am. Water Resour. Assoc.* **43**, 86 (2007).
6. J. D. Allan, *Annu. Rev. Ecol. Evol. Syst.* **35**, 257 (2004).
7. This 5 to 10% issue is based on studies done on many nonmining types of land-use change. Thus far, EPA has not done mining-specific studies on this "threshold" issue (percentage of watershed mined versus impacts on streams) despite many calls for such data.
8. T. L. Negley, K. N. Eshleman, *Hydrol. Process.* **20**, 3467 (2006).
9. B. C. McCormick, K. N. Eshleman, J. L. Griffith, P. A. Townsend, *Water Resour. Res.* **45**, W08401 (2009).
10. J. R. Ferrari, T. R. Lookingbill, B. McCormick, P. A. Townsend, K. N. Eshleman, *Water Resour. Res.* **45**, W04407 (2009).
11. K. S. Paybins *et al.*, *USGS Circular* 1204 (2000); http://pubs.water.usgs.gov/circ1204/.
12. G. J. Pond, M. E. Passmore, F. A. Borsuk, L. Reynolds, C. J. Rose, *J. N. Am. Benthol. Soc.* **27**, 717 (2008).
13. K. J. Hartman *et al.*, *Hydrobiologia* **532**, 91 (2005).
14. J. I. Sams, K. M. Beer, *USGS Water Res. Report* 99-4208 (2000); http://pa.water.usgs.gov/reports/wrir_99-4208.pdf.
15. N. F. Caraco, J. J. Cole, G. E. Likens, *Nature* **341**, 316 (1989).
16. S. B. Joye, J. T. Hollibaugh, *Science* **270**, 623 (1995).
17. M. E. van der Welle, J. G. Roelofs, L. P. Lamers, *Sci. Total Environ.* **406**, 426 (2008).
18. EPA, *Stream Chemistry Report*, part 2 (EPA Region 3, Philadelphia, PA, 2002); http://www.epa.gov/region3/mtntop/pdf/appendices/d/stream-chemistry/MTMVFChemistryPart2.pdf.
19. A. D. Lemly, *Selenium Assessment in Aquatic Ecosystems: A Guide for Hazard Evaluation and Water Quality Criteria* (Springer, New York, 2002).
20. EPA, *Mountaintop Mining/VF Final Programmatic Environmental Impact Statement* (EPA Region 3, Philadelphia, PA, 2005); http://www.epa.gov/region3/mtntop/index.htm.
21. J. M. Conley, D. H. Funk, D. B. Buchwalter, *Environ. Sci. Technol.* **43**, 7952 (2009).
22. S. McAuley, M. D. Kozar, *USGS Report* 5059 (2006); http://pubs.usgs.gov/sir/2006/5059/pdf/sir2006-5059.pdf.
23. M. K. Ghose, S. R. Majee, *Environ. Monit. Assess.* **130**, 17 (2007).
24. M. Hendryx, M. M. Ahern, *Public Health Rep.* **124**, 541 (2009).
25. Mining industry and government organizations recently signed a statement of intent to promote reforestation approaches that improve reclamation [see, e.g., (*34*)]; however, adoption of recommendations is voluntary. Reforestation of a mined site to premined conditions has not been demonstrated.
26. J. A. Simmons *et al.*, *Ecol. Appl.* **18**, 104 (2008).
27. P. Emerson, J. Skousen, P. Ziemkiewicz, *J. Environ. Qual.* **38**, 1821 (2009).
28. B. Y. Amichev, A. J. Burger, J. A. Rodrigue, *For. Ecol. Manage.* **256**, 1949 (2008).
29. P. A. Townsend *et al.*, *Remote Sens. Environ.* **113**, 62 (2009).
30. EPA and ACOE, *Fed. Regist.* **73**, 10 (2008).
31. U.S. District Court, Civil Action No. 3:05-0784, transcript, vol. 3, pp. 34–45; http://palmerlab.umd.edu/MTM/US_District_Court_Civil_Action_Official_transcript_Volume_III.pdf.
32. A. P. Chikkatur, A. D. Sagar, T. L. Sankar, *Energy* **34**, 942 (2009).
33. U.S. Court of Appeals for the 4th District, *Ohio Valley Environmental Coalition* et al. vs. *U.S. ACOE* et al., case 07-1255.
34. Appalachian Regional Reforestation Initiative, www.arri.osmre.gov/FRApproach.shtm.
35. This is contribution no. 4368 of the University of Maryland Center for Environmental Science.


### Supporting Online Material

www.sciencemag.org/cgi/content/full/327/5962/148/DC1

10.1126/science.1180543

MOLECULAR BIOLOGY

# Directing the Centromere Guardian

Histone phosphorylation controls the chromosomal localization of a protein family that functions in chromosome segregation during cell division.

**Jean-Paul Javerzat**

Accurate chromosome segregation during eukaryotic cell division requires the timely release of cohesion between duplicated chromosomes so that they may separate into two daughter cells. Errors in this process have been linked to cancer progression, infertility, and debilitating genetic diseases such as Down syndrome. A surveillance mechanism known as the spindle assembly checkpoint delays this release until all chromosome pairs are properly attached to a structure called the mitotic spindle. The enzyme Bub1 is essential for this checkpoint, but the targets of its phosphorylation activity have been elusive. On page 172 of this issue, Kawashima *et al*. (*1*) report that histone H2A—a protein associated with DNA within chromosomes—is a substrate of Bub1, and that H2A phosphorylation directs subsequent events that control chromatid cohesion and the checkpoint mechanism during the early stages of cell division.

After DNA replication in the S phase of the cell division cycle, the mitotic spindle must know which chromosomes are duplicates so as to segregate them from each other. The linkage of duplicated chromosomes by the protein complex cohesin enables this to occur by creating physically associated pairs. These chromosome pairs (called sister chromatids) attach to microtubules of the mitotic spindle through a kinetochore protein complex that forms on the centromeric region of each chromosome (see the figure). When all chromosome pairs are attached, cohesin is cleaved by the enzyme separase, and sister chromatids move to opposite spindle poles. The spindle assembly checkpoint keeps separase inactive until all chromosomes are attached and properly (bidirectionally) oriented on the spindle (*2*). Here again, cohesion plays a fundamental role. By resisting the pulling forces exerted by spindle microtubules, cohesion generates tension when sister chromatids are properly attached; faulty attachments fail to do so and are actively dismantled.

As expected from its crucial function, cohesion is tightly regulated. A protein family called shugoshin (which means "guardian spirit" in Japanese) plays a central role in this process. Shugoshin was first identified as a protector of cohesion at centromeres during meiosis (the cell division process that produces gametes) (*3*–*6*). During the first meiotic division, the cohesin complex is cleaved and released from chromosomes except for at centromeres, where it is protected by shugoshin, which is associated with the phosphatase PP2A (*7*, *8*). This spared cohesion at centromeres ensures sister chromatid segregation during the second meiotic division. A shugoshin-PP2A complex also functions in vertebrate somatic cells, in which the bulk of cohesin is removed during the initial phase of cell division (prophase), but does not require cleavage. A small amount of cohesin complex is protected by shugoshin at centromeres to ensure sister chromatid cohesion and bidirectional attachment to the mitotic spindle (*9*–*11*). Shugoshin also contributes to the recruitment of the enzyme Aurora B, which promotes bidirectional chromosome attachment by dismantling those that fail to produce tension. (*12*–*14*). Most organisms have two shugoshin members, although the fly *Drosophila melanogaster* and budding yeast have only one. In fission yeast, the model organism used by Kawashima *et al*., the shugoshin protein Sgo1 protects cohesion during meiosis, whereas Sgo2 functions in the sensing of tension-less kinetochores.

How are shugoshins recruited to centromeres? The first hint came from discovering that, during meiosis, the spindle assembly checkpoint component Bub1 is required for protecting centromere cohesion in fission yeast (*15*) and that the phosphorylation activity of Bub1 is necessary for the centromeric localization of shugoshin during meiosis and mitosis (*4*, *9*, *12*, *16*). Additionally, Bub1-dependent centromeric localization of shugoshin contributes to Aurora B recruitment and the sensing of tension-less kinetochores (*12*–*14*).

Kawashima *et al*. found that Bub1 phosphorylates a conserved serine residue at posi-

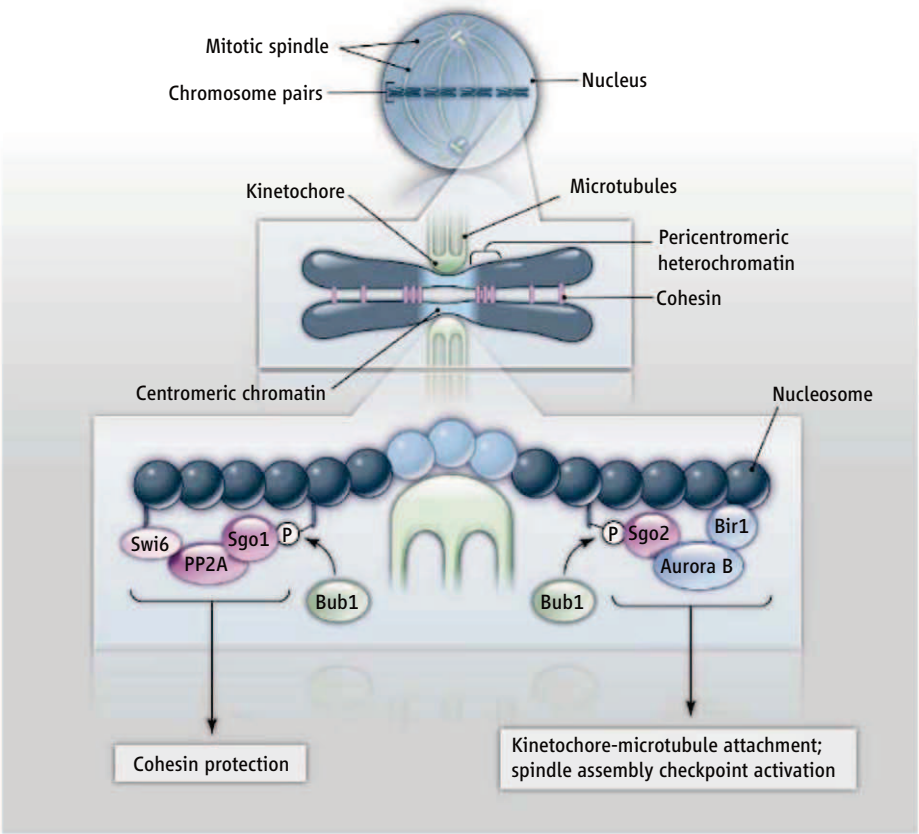


**Directing shugoshins.** Phosphorylation of the nucleosome protein H2A by Bub1 creates a binding site for shugoshin proteins (Sgo1 and Sgo2 in fission yeast). Sgo1 prevents cohesin removal from the centromere in meiosis I whereas Sgo2 recruits Aurora B to monitor proper chromosome attachment to the spindle.

CREDIT: Y. GREENMAN/*SCIENCE*

Institut de Biochimie et Génétique Cellulaires, Université Victor Segalen Bordeaux2/CNRS UMR5095, Bordeaux, 33077 France. E-mail: Jpaul.Javerzat@ibgc.u-bordeaux2.fr

tion 121 of histone H2A in fission yeast. The authors demonstrate that this single phosphorylation event is required for the correct localization and function of Sgo1 and Sgo2 and show that this pathway is conserved from yeast to human.

However, Bub1-mediated phosphorylation of H2A is not the sole molecular determinant of shugoshin localization. In fission yeast, H2A is extensively phosphorylated in a Bub1-dependent manner along chromosome arms and centromeres during interphase of the cell cycle. Yet Sgo2 specifically locates near the ends of chromosomes at this stage, suggesting that additional factors contribute to Sgo2 positioning. During mitosis, H2A phosphorylation is selectively eliminated from the bulk of chromatin but retained at the centromere, where Sgo2 relocation requires Bir1 (a subunit of a protein complex that includes Aurora B). Likewise, in meiosis, Sgo1 is found within the pericentromeric domains and its localization requires the heterochromatin protein Swi6 (*17*). It is therefore a combination of chromatin "marks" that guides shugoshin localization, and phosphorylated H2A is the prerequisite and the common denominator (see the figure).

The identification of Bub1's key substrate raises questions about the roles and regulation of H2A phosphorylation. How is this modification controlled in space and time? The extended pattern of H2A phosphorylation along a chromosome during interphase indicates that targeted dephosphorylation may be instrumental in restraining the histone modification to centromeres as the cell prepares to divide. Is the phosphorylation of H2A specifically at centromeres coupled to the spindle assembly checkpoint? Indeed, it is striking that a component of the checkpoint system tells shugoshin where to go. Upon checkpoint activation at the beginning of every cell division cycle, Bub1 accumulation at kinetochores might increase local H2A phosphorylation and promote the delivery of shugoshin to the right place at the right time. There is, however, no evidence for such a mechanism. Instead, Bub1 at the kinetochore might not be relevant because H2A-dependent recruitment of shugoshin takes place within pericentromeric heterochromatin, not at the kinetochore. Finally, H2A phosphorylation during interphase and the sensitivity of *bub1* fission yeast mutants to a DNA damaging agent suggest that Bub1 might have other chromosomal functions that have yet to be identified.

**References**


1. S. A. Kawashima, Y. Yamagishi, T. Honda, K.-i. Ishiguro, Y. Watanabe, *Science* **327**, 172 (2010); published online 19 November 2009 (10.1126/science.1180189).
2. S. Santaguida, A. Musacchio, *EMBO J.* **28**, 2511 (2009).
3. V. L. Katis, M. Galova, K. P. Rabitsch, J. Gregan, K. Nasmyth, *Curr. Biol.* **14**, 560 (2004).
4. T. S. Kitajima, S. A. Kawashima, Y. Watanabe, *Nature* **427**, 510 (2004).
5. A. L. Marston, W. H. Tham, H. Shah, A. Amon, *Science* **303**, 1367 (2004).
6. K. P. Rabitsch *et al.*, *Curr. Biol.* **14**, 287 (2004).
7. T. S. Kitajima *et al.*, *Nature* **441**, 46 (2006).
8. C. G. Riedel *et al.*, *Nature* **441**, 53 (2006).
9. T. S. Kitajima, S. Hauf, M. Ohsugi, T. Yamamoto, Y. Watanabe, *Curr. Biol.* **15**, 353 (2005).
10. B. E. McGuinness, T. Hirota, N. R. Kudo, J. M. Peters, K. Nasmyth, *PLoS Biol.* **3**, e86 (2005).
11. A. Salic, J. C. Waters, T. J. Mitchison, *Cell* **118**, 567 (2004).
12. Y. Boyarchuk, A. Salic, M. Dasso, A. Arnaoutov, *J. Cell Biol.* **176**, 919 (2007).
13. S. A. Kawashima *et al.*, *Genes Dev.* **21**, 420 (2007).
14. V. Vanoosthuyse, S. Prykhozhij, K. G. Hardwick, *Mol. Biol. Cell* **18**, 1657 (2007).
15. P. Bernard, J. F. Maure, J. P. Javerzat, *Nat. Cell Biol.* **3**, 522 (2001).
16. Z. Tang, Y. Sun, S. E. Harley, H. Zou, H. Yu, *Proc. Natl. Acad. Sci. U.S.A.* **101**, 18012 (2004).
17. Y. Yamagishi, T. Sakuno, M. Shimura, Y. Watanabe, *Nature* **455**, 251 (2008).


10.1126/science.1184770

GEOCHEMISTRY

# Deep Mantle Properties

**Kei Hirose**

High-temperature, high-pressure measurements combined with observation and calculations are providing a better picture of Earth's lower mantle.

The lower mantle extends from 660 to 2890 km below the surface of the Earth. The rocks and minerals of the deep mantle are not accessible in nature, except those occurring infrequently as inclusions in diamond. However, they can be synthesized and examined at the relevant high pressure and temperature conditions in the laboratory. Recent such experimental investigations, as well as theoretical calculations, have suggested that the properties of lower-mantle minerals vary with increasing depth much more than was previously thought. On page 193 of this issue, Irifune *et al.* (*1*) report that iron (Fe) partitioning between the two main lower-mantle constituents, iron–magnesium silicate perovskite (Pv) and iron–magnesium oxide (ferropericlase, Fp), indeed changes in a natural mantle composition for conditions corresponding to depths below 1100 km. The results have profound implications for predicting the properties and dynamics of the deep mantle.

Pyrolite is a model bulk mantle composition, close to that of undifferentiated rock found in the uppermost mantle. Irifune *et al.* carried out high-pressure experiments on such pyrolitic mantle material and found Fe enrichment in Fp at the expense of Fe in Pv. This can be attributed to a high-spin to low-spin transition of Fe in Fp (*2*). Because high pressure favors Fe in a low-spin state with smaller ionic radius, Fe partitions into low-spin Fp relative to high-spin Pv. Previous x-ray emission measurements (*3*) and theoretical calculations (*4*) suggested a broad transition (over ~1000 km thickness) in Fp at plausible lower-mantle temperatures (2000 to 2500 K). In contrast, Irifune *et al.* found that Fe partitioning changed over a much narrower pressure (depth) range (~150 km thickness). The spin transition has been demonstrated to occur also in Pv (*5*), but the pressure range of transition remains controversial (*6*). A signal of spin transition in Pv was not found in their experimental data (*1*).

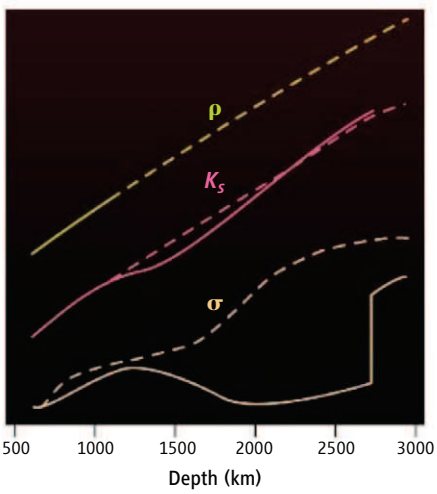


**Properties of Earth's lower mantle.** Measured or calculated profiles for "pyrolite" in the lower mantle (solid lines) (*1*, *9*, *10*) in comparison with geophysical observations (broken lines) (*7*, *11*). ρ, density; $K_s$, adiabatic bulk modulus; σ, electrical conductivity.

Department of Earth and Planetary Sciences, Tokyo Institute of Technology, Meguro, Tokyo 152-8551, Japan. E-mail: kei@geo.titech.ac.jp

Although such abrupt change in Fe distribution makes Fp and Pv denser and lighter, respectively, Irifune *et al*. found no anomaly in the net density of pyrolite. Indeed, the experimentally measured density of pyrolite matches the lower-mantle density profile deduced from seismology (*7*), thus supporting this traditional mantle composition model. On the other hand, the spin transition is known to strongly diminish the bulk modulus (incompressibility) and the electrical conductivity of pyrolite. Both experiment and theory have suggested an appreciable softening of the bulk modulus of Fp over the pressure range of spin transition (~4% reduction as pyrolite) (*8*, *9*) (see the figure). Such an anomaly is not found in the lower-mantle profile of seismologically observed bulk modulus (*7*), possibly because it is within the uncertainty of global seismic data (*9*). Recent laboratory measurements of electrical conductivity of pyrolite have shown that it decreases at depths greater than ~1200 km (*10*), likely attributable to the spin transition in Pv. Such measurements are not in agreement with geomagnetic field data, although observations constraining the lower-mantle conductivity are limited (*11*) (see the figure). The observed high electrical conductivity might suggest that the deep lower mantle is not pyrolitic in composition but includes a substantial amount of subducted oceanic crust, which exhibits much higher conductivity than pyrolite (*10*).

The results presented by Irifune *et al*. are an outcome of recent rapid developments in high-pressure experimental techniques combined with synchrotron x-ray radiation, which now enables precise density measurements up to 47 GPa and 2073 K (corresponding to 1200 km depth) in a large-volume press. These experiments have much better control of sample temperature than the other techniques, such as laser-heated diamond-anvil cell, with which similar experiments were previously performed. Nevertheless, much remains unknown about the composition and properties at greater depths. The nature of the spin transition in Pv is still an open question. A range of geophysical and geochemical observations suggest chemical stratification below ~1600 km depth (*10*, *12*, *13*). Additionally, the lowermost mantle, the bottom several hundred kilometers of the mantle, exhibits complex seismic-wave velocity structure. The recent discovery of silicate post-perovskite, a high-pressure phase of Pv, helps to explain the abrupt shear velocity increase at around 2700 km depth (*14*, *15*). On the other hand, supposed strong chemical heterogeneities in plume upwelling regions underneath Africa and the Pacific are yet to be examined. Further progress in high-pressure experimental techniques will allow us to tackle these unsolved problems in the deep Earth.

**References**


1. T. Irifune *et al*., *Science* **327**, 193 (2010).
2. J. Badro *et al*., *Science* **300**, 789 (2003).
3. J.-F. Lin *et al*., *Science* **317**, 1740 (2007).
4. T. Tsuchiya, R. M. Wentzcovitch, C. R. S. da Silva, S. de Gironcoli, *Phys. Rev. Lett.* **96**, 198501 (2006).
5. J. Badro *et al*., *Science* **305**, 383 (2004).
6. J. Li, in *Post-Perovskite: The Last Mantle Phase Transition*, K. Hirose, J. Brodholt, T. Lay, D. Yuen, Eds. (American Geophysical Union, Washington, DC, 2007), pp. 47–68.
7. A. M. Dziewonski, D. L. Anderson, *Phys. Earth Planet. Inter.* **25**, 297 (1981).
8. J. C. Crowhurst, J. M. Brown, A. F. Goncharov, S. D. Jacobsen, *Science* **319**, 451 (2008).
9. R. M. Wentzcovitch *et al*., *Proc. Natl. Acad. Sci. U.S.A.* **106**, 8447 (2009).
10. K. Ohta *et al*., *Earth Planet. Sci. Lett.*, in press; available at http://dx.doi.org/10.1016/j.epsl.2009.11.042.
11. N. Olsen, *Geophys. J. Int.* **138**, 179 (1999).
12. L. H. Kellogg, B. H. Harger, R. D. van der Hilst, *Science* **283**, 1881 (1999).
13. R. D. van der Hilst, H. Karason, *Science* **283**, 1885 (1999).
14. M. Murakami, K. Hirose, K. Kawamura, N. Sata, Y. Ohishi, *Science* **304**, 855 (2004).
15. A. R. Oganov, S. Ono, *Nature* **430**, 445 (2004).


10.1126/science.1184786

ECOLOGY

# Clarity on Honey Bee Collapse?

The worldwide losses of honey bee colonies continue to puzzle researchers and the beekeeping industry.

**Francis L. W. Ratnieks and Norman L. Carreck**

Over the past few years, the media have frequently reported deaths of honey bee (*Apis mellifera* L.) colonies in the United States, Europe, and Japan. Most reports express opinions but little hard science. A recent historical survey (*1*) pointed out that extensive colony losses are not unusual and have occurred repeatedly over many centuries and locations. Concern for honey bees in the United States has been magnified by their vital role in agriculture. The California almond industry alone is worth $2 billion annually and relies on over 1 million honey bee hives for cross-pollination. So what is killing honey bee colonies worldwide, and what are the implications for agriculture?

In fall 2006 and spring 2007, many U.S. beekeepers encountered hives without adult bees but with abandoned food and brood. It was widely believed that these were symptoms of a new and highly virulent pathogen. In the absence of a known cause, the term "Colony Collapse Disorder" (CCD) was coined. What have we learned about this condition since then? Are the symptoms really novel?

CCD has stimulated a flurry of explanations, ranging from mobile phones and genetically modified crops, which have been dismissed by scientists (*2*, *3*), to pests and diseases, environmental and economic factors, and pesticides, which have received more serious consideration and stimulated much research. This week, for example, comprehensive surveys of honey bee losses in general in 16 countries in North America and Europe are reported (*4*). Although full explanations for these losses are still debatable, the consensus seems to be that pests and pathogens are the single most important cause of colony losses.

There is also growing evidence that the ability of a particular pathogen to kill colonies may depend on other factors, such as the ectoparasitic mite *Varroa destructor*. CCD-like symptoms have often been reported in Europe in colonies infected with this mite (*5*). Its original host was the Asian honey bee *Apis cerana*, but it colonized *A. mellifera* when this bee species was introduced to Asia. *V. destructor* is now present in all major beekeeping regions worldwide except Australia, where CCD symptoms have not been observed. It is not the mite itself that causes bee death, but a range of normally innocuous bee viruses that it carries. Experimental studies (*6*) have shown that *V. destructor* transmits viruses previously considered unimportant to honey bee biology, including slow paralysis virus and Kashmir bee virus, thus causing colony death. Field studies have demonstrated that the incidence and abundance of viral infections in *A. mellifera* have increased substantially since the mite colonized this species of bee. For example, in one study in the UK, the incidence of infection of experimental colonies with deformed

Laboratory of Apiculture and Social Insects, Department of Biological and Environmental Science, University of Sussex, Falmer, Brighton BN1 9QG, UK. E-mail: f.ratnieks@sussex.ac.uk; norman.carreck@sussex.ac.uk

wing virus increased from 0% in 1994–1995 to 100% once the mite was firmly established in the bee population during 1997–1998 (*7*). *V. destructor* has been controlled in various ways, including by acaricides, but in many areas, especially the United States and Europe, the mite has evolved resistance to the most effective chemicals used.

Mite interactions alone cannot, however, account for all losses attributed to CCD. One paradox noticed by researchers early on in the U.S. CCD story is that although *V. destructor* is universally present in affected colonies, mite numbers were often claimed to be small, whereas *V. destructor*–related colony losses elsewhere typically reported thousands of mites per colony (*8*). A possible resolution for the former lies in studies involving *V. destructor* and Kashmir bee virus (*9*), which report that the virus can persist in a colony's worker bees even in the absence of the mite, indicating that direct bee-to-bee virus transmission also occurs. This is not surprising, as this virus was present in *A. mellifera* before the bee was colonized by *V. destructor*. A study of U.S. CCD colonies using whole-genome microarrays found much evidence of viral infection, including by Kashmir bee virus (*10*).

In 2007, a metagenomic study (*11*) compared worker honey bees from dead or dying colonies showing CCD symptoms with workers from thriving hives. The analysis showed that Israeli acute paralysis virus, a previously esoteric virus, was the pathogen most commonly associated with CCD. Although the authors did not claim a causal relationship, this seemed reasonable, given that closely related viruses such as acute bee paralysis virus and Kashmir bee virus can kill colonies when in association with *V. destructor*. However, a 2009 study paints a less clear picture (*12*). Further studies on the pathology of bee infection by Israeli acute paralysis virus are needed and may be guided by studies on the related viruses linked to colony death.

Another pathogen that may be killing colonies is the microsporidian gut parasite *Nosema ceranae*, which also originated in the Asian hive bee *A. cerana*. *N. ceranae* affects adult bees and was recently found in collapsing *A. mellifera* colonies in Spain. Experimental results suggest that it is more virulent than *Nosema apis*, which has long been known to infect *A. mellifera*. However, molecular studies show that *N. ceranae* occurs in thriving colonies in many countries, and analyses of stored bee extracts showed that it was present in *A. mellifera* decades before the onset of CCD. More research is needed to determine how virulent *N. ceranae* really is (*13*).

Foraging honey bees and even whole colonies can be killed by chemicals intended to target other insects. Neonicotinoid systemic insecticides have been blamed for extensive colony collapse, and this has caused much debate. In France, the neonicotinoid compound imidacloprid was banned as a treatment on sunflowers and maize because of concerns that it could contaminate nectar or pollen and thus kill bees, but colony losses continued. After 10 years of research (*14*), it seems unlikely that imidacloprid was responsible for the French bee deaths, but it is conjectured that subtle, sublethal effects of either the compound or its metabolites may occur, perhaps making bees more susceptible to disease.

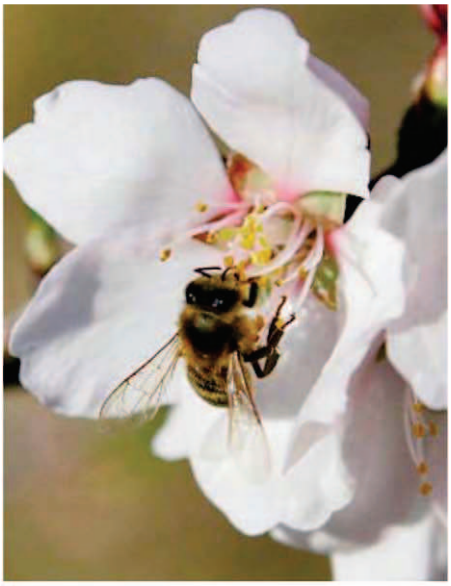

CREDIT: WIKIMEDIA COMMONS

**The mighty honey bee.** Research is still needed to help beekeepers maintain healthy colonies and to determine what is killing colonies in colony collapse disorder. Shown is *A. mellifera.*

The first annual report of the U.S. Colony Collapse Disorder Steering Committee, published in July 2009 (*15*), suggests that CCD is unlikely to be caused by a previously unknown pathogen. Rather, it may be caused by many agents in combination—the interaction between known pests and pathogens, poor weather conditions that diminish foraging, lack of forage (*16*), and management factors such as the use of pesticides and stress caused by long-distance transport of hives to nectar sources or pollination locations. The increasingly technical process of beekeeping itself merits further research as far as its impact on colony health. For example, although pollen substitutes are now widely used, little is known about the interactions between nutrition and disease susceptibility. Further research is also needed to develop effective ways of keeping colonies healthy through good hive management based on appropriate chemical, and other treatments such as "hygienic" bees that remove diseased brood and can be bred using conventional methods. In Europe, the COLOSS (COlony LOSS) network, consisting of 161 members from 40 countries worldwide, is coordinating research efforts and activities by scientists and the beekeeping industry to address these and other issues related to honey bee losses, including CCD (*2*).

In February 2009, the high pollination fee, combined with a temporary reduction in pollination demand due to drought and reduced almond prices, resulted in a surplus of hives in California available to pollinate almonds. But this leaves no room for complacency. Almond pollinating beekeepers had a poor summer in 2009 in the Dakotas and neighboring states, where hives spend the summer making honey, with heavy rains delaying and reducing the honey crop. This delayed chemical treatments for *Varroa* mites, and many colonies were probably in worse than usual condition going into winter back in California. It will be interesting to see what happens in February 2010 when the almonds bloom. On a longer time scale, there is a worrying downward trend in U.S. hives, from six million after World War II to 2.4 million today. Is the future of U.S. commercial beekeeping going to be based on pollinating a few high-value crops? If so, what will be the wider economic cost arising from crops that have modest yield increases from honey bee pollination? These crops cannot pay large pollination fees but have hitherto benefited from an abundance of honey bees providing free pollination.

Given the importance of the honey bee to mankind, the progress made in understanding CCD and colony losses in general is encouraging. But further research on honey bee health and well-being is needed.

**References**


1. B. P. Oldroyd, *PLoS Biol.* **5**, e168 (2007).
2. L. A. Malone, M.-H. Pham-Delègue, *Apidologie (Celle)* **32**, 287 (2001).
3. T. A. Mixon *et al.*, *Science of Bee Culture* **1**, 22 (2009).
4. P. Neumann, N. L. Carreck, *J. Apic. Res.* **49**, 1 (2010).
5. N. L. Carreck, B. V. Ball, J. K. Wilson, M. F. Allen, in *Proceedings of XXXIXth International Apicultural Congress, Dublin, Ireland, 21-26/8/2005,* pp. 32–33.
6. B. V. Ball, in *Varroa! Fight the Mite*, P. A. Munn, H. R. Jones, Eds. (International Bee Research Association, Cardiff, UK, 1997), pp. 11–15.
7. N. L. Carreck, B. V. Ball, J. K. Wilson, *Apiacta* **37**, 44 (2002).
8. S. J. Martin, *J. Appl. Ecol.* **38**, 1082 (2001).
9. N. L. Carreck, *Proceedings of XXXXIst International Apicultural Congress, Montpellier, France, 15th–20th September 2009,* p. 146.
10. R. M. Johnson *et al.*, *Proc. Natl. Acad. Sci. U.S.A.* **106**, 14790 (2009).
11. D. L. Cox-Foster *et al.*, *Science* **318**, 283 (2007); published online 5 September 2007 (10.1126/science.1146498).
12. D. vanEngelsdorp *et al.*, *PLoS ONE* **4**, e6481 (2009).
13. R. J. Paxton, *J. Apic. Res.* **49**, 80 (2010).
14. C. Maus *et al.*, *Bull. Insectology* **56**, 51 (2003).
15. CCD Steering Committee, *Colony Collapse Disorder Progress Report* (U.S. Department of Agriculture, Washington, DC, 2009).
16. D. Naug, *Biol. Conserv.* **142**, 2369 (2009).


10.1126/science.1185563

ECOLOGY

# Valuing Common Species

**Kevin J. Gaston**

Ecologically common species play key roles in terrestrial and marine ecosystems, yet are also the main victims of habitat loss, ecosystem degradation, and overexploitation.

Aldo Leopold's dictum that "To keep every cog and wheel is the first precaution of intelligent tinkering" (*1*) has been oft repeated in the context of environmental management. The argument is beguilingly simple. In the absence of a detailed understanding of what each species does in an ecosystem, it would be foolish to allow the loss of any one of them. It is the precautionary principle writ large and, given its enormous ramifications for the ways in which people interact with the natural world, ecologists have spent much intellectual energy, time, and resources in determining whether it has a strong empirical basis (*2*). Indeed, some of the best-known recent ecological experiments have examined the consequences of varying the numbers of species in a small area on ecosystem function. This focus assumes that the importance of retaining Leopold's cogs and wheels lies mostly in the differences between them. However, a growing body of work on common species underlines that having sufficient copies of some key pieces may be equally, and perhaps often more, important.

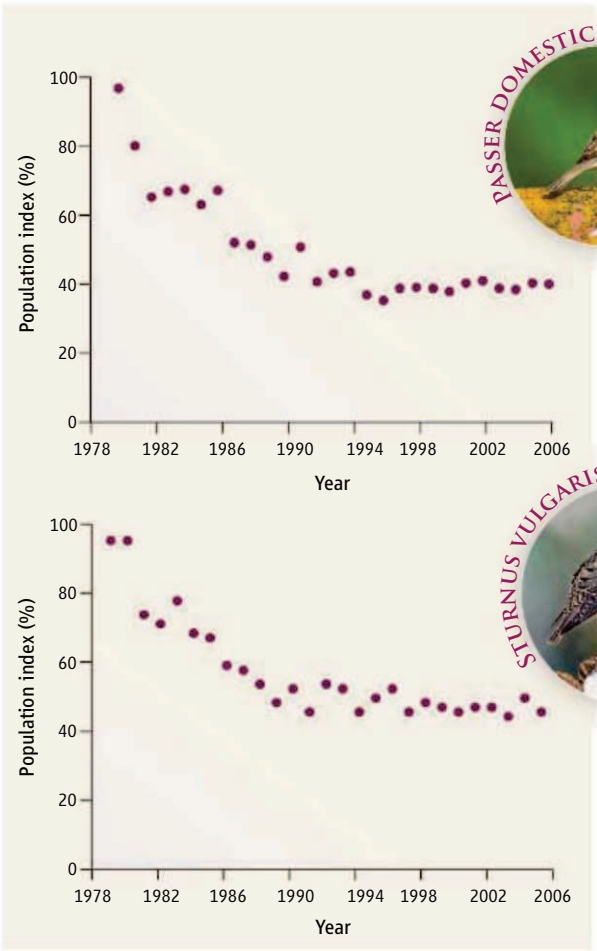


**Common yet declining.** Some of the most familiar common species are in marked decline. For example, European populations of the house sparrow (*Passer domesticus*) and the starling (*Sturnus vulgaris*) have fallen dramatically. The trends shown were determined from annual national breeding bird surveys (*17*).

Arguably, the importance of naturally common species—those that are abundant and widespread—in shaping the world around us is so blatant that it is easily overlooked. Within any given taxonomically defined assemblage (such as vascular plants, bees, amphibians, or birds), such species are in the distinct minority—the state of being very common is actually very rare—but they contribute much of the structure, biomass, and energy turnover of the majority of terrestrial and marine systems (*3*, *4*). They may exert a profound influence on the prevailing environmental conditions experienced by other species and thus those that can coexist. Even in tropical forest landscapes, some of the most species-rich ecosystems that exist, it is not the full diversity of trees that is most apparent but the smaller number of species that have come to dominate.

Few experiments have been conducted explicitly to determine the contribution of common species to ecosystem function. However, those that have been done confirm the importance of these species. In particular systems, common species can, for example, be responsible for the bulk of primary production, carbon storage and flows, and sediment mixing (*5*–*8*). Moreover, meta-analyses of the results of experiments that have manipulated species richness have shown that the standing stock (total abundance or biomass) and resource depletion found in the experimental treatments with most species tend to be similar to those of the most productive species in single-species treatments (*9*). This result might be explained by the sampling effect: Assemblages with larger numbers of species are more likely to contain those species that are most productive.

In consequence, common species underpin the provision of many ecosystem services, the benefits that ecosystems provide to people. This does not pertain solely to the more familiar supporting services (such as soil formation, primary production, nutrient cycling, and water cycling) and regulating services (such as air quality regulation, climate regulation, water regulation, and pollination). There is also growing evidence that physical and visual encounters with the natural world positively influence human health and well-being, most noticeably in urban areas where such access is limited but where most people live (*10*–*12*). Inevitably, it is species that are common within cities (when native, they are often also common more widely) that are chiefly responsible for these interactions.

The null expectation is that the contribution of common species to ecosystem structure, function, and services will be strictly proportional to their abundance. However, the extent to which this expectation is met, or to which common species contribute suprapoportionally (that is, they are keystone species) or subproportionally, remains poorly understood.

Ecologists and evolutionary biologists have found that common species also contribute to structuring the world around us in less obvious ways. For instance, they disproportionately influence spatial patterns of variation in species richness and species turnover (*13*, *14*), provide temporal continuity to

Biodiversity and Macroecology Group, Department of Animal and Plant Sciences, University of Sheffield, Sheffield S10 2TN, UK. E-mail: k.j.gaston@sheffield.ac.uk

assemblage structure through greater species longevity (*15*), and exhibit some of the classical latitudinal and altitudinal patterns of variation in body size, coloration, and reproductive investment that can result in the same species looking and behaving differently in different parts of the world (*16*).

The importance of the role that common species play would perhaps largely be of interest only to biologists if they remained common. However, systematic declines are now frequent (see the figure), with common species lying at the heart of each of the major pressures on biodiversity.

First, common species are the main victims of habitat loss, fragmentation, and degradation. Indeed, to a first approximation, common species are habitat loss, yet our awareness of this fact is dulled by the presentation of statistics in terms of areal declines of forests, grasslands, coral reefs, and the like, rather than the numbers of individuals that have been removed.

Second, common species are the main objects of large-scale overexploitation. Although many species may be involved, the vast majority of the resources resulting from logging, fishing, and the bushmeat trade come from just a few. Sustainable use is principally a matter of how we deal with common species.

Third, common species are frequent casualties of the invasion of species, whether after accidental or intentional introduction, that are alien to an area. Indeed, some of the environmentally and economically most important alien species are those that have killed or replaced the natural dominants.

Finally, it is the impacts of habitat loss, overexploitation, and invasive species on common species that lead to the most pronounced resultant cascades of reductions and losses of other species, because common species shape their environments and are involved in large numbers of biotic interactions (such as herbivory, predation, and parasitism).

One might perhaps argue that the declines of previously common species are of limited concern, because others will increase in abundance and distribution to take their places. In some cases, it is doubtless true that other species will come to dominance, although these typically tend to be rather different in biological characteristics (for example, smaller sizes, shorter generation times, and greater propensity for boom-and-bust dynamics) and in the ecosystem services that they provide (a grassland is not a forest, and jellyfish-dominated oceans do not provide large quantities of fish for human consumption). Moreover, in an increasing number of cases, a troubling dynamic appears to be playing out, with declines in common species reflecting large net losses in the numbers of individuals of an assemblage (*4*). Many examples come from intensively used areas of agriculture and urbanization in the developed world, perhaps presaging such problems elsewhere. Previously common species, including the rocky mountain grasshopper and the passenger pigeon, have been driven extinct through anthropogenic activities. However, typically, the more substantive concern is the extinction of commonness, or the ecological and functional extinction of common species.

None of this is to say that rare species are unimportant: There is ample evidence to the contrary. Rather, we need to give weight both to retaining the different kinds of Leopold's cogs and wheels and to ensuring that we have sufficient of each.


**References and Notes**

1. L. B. Leopold, Ed., *Round River: From the Journal of Aldo Leopold* (Oxford Univ. Press, New York, 1953).
2. D. U. Hooper *et al*., *Ecol. Monogr.* **75**, 3 (2005).
3. J. P. Grime, *J. Ecol.* **86**, 902 (1998).
4. K. J. Gaston, R. A. Fuller, *Trends Ecol. Evol.* **23**, 14 (2008).
5. M. D. Smith, A. K. Knapp, *Ecol. Lett.* **6**, 509 (2003).
6. M. Solan *et al*., *Science* **306**, 1177 (2004).
7. D. E. Bunker *et al*., *Science* **310**, 1029 (2005).
8. B. W. Taylor *et al*., *Science* **313**, 833 (2006).
9. B. J. Cardinale *et al*., *Nature* **443**, 989 (2006).
10. R. Mitchell, F. Popham, *J. Epidemiol. Community Health* **61**, 681 (2007).
11. T. S. Nielsen, K. B. Hansen, *Health Place* **13**, 839 (2007).
12. J. F. Bell, J. S. Wilson, G. C. Liu, *Am. J. Prev. Med.* **35**, 547 (2008).
13. K. J. Gaston *et al*., *Proc. R. Soc. Lond. B. Biol. Sci.* **274**, 1567 (2007).
14. A. L. Šizling *et al*., *Am. Nat.* **174**, 82 (2009).
15. D. Jablonski, G. Hunt, *Am. Nat.* **168**, 556 (2006).
16. K. J. Gaston *et al*., *J. Biogeogr.* **35**, 483 (2008).
17. Data from European Bird Census Council/Royal Society for the Protection of Birds/BirdLife/Statistics Netherlands; see www.ebcc.info/pecbm.html.


10.1126/science.1182818

PHYSICS

# Electron Nematic Phases Proliferate

**Eduardo Fradkin[1] and Steven A. Kivelson[2]**

A form of electron ordering similar to that of molecules in liquid crystals has been observed in an iron-based superconductor.

Even though electrons in solids form a dense and strongly interacting fluid, electrons in many metals can also be considered as a weakly interacting quantum gas of "quasiparticles." Like a gas, the electron fluid is essentially homogeneous and isotropic. On the other hand, if the electrons interact sufficiently strongly, they crystallize, freezing into an insulating state that exhibits density modulations that are periodic in space. However, both of these conventional descriptions fail dramatically in many of the most interesting electronic materials discovered in the past two decades. In these materials, the electrons appear to organize into phases with a spatial structure that partially resembles the electron crystal but is still a conducting fluid. The behavior of these materials has the characteristics of both, seemingly opposite, states. On page 181 of this issue, Chuang *et al*. (*1*) report the observation of such a phase, in a scanning tunneling microscopy (STM) study of an iron-based high-temperature superconductor (*2*).

Insight into the behavior of strongly interacting electron fluids can be gleaned from an analogy to classical liquid crystals. For instance, nematic liquid crystals are uniform fluids made of "cigar-shaped" molecules, but alignment of the molecules causes some of their properties to be anisotropic. A strongly interacting system of electrons can also exhibit an anisotropic conducting state, an electron nematic. Alternatively, the molecules of a classical liquid crystal can arrange themselves into layered structures, called smectics. In the electronic analog, the density is modulated in one direction, forming a "stripe phase," an electron smectic. More generally, one can envision a host of exotic quantum electronic liquid crystalline phases (*3*).

The phase transitions between liquid crystalline phases are also interesting. For instance, at temperatures where the smectic phase has just "melted" to form a nematic, remnants of the smectic ordering appear in the form of short-range density wave order. Correspondingly, an electron nematic phase near a stripe phase can be pictured as a partially melted stripe phase (see the figure). However, quantum effects and the presence of additional degrees of freedom are important in electronic liquid crystalline phases,

In common with the copper oxide high-temperature superconductors, the iron-based "Fe pnictides" are layered materials in which

[1]Department of Physics, University of Illinois, Urbana, IL 61801, USA. [2]Department of Physics, Stanford University, Stanford, CA 94305, USA. E-mail: efradkin@illinois.edu

magnetism, which reflects strong correlations between the electrons, plays a key role (*4*). Whereas previous STM studies of various Fe pnictides have revealed poor-quality surfaces, Chuang *et al*. found that a particular Fe-pnictide superconductor—$CaFe_2As_2$ lightly doped with cobalt—has sufficiently clean and flat surfaces for the images to achieve atomic-scale resolution. This enabled them to study quasiparticle interference effects. What makes the surfaces of this particular Fe pnictide so perfect is still unclear.

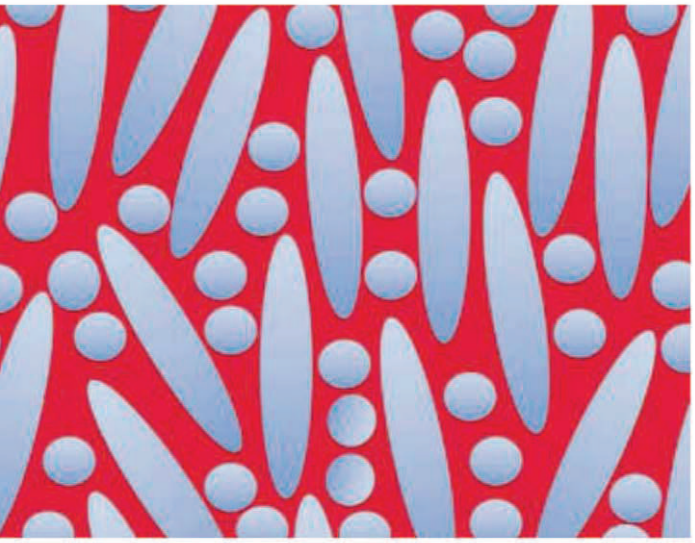

**Electron nematics as melted stripe states.** An electronic nematic state, such as the one seen in the experiments of Chuang *et al.*, can be regarded as a melted (quantum or thermal) stripe phase. The result is an electronically uniform state that retains the orientational order of the stripe.

The STM data of Chuang *et al*. show several fascinating and unanticipated features. In particular, they present clear evidence of nanoscale electronic structures that run in one direction with a characteristic scale of 8*a*, where *a* is the spacing between Fe atoms. These structures apparently produce a dramatic anisotropy in the quasiparticle "dispersion" (i.e., the relation between the energy and the momentum). The quasiparticle dispersion is determined indirectly in STM by looking at the characteristic dispersive interference patterns at different values of the tip bias voltage.

On the basis of such an analysis, Chuang *et al*. find an essentially one-dimensional dispersion relation; the quasiparticle energy is only a function of the component of their momentum oriented parallel to the nanoscale structures. Conversely, in the transverse direction, the same quasiparticle dispersion is repeated displaced by an amount $2\pi/8a$ in momentum space.

In a strongly correlated system, quantum liquid crystal phases result from the spontaneous organization of the electrons into mesoscale structures by various mechanisms such as frustrated phase separation (*5*). Where this description applies, the electron nematic can be regarded as a melted stripe phase. A key consequence is that low-energy (slow) fluctuations occur in the nematic that have the character of the nearby stripe state, a "fluctuating stripe state" (*6*). However, this is not the only pathway to an electron nematic. This phase may also arise from the breakdown of a conventional metallic state caused by a "Pomeranchuk instability" of a conventional Fermi liquid. The structure of a Fermi liquid is dominated by the Pauli exclusion principle: All states with energy less than the Fermi energy are occupied, and all those with higher energy are empty. The result is a well-defined "Fermi surface" in momentum space, which is the surface that separates the occupied and unoccupied states. In the Pomeranchuk picture of the nematic transition, the Fermi surface undergoes a spontaneous distortion to a shape with less symmetry than that of the underlying crystal (*7*–*9*). In both the melted-stripe and the Pomeranchuk descriptions, the electron nematic behaves as an anisotropic metal, but where the Pomeranchuk description applies, no fluctuating stripe correlations appear at low energies.

Structural studies of the bulk material have shown that Fe pnictides at low enough doping concentrations exhibit a small structural distortion that distinguishes the otherwise equivalent x and y directions (which crystallographers call "a" and "b") in the Fe-pnictide layers. This distortion had already been interpreted theoretically as evidence for an electron nematic state in this system (*10*–*13*) that is driven by electronic correlation effects. Preliminary evidence in favor of this interpretation came from the unusually strong magnetic anisotropy detected in neutron scattering experiments on $CaFe_2As_2$ and LaOFeAs (*3*).

The STM data of Chuang *et al*. apparently confirm this interpretation but also raise more questions. The observation of a characteristic nanoscale structure strongly suggests that this system must be regarded as a "melted stripe" phase, and that it is likely close to a smectic (stripe) nematic quantum phase transition (*14*), rather than to a Pomeranchuk instability from a Fermi liquid (*7*–*9*). However, bulk diffraction studies have yet to detect any evidence of this nanoscale electronic structure.

In recent years, electronic nematic states have been discovered experimentally in an increasing number of diverse systems, including the two-dimensional electron gas in a large magnetic field (*15*), the bilayer ruthenate $Sr_3Ru_2O_7$ (*16*), and the cuprate superconductors $YBa_2Cu_3O_{6+x}$ (*17*–*19*) and $Bi_2Sr_2CaCu_2O_{8+x}$ (*20*, *21*). Electronic nematic order is fragile and can be disrupted at long length scales by the effects of local disorder, which is present to varying degrees in all of these systems. The use of local probes, such as STM, is particularly important in this context, as they can be used to detect local nematic order over nanoscopic length scales (*4*, *20*, *21*). The observation of electronic nematic order (*22*, *23*) in several different high-temperature superconductors in fact suggests a common underlying mechanism for both superconducting and nematic order. Rather than being competing forms of ordering, they may actually arise together.

**References and Notes**


1. T.-M. Chuang *et al*., *Science* **327**, 181 (2010).
2. Y. Kamihara *et al*., *J. Am. Chem. Soc.* **130**, 3296 (2008).
3. S. A. Kivelson, E. Fradkin, V. J. Emery, *Nature* **393**, 550 (1998).
4. J. Zhao *et al*., *Nat. Phys.* **5**, 555 (2009).
5. V. J. Emery, S. A. Kivelson, *Physica C* **209**, 597 (1993).
6. S. A. Kivelson *et al*., *Rev. Mod. Phys.* **75**, 1201 (2003).
7. V. Oganesyan, S. A. Kivelson, E. Fradkin, *Phys. Rev. B* **64**, 195109 (2001).
8. Ch. J. Halboth, W. Metzner, *Phys. Rev. Lett.* **85**, 5162 (2000).
9. H.-Y. Kee, E. H. Kim, C.-H. Chung, *Phys. Rev. B* **68**, 245109 (2003).
10. C. Fang *et al*., *Phys. Rev. B* **77**, 224509 (2008).
11. C. Xu, Y. Qi, S. Sachdev, *Phys. Rev. B* **78**, 134507 (2008).
12. W.-C. Lee, C. Wu, *Phys. Rev. Lett.* **103**, 176101 (2009).
13. H. Zhai, F. Wang, D.-H. Lee, *Phys. Rev. B* **80**, 064517 (2009).
14. K. Sun *et al*., *Phys. Rev. B* **78**, 085124 (2008).
15. K. B. Cooper *et al*., *Phys. Rev. B* **65**, 241313 (2002).
16. R. A. Borzi *et al*., *Science* **315**, 214 (2007); published online 22 November 2006 (10.1126/science.1134796).
17. Y. Ando *et al*., *Phys. Rev. Lett.* **88**, 137005 (2002).
18. V. Hinkov *et al*., *Science* **319**, 597 (2008); published online 10 January 2008 (10.1126/science.1152309).
19. R. Daou ***et al***., http://arXiv.org/abs/0909.4430 (2009).
20. C. Howald, H. Eisaki, N. Kaneko, A. Kapitulnik, *Proc. Natl. Acad. Sci. U.S.A.* **100**, 9705 (2003).
21. Y. Kohsaka *et al*., *Science* **315**, 1380 (2007); published online 7 February 2007 (10.1126/science.1138584).
22. For a recent review of electronic nematic order, see (*23*) and references therein.
23. E. Fradkin *et al.*, http://arXiv.org/abs/0910.4166 (2009).


24. Supported by NSF grants DMR 0758462 (E.F.) and DMR 0531196 (S.A.K.), and by the Office of Science, U.S. Department of Energy, under contract DE-FG02-91ER45439 through the Frederick Seitz Materials Research Laboratory at the University of Illinois (E.F.) and contract DE-FG02-06ER46287 through the Geballe Laboratory of Advanced Materials at Stanford University (S.A.K.).

10.1126/science.1183464

AAAS, publisher of *Science*

# 2010 Annual Meeting

## *Bridging Science and Society*

**18—22 February • San Diego**

## The place for celebrations is the AAAS Annual Meeting

- 25 Years of science education reform through AAAS Project 2061
- 50 Years of accomplishments in higher education and academic research by the University of California, San Diego
- 60 Years of discovery through support from the U.S. National Science Foundation
- 350 Years of scientific achievement and endeavor by the Royal Society, the world's oldest science academy
- And celebrate one of the greatest inventions of the 20th century — the laser

**Get program details and take advantage of early-bird registration and hotel discounts at:**
http://www.aaas.org/meetings

**Follow us in cyberspace at:**
http://www.facebook.com/AAAS.Science and http://twitter.com/#search?q=AAAS10

**Reporters: The EurekAlert! Web site hosts the AAAS Meeting Newsroom. Reporters can obtain details and register at:**
www.eurekalert.org/aaasnewsroom

AAAS
ADVANCING SCIENCE, SERVING SOCIETY

**Peter C. Agre, M.D.**
AAAS President and
2010 Program Chair

Dear Colleagues,

**On behalf of the AAAS Board of Directors, it is my distinct honor to invite you to the 176th Meeting of**

## President's Address

### Peter C. Agre, M.D.

**AAAS President; Director, Malaria Research Institute, Johns Hopkins Bloomberg School of Public Health**

Agre shared the 2003 Nobel Prize in Chemistry with Roderick MacKinnon of Rockefeller University for the discovery of aquaporins, the key proteins that transport water across cell membranes. Not long after receiving the Nobel Prize, Agre began working to extend his studies of aquaporins to malaria, addressing the question of whether or not aquaporins could be exploited as a means of treating or preventing the disease. Initial results led his laboratory to focus on malaria as its primary area of study. As director of the Malaria Research Center, he oversees 19 Hopkins faculty members who concentrate on advancing basic science to develop new methods in malaria prevention and treatment. Agre is a member of the National Academy of Sciences (NAS), chair of the NAS Committee on Human Rights, and a Fellow of AAAS.

## Plenary Speakers

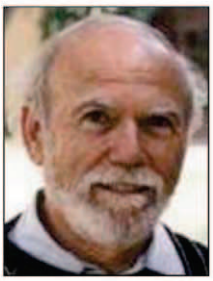

### Barry C. Barish, Ph.D.

**Director, Global Design Effort for the International Linear Collider (ILC); Linde Professor of Physics, emeritus, California Institute of Technology**
***Lecture Title To Be Determined***

Among Barish's noteworthy experiments were those performed at Fermilab using high-energy neutrino collisions. These experiments were among the first to observe the weak neutral current, a linchpin of electroweak unification theories. Today he directs the ILC, the highest priority future project for particle physics worldwide that promises to complement the Large Hadron Collider at CERN in exploring the TeV energy scale. In the 1980s, Barish initiated an ambitious international effort to build a sophisticated underground detector which provided some key evidence that neutrinos have mass. As director of the Laser Interferometer Gravitational-Wave Observatory Laboratory from 1997 to 2005, he led a team of scientists who built two facilities to detect and study gravitational waves from astrophysical sources. Barish is a member of the National Academy of Sciences and is an AAAS Fellow.

### Carol W. Greider, Ph.D.

**Daniel Nathans Professor; Director, Department of Molecular Biology and Genetics; Professor of Oncology, Johns Hopkins University School of Medicine**
***Telomerase and the Consequences of Telomere Dysfunction***

Greider, one of the world's pioneering researchers on the structure of telomeres, was awarded the 2009 Nobel Prize in physiology or medicine by the Royal Swedish Academy of Sciences along with Elizabeth Blackburn and Jack W. Szostak. While a 23-year-old graduate student at the University of California, Berkeley, working together with Blackburn, Greider discovered the enzyme telomerase and later, in her own lab, she cloned its RNA component. This work laid the foundation for studies that have linked telomerase and telomeres to human cancer and age-related degenerative disease. It represents another example of curiosity-driven basic research that has direct medical implications.

### Eric S. Lander, Ph.D.

**Director, The Broad Institute of MIT and Harvard University; Co-Chair, President's Council of Advisors on Science and Technology (PCAST)**
***Science and Technology in the First Year of the New Administration***

Lander is widely known as one of the driving forces behind today's revolution in genomics, the study of all of the genes in an organism and how they function together in health and disease. He also is co-chair of President Obama's council of science and technology advisers. PCAST is an advisory group of the nation's leading scientists and engineers who directly advise the President and make policy recommendations in the many areas where understanding of science, technology, and innovation is key to strengthening the economy and forming policy. Lander also was one of the principal leaders of the Human Genome Project and is a member of both the National Academy of Sciences and Institute of Medicine. He is also an AAAS Fellow.

### Marcia McNutt, Ph.D.

**Director, U.S. Geological Survey; Science Adviser to the Secretary, U.S. Department of the Interior *(invited)***
***Science Below the Sea***

McNutt's appointment in 2009 marked a milestone for USGS — she is the first female director in the agency's 130-year history. She directs a multi-disciplinary organization that focuses on biology, geography, geology, geospatial information, and water, and is dedicated to studying the landscape, natural resources, and natural hazards. Most recently she served as president and chief executive officer of the Monterey Bay Aquarium Research Institute. Her biography includes a broad range of research interests and numerous honors and awards. She has participated in 15 major oceanographic expeditions and served as chief scientist on more than half of them. She is a member of the National Academy of Sciences and the American Academy of Arts and Sciences, and a Fellow of AAAS.

# Topical Lecture Series

## Karen Emmorey
Director, Laboratory for Language and Cognitive Neuroscience, and Professor of Speech, Language, and Hearing Sciences, San Diego State University
***Neural and Cognitive Underpinnings of Language Across Modalities***

## Robert T. Fraley
Executive Vice President and Chief Technology Officer of Monsanto Co., St Louis, Missouri
***Sustainable Solutions for Doubling Crop Productivity by 2030***

## Lawrence S. B. Goldstein
Director, Stem Cell Research Program, and Professor of Cellular and Molecular Medicine, University of California, San Diego
***The Future of Stem Cell Research***

## James J. Heckman
Henry Schultz Distinguished Service Professor of Economics, University of Chicago, and Distinguished Chair of Microeconometrics, University College, London and University College, Dublin
***Economics, Psychology, and Biology of Early Childhood Development***

## Kristina M. Johnson
Under Secretary for Energy, U.S. Department of Energy, Washington, D.C.
***An Integrated Approach to a Low Carbon Energy Future***

## Thomas Hillman Jordan
Director, Southern California Earthquake Center, and the W. M. Keck Professor of Earth Sciences, University of Southern California
***Understanding Earthquakes Through Large-Scale Simulations***

## Stephen R. Palumbi
Professor of Biological Sciences, Stanford University
***How Marine Species React and Adjust to Ocean Acidification and Climate Change***

## Kellogg Schwab
Associate Professor and Director of the Center for Water and Health, Johns Hopkins Bloomberg School of Public Health
***Improving Access to Potable Water Throughout The World***

## Steffanie Strathdee
Associate Dean of Global Health Sciences, Harold Simon Professor, and Chief of the Division of Global Public Health, School of Medicine, University of California, San Diego
***Infectious Diseases Have No Passport: Battling HIV, TB, and STDs on the Mexico-U.S. Border***

## Jay Vavra
Biology Teacher, The Gary and Jerri-Ann Jacobs High Tech High, San Diego, CA
***The Case for Original Research in the High School Science Classroom***

2010 GEORGE SARTON MEMORIAL LECTURE

## Jed Z. Buchwald
Doris and Henry Dreyfuss Professor of History, California Institute of Technology
***Knowledge in the Early Modern Era: The Origins of Experimental Error***

# Seminar Tracks

Day-long seminars address topics that build bridges between science and society.

## Translational and Personalized Medicine

### Friday, 19 February

Translational research transforms scientific discoveries from the laboratory bench into practical clinical applications at the patient's bedside. This seminar focuses on the challenges and opportunities in translating the burgeoning science and technology of genomics into a greater understanding of human diseases and personalized treatment.

**Evaluating and Funding Translational Research**

*Organized in cooperation with the journal,* Science Translational Medicine

*Organized by* Maria T. Vassileva, Foundation for the National Institutes of Health; Juli Staiano, AAAS Development; Katrina Kelner, *Science Translational Medicine*

**SPEAKERS**
Eric J. Topol, The Scripps Research Institute, La Jolla, CA
*Outcomes of the NIH Roadmap: Impact on Translational Medicine*
Gail Cassell, Eli Lilly and Co., Indianapolis, IN
*The FDA Critical Path Initiative: A Perspective of the First Four Years*
Ellen V. Sigal, Friends of Cancer Research, Arlington, VA
*Novel Funding Models for Translational Research*

**DISCUSSANT**
Gary Firestein, University of California, San Diego

**Genome Analyses and Sequencing To Advance Drug Discovery and Treatment**

*Organized by* William Evans, St. Jude Children's Research Hospital

**SPEAKERS**
Richard Wilson, Washington University School of Medicine, St. Louis
*Discovery of Poly-Genetic Determinants of Diseases Through Whole Genome Sequencing*
Mary Relling, St. Jude Children's Research Hospital, Memphis, TN
*Genetics of Racial Differences in Drug Response, Disease Risk, and Health Disparities*
Dan Roden, Vanderbilt University School of Medicine, Nashville, TN
*Challenges and Opportunities in the Assembly of Population Pharmacogenomics*

**DISCUSSANTS**
Scott Weiss, Harvard Medical School, Boston, MA
William Evans, St. Jude Children's Research Hospital, Memphis, TN

**The Road to Personalized Medicine**

*Organized by* Donna L. Mendrick, U.S. Food and Drug Administration; Vishal S. Vaidya, Harvard Medical School

**SPEAKERS**
Ivan Rusyn, University of North Carolina, Chapel Hill
*Modeling Toxicity in the Population Using Experimental Models*
Vishal S. Vaidya, Harvard Medical School, Boston, MA
*Bench to Bedside Detection of Kidney Toxicity*
Maryellen de Mars, Critical Path Institute, Tucson, AZ
*Using Genetic Information To Predict and Prevent Drug Toxicity*

**DISCUSSANT**
Donna L. Mendrick, U.S. Food and Drug Administration, Silver Spring, MD

## Marine Sciences and Society

### Saturday, 20 February

The oceans provide us with many economic and aesthetic benefits as well as vital ecosystem services. These include seafood, pharmaceuticals, minerals, recreation, and much of the oxygen we breathe. Evaluating available science and unique aspects of marine systems is critical to successful ocean stewardship.

### Does Size Matter? Rationales for Large Marine Reserves

*Organized by* Emily Frost and Angela T. Bednarek, The Pew Charitable Trusts; Terry Hughes, James Cook University, Australia

**MODERATOR**
Jane Lubchenco, National Oceanic and Atmospheric Administration, Washington, DC

**SPEAKERS**
Stuart L. Pimm, Duke University, Durham, NC
*Large Terrestrial Protected Areas and Lessons for the Marine Environment*
Stephen R. Palumbi, Stanford University, CA
*Spreading the Wealth: Design and Function of Highly Protected Reserve Networks*
Terry Hughes, James Cook University, Townsville, Australia
*Proving the Benefits of Very Large Marine Reserves*

**DISCUSSANT**
Jay Nelson, The Pew Charitable Trusts, Philadelphia, PA

### Marine Spatial Planning: A New Approach for Balancing Ocean Uses and Ecosystem Health

*Organized by* Morgan Gopnik, Nicholas Institute for Environmental Policy Solutions; Mary Turnipseed, Duke University

**SPEAKERS**
Larry Crowder, Duke University, Beaufort, NC
*The Science and Management of Coupled Social-Ecological Systems in the Ocean*
Kevin St. Martin, Rutgers, The State University of New Jersey, New Brunswick
*Mapping Communities: Linking People to Ocean Spaces*
Andrew Rosenberg, University of New Hampshire, Durham
*Advancing Ocean Planning in Massachusetts: The Role of a Unique Stakeholder Coalition*
Mary Turnipseed, Duke University, Durham, NC
*Re-Imagining the Public Trust Doctrine To Inform U.S. Marine Spatial Planning*
Jo Foden, University of East Anglia, Norwich, United Kingdom
*Evaluating Marine Plans: Lessons Learned from Aquatic Environmental Assessments*
Fanny Douvere, UNESCO, Paris
*Marine Spatial Planning: A Step-by-Step Approach Toward Ecosystem-Based Management*

### Arctic Sea-Ice Loss: What This Means for the Conservation of Arctic Marine Ecosystems

*Organized by* Tara Connelly and Gabriela Chavarria, Natural Resources Defense Council

**SPEAKERS**
John Walsh, University of Alaska, Fairbanks
*Climate Change in the Arctic: What Are the Signs and What Is Predicted?*
Jacqueline Grebmeier, University of Tennessee, Knoxville
*The Potential Effect of Sea-Ice Loss on Arctic Marine Ecosystems*
Frances Beinecke, Natural Resources Defense Council, Washington, DC
*Role of the Aspen Institute's Commission on Arctic Climate Change in the Arctic*

**DISCUSSANT**
Charles Clusen, Natural Resources Defense Council, Washington, DC

## History and Future of Laser Technology

### Sunday, 21 February

A prominent example of the impact that pure scientific research can have on society is the story of the laser. The 50th anniversary of the first working laser takes place in 2010. From DVD players to eye surgery, the laser is one of the greatest inventions of the 20th century and has revolutionized daily life.

### Celebrating the Birth of the Laser: A Look Back After 50 Years

*Organized by* Alan Chodos, American Physical Society, College Park, MD; Anthony J. Campillo, Optical Society of America, Washington, DC

**SPEAKERS**
Anthony Siegman, Stanford University, CA
*How the Laser Came To Be*
William B. Bridges, California Institute of Technology, Pasadena
*Gas Lasers: The Early Years*
Jeff Hecht, *Laser Focus World,* Auburndale, MA
*Looking Back at How the Laser Evolved*

### Next Generation of Extreme Optical Tools and Applications

*Organized by* Christopher Ebbers, Lawrence Livermore National Laboratory

**SPEAKERS**
Robert L. Byer, Stanford University, CA
*Quantum Noise Limited Lasers and the Search for Gravitational Waves*
Margaret Murnane, University of Colorado, Boulder
*Attosecond Light and Science at the Time-Scale of Electron Motion*
Christopher Barty, Lawrence Livermore National Laboratory, Livermore, CA
*Revolutionizing Isotope Science and Applications with Laser-Like Gamma-Rays*
Keith Hodgson, SLAC National Accelerator Laboratory, Menlo Park, CA
*Next Generation X-Ray Lasers and Applications*
Toshiki Tajima, Max Planck Institute for Quantum Optics, Garching, Germany
*Relativistic Optics and Applications with Ultra-Intense Lasers*
Wim Leemans, Lawrence Berkeley National Laboratory, Livermore, CA
*Laser-Based Particle Acceleration and the Path to TeV Physics*

### Lasers at the Extreme: Ultra-Cold, Ultra-Fast, and Ultra-Hot Uses

*Organized by* Thomas M. Baer, Stanford Photonics Research Institute

**SPEAKERS**
William D. Phillips, National Institute of Standards and Technology, Gaithersburg, MD
*Laser Cooling and Trapping: Making the Coldest Stuff in the Universe*
David N. Payne, University of Southampton, United Kingdom
*How Lasers and Glass Fibers Changed Our World*
Edward Moses, Lawrence Livermore National Laboratory, Livermore, CA
*National Ignition Facility: Creating Star Power in the Laboratory*

# Special Session

## 2010 Forum for Sustainability Science Programs

### Thursday, 18 February

**1:00PM–6:00PM**

*Organized by* Arnim Wiek, Arizona State University, Tempe; Amy Fuller, AAAS International Office, Washington, DC

As sustainability considerations rise on both the domestic and international agenda, policy makers at all levels of governance increasingly look to scientists and engineers to provide guidance in creating sustainable societies. Universities have responded by developing academic and research programs in Science and Technology for Sustainable Development or "Sustainability Science" that undertake practical, place-based research to provide decision-support for addressing sustainability challenges.

These inherently interdisciplinary, society-focused programs have converged on the AAAS Annual Meeting as the most appropriate meeting place for networking and exchanging ideas. Beginning with the 2007 Annual Meeting in San Francisco, the AAAS Center for Science, Technology, and Sustainability has convened the AAAS Forum for Sustainability Science Programs.

An important prerequisite to development of course content and curriculum development is having a clear understanding of the core competencies expected of program graduates. The 2010 Forum will focus on this with the ultimate goal of a set of commonly agreed-upon competencies. For more information on this invitation-only event, contact Amy Fuller at afuller@aaas.org.

# Symposium Tracks

## Beyond the Classroom

**Building Bridges Between Ocean Scientists, Educators, and Students**
*Organized by* Gwen Noda, University of California, Los Angeles; Linda Duguay, University of Southern California, Los Angeles

**Civic Scientific Literacy in Developed and Developing Countries**
*Organized by* Jon D. Miller, Michigan State University, East Lansing; Rajesh Shukla, National Council of Applied Economic Research, New Delhi, India

**Learning Science in Informal Environments**
*Organized by* Bruce V. Lewenstein, Cornell University, Ithaca, NY

**Mind Changes: Can Out-of-School Learning Contribute to Evolution Literacy?**
*Organized by* Martin Weiss, New York Hall of Science, New York City

**Reemergence of Science, Technology, and Education as Priorities in the Arab World**
*Organized by* Ashley Dougherty and Cindi Warren Mentz, U.S. Civilian Research Development Foundation, Arlington, VA

**Scientific Foundations for Future Physicians**
Organized by Jodi Lubetsky and Anthony Mazzaschi, Association of American Medical Colleges, Washington, DC

**Strategies for Diaspora To Be Enablers of S&T Capacity-Building in Their Homelands**
*Organized by* Pallavi Phartiyal, AAAS Science and Policy Programs, Washington, DC; Lara Campbell, CUBRC Center for International Science and Technology Advancement, Washington

**Tomorrow's Scientists and Engineers**
*Organized by* Jon D. Miller, Michigan State University, East Lansing; Greg Pearson, National Academy of Engineering, Washington, DC

**Top-Down or Bottom-Up? Comparing European and U.S. Gender Policies in Science**
*Organized by* Marina Marchetti, European Commission, Directorate General for Research, Brussels, Belgium

**Women and Men in the Scientific Work Force: Issues of Networks, Partners, and Ethics**
*Organized by* Julia E. Melkers, Georgia Institute of Technology, Atlanta

## Cognitive Function and Development

**The Brain on Trial: Neuroscience Evidence in the Courtroom**
*Organized by* Deborah Runkle and Mark S. Frankel, AAAS Science and Policy Programs, Washington, DC

**From Gene Discovery to Cell Biology in Psychiatry: An Emerging Case**
*Organized by* Tyrone Cannon, University of California, Los Angeles

**Language Learning in Deaf Children: Integrating Research on Speech, Gesture, and Sign**
*Organized by* Jenny Saffran, University of Wisconsin, Madison

**Language Processing for Science and Society**
*Organized by* Annie Zaenen, Palo Alto Research Center, CA

**The Long Reach of Early Childhood Poverty: Pathways and Impacts**
*Organized by* Greg J. Duncan, University of California, Irvine

**Music-Language Interactions in the Brain: From the Brainstem to Broca's Area**
*Organized by* Aniruddh D. Patel, Neurosciences Institute, San Diego, CA

**Role of Sleep in Memory from Development to Old Age**
*Organized by* Sara C. Mednick, University of California, San Diego

**Stress and the Central Role of the Brain in Health Inequities**
*Organized by* Michael J. Zigmond, University of Pittsburgh, PA; Bruce S. McEwen, Rockefeller University, New York City

**Traumatic Brain Injury: The Violent and Silent Epidemic**
*Organized by* Mahlon DeLong and David Wright, Emory University School of Medicine, Atlanta, GA

**Unexpected Discoveries on Brain Function and Development from Model Organisms**
*Organized by* S. Lawrence Zipursky, University of California, Los Angeles; Barbara Illman, U.S. Forest Service, Madison, WI

## Communicating Science

**Communicating Science to the Public: Culture and Social Context in East Asia**
*Organized by* Masataka Watanabe, Japan Science and Technology Agency, Tokyo, Japan; Sook-Kyoung Cho, Korea Foundation for the Advancement of Science and Creativity, Seoul; Sun Mengxin, China Association for Science and Technology, Beijing

**Communicating on the State and Local Level: How Can Scientists Support Policy-Makers?**
*Organized by* Peyton West and Erin Heath, AAAS Science and Policy Programs, Washington, DC

**Covering Global Climate Change and Adaptation from the Ground Up**
*Organized by* Cristine Russell, Harvard University, Cambridge, MA; Deborah Blum, University of Wisconsin, Madison; Phillip Hilts, MIT's Knight Science Journalism Fellowships, Cambridge, MA

**Earthquake Science and Advocacy: Helping Californians Live Along the San Andreas Fault**
*Organized by* Mark L. Benthien, Southern California Earthquake Center, Los Angeles

**Eyes on Screen: Communicating Science in the New Information Age**
*Organized by* Sharon Dunwoody, University of Wisconsin, Madison; Lynne Friedmann, Friedmann Communications, Solana Beach, CA

**Facing the Uncertain Future of International Science Journalism**
*Organized by* Cristine Russell, Harvard University, Cambridge, MA; James Cornell, International Science Writers Association, Tucson, AZ; Donald Kennedy, Stanford University, CA

**Genetics and Ethics: Different Views on the Human Condition**
*Organized by* Walter Doerfler, University of Cologne, Erlangen, Germany; Hans G. Ulrich, Erlangen University, Germany

**Plato's Progeny: Academies of Science**
*Organized by* Lynn E. Elfner, Ohio Academy of Science, Columbus; Jay B. Labov, National Research Council, Washington, DC

**Science in the Theater**
*Organized by* Vince LiCata, Louisiana State University, Baton Rouge

**Science Meets Society: Walking the Talk**
*Organized by* Viviane Willis-Mazzichi and Raffaella Di Iorio, European Commission, Joint Research Center, Brussels, Belgium

**Watching the Watchmen and Cheering the Heroes: The Science of Superheroes**
*Organized by* Cortney Riese Sloan and Ann Merchant, National Academies, Washington, DC; Jennifer Ouellette, National Academy of Sciences, Los Angeles, CA

## Education in the Classroom

**Can Singapore Mathematics Enhance Student Learning in the United States?**
*Organized by* Patsy Wang-Iverson, Gabriella and Paul Rosenbaum Foundation, Stockton, NJ

**Demonstrating the Legal Sustainability of Effective STEM Diversity Programs**
*Organized by* Daryl E. Chubin, AAAS Education and Human Resources, Washington, DC

**Education Research at Minority-Serving Institutions: What Have We Learned?**
*Organized by* Marilyn J. Suiter, National Science Foundation, Arlington, VA

**First-Person Solvers? Learning Mathematics in a Video Game**
*Organized by* Keith Devlin, Stanford University, CA

**Role of Community Colleges in Increasing Minority Students in the STEM Pipeline**
*Organized by* Anne Jane MacLachlan, University of California, Berkeley

**Science Literacy: How To Train Teachers, Engage Students, and Maximize Learning**
*Organized by* Michael W. Klymkowsky, University of Colorado, Boulder

**Scientific Approaches to Teaching Science in K-16 Education**
*Organized by* Robert E. Fay, Westat, Bethesda, MD

**TIMSS 2007: Exploring the Dramatic Improvements in Performance in Two States**
*Organized by* Patsy Wang-Iverson, Gabriella and Paul Rosenbaum Foundation, Stockton, NJ

**Visualizations in the Mind and in the World: Implications for STEM Education**
*Organized by* Mary Hegarty, University of California, Santa Barbara

**Worlds of Wonder: Can Video Games Teach Science?**
*Organized by* Yasmin Kafai, University of Pennsylvania, Philadelphia; Douglas Clark, Vanderbilt University, Nashville, TN

## Energy Today and Tomorrow

**Advanced Nuclear Energy Concepts for a Safe, Sustainable, Carbon-Free Future**
*Organized by* Tomas Diaz de la Rubia, Lawrence Livermore National Laboratory, Livermore, CA; Robert Rosner, Argonne National Laboratory, Argonne, IL

**Biofuels' Uncertain Future: Unraveling the Science and Politics of Indirect Land Use**
*Organized by* Holly K. Gibbs, Stanford University, CA; Richard Plevin, University of California, Berkeley

**Combating Global Emissions: The Urgent Need for a New Strategy in the Asia-Pacific Rim**
*Organized by* Ellyn M. Murphy and Yong Wang, Pacific Northwest National Laboratory, Richland, WA

**Consequences of Changes in Energy Return on Energy Invested**
*Organized by* Carey King, University of Texas, Austin

**Gray Is the New Green: How Energy Recycling Curbs Both Global Warming and Power Costs**
*Organized by* Thomas Casten, Recycled Energy Development, Westmont, IL

**Nanotechnology: Will Nanomaterials Revolutionize Energy Applications?**
*Organized by* S. Thomas Picraux, Los Alamos National Laboratory, Los Alamos, NM

**Smart and Secure Transmission Grids To Realize U.S. and E.U. Renewable Energy Potentials**
*Organized by* Gianluca Fulli and Giovanni De Santi, European Commission, Joint Research Center, Petten, Netherlands

**Societal Strategies for Addressing the Climate and Energy Challenge**
*Organized by* Jane C.S. Long, Lawrence Livermore National Laboratory, Livermore, CA

**Nuclear Waste Management: From Public Perception to Industrial Reality**
*Organized by* Didier J. Haas, European Commission, Joint Research Center, Brussels, Belgium

**Toward Green Mobility: Integrating Electric Drive Vehicles and Smart Grid Technology**
*Organized by* Kathryn Clay, Alliance for Automotive Manufacturers, Washington, DC; Tina Kaarsberg, U.S. Department of Energy, Washington, DC

**Urban Design and Energy Demand: Transforming Cities for an Eco-Energy Future**
*Organized by* Nancy Levinson, Arizona State University, Tempe

## Global Science and Policy

**Bottom-of-the-Economic-Pyramid Technological Solutions: Lessons from Success Stories**
*Organized by* William S. Kisaalita, University of Georgia, Athens

**Building International Security Through Lab-to-Lab Exchanges**
*Organized by* Benn Tannenbaum, AAAS Center for Science, Technology, and Security Policy, Washington DC

**Information Technologies and Remote Sensing for Understanding Human Rights Violations**
*Organized by* Lars Bromley, AAAS International Office, Washington, DC

**Mobilizing East Asian Science and Technology To Address Critical Global Challenges**
*Organized by* Asuka Hoshikoshi and Yuko Nagano, National Institute of Science and Technology Policy, Tokyo, Japan

**The Next Big Thing: Keys in the Transformation from Science to Society**
*Organized by* Gerald Hane, Q-Paradigm, Rockville, MD

**Oceans Apart? Transatlantic Perspectives on Public Research and Business Innovation**
*Organized by* Eamonn Cahill, Office of the Chief Scientific Adviser, Dublin, Ireland

**Privacy in a New Global Context: Trapped Between Culture, Laws, and Technology**
*Organized by* Stephan Lechner, JRC Institute for the Protection and Security of the Citizen, Ispra, Italy; Aidan Gilligan, European

Commission, Joint Research Center, Brussels, Belgium

**Science Academies in Society**
*Organized by* Daniel Schaffer and Tasia Asakawa, Academy of Sciences for the Developing World, Trieste, Italy

**What Went Wrong with the Global Economy?**
*Organized by* Rolf Sinclair, Center for Scientific Studies, Valdivia, Chile; J. Doyne Farmer, Santa Fe Institute, NM

**When Science Goes Global, Can Everybody Win?**
*Organized by* Sieglinde Gruber, Alessandro Damiani, and Mary Kavanagh, European Commission, Directorate General for Research, Brussels, Belgium

**Working Together for the Public: Challenges for Verification of Nuclear Activities**
*Organized by* Aidan Gilligan, European Commission, Joint Research Center (JRC), Brussels, Belgium

## Health, Medicine, and the Environment

**Applying Biogenomics to Ecology: From the Molecular to the Ecosystem Level**
*Organized by* Teresa Lettieri, JRC Institute for Environment and Sustainability, Ispra, Italy

**A California Roadmap for Identifying Chemicals that Affect Breast Cancer Risk**
*Organized by* Sarah Janssen, Natural Resources Defense Council (NRDC), San Francisco, CA; Gabriela Chavarria, NRDC, Washington, DC

**Consequences of Endocrine Disrupting Agents in the Laboratory and Home**
*Organized by* John G. Vandenbergh, North Carolina State University, Raleigh; A. Wallace Hayes, Harvard School of Public Health, Andover, MA

**False Discoveries and Statistics: Implications for Health and the Environment**
*Organized by* Ron Brookmeyer, Johns Hopkins Bloomberg School of Public Health, Baltimore, MD; Robert E. Fay, Westat, Bethesda, MD

**The Impact of Genomics**
*Organized by* Stephen G. Oliver, University of Cambridge, United Kingdom

**Innate Immunity: Theme and Variations**
*Organized by* David H. Raulet, University of California, Berkeley; Christine A. Biron, Brown University, Providence, RI; Sondra Schlesinger, Washington University School of Medicine, St. Louis, MO

**Moving Across Scales: Mathematics for Investigating Biological Hierarchies**
*Organized by* Louis J. Gross, University of Tennessee, Knoxville

**Mutators Versus Antimutators in Evolution and Medicine**
*Organized by* Robert C. von Borstel, University of Alberta, Edmonton, Canada

**One Health: Attaining Optimal Health for People, Animals, and the Environment**
*Organized by* Barbara Hyde, American Society for Microbiology, Washington, DC

**Protecting the Consumer: Can "Omics" Keep the Promise?**
*Organized by* Aidan Gilligan, European Commission, Joint Research Center, Brussels, Belgium

**Rethinking the Science, Biology, and Importance of Stem Cells in Regenerative Medicine**
*Organized by* Irving Weissman, Stanford University School of Medicine, Palo Alto, CA; Sondra Schlesinger, Washington University School of Medicine, St. Louis, MO; Carol Newlon, University of Medicine and Dentistry of New Jersey, Newark

**Science of the Small: Nano-Bio-Technology Under the Biological Microscope**
*Organized by* Barbara Illman, U.S. Forest Service, Madison, WI; Vicki Colvin, Rice University, Houston, TX

## Physical Sciences Frontiers

**50 Years of Exobiology and Astrobiology: Past, Present, and Future Life in the Universe**
*Organized by* Linda Billings, George Washington University, Washington, DC; Jeffrey Bada, University of California, San Diego

**Are Neutrinos the Reason We Exist?**
*Organized by* Kurt Riesselmann, Fermi National Accelerator Laboratory, Batavia, IL

**The Arrow of Time**
*Organized by* Sean M. Carroll, California Institute of Technology, Pasadena

**Astrobiology and the Future: Science, Ethics, and Societal Issues on Earth and Beyond**
*Organized by* Margaret Race, SETI Institute, Mountain View, CA

**Doomsday Versus Discovery**
*Organized by* Renilde Vanden Broeck, CERN, Geneva, Switzerland; Katie Yurkewicz, Fermi National Accelerator Laboratory, Batavia, IL

**How Computational Science Is Tackling the Grand Challenges Facing Science and Society**
*Organized by* Edward Seidel, Carmen Whitson, and José Muñoz, National Science Foundation, Arlington, VA

**Managing the Exaflood: Enhancing the Value of Networked Data for Science and Society**
*Organized by* Bonnie C. Carroll, Information International Associates Inc., Oak Ridge, TN; Paul F. Uhlir, National Research Council, Washington, DC

**Particles and People: How Basic Physics Benefits Society**
*Organized by* Elizabeth Clements and Katie Yurkewicz, Fermi National Accelerator Laboratory, Batavia, IL

**Physics and Art: A Gateway to the Sciences**
*Organized by* Christopher M. Smith, Center for Theoretical Biological Physics, La Jolla, CA

**Real Numbers: Mathematical Technologies for Counterterrorism and Border Security**
*Organized by* Jonathan D. Farley, Johannes Kepler University Linz, Austria; Tony Harkin, Rochester Institute of Technology, NY; Anice Anderson, Rose-Hulman Institute of Technology, Terre Haute, IN

**SETI Turns 50**
*Organized by* Jill C. Tarter, SETI Institute, Mountain View, CA

**Traffic, Crowds, and Society**
*Organized by* Nicola Bellomo, Polytechnic University of Turin, Torino, Italy; Andrea Bertozzi, University of California, Los Angeles

**What's Next for the Net? The Internet of Things and Ubiquitous Computing**
*Organized by* Michael R. Nelson, Georgetown University, Washington, DC

## Protecting Marine Resources

**Adam Smith Meets Jacques Cousteau: Using Economics To Protect Marine Resources**
*Organized by* Benjamin Halpern, University of California, Santa Barbara; Anne Guerry, National Oceanic and Atmospheric Administration (NOAA) Northwest Fisheries Science Center, Seattle, WA

**Confronting Ocean Acidification: Options for Management and Policy**
*Organized by* Susan Park, National Research Council, Washington, DC; Victoria J. Fabry, California State University, San Marcos

**Denial, Detente, and Decisions: Fisheries Science at the Crossroads**
*Organized by* Alison Rieser, University of Hawaii at Manoa, Honolulu, HI; John Lynham, University of Hawaii at Manoa, Honolulu, HI

**Designing the Future Ocean: Baseline Data Needs for Marine Spatial Planning**
*Organized by* Alison Chase and Lisa Suatoni, Natural Resources Defense Council (NRDC), New York City; Gabriela Chavarria, NRDC, Washington, DC

**Ensuring Marine Policy Is Responsive to Social Dynamics and Management Experience**
*Organized by* Patrick Christie, University of Washington, Seattle; Richard Pollnac, University of Rhode Island, Kingston

**Land-Ocean Linkages and Dynamics of High-Productivity Ecosystems in the Sea of Cortes**
*Organized by* Exequiel Ezcurra, University of California, Riverside

**Limits to Sustainability of Coral Reef Fisheries**
*Organized by* Ayana Elizabeth Johnson, University of California, San Diego

**Management and Governance in a Melting Marine Arctic: Challenges and Opportunities**
*Organized by* Lisa Speer, NRDC, New York City; Gabriela Chavarria, NRDC, Washington, DC

**Marine Reserves in a Changing World: Connecting Research with Human Needs**
*Organized by* Steven Gaines, University of California, Santa Barbara; Kirsten Grorud-Colvert, Oregon State University, Corvallis; Sarah Lester, University of California, Santa Barbara

**One Fish, Two Fish, Red Fish, New Fish: Society Needs Marine Biodiversity Research**
*Organized by* Heather Mannix, Consortium for Ocean Leadership, Washington, DC

**Unraveling the Mysteries of the Deep: Effects of Human Activities on Marine Megafauna**
*Organized by* Rebecca Lewison, San Diego State University, CA

**Will Coral Reefs Disappear? Separating Fact from Conjecture**
*Organized by* Joanie Kleypas, National Center for Atmospheric Research, Boulder, CO; Kimberley Yates, U.S. Geological Survey, St. Petersburg, FL

## Public Health and Wellness

**Children of Assisted Reproductive Technologies: Their Health and New Genetic Issues**
*Organized by* Marvin L. Meistrich, University of Texas M.D. Anderson Cancer Center, Houston

**Decoding the Secret Pathologies of Dolphins: Significance for Human and Ocean Health**
*Organized by* Carolyn Sotka, National Oceanic and Atmospheric Administration (NOAA) Oceans and Human Health Initiative, Charleston, SC; Paul Sandifer, NOAA Oceans and Human Health Initiative, Charleston, SC

**Food Allergies: The Enemy Within**
*Organized by* Aidan Gilligan, European Commission, Joint Research Center (JRC), Brussels, Belgium; Doris Florian, JRC Institute for Reference Materials and Measurements, Geel, Belgium

**Healthy and Plentiful Animal-Based Foods: Science Offers New Possibilities**
*Organized by* Rodney A. Hill, University of Idaho, Moscow; Larry Branen, University of Idaho, Coeur d'Alene

**Impact of Biomedical Progress on Health Span and Health Care of the Elderly**
*Organized by* Edward J. Goetzl, University of California, San Francisco

**Improving Oral Health: Smiles for Life**
*Organized by* Huw F. Thomas, University of Alabama, Birmingham

**Repairing Our DNA: Bridging Molecular Mechanism and Human Health**
*Organized by* Graham C. Walker, Massachusetts Institute of Technology, Cambridge

**Science in Motion: Addressing Complex Health Problems Through Upstream Solutions**
*Organized by* Patricia L. Mabry, Christine Bachrach, and Dana M. Sampson, National Institutes of Health, Bethesda, MD

**The Science of Well-Being and Implications for Societal Quality of Life**
*Organized by* Ed Diener, University of Illinois, Urbana-Champaign

**Targeting HIV/AIDS Prevention: New Research and Future Avenues**
*Organized by* Rochelle A. Diamond, California Institute of Technology, Pasadena; Andrew M. Hebbeler, Gladstone Institute of Virology and Immunology, San Francisco, CA

**Tracking and Tracing Our Food Supply: The Way Forward**
*Organized by* Ewen C. Todd, Michigan State University, East Lansing

**Translating the Science of Vector-Borne Disease to the Improvement of Global Health**
*Organized by* Nancy E. Beckage, University of California, Riverside; Joseph M. Vinetz, University of California, San Diego

## Responding to Environmental Change

**Algae for Food, Feed, Fiber, Freshwater, and Fuel**
*Organized by* Michael Webber, University of Texas, Austin

**America's Climate Choices: Potential Strategies for a U.S. Response to Climate Change**
*Organized by* Ian Kraucunas, National Academy of Sciences, Washington, DC; Thomas Dietz, Michigan State University, East Lansing; Thomas J. Wilbanks, Oak Ridge National Laboratory, TN

**Can Geoengineering Save Us from Global Warming?**
*Organized by* Alan Robock, Rutgers University, New Brunswick, NJ; Margaret Leinen, Climos Inc., Alexandria, VA

**Can Science Feed the World?**
*Organized by* Tracey Elliott, Royal Society, London, United Kingdom

**Climate Change in Working Landscapes: Sustainability Science and Policy Perspectives**
*Organized by* Ashwini Chhatre, University of Illinois, Urbana-Champaign

**Coastal Adaptation**
*Organized by* So-Min Cheong, University of Kansas, Lawrence; Robert Nicholls, University of Southampton, United Kingdom

**Co-Evolution of Science and Society for Sustainability Innovation**
*Organized by* Masaru Yarime, University of Tokyo, Japan

**Geoengineering the Climate: The Royal Society Study**
*Organized by* Tracey Elliott, Royal Society, London, United Kingdom

**Greening Cities Through Media, Education, and Science**
*Organized by* Marla S. McIntosh, University of Maryland, College Park; Albert G. Medvitz, McCormack Sheep and Grain, Rio Vista, CA

**Human Dimensions of Geoengineering**
*Organized by* Brad Allenby, Arizona State University, Tempe; Peter A. Wilderer, European Academy of Sciences and Arts, Schliersee, Germany

**Infusing Science into Sustainable, Master-Planned Communities**
*Organized by* Carla Carlson, University of Minnesota, Minneapolis

**Research Translation and Environmental Health: A U.S.-Mexico Border Initiative**
*Organized by* Keith Pezzoli, University of California, San Diego

## Science, Policy, and Economics

**The American Community Survey and the Census: A New Foundation for the Social Sciences**
*Organized by* William Eddy, Carnegie Mellon University, Pittsburgh, PA

**DNA Identifiability: Ethical Issues and Policy Challenges**
*Organized by* Joel T. Wu and Barbara Koenig, Mayo Clinic, Rochester, MN

**Ethical and Societal Dimensions of Biosecurity and Dual-Use Research**
*Organized by* Lida Anestidou and Jo Husbands, National Academies, Washington, DC

**The Future of the National Science Foundation on Its 60th Anniversary**
*Organized by* John Tsapogas and Ann Ferrante, National Science Foundation, Arlington, VA

**Intelligence of Dolphins: Ethical and Policy Implications**
*Organized by* Stephanie J. Bird, Science and Engineering Ethics, Wrentham, MA; Thomas I. White, Loyola Marymount University, Redondo Beach, CA; Dena K. Plemmons, University of California, San Diego

**Mathematics and the Analysis of Fairness in Political Processes**
*Organized by* Michael A. Jones, Mathematical Reviews, Ann Arbor, MI

**Past, Present, and Future of Forensic Science in the United States**
*Organized by* Sarah P. Chu, Innocence Project, New York City

**Scientific Rationality and Policy-Making: Making Their Marriage Work**
*Organized by* Aidan Gilligan, European Commission, Joint Research Center, Brussels, Belgium

**Speaking Scientific Truth to Power**
*Organized by* Lisa M. Lambert, Maria Trainer, and Christina Stachulak, Council of Canadian Academies, Ottawa

**Using GIS and Spatial Analysis To Better Understand Patterns and Causes of Violence**
*Organized by* William Alex Pridemore, Indiana University, Bloomington

**Value and Limits of Scientific Research: Past and Future R&D Budgets**
*Organized by* Joanne P. Carney, AAAS Science and Policy Programs, Washington, DC; Tobin L. Smith, Association of American Universities, Washington, DC; Jennifer Poulakidas, Association of Public and Land-Grant Universities, Washington, DC

**A Wobbly Three-Legged Stool: Science, Politics, and the Public**
*Organized by* Lewis M. Branscomb, University of California, San Diego

## Understanding Environmental Change

**Bridging Science and Society for Sustainability: The Role of Visualization**
*Organized by* Arnim Wiek, Arizona State University, Tempe; Villy Christensen, University of British Columbia, Vancouver, Canada

**Dust in the Earth System**
*Organized by* E. Arthur Bettis III, University of Iowa, Iowa City; Paul M. Bertsch, University of Kentucky, Lexington; Nicholas Lancaster, Desert Research Institute, Reno, NV

**Getting to the Roots of Agricultural Productivity**
*Organized by* Daniel Bush, Colorado State University, Fort Collins; Jonathan Lynch, Pennsylvania State University, University Park

**Global Food Security, Land Use, and the Environment: Future Challenges**
*Organized by* Jonathan A. Foley and David Tilman, University of Minnesota, St. Paul, MN

**Integrated Science for Society and the Environment**
*Organized by* G. Philip Robertson, Michigan State University, Hickory Corners; Scott L. Collins, University of New Mexico, Albuquerque

**Preserving the Global Commons Through Conservation and Cooperation**
*Organized by* Jennifer Jacquet, University of British Columbia Fisheries Center, Vancouver, Canada; John Hocevar, Greenpeace USA, Austin, TX

**Progress in the Use of Earth Observation for Fighting Hunger**
*Organized by* Oliver Leo, JRC Institute for the Protection and Security of the Citizen, Ispra, Italy

**Sea Ice in the Changing Climate: Modeling a Multiscale Nonlinear System**
*Organized by* Kenneth M. Golden, University of Utah, Salt Lake City

**Sustainability Science: Transformative Research Beyond Scenario Studies**
*Organized by* Arnim Wiek, Arizona State University, Tempe; Katja Brundiers, Arizona State University, Tempe

**Understanding Climate-Change Skepticism: Its Sources and Strategies**
*Organized by* Riley E. Dunlap, Oklahoma State University, Stillwater

**Up in Flames: Fire in a Changing Environment**
*Organized by* Susan G. Conard, U.S. Forest Service (retired), Silver Spring, MD

AAAS, publisher of *Science*,
thanks the sponsors and supporters of the

# 2010 Annual Meeting

## *Bridging Science and Society*

**18—22 February ▸ San Diego**

Presenting Sponsor

SUBARU

In addition generous funding for AAAS Awards is provided by the ***Kavli Foundation*** and ***Affymetrix.***

## Be part of a proven equation:

Your Organization + AAAS Annual Meeting = Global Visibility

**Call today about the benefits of sponsorships currently available:**

Jill C. Perla
AAAS Meetings
Direct Dial: (202) 326-6736
E-mail: jperla@aaas.org

AAAS
ADVANCING SCIENCE, SERVING SOCIETY

# CRISPR/Cas, the Immune System of Bacteria and Archaea

**Philippe Horvath[1]* and Rodolphe Barrangou[2]***

**Microbes rely on diverse defense mechanisms that allow them to withstand viral predation and exposure to invading nucleic acid. In many Bacteria and most Archaea, clustered regularly interspaced short palindromic repeats (CRISPR) form peculiar genetic loci, which provide acquired immunity against viruses and plasmids by targeting nucleic acid in a sequence-specific manner. These hypervariable loci take up genetic material from invasive elements and build up inheritable DNA-encoded immunity over time. Conversely, viruses have devised mutational escape strategies that allow them to circumvent the CRISPR/Cas system, albeit at a cost. CRISPR features may be exploited for typing purposes, epidemiological studies, host-virus ecological surveys, building specific immunity against undesirable genetic elements, and enhancing viral resistance in domesticated microbes.**

Microbes have devised various strategies that allow them to survive exposure to foreign genetic elements. Although outpopulated and preyed upon by abundant and ubiquitous viruses, microbes routinely survive, persist, and occasionally thrive in hostile and competitive environments. The constant exposure to exogenous DNA via transduction, conjugation, and transformation have forced microbes to establish an array of defense mechanisms that allow the cell to recognize and distinguish incoming "foreign" DNA, from "self" DNA and to survive exposure to invasive elements. These systems maintain genetic integrity, yet occasionally allow exogenous DNA uptake and conservation of genetic material advantageous for adaptation to the environment. Certain strategies, such as prevention of adsorption, blocking of injection, and abortive infection, are effective against viruses; other defense systems specifically target invading nucleic acid, such as the restriction-modification system (R-M) and the use of sugar-nonspecific nucleases. Recently, an adaptive microbial immune system, clustered regularly interspaced short palindromic repeats (CRISPR) has been identified that provides acquired immunity against viruses and plasmids.

CRISPR represents a family of DNA repeats found in most archaeal (~90%) and bacterial (~40%) genomes (*1*–*3*). Although the initial discovery of a CRISPR structure was made fortuitously in *Escherichia coli* in 1987, the acronym was coined in 2002, after similar structures were observed in genomes of various Bacteria and Archaea (*1*). CRISPR loci typically consist of several noncontiguous direct repeats separated by stretches of variable sequences called spacers (which mostly correspond to segments of captured viral and plasmid sequences) and are often adjacent to *cas* genes (CRISPR-associated) (Fig. 1). *cas* genes encode a large and heterogeneous family of proteins that carry functional domains typical of nucleases, helicases, polymerases, and polynucleotide-binding proteins (*4*). CRISPR, in combination with Cas proteins, forms the CRISPR/Cas systems. Six "core" *cas* genes have been identified, including the universal markers of CRISPR/Cas systems *cas1* (COG1518) and *cas2* (COG1343, COG3512, occasionally in a fused form with other *cas* genes). Besides the *cas1* to *cas6* core genes, subtype-specific genes and genes encoding "repeat-associated mysterious proteins" (RAMP) have been identified and grouped into subtypes functionally paired with particular CRISPR repeat sequences (*4*–*8*). The size of CRISPR repeats and spacers varies between 23 to 47 base pairs (bp) and 21 to 72 bp, respectively. Generally, CRISPR repeat sequences are highly conserved within a given CRISPR locus, but a large assortment of repeat sequences has been shown across microbial species (*1*, *9*). Most repeat sequences are partially palindromic, having the potential to form stable, highly conserved secondary structures (*7*). The number

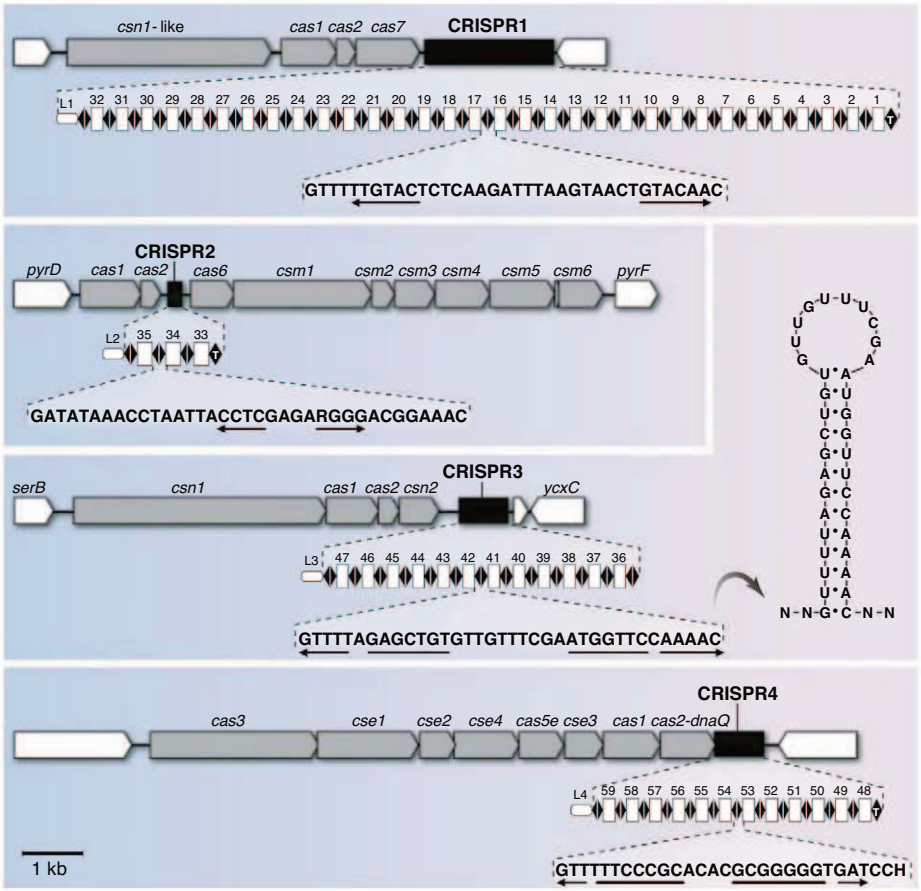


**Fig. 1.** Overview of the four CRISPR/*cas* systems present in *Streptococcus thermophilus* DGCC7710. For each system, gene organization is depicted on the top, with *cas* genes in gray, and the repeat-spacer array in black. Below the gene scheme, the repeat and spacer (captured phage or plasmid nucleic acid) content is detailed as black diamonds (T, terminal repeat) and white rectangles, respectively. Bottom line, consensus repeat sequence. L1 to L4, leader sequences. The predicted secondary structure of the CRISPR3 repeat is shown on the right. *S. thermophilus* CRISPR2, CRISPR3, and CRISPR4 systems are homologous to the CRISPR systems of *Staphylococcus epidermidis* (*20*), *Streptococcus mutans* (*19*), and *E. coli* (*28*), respectively.

[1]Danisco France SAS, BP10, F-86220 Dangé-Saint-Romain, France. [2]Danisco USA, Inc., 3329 Agriculture Drive, Madison, WI 53716, USA.

*To whom correspondence should be addressed. E-mail: philippe.horvath@danisco.com (P.H.), rodolphe.barrangou@danisco.com (R.B.)

of repeat-spacer units is documented to reach 375 (*Chloroflexus* sp. Y-400-fl), but most loci commonly contain fewer than 50 units, as exemplified in lactic acid bacteria genomes (*8*). Microbes may contain more than one CRISPR locus; up to 18 such loci have been identified in *Methanocaldococcus jannaschii*, totaling more than 1% of the genome (*10*). CRISPRs are typically located on the chromosome, although some have been identified on plasmids (*11*–*13*).

The CRISPR loci have highly diverse and hypervariable spacer sequences, even between closely related strains (*14*–*16*), which were initially exploited for typing purposes. A variety of putative roles for CRISPR sequences was originally suggested, including chromosomal rearrangement, modulation of expression of neighboring genes, target for DNA binding proteins, replicon partitioning, and DNA repair (*5*). In 2005, three independent in silico studies reported homology between spacer sequences and extrachromosomal elements, such as viruses and plasmids (*11*, *14*, *15*). This led to the hypothesis that CRISPR may provide adaptive immunity against foreign genetic elements (*6*).

### A Vast Spectrum of Immunity

In 2007, it was shown in *Streptococcus thermophilus* that during natural generation of phage-resistant variants, bacteria commonly alter their CRISPR loci by polarized (i.e., at the leader end) incorporation of CRISPR repeat-spacer units (Fig. 1) (*17*, *18*), consistent with observed spacer hypervariability at the leader end of CRISPR loci in various strains (*14*, *16*). The integrated sequences were identical to those of the phages used in the challenge, which suggested that they originate from viral nucleic acid. To determine whether CRISPR impacts phage resistance, spacer content was altered via genetic engineering, which showed that spacer addition can provide novel phage resistance, whereas spacer deletion could result in loss of phage resistance (*17*). These findings were confirmed in *Streptococcus mutans*, where phage-resistant mutants acquired novel CRISPR spacers with sequences matching the phage genome, in vitro and in vivo (*19*). Although the ubiquitous and predatory nature of phages may explain the overwhelming representation of phage sequences in CRISPR loci, CRISPR spacers can also interfere with both plasmid conjugation and transformation, as shown in *Staphylococcus epidermidis* (*20*). Furthermore, several metagenomic studies investigating host-virus populations dynamics showed that CRISPR loci evolve in response to viral predation and that CRISPR spacer content and sequential order provide insights both historically and geographically (*21*–*24*).

The ability to provide defense against invading genetic elements seems to render CRISPR/Cas systems particularly desirable in hostile environments and may explain their propensity to be transferred horizontally between sometimes distant organisms (*12*). There is extensive evidence that defense systems such as CRISPR have

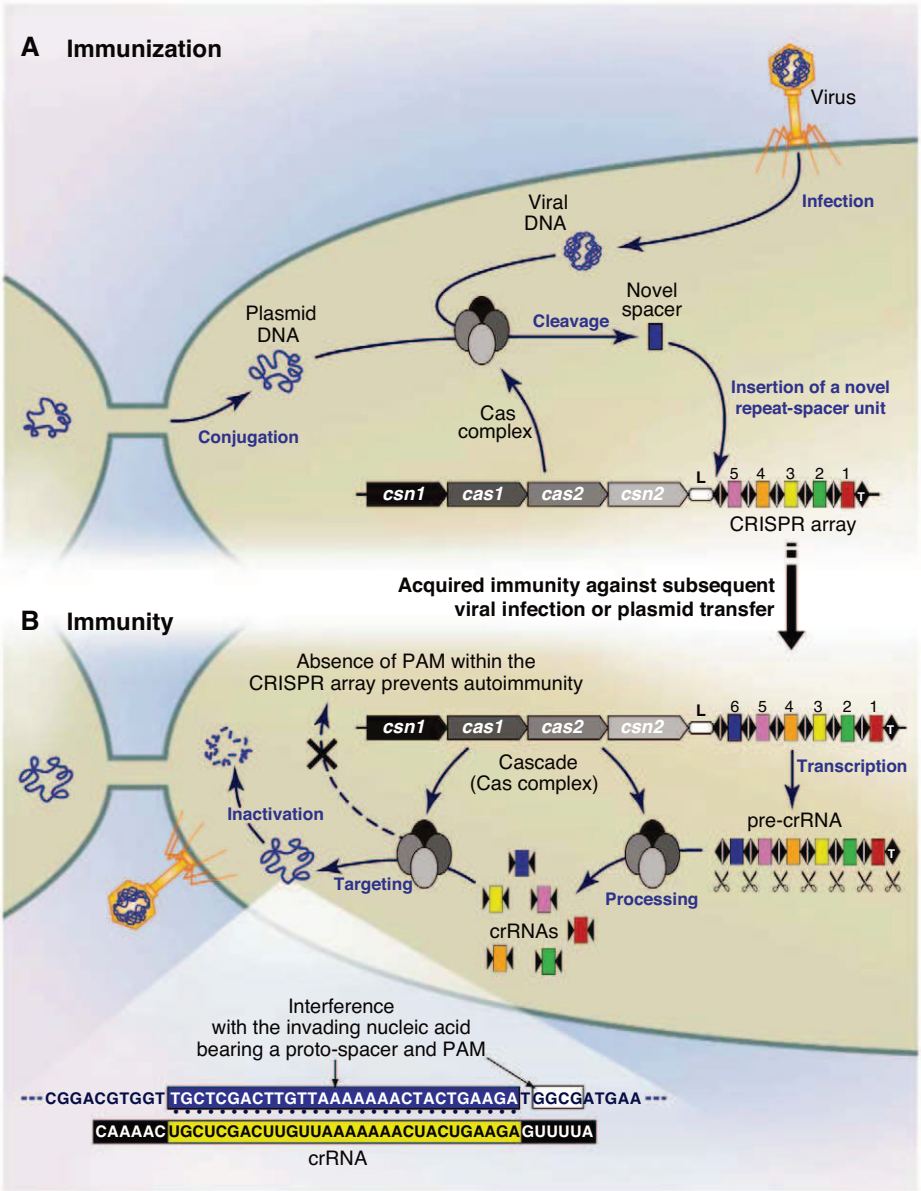


**Fig. 2.** Overview of the CRISPR/Cas mechanism of action. (**A**) Immunization process: After insertion of exogenous DNA from viruses or plasmids, a Cas complex recognizes foreign DNA and integrates a novel repeat-spacer unit at the leader end of the CRISPR locus. (**B**) Immunity process: The CRISPR repeat-spacer array is transcribed into a pre-crRNA that is processed into mature crRNAs, which are subsequently used as a guide by a Cas complex to interfere with the corresponding invading nucleic acid. Repeats are represented as diamonds, spacers as rectangles, and the CRISPR leader is labeled L.

undergone horizontal transfer between genomes, notably differences observed in codon bias, GC content variability, their presence on mobile genetic elements, the presence of neighboring insertion sequence elements, and their variable presence and location in closely related genomes. This is in agreement with the lack of congruence between the phylogenetic relation of various CRISPR elements and that of the organisms in which they are found (*8*, *12*). This horizontal gene transfer may be mediated by plasmids, megaplasmids, and even prophages, all of which are documented to carry CRISPR loci (*2*).

Given the variety of defense systems in microbes and their role in controlling the presence of plasmids, prophages, transposons, and, perhaps, chromosomal sequences, studies should investigate whether CRISPR/Cas systems preferentially target certain elements and could determine whether they are symbiotic or mutually exclusive with other defense systems.

### Idiosyncrasies of the CRISPR/Cas Mechanism of Action

The mechanism by which CRISPR provides resistance against foreign genetic elements is not fully characterized (Fig. 2). Even so, the functional link between Cas and CRISPR repeats has been inferred from the congruence observed between their sequence patterns. *cas* genes provide

CRISPR-encoded immunity, because inactivating the CRISPR1-associated *cas7* gene (Fig. 1) impairs the ability of the host to integrate novel CRISPR spacers after phage exposure (*17*), which suggests that it is necessary for recognizing foreign nucleic acid and/or integrating the novel repeat-spacer unit. Cas1 appears to be a double-stranded DNA (dsDNA) endonuclease involved in the immunization process (*25*). It has also been proposed that Cas2 may act as a sequence-specific endoribonuclease that cleaves uracil-rich single-stranded RNAs (ssRNAs) (*26*). The mechanistic steps involved in invasive element recognition, novel repeat manufacturing, and spacer selection and integration into the CRISPR locus remain uncharacterized.

Although some Cas proteins are involved in the acquisition of novel spacers, others provide CRISPR-encoded phage resistance and interfere with invasive genetic elements. Mechanistically, although defense is spacer-encoded, the information that lies within the CRISPR repeat-spacer array becomes available to the Cas machinery through transcription. The CRISPR leader, defined as a low-complexity, A/T-rich, noncoding sequence, located immediately upstream of the first repeat, likely acts as a promoter for the transcription of the repeat-spacer array into a CRISPR transcript, the pre-crRNA (*13*, *27*). The full-length pre-crRNA is subsequently processed into specific small RNA molecules that correspond to a spacer flanked by two partial repeats (*27*–*29*). In *E. coli*, processing is achieved by a multimeric complex of Cas proteins named Cascade (CRISPR-associated complex for antiviral defense), which specifically cleaves the pre-crRNA transcript within the repeat sequence to generate small CRISPR RNAs, crRNAs (*28*). Similarly, in *Pyrococcus,* Cas6 is an endoribonuclease that cleaves the pre-crRNA transcript into crRNA units that include a partial [8-nucleotide (nt)] repeat sequence at the 5′ end, as part of the Cas-crRNA complex (*27*, *29*, *30*). The crRNAs seem to specifically guide the Cas interference machinery toward foreign nucleic acid molecules that match its sequence, which leads ultimately to degradation of the invading element (*30*). The involvement of *cas* genes in CRISPR defense was originally demonstrated when inactivating the CRISPR1-associated *csn1*-like gene (Fig. 1) resulted in loss of phage resistance despite the presence of matching spacers (*17*).

The observation that CRISPR spacers match both sense and antisense viral DNA led to the hypothesis that some CRISPR/Cas systems may target dsDNA, and this was confirmed by disruption of target DNA with an intron (the excision of which restores the native mRNA) on a plasmid that allows conjugation despite the presence of a matching CRISPR spacer (*20*). Conversely, the *Pyrococcus* CRISPR effector complex, a ribonucleoprotein complex that consists of crRNA and Cas proteins, targets invader RNA by complementary-dependent cleavage, in vitro (*30*). Given the large diversity of CRISPR/Cas systems in Bacteria and Archaea (*4*, *6*), it is likely that both DNA and RNA may be targets. More information is needed to establish and understand what the functional differences are among distinct CRISPR/Cas systems.

The initial hypothesis that CRISPR may mediate microbial immunity via RNA interference (RNAi) (*6*) is misguided. RNAi allows eukaryotic organisms exposed to foreign genetic material to silence the invading nucleic acid sequence before or after it integrates into the host chromosome, and/or to subvert cellular processes through a small interfering RNA guide (*31*). A key difference between RNAi and CRISPR-encoded immunity lies in the enzymatic machinery involved. Although both are mediated by a guide RNA in an inhibitory ribonucleoprotein complex, only Dicer, Slicer, and the RNA-induced silencing complex (RISC) may have analogous counterparts (*6*, *30*). Mechanistically, although the short RNA duplexes at the core of RNAi are typically 21 to 28 nt in length (*32*), crRNAs are larger, because they contain a CRISPR spacer (23 to 47 nt) flanked by partial repeats. Also, RNA-dependent transcription generating dsRNA and using the cleaved target RNA seen in RNAi have not been characterized in the CRISPR/Cas systems. In other ways, the sequence-specific and adaptive CRISPR/Cas systems share similarities with the vertebrate adaptive immune system, although CRISPR spacers are DNA-encoded and can be inherited by the progeny.

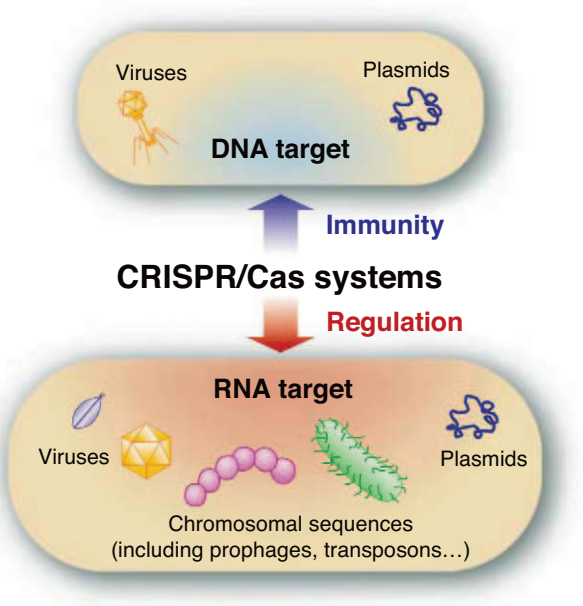


**Fig. 3.** CRISPR interference. The CRISPR/Cas systems may target either DNA or RNA to interfere with viruses, plasmids, prophages, or other chromosomally encoded sequences.

### Circumventing CRISPR-Based Immunity

Even though CRISPR can provide high levels of phage resistance, a relatively small proportion of viruses retain the ability to infect the "immunized" host. These viral particles have specifically mutated the proto-spacer (sequence within the invading nucleic acid that matches a CRISPR spacer), with a single point mutation that allows the viruses to overcome immunity, which indicates that the selective pressure imposed by CRISPR can rapidly drive mutation patterns in viruses (*17*, *18*, *23*). Analysis of phage sequences adjacent to proto-spacers revealed the presence of conserved sequences, called CRISPR motifs (*13*, *16*, *18*, *19*, *33*, *34*), or proto-spacer adjacent motifs (PAMs) (*35*). Phages may also circumvent the CRISPR/Cas system by mutating the CRISPR motif (*18*), which indicates that it is involved in CRISPR-encoded immunity. Additionally, CRISPR motif mutation can result in loss of phage resistance despite the presence of a matching CRISPR spacer (*34*). The absence of this motif in the CRISPR locus likely allows the system to act on the invading target DNA specifically and precludes an "autoimmune" response on the host chromosome (Fig. 2). Such a motif may not be necessary in CRISPR/Cas systems targeting RNA. Although proto-spacers seem to be randomly located on phage genomes, a given CRISPR spacer may be acquired independently by different lineages. It is thus tempting to speculate that CRISPR motifs also play a key role in the selection of spacers.

These mutations may have an impact on the amino acid sequence, as either nonsynonymous mutations or premature stop codons that truncate the viral protein (*18*). In addition to mutations, phages may also circumvent CRISPR-encoded immunity via deletion of the target sequence (*18*, *21*). This perhaps indicates a strong cost associated with circumventing the CRISPR/Cas systems. Alternative strategies that allow viruses to escape CRISPR, such as suppressors that could interfere with crRNAs biogenesis or Cas machinery remain uncovered. Defense tactics employed by viruses to circumvent the CRISPR/Cas systems are yet another critical difference between RNAi and CRISPR: Eukaryotic viruses may express inhibitors such as dsRNA-binding proteins that interfere with the RNA silencing machinery (*32*), which are yet to be identified in response to CRISPR, whereas microbial viruses specifically mutate or recombine (*21*) the sequence

corresponding to the CRISPR spacer or that of the PAM.

The impact of CRISPR on phage genomes is illustrated by extensive genome recombination events observed in environmental phage populations in response to CRISPR (*21*). This contrasts with the fact that acquisition of novel CRISPR spacers does not seem to have a fitness cost for the host, apart from maintaining the CRISPR/Cas system as active.

Although it seems intuitive that CRISPR loci should not be able to expand indefinitely (*21*, *36*), little is known about the parameters that define the optimal and maximum size of a CRISPR locus. Also, the fitness cost of CRISPR expansion in the host should be compared with that of CRISPR evasion in the virus populations, so as to determine whether prey or predators incur the higher evolutionary cost of this genetic warfare.

Although CRISPR loci primarily evolve via polarized addition of novel spacers at the leader end of the locus after phage exposure, internal spacer deletions have also been reported, likely occurring via homologous recombination between CRISPR repeats (*1*, *16*, *18*). Perhaps this allows the host to limit the expansion of the CRISPR locus so that the relative size of the locus does not increase to a detrimental level. The propensity of spacers located at the trailer end (opposite to the leader end) to be deleted preferentially would mitigate the loss of fitness associated with the deletion, because ancestral spacers would arguably provide resistance against viruses that were historically, but are not currently, present in the environment. The combination of locus expansion via spacer acquisition and contraction via spacer loss, in the context of rapid evolution in space and time because of viral predation, which generate a high level of spacer polymorphism, suggests that CRISPR loci undergo dynamic and rapid turnover on evolutionary time scales (*16*, *21*, *36*). Indeed, in microbes with an active system, CRISPR loci have been shown to be the most hypervariable genomic regions (*21*).

## Applications and Future Directions

A priori, the concurrent presence of distinct defense systems against foreign genetic elements in Bacteria and Archaea seems inefficient and redundant, although it might reflect functional preferences and increased fitness. Because all defense mechanisms have their advantages and caveats, the accumulation and combination of different systems would increase the selective pressure on invading elements and, consequently, could increase the chances of host survival by using multiple hurdles.

Because CRISPR spacers correspond to prior episodes of phage and plasmid exposure, they provide a historical and geographical—although limited—perspective as to the origin and paths of a particular strain, which may be used for ecological and epidemiological studies. Many intrinsic aspects of CRISPR-based immunity have provided avenues for industrial applications, including exploiting hypervariability for typing purposes, driving viral evolution, predicting and modulating virus resistance in domesticated microbes, and performing natural genetic tagging of proprietary strains. The inheritable nature of the CRISPR spacer content provides potential for perennial use of industrial microbes. Alternatively, the ability of CRISPR/Cas systems to impede the transfer of particular nucleic acid sequences (such as phage or plasmid DNA) into a host might be exploited via genetic engineering to specifically preclude the dissemination of undesirable genetic elements, such as antibiotic-resistance markers and genes harmful to humans and other living organisms. It may also be designed to limit the intracellular spread of mobile genetic elements such as insertion sequences and transposons. In addition to providing immunity, CRISPR/Cas systems that target RNA have the potential to affect the transcript stability of chromosomal elements (Fig. 3).

Although significant progress has been made in the last few years, many mechanistic aspects remain uncovered, notably vis-à-vis the immunization process (key elements involved in spacer selection and integration between repeats and/or possible involvement of degenerate infectious particles in building immunity) and the interference mechanism (other cellular components involved). Also, more knowledge is desirable regarding the elements necessary to have functional CRISPR/Cas systems and the basis for the absence of CRISPR in 60% of Bacteria.

### References and Notes


1. R. Jansen, J. D. Embden, W. Gaastra, L. M. Schouls, *Mol. Microbiol.* **43**, 1565 (2002).
2. R. Sorek, V. Kunin, P. Hugenholtz, *Nat. Rev. Microbiol.* **6**, 181 (2008).
3. J. van der Oost, M. M. Jore, E. R. Westra, M. Lundgren, S. J. Brouns, *Trends Biochem. Sci.* **34**, 401 (2009).
4. D. H. Haft, J. Selengut, E. F. Mongodin, K. E. Nelson, *PLOS Comput. Biol.* **1**, e60 (2005).
5. K. S. Makarova, L. Aravind, N. V. Grishin, I. B. Rogozin, E. V. Koonin, *Nucleic Acids Res.* **30**, 482 (2002).
6. K. S. Makarova, N. V. Grishin, S. A. Shabalina, Y. I. Wolf, E. V. Koonin, *Biol. Direct* **1**, 7 (2006).
7. V. Kunin, R. Sorek, P. Hugenholtz, *Genome Biol.* **8**, R61 (2007).
8. P. Horvath *et al.*, *Int. J. Food Microbiol.* **131**, 62 (2009).
9. I. Grissa, G. Vergnaud, C. Pourcel, *BMC Bioinformatics* **8**, 172 (2007).
10. R. K. Lillestøl, P. Redder, R. A. Garrett, K. Brügger, *Archaea* **2**, 59 (2006).
11. F. J. Mojica, C. Díez-Villaseñor, J. García-Martínez, E. Soria, *J. Mol. Evol.* **60**, 174 (2005).
12. J. S. Godde, A. Bickerton, *J. Mol. Evol.* **62**, 718 (2006).
13. R. K. Lillestøl *et al.*, *Mol. Microbiol.* **72**, 259 (2009).
14. C. Pourcel, G. Salvignol, G. Vergnaud, *Microbiology* **151**, 653 (2005).
15. A. Bolotin, B. Quinquis, A. Sorokin, S. D. Ehrlich, *Microbiology* **151**, 2551 (2005).
16. P. Horvath *et al.*, *J. Bacteriol.* **190**, 1401 (2008).
17. R. Barrangou *et al.*, *Science* **315**, 1709 (2007).
18. H. Deveau *et al.*, *J. Bacteriol.* **190**, 1390 (2008).
19. J. R. van der Ploeg, *Microbiology* **155**, 1966 (2009).
20. L. A. Marraffini, E. J. Sontheimer, *Science* **322**, 1843 (2008).
21. A. F. Andersson, J. F. Banfield, *Science* **320**, 1047 (2008).
22. V. Kunin *et al.*, *Genome Res.* **18**, 293 (2008).
23. J. F. Heidelberg, W. C. Nelson, T. Schoenfeld, D. Bhaya, N. Ahmed, *PLoS ONE* **4**, e4169 (2009).
24. N. L. Held, R. J. Whitaker, *Environ. Microbiol.* **11**, 457 (2009).
25. B. Wiedenheft *et al.*, *Structure* **17**, 904 (2009).
26. N. Beloglazova *et al.*, *J. Biol. Chem.* **283**, 20361 (2008).
27. C. Hale, K. Kleppe, R. M. Terns, M. P. Terns, *RNA* **14**, 2572 (2008).
28. S. J. Brouns *et al.*, *Science* **321**, 960 (2008).
29. J. Carte, R. Wang, H. Li, R. M. Terns, M. P. Terns, *Genes Dev.* **22**, 3489 (2008).
30. C. R. Hale *et al.*, *Cell* **139**, 945 (2009).
31. C. C. Mello, D. Conte Jr., *Nature* **431**, 338 (2004).
32. G. Meister, T. Tuschl, *Nature* **431**, 343 (2004).
33. S. A. Shah, N. R. Hansen, R. A. Garrett, *Biochem. Soc. Trans.* **37**, 23 (2009).
34. E. Semenova, M. Nagornykh, M. Pyatnitskiy, I. I. Artamonova, K. Severinov, *FEMS Microbiol. Lett.* **296**, 110 (2009).
35. F. J. Mojica, C. Díez-Villaseñor, J. García-Martínez, C. Almendros, *Microbiology* **155**, 733 (2009).
36. G. W. Tyson, J. F. Banfield, *Environ. Microbiol.* **10**, 200 (2008).



37. We thank our colleagues P. Boyaval, C. Fremaux, D. Romero, and E. Bech Hansen for their support and scientific contributions, and S. Moineau, V. Siksnys, and J. Banfield for their insights and expertise. This work was supported by Danisco A/S. P.H. and R.B. have submitted patent applications relating to various uses of CRISPR.

10.1126/science.1179555

# Punishers Benefit From Third-Party Punishment in Fish

Nichola J. Raihani,[1]* Alexandra S. Grutter,[2] Redouan Bshary[3]

Human studies show that uninvolved bystanders often pay to punish defectors (*1*, *2*). Such behavior has typically been interpreted in terms of group-level benefits (*3*) despite theoretical predictions that third-party punishment can yield individual benefits to the punisher (*4*). Here, we show that male cleaner fish, *Labroides dimidiatus*, punish their female partners if females cheat while inspecting model clients. Punishment promotes female cooperation, yielding direct foraging benefits to the male. This finding demonstrates empirically that third-party punishment can evolve via self-serving tendencies.

When servicing clients, cleaners either cooperate by removing ectoparasites or cheat by taking a bite of mucus. Cleaners prefer to eat mucus (*5*) but risk clients terminating the interaction if they do (*6*). The conflict of interest between cleaner and client is less pronounced during inspections by cleaner pairs than during singleton inspections (*7*). Increased service quality during pair inspections was interpreted as resulting from female cooperation, both under natural conditions and in the laboratory where Plexiglas (acrylic plastic) plates serve as model clients. Larger males regularly chased smaller female partners if females caused clients to leave, particularly in the laboratory (*7*). This male behavior is peculiar because clients, not males, are the victims of biting females. Despite this fact, it is possible that male chasing could cause females to behave more cooperatively in future interactions. If males benefit personally through increased foraging success, then the males' behavior represents third-party punishment that evolves via self-regarding, rather than altruistic, tendencies.

Cleaners were trained to feed off model clients (Plexiglas plates) containing two food types: preferred prawn and less-preferred fish flake (*8*). Eating prawn corresponded to cheating the client by eating mucus, whereas eating flake corresponded to cooperating by removing ectoparasites. Eating prawn resulted in the immediate removal of the plate. We replicated earlier results (*7*) that males more often chased females when the latter's behavior caused plate removal (Wilcoxon signed-rank test, $n = 8$, $V$ (rank sum of positive values of $x = y$) $= 21$, $P = 0.036$). After being chased, females were less likely to eat prawn again in the second plate presentation 60 s later (Wilcoxon signed-rank test, $n = 8$, $V = 34$, $P = 0.030$; Fig. 1A) and fed against their preference, eating a higher ratio of flake to prawns (Wilcoxon signed-rank test, $n = 8$, $V = 36$, $P = 0.008$; Fig. 1B). This allowed males to increase their food intake in the second presentation (Wilcoxon signed-rank test, $n = 8$, $V = 28$, $P = 0.02$; Fig. 1C). Conversely, when chasing was prevented with a temporary partition, females that cheated in the first presentation were equally likely to cheat in the second one (Wilcoxon signed-rank test, $n = 8$, $V = 11$, $P = 0.67$; Fig. 1A) and did not eat a higher ratio of flake to prawn items (Wilcoxon signed-rank test, $n = 8$, $V = 8$, $P = 0.35$; Fig. 1B), and male foraging efficiency did not improve (Wilcoxon signed-rank test, $n = 8$, $V = 17.5$, $P = 1.0$; Fig. 1C). In nature, male cleaners may benefit if they punish cheating females, even though clients are the primary victims. The establishment of self-serving third-party punishment in response to personal losses may be a key step toward third-party punishment without current involvement as in humans (*2*).


**References and Notes**

1. E. Fehr, U. Fischbacher, *Evol. Hum. Behav.* **25**, 63 (2004).
2. E. Fehr, S. Gächter, *Nature* **415**, 137 (2002).
3. R. Boyd, H. Gintis, S. Bowles, P. J. Richerson, *Proc. Natl. Acad. Sci. U.S.A.* **100**, 3531 (2003).
4. K. Jaffe, *Acta Biotheor.* **52**, 155 (2004).
5. A. S. Grutter, R. Bshary, *Proc. Biol. Sci.* **270** (suppl. 2), S242 (2003).
6. R. Bshary, A. S. Grutter, *Anim. Behav.* **63**, 547 (2002).
7. R. Bshary, A. S. Grutter, A. S. T. Willener, O. Leimar, *Nature* **455**, 964 (2008).
8. Materials and methods are available as supporting material on *Science* Online.


9. We thank M. Cant, A. Ridley, and A. Thornton for commenting on earlier versions of this manuscript and L. Brun, A. Bshary, A. Pinto, D. Rappaz, and M. Soares for assistance in the field. N.J.R. is funded by the Zoological Society of London, R.B. by the Swiss Science Foundation, and A.S.G. by the University of Queensland.


**Supporting Online Material**

www.sciencemag.org/cgi/content/full/327/5962/171/DC1
Materials and Methods
Fig. S1

8 October 2009; accepted 23 November 2009
10.1126/science.1183068

[1]Institute of Zoology, Zoological Society of London, Regent's Park, London NW1 4RY, UK. [2]Institut de Biologie, Universitè de Neuchâtel, CH-2009 Neuchâtel, Switzerland. [3]School of Biological Sciences, The University of Queensland, Brisbane Qld 4072, Australia.

*To whom correspondence should be addressed. E-mail: nichola.raihani@ioz.ac.uk

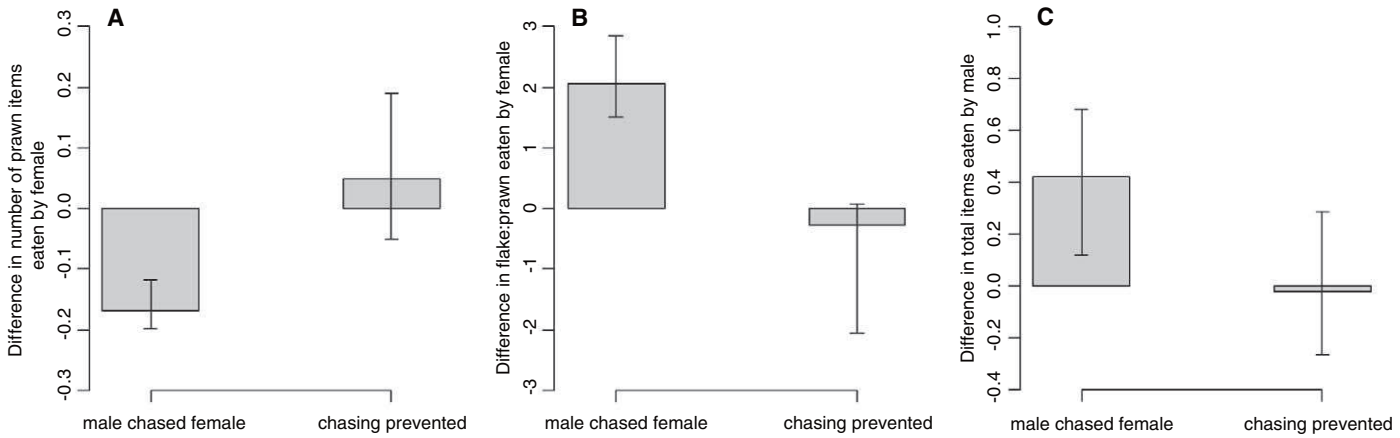


**Fig. 1.** Median difference according to treatment in (**A**) the number of prawn items eaten by females, (**B**) the ratio of flake to prawn items eaten by females, and (**C**) the total number of food items eaten by the male. For each pair, we first calculated (A) mean number of prawn items female ate, (B) mean ratio of flake to prawn items female ate, and (C) mean number of food items male ate in first and second presentations, respectively. Differences for each pair were calculated by subtracting mean (presentation one) from mean (presentation two). The median of these differences and the interquartile range were then calculated and are presented in the figure (gray boxes and bars, respectively).

# Phosphorylation of H2A by Bub1 Prevents Chromosomal Instability Through Localizing Shugoshin

Shigehiro A. Kawashima,[1] Yuya Yamagishi,[1,2]* Takashi Honda,[1,3]* Kei-ichiro Ishiguro,[1] Yoshinori Watanabe[1,2,3]†

Bub1 is a multi-task protein kinase required for proper chromosome segregation in eukaryotes. Impairment of Bub1 in humans may lead to chromosomal instability (CIN) or tumorigenesis. Yet, the primary cellular substrate of Bub1 has remained elusive. Here, we show that Bub1 phosphorylates the conserved serine 121 of histone H2A in fission yeast *Schizosaccharomyces pombe*. The *h2a-SA* mutant, in which all cellular H2A-S121 is replaced by alanine, phenocopies the *bub1* kinase-dead mutant (*bub1-KD*) in losing the centromeric localization of shugoshin proteins. Artificial tethering of shugoshin to centromeres largely restores the *h2a-SA* or *bub1-KD*–related CIN defects, a function that is evolutionally conserved. Thus, Bub1 kinase creates a mark for shugoshin localization and the correct partitioning of chromosomes.

The precise partition of chromosomes to daughter cells is essential for maintaining the integrity of genomes (*1*, *2*). When sister chromatid kinetochores are captured by spindle microtubules from opposite poles (bipolar attachment), sister chromatids are held together by the cohesin complex (*3*–*5*). The shugoshin protein phosphatase 2A (PP2A) complex protects centromeric cohesin during mitotic prophase in animal cells and more generally during meiosis I (*6*–*8*). When all sister chromatids have achieved biorientation, the anaphase-promoting complex (APC)–dependent degradation of securin liberates separase, which cleaves the cohesin subunit Rad21 (or Rec8 in meiosis), resulting in the separation of sister chromatids (*3*, *4*, *9*). The spindle assembly checkpoint (SAC) senses unattached kinetochores or a lack of tension and, by inhibiting the APC, prevents premature entry to anaphase. Aurora B destabilizes erroneous attachments and activates the SAC, which monitors the lack of tension (*10*, *11*). Shugoshin also loads the Aurora B complex to centromeres and ensures the bipolar attachment of kinetochores (*12*–*14*).

The conserved SAC protein kinase Bub1 is a tumor suppressor (*15*, *16*). The N-terminal nonkinase domain of Bub1 recruits SAC components to kinetochore, whereas Bub1 kinase activity plays a role in chromosome congression and an auxiliary role in SAC activation (*17*–*22*). The centromeric localization of shugoshin seems to depend on Bub1 (*14*, *23*–*26*). Although several candidates for Bub1 substrates have been suggested (*14*, *22*, *27*), the canonical substrate still remains to be identified even in genetically tractable organisms such as yeast. Therefore, the molecular entity of the downstream of Bub1 remains a longstanding enigma and controversial issue.

**Bub1 phosphorylates H2A Ser$^{121}$.** To identify substrates of the Bub1 kinase, we prepared a chromatin fraction from a fission yeast cell extract and mixed it with [$\gamma$-$^{32}$P] adenosine 5′-triphosphate (ATP) and recombinant Bub1 protein (*28*). A major phosphorylation was detected in the ~15 kDa range, close to histone H2A and H2B (Fig. 1A). This phosphopeptide was precipitated by an antibody to H2A (Fig. 1B). We confirmed this by tagging endogenous H2A with FLAG (H2Aα and H2Aβ, encoded by *hta1*$^+$ and *hta2*$^+$, were both tagged) and immunoblotting the major phosphopeptide, which was migrated more slowly in the *h2a*$^+$*-flag* strain (Fig. 1C). Recombinant H2A proteins are efficiently phosphorylated by Bub1 but not by Aurora B in vitro (Fig. 1D). Phosphorylation by Bub1 is abolished in H2A lacking the C-terminal tail but not in H2A lacking the N-terminal tail (fig. S1). Amino acid substitution and phospho–amino acid analysis identified Ser 121 as the phosphorylation site of H2A by Bub1 in vitro (Fig. 1, E and F). Antibodies that specifically recognize phosphorylated H2A-S121 (H2A-pS121) gave an H2A-pS121 signal in wild-type cells. This signal was abolished in cell extracts prepared from *h2a-SA* cells, in which Ser 121 is replaced with alanine (H2A-S121A) in both the *hta1*$^+$ and *hta2*$^+$ genes (Fig. 1G). We made a kinase–dead point mutation allele of *bub1* (*bub1-KD*) (fig. S2) and examined the phosphorylation of H2A-S121 in cell extracts prepared from *bub1-KD* cells. H2A-S121 phosphorylation was completely abolished in *bub1-KD* cells, although a similar amount of H2A was detected (Fig. 1G). Thus, H2A-S121 is an in vivo substrate of Bub1 kinase in fission yeast.

***h2a-SA* phenocopies *bub1-KD*.** Although *h2a-SA* cells are viable, they show a similar level of hypersensitivity to the microtubule-destabilizing drug thiabendazole (TBZ) as *bub1-KD* cells but to a lesser extent than *bub1*Δ cells (Fig. 2A). *bub1-KD* cells, but not *bub1*Δ cells, arrested at prometaphase when spindle formation was abolished (Fig. 2B). However, when sister chromatid cohesion was inactivated and thus tension was

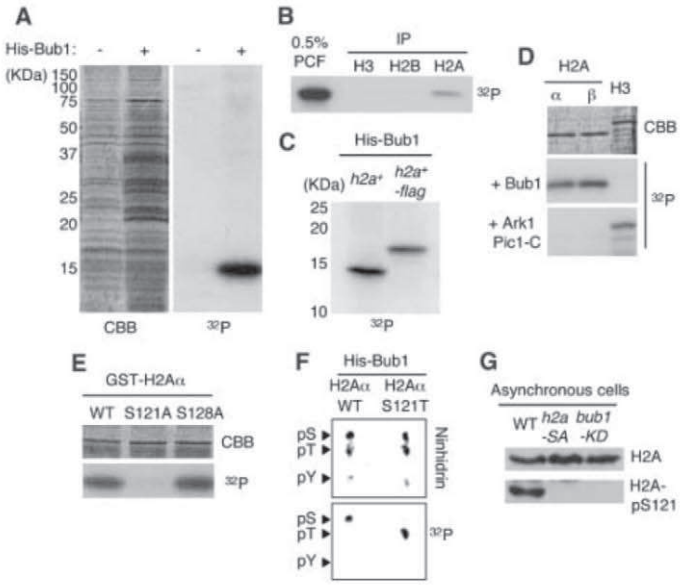


**Fig. 1.** H2A-S121 is phosphorylated by Bub1. (**A**) Chromatin fractions were incubated with or without recombinant His-Bub1 in the presence of [$\gamma$-$^{32}$P]ATP. The incorporation of the radioactive phosphate group was visualized by means of autoradiography ($^{32}$P), and protein loading was analyzed through staining with Coomassie Brilliant Blue (CBB). (**B**) The phosphorylated chromatin fraction (PCF) was denatured and immunoprecipitated with the indicated antibodies. (**C**) Chromatin fractions from *h2a*$^+$ or *h2a*$^+$*-flag* cells were phosphorylated as in (A). (**D**) Recombinant H2Aα, H2Aβ, and H3 were phosphorylated with His-Bub1 or GST-Ark1 and GST-Pic1-C. (**E**) The indicated mutants of GST-H2Aα were phosphorylated with His-Bub1. (**F**) Phospho–amino acid analysis of H2Aα and H2Aα-S121T phosphorylated by Bub1. (**G**) Cell extracts prepared from the indicated cells were immunoblotted for H2A-pS121 and H2A.

[1]Laboratory of Chromosome Dynamics, Institute of Molecular and Cellular Biosciences, University of Tokyo, Yayoi, Tokyo 113-0032, Japan. [2]Graduate Program in Biophysics and Biochemistry, Graduate School of Science, University of Tokyo, Yayoi, Tokyo 113-0032, Japan. [3]Graduate School of Agricultural and Life Science, University of Tokyo, Yayoi, Tokyo 113-0032, Japan.

*These authors contributed equally to this work.
†To whom correspondence should be addressed. E-mail: ywatanab@iam.u-tokyo.ac.jp

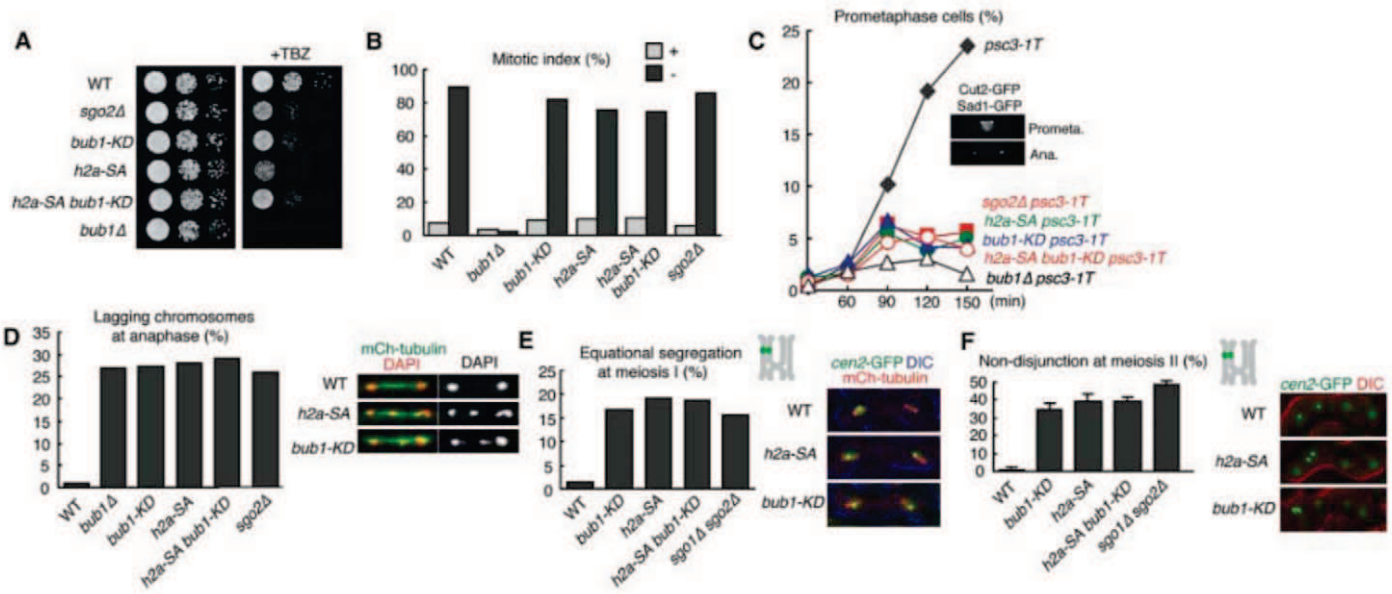


**Fig. 2.** Similar chromosomal instability (CIN) defects of *bub1-KD*, *h2a-SA*, and shugoshin mutants. (**A**) Serial dilution assay (12.5 μg/ml TBZ). (**B**) The indicated cells carrying a mutation of β-tubulin (*nda3-KM311*) were cultured at permissive temperature (+) or restrictive temperature (–) and scored for mitotic index ($n$ > 200 cells). (**C**) The indicated temperature-sensitive cohesin mutants (*psc3-1T*) were arrested at the $G_1$/S phase by adding hydroxyurea (HU) and released by increasing the temperature. Prometaphase (spindle pole body–duplicated and securin/Cut2 positive) cells were counted at each time point ($n$ > 200 cells). (**D**) The indicated strains expressing mCherry-Atb2 (α2-tubulin) were examined for frequencies of lagging chromosomes in anaphase cells ($n$ > 100 cells). Examples are shown at the right. (**E**) One of the homologs marked with *cen2*–green fluorescent protein (GFP) was monitored for segregation during meiosis I in the indicated zygotes. The number of cells that had undergone equational segregation in meiosis I was examined by monitoring metaphase II cells ($n$ > 100 zygotes). (**F**) One of the homologs marked with *cen2*-GFP was monitored for segregation during meiosis II in the indicated zygotes ($n$ > 200 zygotes).

**Fig. 3.** Forced enrichment of shugoshins in centromeres suppresses the CIN defects of *bub1-KD* or *h2a-SA* cells. (**A**) The signals of Sgo2-GFP expressed from the endogenous promoter were measured in metaphase in the indicated cells. Error bars represent SEM ($n$ = 16 cells). (**B**) Sgo1-GFP expressed from the endogenous promoter was detected in metaphase I in the indicated cells. The metaphase I spindle was visualized with mCherry-Atb2. Sgo1 signals were detected only in wild-type cells ($n$ > 50 zygotes). (**C**) The indicated *pcs3-1T* strains were arrested at the $G_1$/S phase and released by raising the temperature. Prometaphase cells were counted at each time point ($n$ > 200 cells). (**D**) The indicated cells were examined for frequencies of lagging chromosomes at anaphase ($n$ > 100 cells). (**E**) The signal intensity of Ark1-GFP in metaphase cells was measured. Error bars represent SEM ($n$ > 25 cells). (**F**) One of the homologs marked with *cen2*-GFP was monitored for segregation during meiosis II in the indicated zygotes ($n$ > 200 zygotes). (**G**) Par1-mCherry was detected at metaphase I. (**H**) Schematic depiction of the Bub1 pathway regulating chromosome segregation.

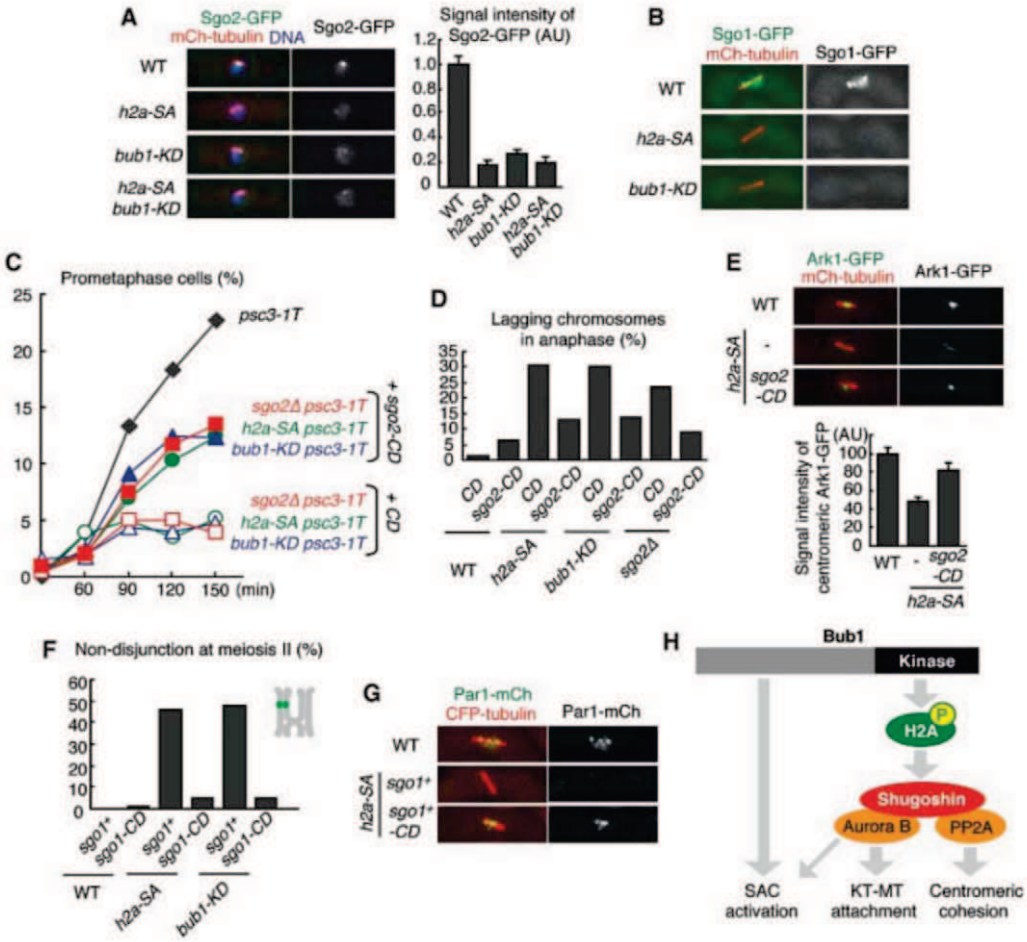

abolished between sister chromatids, *bub1-KD* cells showed the same defect in activating the SAC as *bub1*Δ cells (Fig. 2C). Thus, although the N-terminal non-kinase domain of Bub1 may fully contribute to the SAC, the kinase activity plays a limited role in the SAC activation. In this regard, *h2a-SA* cells behave exactly like *bub1-KD* cells (Fig. 2, B and C). Bub1 is required for the proper attachment of the kinetochore to microtubules (*29*), which was similarly impaired in both *bub1-KD* and *bub1*Δ cells (Fig. 2D), implying that the attachment is predominantly governed by the kinase activity rather than non-kinase function of Bub1. *h2a-SA* cells show similar defects in attachment (Fig. 2D).

In meiosis I, sister kinetochores are captured from the same pole (monopolar attachment), whereas homologous chromosomes are captured from the opposite poles. Bub1 ensures monopolar attachment by preventing merotelic attachment of paired sister kinetochores (*30*). At anaphase I, sister chromatid cohesin (or Rec8 cohesin) is released only along the arms, whereas centromeric cohesin is persistent, which ensures faithful disjunction at meiosis II. Bub1 is required for this protection of Rec8 cohesin at centromeres (*31*). We confirmed that *bub1-KD* cells display defects in the monopolar attachment at meiosis I (Fig. 2E) and in the centromeric protection of Rec8 cohesin (fig. S3), which results in nondisjunction at meiosis II (Fig. 2F). *h2A-SA* cells show nearly identical defects in monopolar attachment and centromeric protection (Fig. 2, E and F), whereas the phospho-mimic *h2a-SE* mutation suppresses the defect of centromeric protection in *bub1-KD* cells (fig. S4). Because the *bub1-KD h2a-SA* double mutant shows no additive defects in either mitotic or meiotic chromosome segregation (Fig. 2), these results argue that H2A-S121 phosphorylation and Bub1 kinase activity act in the same pathway and that H2A is a predominant cellular substrate for Bub1 kinase in fission yeast.

**H2A-S121 phosphorylation regulates shugoshin localization.** Bub1 is required for the localization of shugoshin (*14*, *23*–*26*, *32*), and H2A-pS121 might mediate this linkage. Fission yeast shugoshin Sgo2 is expressed in both mitosis and meiosis and is required for loading the Aurora B complex to centromeres, preventing merotelic attachment, and activating the SAC that senses lack of tension (*12*, *13*, *30*), whereas Sgo1 is meiosis-specific and required for loading PP2A and protecting centromeric cohesion presumably by dephosphorylating cohesin (*6*, *7*). The centromeric localization of Sgo2 is abolished in *h2a-SA* cells, such as in *bub1-KD* cells, during both mitosis and meiosis (Fig. 3A and fig. S5), and the mitotic defects in the SAC and kinetochore attachment of *h2a-SA* or *bub1-KD* cells are reproduced in *sgo2*Δ cells (Fig. 2, B to D). Similarly, the localization of meiosis-specific Sgo1 is abolished in *bub1-KD* or *h2a-SA* zygotes (Fig. 3B), accounting for the nearly identical defects in centromeric protection during meiosis

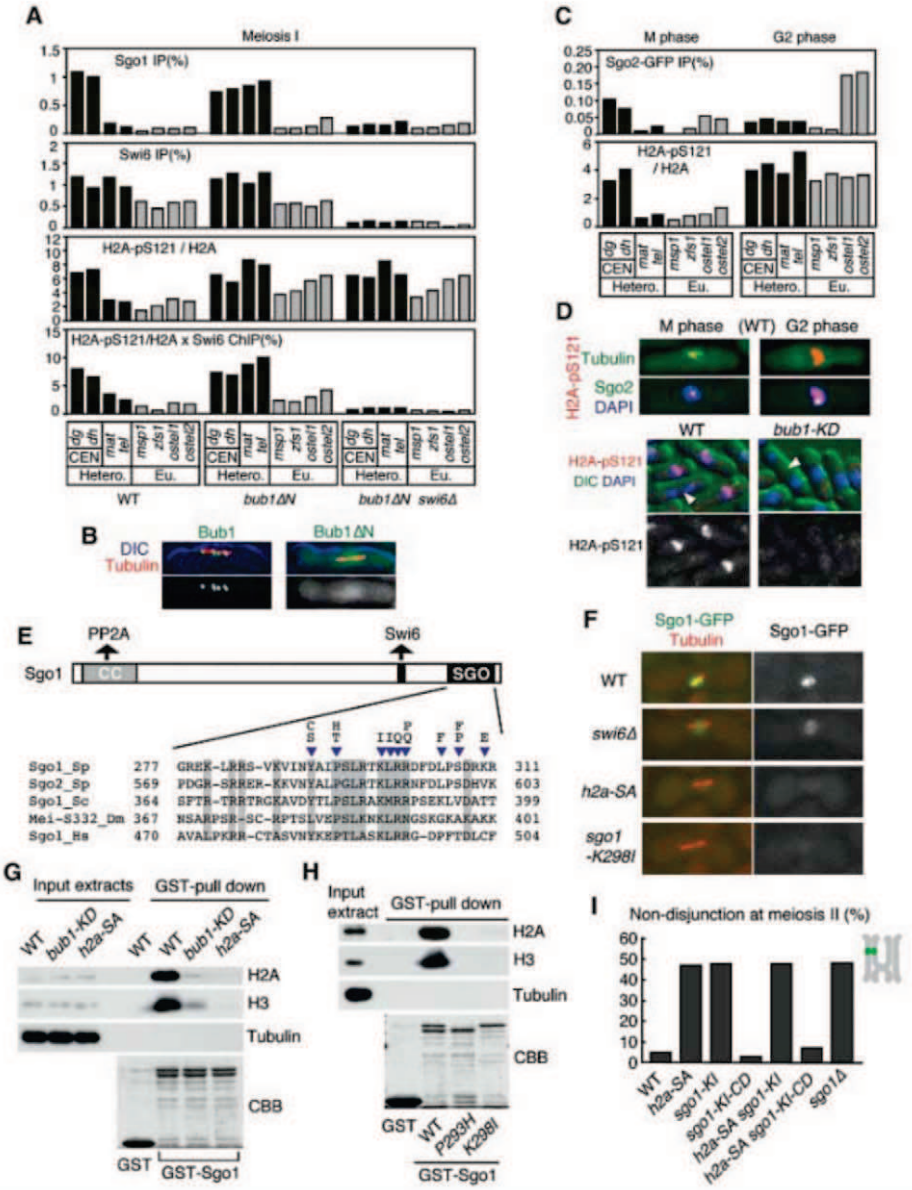


**Fig. 4.** Association between the SGO motif and nucleosomes containing H2A-pS121 is required for the chromosomal localization of shugoshin. (**A**) ChIP analysis was used to measure Sgo1, Swi6, H2A-pS121, and H2A throughout the heterochromatic centromere (*dg* and *dh*), mating type locus (*mat*), and telomere (*tel*); euchromatic arm region (*msp1* and *zfs1*); and outer subtelomere (*ostel1* and *ostel2*) in the indicated strains at metaphase I. Values of H2A-pS121/H2A multiplied by Swi6 ChIP (in percent) are compared with those of Sgo1 ChIP (in percent), revealing a good correlation along the chromosome. (**B**) Bub1-GFP and Bub1ΔN-GFP were detected in cells at metaphase I. (**C**) ChIP analysis was used to measure Sgo2, Swi6, H2A-pS121, and H2A in asynchronous ($G_2$) or M phase–arrested (M) *nda3-KM311* cells. (**D**) Immunostaining for Sgo2, H2A-pS121, tubulin, and DNA in wild-type cells (top) and for H2A-pS121 and DNA in the indicated cells (bottom). Arrowheads indicate anaphase cells. (**E**) A schematic of the Sgo1 protein showing the PP2A-interacting coiled-coil region (CC), Swi6/HP1–interacting motif (black box), and SGO motif (SGO). Arrowheads indicate the mutations isolated in a genetic screening (fig. S13), which abolish Sgo1 localization. (**F**) Sgo1 localization was examined at metaphase I in the indicated strains. (**G**) Cell extracts prepared from the indicated strains were pulled down with GST-Sgo1 or GST and analyzed by means of immunoblotting with antibodies to H3, H2A, and tubulin. Input extracts are also shown (0.5%). (**H**) Cell extracts prepared from wild-type cells were pulled down with the indicated Sgo1 mutant proteins fused with GST and analyzed as in (G). (**I**) One of the homologs marked with *cen2*-GFP was monitored for segregation during meiosis II in the indicated zygotes at 26.5°C ($n$ > 200 zygotes).

of these mutants (Fig. 2F and fig. S3). Consistently, the centromeric localization of shugoshin effectors Aurora B and PP2A is impaired in *h2a-SA* and *bub1-KD* cells such as in shugoshin-deleted cells (fig. S6). We conclude that shugoshin localization and functions are largely abolished in *h2a-SA* cells as well as in *bub1-KD* cells.

If localization of shugoshin is the major function of H2A-S121 phosphorylation, then forced localization of Sgo1 and Sgo2 should restore the defects in *h2a-SA* or *bub1-KD* cells. We fused Sgo1 and Sgo2 C-terminal ends to the chromo domain (CD), which binds to Lys-9–methylated histone H3 principally located at the centromeric heterochromatin. Sgo2-CD, which localizes at centromeres in the absence of H2A-S121 phosphorylation (fig. S7), partially (~60%) restored the defects in the SAC and kinetochore attachment in *h2a-SA* and *bub1-KD* cells during mitosis (Fig. 3, C and D). Likewise, the expression of Sgo2-CD partially (~60%) complements *sgo2*Δ (Fig. 3, C and D). Given that Sgo2 is mainly required for the centromeric localization of Aurora B and that this localization is indeed restored by Sgo2-CD in *h2a-SA* cells (Fig. 3E), our results imply that one of the functions of Bub1 kinase in vivo is the localization and/or activation of Aurora B at centromeres, which regulates attachment and the SAC. Moreover, nondisjunction at meiosis II, which originates from defects in centromeric protection during meiosis I, was fully restored in *h2a-SA* or *bub1-KD* cells by expressing Sgo1-CD and restoring PP2A localization at centromeres (Fig. 3, F and G). Collectively, these results argue that the primary readout of Bub1 kinase activity in vivo is the localization of both Sgo1 and Sgo2 to centromeres, in which they recruit PP2A and Aurora B, respectively. H2A-pS121 is the principal mediator of the crucial link between Bub1 kinase and the shugoshin action.

**H2A-pS121 nucleosomes associate with shugoshin.** The centromeric localization of Sgo1 in meiosis I depends largely on the specific association with heterochromatin protein Swi6 (*Schizosaccharomyces pombe* HP1 homolog) (*33*). However, chromatin immunoprecipitation (ChIP) assay indicates that Swi6 localizes not only to the centromeric region but also to the mating type (*mat*) locus and telomeres (*34*), despite the fact that Sgo1 is exclusively centromeric (*33*) (Fig. 4A). H2A-S121 phosphorylation is most enriched at the centromere but not other heterochromatic regions at metaphase I (Fig. 4A), which is consistent with the fact that Bub1 localizes at centromeres at this stage (*31*) (fig. S8) and that this phosphorylation as well as Sgo1 localization are totally dependent on Bub1 (fig. S8). To delineate the requirement of H2A-S121 phosphorylation and heterochromatin

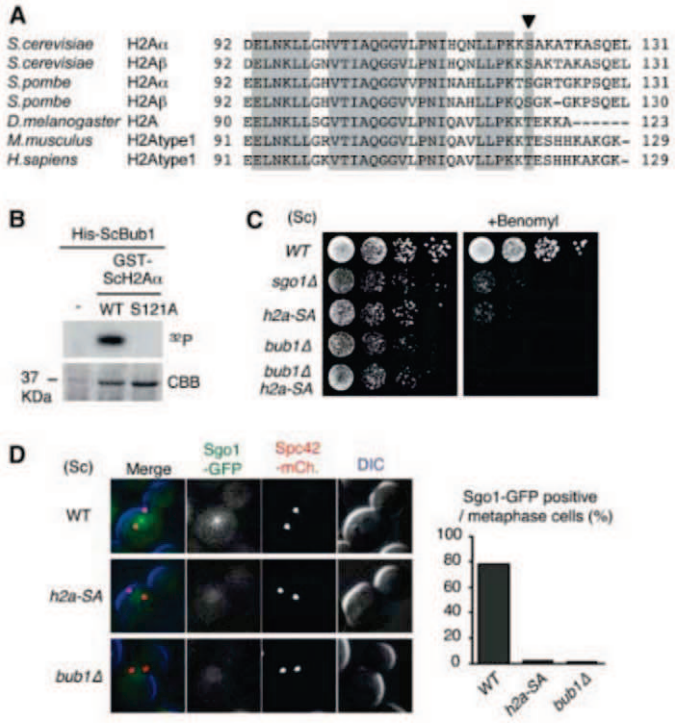


**Fig. 5.** Bub1-H2A-shugoshin pathway is conserved in budding yeast. (**A**) Alignment of the C-tail of histone H2A (amino acids are numbered excluding the first methionine). Ser 121 (arrowhead) and the preceding sequence are widely conserved among eukaryotes. (**B**) GST-ScH2A (wild-type or S121A) proteins were incubated with His-ScBub1 in the presence of [$\gamma$-$^{32}$P]ATP for 30 min at 30°C. (**C**) Serial dilution assay (10 μg/ml Benomyl). (**D**) ScSgo1-GFP was detected at metaphase (mitotic spindle indicated by separated Spc42 signals) in wild-type, *h2a-SA*, and *bub1* cells. Quantification of Sgo1-GFP–positive cells at metaphase is shown ($n$ > 100 cells).

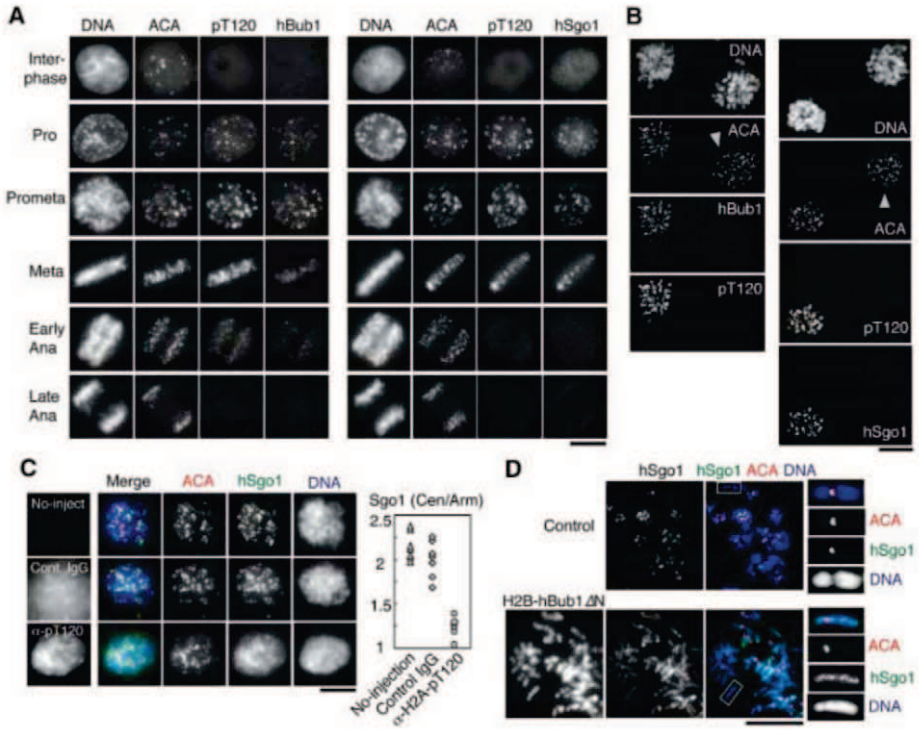


**Fig. 6.** Bub1-H2A-shugoshin pathway is conserved in humans. (**A**) Cycling HeLa cells were spun onto glass slides after fixation and stained with antibody to H2A-pT120 and anti-centromere antibodies (ACA) as well as antibodies to hBub1 (left) or hSgo1 (right). DNA was counterstained with Hoechst 33342. (**B**) HeLa cells treated with Bub1 siRNA were arrested at prometaphase by nocodazole and MG132 for 3 hours. Immunostaining was performed as in (A). Arrowheads indicate a Bub1-negative cell (left) and an H2A-pT120 negative cell (right), respectively. (**C**) Cells injected with antibody to H2A-pT120 or control immunoglobulin G (IgG) were arrested at prometaphase by nocodazole and stained with antibody to hSgo1 and ACA. The injected antibodies and DNA were also stained. The ratio of centromere and arm Sgo1 signals was quantified. (**D**) HeLa cells expressing H2B-Bub1ΔN-GFP were depleted for endogenous Bub1 by means of RNA interference, subjected to chromosome spreads, and stained with antibody to hSgo1 and ACA. Magnified images of paired sister chromatids are shown on the left. Scale bars, 10 μm.

for Sgo1 localization, we expressed a Bub1-kinase domain lacking the N-terminal regulatory region (Bub1ΔN), which showed uniform localization within the nucleus at metaphase I (Fig. 4B). ChIP assay indicated that the phosphorylation of H2A-S121 is elevated along the entire chromosome length in *bub1ΔN* cells at metaphase I (Fig. 4A). Consequently, Sgo1 localization, which is usually limited to the centromeres, extended to all heterochromatic regions including the *mat* locus and telomeres but not to euchromatic regions (Fig. 4A). The expanded Sgo1 localization was overall abolished by introducing the *swi6*Δ mutation (Fig. 4A). These results indicate that the localization of Sgo1 can largely be defined by a synergetic action of Swi6 and H2A-pS121 (Fig. 4A). The pattern of H2A-pS121 is invariable in *swi6*Δ cells (Fig. 4A and fig. S8), and heterochromatin formation is intact in *h2a-SA* cells (fig. S9), implying that these two pathways are assembled independently and converge into the regulation of the Sgo1 localization.

The regulation of Sgo2 localization is not identical to that of Sgo1 because Sgo2 locates at the outer subtelomeric region in the $G_2$ phase in a heterochromatin-independent manner (Fig. 4C and fig. S10) while accumulating at centromeres in the M phase, depending on Bir1 (a subunit of the chromosome passenger complex) (*12*, *13*). Crucially, however, the localization of Sgo2 in both $G_2$ and M phases is largely abolished in *bub1-KD* and *h2a-SA* cells (Fig. 3A and fig. S11). These results indicate that H2A-pS121 promotes the association of Sgo2 with chromatin, regardless of whether it is centromeric or outer subtelomeric. H2A-S121 is phosphorylated along the entire chromosome length in the $G_2$ phase, whereas it is limited to centromeres in the M phase (Fig. 4, C and D), and both phosphorylations are dependent on Bub1 (Fig. 4D and fig. S12). Thus, phosphorylation of H2A-S121 directs the chromosomal association of shugoshin, whereas additional factors such as heterochromatin, Bir1, or some outer subtelomeric chromatin may affect localization and timing. Enrichment of H2A-pS121 at centromeres during the M phase, which is carried out by the accumulation of Bub1, is crucial in order to restrain the shugoshin localization to centromeres at this stage.

Shugoshin family proteins, albeit conserved among all eukaryotes, share limited similarities in amino acid sequence in the basic region near the C terminus, which we now denote the SGO (shugoshin) motif (Fig. 4E). Screening for mutations that abolish Sgo1 localization (fig. S13), we identified several intragenic mutations, all of which mapped in the SGO motif (Fig. 4E). The mutant proteins preserved the ability to associate with Swi6 in the immunoprecipitation assay (fig. S14), which is consistent with the fact that the Swi6-interacting sequences locate outside the SGO motif of Sgo1 (*33*) (Fig. 4E). Analogous mutations within the SGO motif of Sgo2 abolished the chromatin localization (fig. S11). Although we could not detect the association of nucleosomes with Sgo1 in the immunoprecipitation assay, we could detect it in a pull-down assay, suggesting that their association is not stable. The glutathione *S*-transferase (GST)–Sgo1 protein pulls down the nucleosomes from cell extracts prepared from wild-type cells but not from cell extracts prepared from *bub1-KD* or *h2a-SA* cells (Fig. 4G). Moreover, the mutations in the SGO motif (Sgo1-P293H and -K298I) lost the ability to pull down the nucleosomes even from wild-type cell extracts (Fig. 4H). These results indicate that Sgo1 associates with nucleosomes containing H2A-pS121 through the conserved SGO motif, although further molecular details of the association remain to be studied. To delineate the requirement of the SGO motif for protein function, we fused Sgo1-K298I with the CD and expressed it from the endogenous promoter. Sgo1-K298I-CD can perform its full function in protecting cohesion, and this is also true in *h2a-SA* cells (Fig. 4I). These results argue that the conserved SGO motif is required exclusively for shugoshin localization.

**Conservation of the Bub1-H2A-shugoshin pathway.** The requirement of Bub1 for shugoshin localization is conserved in budding yeast *Saccharomyces cerevisiae* (*26*, *32*), which lacks the HP1 protein. Recombinant ScH2A was phosphorylated by Bub1 in vitro at the conserved Ser 121 (Fig. 5, A and B). To examine the conservation of the Bub1-H2A-shugoshin pathway, we constructed budding yeast *h2a-SA* strain by expressing mutant H2A-S121A from the low copy centromere-plasmid in cells, in which all H2A genes were deleted (*35*). Like budding yeast *Scsgo1*Δ cells (*36*), *Sch2a-SA* cells were viable and showed sensitivity to the spindle-poison benomyl, though to a lesser extent than *Scbub1*Δ cells (Fig. 5C). These results mirror those in fission yeast. Crucially, ScSgo1 localization was abolished in *Sch2a-SA* cells as well as in *Scbub1*Δ cells (Fig. 5D). Together, these results suggest that shugoshin localization and function are also mediated by Bub1 and H2A phosphorylation in budding yeast.

We next investigated the conservation of the Bub1 kinase pathway in mammals. Because human H2A is phosphorylated by hBub1 in vitro at the conserved Thr 120 (equivalent to yeast H2A-S121), we raised antibodies that recognize this phosphorylation (fig. S15). Immunostaining of HeLa cells indicated that H2A-pT120 colocalizes with hBub1, which together with hSgo1 accumulate at centromeres during prometa- and metaphase in the cell cycle (Fig. 6A). The staining of H2A-pT120 as well as hSgo1 is abolished selectively in hBub1-depleted cells, but not in hBub1-positive cells, after treatment with hBub1 small interfering RNA (siRNA) (Fig. 6B). The injection of antibody to H2A-pT120 interferes with the centromeric localization of hSgo1 (Fig. 6C), suggesting that H2A-pT120 plays a role in hSgo1 localization at centromeres. Moreover, when the Bub1 kinase domain (hBub1ΔN) was fused with H2B and ectopically localized on the chromosome arms in Bub1-depleted cells, H2A-T120 was extensively phosphorylated on the whole chromosome (fig. S16), indicating that the localization of hBub1 kinase usually defines the centromere-specific phosphorylation of H2A-T120. Accordingly, hSgo1 localized along the whole chromosome length in H2B-hBub1ΔN cells (Fig. 6D), indicating that H2A-pT120 plays a predominant role in defining shugoshin localization sites on the human chromosomes, although HP1 may contribute to the maintenance of shugoshin at centromeres (*33*). To examine the conservation in meiosis, we stained mouse spermatocytes to localize mBub1, H2A-pT120, and mSgo2 [a predominant shugoshin in meiotic cells (*37*, *38*)]. H2A-pT120 and mSgo2 accumulate at centromeres during prometa- and metaphase I, when mBub1 accumulates at centromeres (fig. S17). Collectively, these results suggest that H2A-pT120 is an in vivo substrate of Bub1 kinase in mammals and that shugoshin localization at centromeres depends on the Bub1-dependent phosphorylation of H2A-T120 in somatic cells and presumably in germ cells as well.

**Discussion.** We report here that the conserved C-tail of histone H2A is a primary cellular substrate of Bub1 kinase because almost all *bub1-KD* defects including the SAC, kinetochore attachment, and centromeric protection are precisely phenocopied in *h2a-SA* cells of fission yeast. Because most mitotic and meiotic defects associated with *bub1-KD* or *h2a-SA* are efficiently suppressed by tethering shugoshin proteins at centromeres, we reason that the centromeric localization of shugoshin is the ultimate readout of the kinase activity of Bub1 in fission yeast. Analyses of budding yeast and mammalian cells suggest that this cascade is evolutionally conserved. A previous study in *Drosophila* identified nucleosomal histone kinase-1 (NHK-1) as the kinase for H2A-T119 (equivalent to fission yeast H2A-S121) in vitro (*39*), although this kinase is not relevant to the phosphorylation of H2A-T119 in mitotic cells (*40*). Our study suggests that the mitotic kinase for H2A in *Drosophila* may be Bub1. Previous mutational analyses of budding yeast histone H2A suggest that H2A-S121 plays a role in DNA repair (*41*). Consistently, we found that *bub1-KD* and *h2a-SA* cells, but not *sgo2*Δ cells, show sensitivity to a DNA-damaging agent (fig. S18), implying that the phosphorylation of H2A-S121 by Bub1 plays an additional role in DNA repair during interphase. Our findings in fission yeast mitosis and meiosis spotlight a crucial link between H2A phosphorylation and chromosomal instability, which may lead to tumorigenesis or birth defects in humans, and therefore are useful for future studies in those fields.

**References and Notes**

1. K. W. Yuen, B. Montpetit, P. Hieter, *Curr. Opin. Cell Biol.* **17**, 576 (2005).
2. A. J. Holland, D. W. Cleveland, *Nat. Rev. Mol. Cell Biol.* **10**, 478 (2009).
3. K. Nasmyth, C. H. Haering, *Annu. Rev. Biochem.* **74**, 595 (2005).

4. J. M. Peters, A. Tedeschi, J. Schmitz, *Genes Dev.* **22**, 3089 (2008).
5. I. Onn, J. M. Heidinger-Pauli, V. Guacci, E. Unal, D. E. Koshland, *Annu. Rev. Cell Dev. Biol.* **24**, 105 (2008).
6. T. S. Kitajima *et al*., *Nature* **441**, 46 (2006).
7. C. G. Riedel *et al*., *Nature* **441**, 53 (2006).
8. Y. Watanabe, *Curr. Opin. Cell Biol.* **17**, 590 (2005).
9. F. Uhlmann, *Curr. Biol.* **13**, R104 (2003).
10. T. U. Tanaka, *Chromosoma* **117**, 521 (2008).
11. B. A. Pinsky, C. Kung, K. M. Shokat, S. Biggins, *Nat. Cell Biol.* **8**, 78 (2006).
12. V. Vanoosthuyse, S. Prykhozhij, K. G. Hardwick, *Mol. Biol. Cell* **18**, 1657 (2007).
13. S. A. Kawashima *et al*., *Genes Dev.* **21**, 420 (2007).
14. Y. Boyarchuk, A. Salic, M. Dasso, A. Arnaoutov, *J. Cell Biol.* **176**, 919 (2007).
15. B. T. Roberts, K. A. Farr, M. A. Hoyt, *Mol. Cell. Biol.* **14**, 8282 (1994).
16. K. Jeganathan, L. Malureanu, D. J. Baker, S. C. Abraham, J. M. van Deursen, *J. Cell Biol.* **179**, 255 (2007).
17. H. Sharp-Baker, R. H. Chen, *J. Cell Biol.* **153**, 1239 (2001).
18. C. D. Warren *et al*., *Mol. Biol. Cell* **13**, 3029 (2002).
19. T. Kiyomitsu, C. Obuse, M. Yanagida, *Dev. Cell* **13**, 663 (2007).
20. S. Yamaguchi, A. Decottignies, P. Nurse, *EMBO J.* **22**, 1075 (2003).
21. C. Klebig, D. Korinth, P. Meraldi, *J. Cell Biol.* **185**, 841 (2009).
22. G. L. Williams, T. M. Roberts, O. V. Gjoerup, *Cell Cycle* **6**, 1699 (2007).
23. T. S. Kitajima, S. A. Kawashima, Y. Watanabe, *Nature* **427**, 510 (2004).
24. Z. Tang, Y. Sun, S. E. Harley, H. Zou, H. Yu, *Proc. Natl. Acad. Sci. U.S.A.* **101**, 18012 (2004).
25. T. S. Kitajima, S. Hauf, M. Ohsugi, T. Yamamoto, Y. Watanabe, *Curr. Biol.* **15**, 353 (2005).
26. J. Fernius, K. G. Hardwick, *PLoS Genet.* **3**, e213 (2007).
27. Z. Tang, H. Shu, D. Oncel, S. Chen, H. Yu, *Mol. Cell* **16**, 387 (2004).
28. Materials and methods are available as supporting material on *Science* Online.
29. P. Bernard, K. Hardwick, J. P. Javerzat, *J. Cell Biol.* **143**, 1775 (1998).
30. S. Hauf *et al*., *EMBO J.* **26**, 4475 (2007).
31. P. Bernard, J. F. Maure, J. P. Javerzat, *Nat. Cell Biol.* **3**, 522 (2001).
32. B. M. Kiburz *et al*., *Genes Dev.* **19**, 3017 (2005).
33. Y. Yamagishi, T. Sakuno, M. Shimura, Y. Watanabe, *Nature* **455**, 251 (2008).
34. H. P. Cam *et al*., *Nat. Genet.* **37**, 809 (2005).
35. J. N. Hirschhorn, A. L. Bortvin, S. L. Ricupero-Hovasse, F. Winston, *Mol. Cell. Biol.* **15**, 1999 (1995).
36. V. B. Indjeian, B. M. Stern, A. W. Murray, *Science* **307**, 130 (2005).
37. J. Lee *et al*., *Nat. Cell Biol.* **10**, 42 (2008).
38. E. Llano *et al*., *Genes Dev.* **22**, 2400 (2008).
39. H. Aihara *et al*., *Genes Dev.* **18**, 877 (2004).
40. A. L. Brittle, Y. Nanba, T. Ito, H. Ohkura, *Exp. Cell Res.* **313**, 2780 (2007).
41. A. C. Harvey, S. P. Jackson, J. A. Downs, *Genetics* **170**, 543 (2005).
42. We thank S. Hauf for critically reading the manuscript, F. Winston and the Yeast Genetic Resource Center for yeast strains, H. Masumoto for methods, and S. Ihara for injection instructions. We also thank all the members of our laboratory for their valuable support and discussion. This work was supported in part by the Japan Society for the Promotion of Science Research Fellowship (to. S.A.K. and Y.Y.) and Grant-in-Aid for Young Scientists (to K.I.), the Global Centers of Excellence Program, and a Grant-in-Aid for Specially Promoted Research (to Y.W.) from the Ministry of Education, Culture, Sports, Science and Technology of Japan.

**Supporting Online Material**

www.sciencemag.org/cgi/content/full/1180189/DC1
Materials and Methods
Figs. S1 to S18
Table S1
References

5 August 2009; accepted 6 November 2009
Published online 19 November 2009;
10.1126/science.1180189
Include this information when citing this paper.



# Quantum Criticality in an Ising Chain: Experimental Evidence for Emergent $E_8$ Symmetry

**R. Coldea,[1]* D. A. Tennant,[2] E. M. Wheeler,[1]† E. Wawrzynska,[3] D. Prabhakaran,[1] M. Telling,[4] K. Habicht,[2] P. Smeibidl,[2] K. Kiefer[2]**

**Quantum phase transitions take place between distinct phases of matter at zero temperature. Near the transition point, exotic quantum symmetries can emerge that govern the excitation spectrum of the system. A symmetry described by the $E_8$ Lie group with a spectrum of eight particles was long predicted to appear near the critical point of an Ising chain. We realize this system experimentally by using strong transverse magnetic fields to tune the quasi–one-dimensional Ising ferromagnet $CoNb_2O_6$ (cobalt niobate) through its critical point. Spin excitations are observed to change character from pairs of kinks in the ordered phase to spin-flips in the paramagnetic phase. Just below the critical field, the spin dynamics shows a fine structure with two sharp modes at low energies, in a ratio that approaches the golden mean predicted for the first two meson particles of the $E_8$ spectrum. Our results demonstrate the power of symmetry to describe complex quantum behaviors.**

Symmetry is present in many physical systems and helps uncover some of their fundamental properties. Continuous symmetries lead to conservation laws; for example, the invariance of physical laws under spatial rotation ensures the conservation of angular momentum. More exotic continuous symmetries have been predicted to emerge in the proximity of certain quantum phase transitions (QPTs) (*1*, *2*). Recent experiments on quantum magnets (*3*–*5*) suggest that quantum critical resonances may expose the underlying symmetries most clearly. Remarkably, the simplest of systems, the Ising chain, promises a very complex symmetry, described mathematically by the $E_8$ Lie group (*2*, *6*–*9*). Lie groups describe continuous symmetries and are important in many areas of physics. They range in complexity from the U(1) group, which appears in the low-energy description of superfluidity, superconductivity, and Bose-Einstein condensation (*10*, *11*), to $E_8$, the highest-order symmetry group discovered in mathematics (*12*), which has not yet been experimentally realized in physics.

The one-dimensional (1D) Ising chain in transverse field (*10*, *11*, *13*) is perhaps the most-studied theoretical paradigm for a quantum phase transition. It is described by the Hamiltonian

$$H = \Sigma_i - JS_i^z S_{i+1}^z - hS_i^x \qquad (1)$$

where a ferromagnetic exchange $J > 0$ between nearest-neighbor spin-½ magnetic moments $\mathbf{S}_i$ arranged on a 1D chain competes with an applied external transverse magnetic field $h$. The Ising exchange $J$ favors spontaneous magnetic order along the $z$ axis ($|\uparrow\uparrow\uparrow \cdots \uparrow\rangle$ or $|\downarrow\downarrow\downarrow \cdots \downarrow\rangle$), whereas the transverse field $h$ forces the spins to point along the perpendicular $+x$ direction ($|\rightarrow\rightarrow\rightarrow \cdots \rightarrow\rangle$). This competition leads to two distinct phases, magnetically ordered and quantum paramagnetic, separated by a continuous transition at the critical field $h_C = J/2$ (Fig. 1A). Qualitatively, the magnetic field stimulates quantum tunneling processes between ↑ and ↓ spin states and these zero-point quantum fluctuations "melt" the magnetic order at $h_C$ (*10*).

To explore the physics of Ising quantum criticality in real materials, several key ingredients are required: very good one-dimensionality of the magnetism to avoid mean-field effects of higher dimensions, a strong easy-axis (Ising) character, and a sufficiently low exchange energy $J$ of a few meV that can be matched by experimentally attainable magnetic fields (10 T ~ 1 meV) to access the quantum critical point. An excellent model system to test this physics is the insulating quasi-1D Ising ferromagnet $CoNb_2O_6$ (*14*–*16*), where magnetic $Co^{2+}$ ions are arranged into near-isolated zigzag chains along the $c$ axis with strong easy-

[1]Clarendon Laboratory, Department of Physics, University of Oxford, Oxford OX1 3PU, UK. [2]Helmholtz-Zentrum Berlin für Materialien und Energie, Lise Meitner Campus, Glienicker Str. 100, D-14109 Berlin, Germany. [3]H. H. Wills Physics Laboratory, University of Bristol, Bristol BS8 1TL, UK. [4]ISIS, Rutherford Appleton Laboratory, Chilton, Didcot OX11 0QX, UK.

*To whom correspondence should be addressed. E-mail: r.coldea@physics.ox.ac.uk

†Present address: Helmholtz-Zentrum Berlin für Materialien und Energie, Lise Meitner Campus, Glienicker Str. 100, D-14109 Berlin, Germany.

axis anisotropy due to crystal field effects from the distorted $CoO_6$ local environment (Fig. 1B). Large single crystals can be grown (*17*), which is an essential precondition for measurement of the crucial spin dynamics with neutron scattering.

$CoNb_2O_6$ orders magnetically at low temperatures below $T_{N1}$ = 2.95 K, stabilized by weak interchain couplings. The chains order ferromagnetically along their length with magnetic moments pointing along the local Ising direction, contained in the crystal (*ac*) plane (*18*). To tune to the critical point, we apply an external magnetic field along the *b* axis, transverse to the local Ising axis. Figure 1C shows that the external field suppresses the long-range 3D magnetic order favored by the Ising exchange in a continuous phase transition at a critical field $B_C$ = 5.5 T.

Expected excitations for the model in Eq. 1 consist of (i) pairs of kinks, with the cartoon representation $|\uparrow\uparrow\downarrow\downarrow_z\ldots\rangle$, below $B_C$, and (ii) spin-flip quasiparticles $|\rightarrow\rightarrow\leftarrow\rightarrow_x\ldots\rangle$ above $B_C$. The kinks interpolate between the two degenerate ground states with spontaneous magnetization along the +*z* or –*z* axis, respectively. Neutrons scatter by creating a pair of kinks (Fig. 2A). The results in Fig. 2, B and C, show that in the ordered phase below $B_C$ the spectrum is a bow tie–shaped continuum with strongly dispersive boundaries and large bandwidth at the zone center ($L$ = 0), which we attribute to the expected two-kink states. This continuum increases in bandwidth and lowers its gap with increasing field, as the applied transverse field provides matrix elements for the kinks to hop, directly tuning their kinetic energy. Above $B_C$ a very different spectrum emerges (Fig. 2E), dominated by a single sharp mode. This is precisely the signature of a quantum paramagnetic phase. In this phase the spontaneous ferromagnetic correlations are absent, and there are no longer two equivalent ground states that could support kinks. Instead, excitations can be understood in terms of single spin reversals opposite to the applied field that cost Zeeman energy in increasing field. The fundamental change in the nature of quasiparticles observed here (compare Fig. 2, C and E) does not occur in higher-dimensional realizations of the quantum Ising model. The kinks are a crucial aspect of the physics in one dimension, and their spectrum of confinement bound states near the transition field will be directly related to the low-energy symmetry of the critical point.

The very strong dimensionality effects in 3D systems stabilize sharp spin-flip quasiparticles in both the ordered and paramagnetic phases, as indeed observed experimentally in the 3D dipolar-coupled ferromagnet $LiHoF_4$ (*19*, *20*). In contrast, weak additional perturbations in the 1D Ising model, in particular a small longitudinal field $-h_z\Sigma_i S_i^z$, should lead to a rich structure of bound states (*6*, *7*, *9*). Such a longitudinal field, in fact, arises naturally in the case of a quasi-1D magnet: In the 3D magnetically ordered phase at low temperature, the weak couplings between the magnetic chains can be replaced in a first approximation by a local, effective longitudinal mean field (*21*), which scales with the magnitude of the ordered moment $\langle \mathbf{S}^z \rangle$ [$h_z = \Sigma_\delta J_\delta \langle \mathbf{S}^z \rangle$ where the sum extends over all interchain bonds with exchange energy $J_\delta$]. If the 1D Ising chain is precisely at its critical point ($h = h_C$), then the bound states stabilized by the additional longitudinal field $h_z$ morph into the "quantum resonances" that are a characteristic fingerprint of the emergent symmetries near the quantum critical point. Nearly two decades ago, Zamolodchikov (*2*) proposed precisely

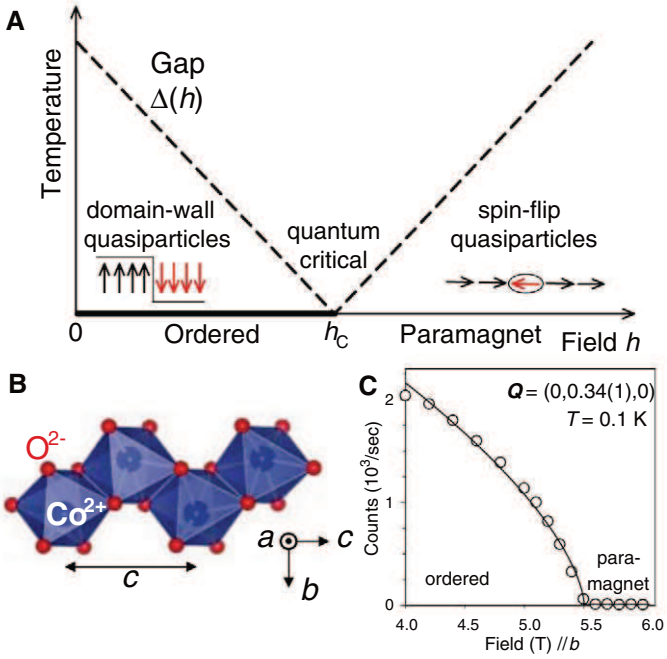


**Fig. 1.** (**A**) Phase diagram of the Ising chain in transverse field (Eq. 1). Spin excitations are pairs of domain-wall quasiparticles (kinks) in the ordered phase below $h_C$ and spin-flip quasiparticles in the paramagnetic phase above $h_C$. The dashed line shows the spin gap. (**B**) $CoNb_2O_6$ contains zigzag ferromagnetic Ising chains. (**C**) Intensity of the 3D magnetic Bragg peak as a function of applied field observed by neutron diffraction (*27*).

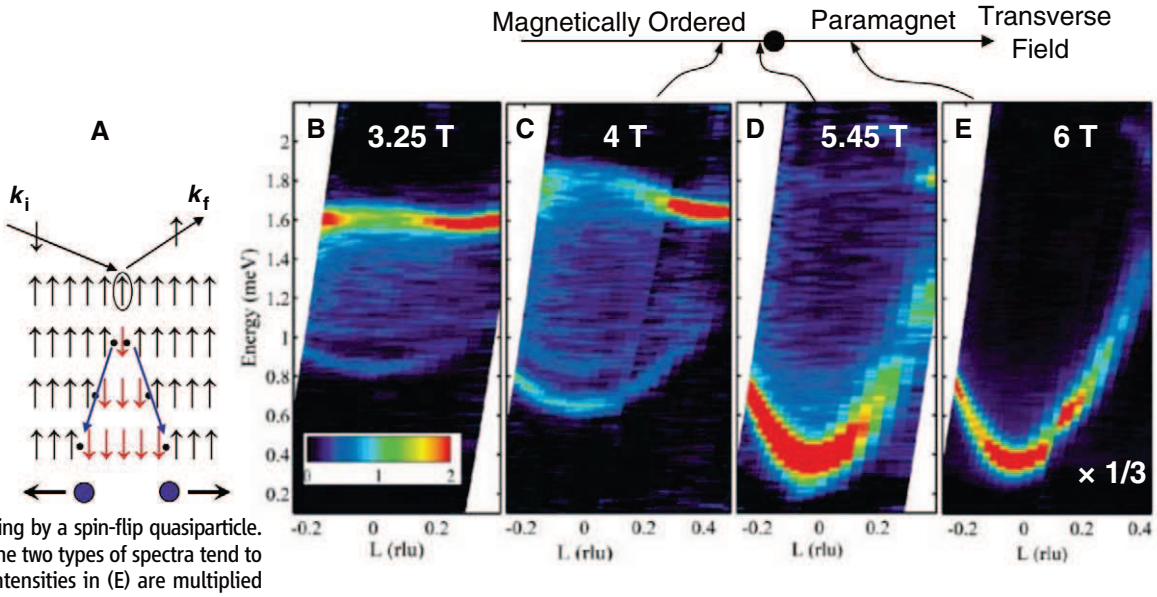


**Fig. 2.** (**A**) Cartoon of a neutron spin-flip scattering that creates a pair of independently propagating kinks in a ferromagnetically ordered chain. (**B** to **E**) Spin excitations in $CoNb_2O_6$ near the critical field as a function of wave vector along the chain (in rlu units of $2\pi/c$) and energy (*18*). In the ordered phase [(B) and (C)], excitations form a continuum due to scattering by pairs of kinks [as illustrated in (A)]; in the paramagnetic phase (E), a single dominant sharp mode occurs, due to scattering by a spin-flip quasiparticle. Near the critical field (D), the two types of spectra tend to merge into one another. Intensities in (E) are multiplied by $^1/_3$ to make them comparable to the other panels.

eight "meson" bound states (the kinks playing the role of quarks), with energies in specific ratios given by a representation of the $E_8$ exceptional Lie group (*2*). Before discussing the results near the QPT, we first develop a more sophisticated model of the magnetism in $CoNb_2O_6$ including confinement effects at zero field, where conventional perturbation theories are found to hold.

The zero-field data in Fig. 3A reveal a gapped continuum scattering at the ferromagnetic zone center ($L = 0$) due to kink pairs, which are allowed to propagate even in the absence of an external field. This is caused by sub-leading terms in the spin Hamiltonian. Upon cooling to the lowest temperature of 40 mK, deep in the magnetically ordered phase, the continuum splits into a sequence of sharp modes (Fig. 3B). At least five modes can be clearly observed (Fig. 3E), and they exist over a wide range of wave vectors and have a quadratic dispersion (open symbols in Fig. 3D). These data demonstrate the physics of kink confinement under a linear attractive interaction (*6*–*9*). In the ordered phase, kink propagation upsets the bonds with the neighboring chains (Fig. 3G) and therefore requires an energy cost $V(x)$ that grows linearly with the kink separation $x$, $V(x) = \lambda|x|$, where the "string tension" $\lambda$ is proportional to the ordered moment magnitude $\langle \mathbf{S}^z \rangle$ and the interchain coupling strength [$\lambda = 2h_z\langle \mathbf{S}^z \rangle/\tilde{\mathbf{c}}$, where $h_z = \Sigma_\delta J_\delta \langle \mathbf{S}^z \rangle$ is the longitudinal mean field of the interchain couplings and $\tilde{\mathbf{c}} = c/2$ is the lattice spacing along the chain].

The essential physics of confinement is apparent in the limit of small $\lambda$ for two kinks near the band minimum, where the one-kink dispersion is quadratic: $\varepsilon(k) = m_o + \hbar^2k^2/(2\mu)$. In this case, the Schrödinger's equation for the relative motion of two kinks in their center-of-mass frame is

$$-\frac{\hbar^2}{\mu}\frac{d^2\varphi}{dx^2} + \lambda|x|\varphi = (m - 2m_o)\varphi \qquad (2)$$

(*6*–*9*, *22*), which has only bound-state solutions with energies (also called masses)

$$m_j = 2m_o + z_j\lambda^{2/3}\left(\frac{\hbar^2}{\mu}\right)^{1/3} \qquad j = 1, 2, 3, \ldots \qquad (3)$$

The bound states are predicted to occur above the threshold $2m_o$ for creating two free kinks in a specific sequence given by the prefactors $z_n$, the negative zeros of the Airy function $\mathrm{Ai}(-z_n) = 0$, $z_j = 2.33, 4.08, 5.52, 6.78, 7.94$, etc. (*18*). The very nontrivial sequencing of the spacing between levels at the zone center agrees well with the measured energies of all five observed bound states (Fig. 3H), indicating that the weak confinement limit captures the essential physics.

A full modeling of the data throughout the Brillouin zone can be obtained (*18*) by considering an extension of Eq. 2 to finite wave vectors and adding a short-range interaction between kinks, responsible for stabilizing the observed bound state near the zone boundary $L = -1$. Interestingly, this is a kinetic bound state; that is, it is stabilized by virtue of the extra kinetic energy gained by two kinks if they hop together as a result of their short-range interaction, as opposed to the Zeeman ladder of confinement bound states (near $L = 0$), stabilized by the potential energy $V(x)$. The good agreement with the dispersion relations of all the bound states observed (Fig. 3D), as well as the overall intensity distribution (compare Fig. 3, B and F), shows that an effective model of kinks with a confinement interaction can quantitatively describe the complete spin dynamics.

Having established the behavior at zero field, we now consider the influence of the QPT at high field. Figure 4C shows that the excitation gap decreases upon approaching the critical field (as quantum tunneling lowers the energy of the kink quasiparticles), then increases again above $B_C$ in

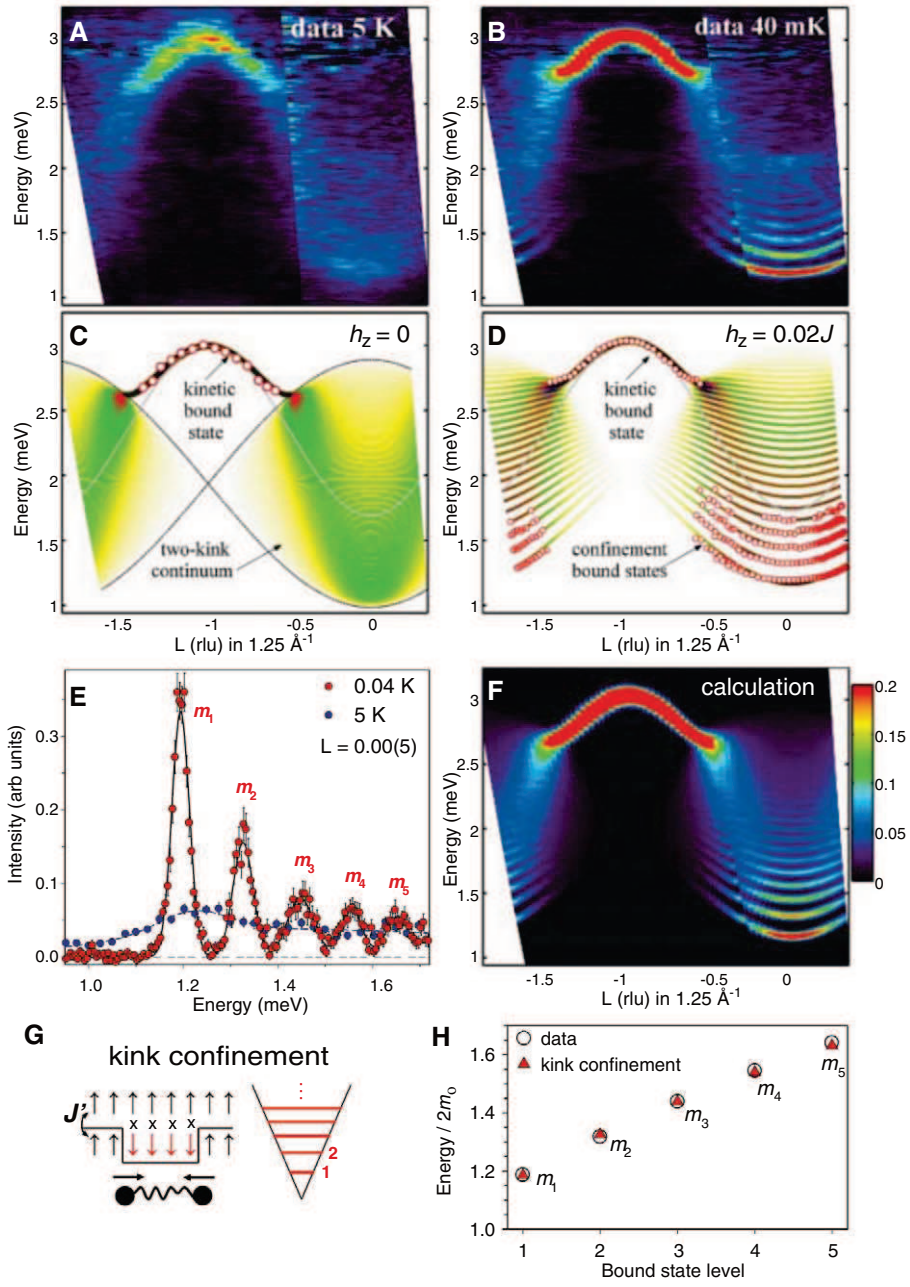


**Fig. 3.** Zero-field spin excitations in $CoNb_2O_6$. (**A**) In the 1D phase above $T_{N1}$, a broad continuum occurs near the zone center ($L = 0$) due to scattering by pairs of unbound kinks. (**B**) The continuum splits into a Zeeman ladder of two-kink bound states deep in the ordered phase. (**C** and **D**) Model calculations (*18*) for $h_z = 0$ and $0.02J$ to compare with data in (A) and (B), respectively. In (C) the thick dashed line is the kinetic two-kink bound state stable only outside the two-kink continuum (bounded by the dashed-dotted lines). Open symbols in (C) and (D) are peak positions from (A) and (B), respectively. (**E**) Energy scan at the zone center observing five sharp modes [red and blue circles are data from (B) and (A), respectively; solid line is a fit to Gaussians]. (**F**) Dynamical correlations $S^{xx}(k,\omega)$ (*18*) convolved with the instrumental resolution to compare with data in (B). (**G**) In the ordered phase, kink separation costs energy as it breaks interchain bonds $J'$, leading to an effective linear "string tension" that confines kinks into bound states. (**H**) Observed and calculated bound-state energies.

the paramagnetic phase as a result of the increase in Zeeman energy cost for spin-flip quasiparticles. In a quasi-1D system such as $CoNb_2O_6$ with finite interchain couplings, a complete gap softening is only expected (*23*) at the location of the 3D magnetic long-range order Bragg peaks, which occur at a finite interchain wave vector $\mathbf{q}_\perp$ that minimizes the Fourier transform of the antiferromagnetic interchain couplings; the measurements shown in Fig. 4C were in a scattering plane where no magnetic Bragg peaks occur, so an incomplete gap softening would be expected here, as indeed was observed.

For the critical Ising chain, a gapless spectrum of critical kinks is predicted (Fig. 4F). Adding a finite longitudinal field $h_z$ generates a gap and stabilizes bound states (Fig. 4G). In the scaling limit sufficiently close to the quantum critical point (i.e., $h_z \ll J$, $h = h_C$), the spectrum is predicted to have eight particles with energies in specific ratios (given by a representation of the $E_8$ Lie group) with the first mass at $\mathbf{m}_1/J = C(h_z/J)^{8/15}$, $C \approx 1.59$ (*2*). The predicted spectrum for such an off-critical Ising chain to be observed by neutron scattering is illustrated in Fig. 4E for the dominant dynamical correlations $S^{zz}(k = 0,\omega)$ for which quantitative calculations are available (*7*): Two prominent sharp peaks due to the first two particles $\mathbf{m}_1$ and $\mathbf{m}_2$ are expected at low energies below the onset of the continuum of two $\mathbf{m}_1$ particles (*24*).

The neutron data taken just below the critical field (Fig. 4, A and B) are indeed consistent with this highly nontrivial prediction of two prominent peaks at low energies, which we identify with the first two particles $\mathbf{m}_1$ and $\mathbf{m}_2$ of the off-critical Ising model. Figure 4D shows how the ratio of the energies of those peaks varies with increasing field and approaches closely (near 5 T just below the 3D critical field of 5.5 T) the golden ratio $\mathbf{m}_2/\mathbf{m}_1 = (1 + \sqrt{5})/2 = 1.618$ predicted for the $E_8$ masses. We identify the field where the closest agreement with the $E_8$ mass ratio is observed as the field $B_C^{1D}$ where the 1D chains would have been critical in the absence of interchain couplings (*25*). Indeed, it is in this regime (*21*) that the special quantum critical symmetry theory would be expected to apply.

Our results show that the exploration of continuous quantum phase transitions can open up avenues to experimentally realize otherwise inaccessible (*1*, *26*) correlated quantum states of matter with complex symmetries and dynamics.

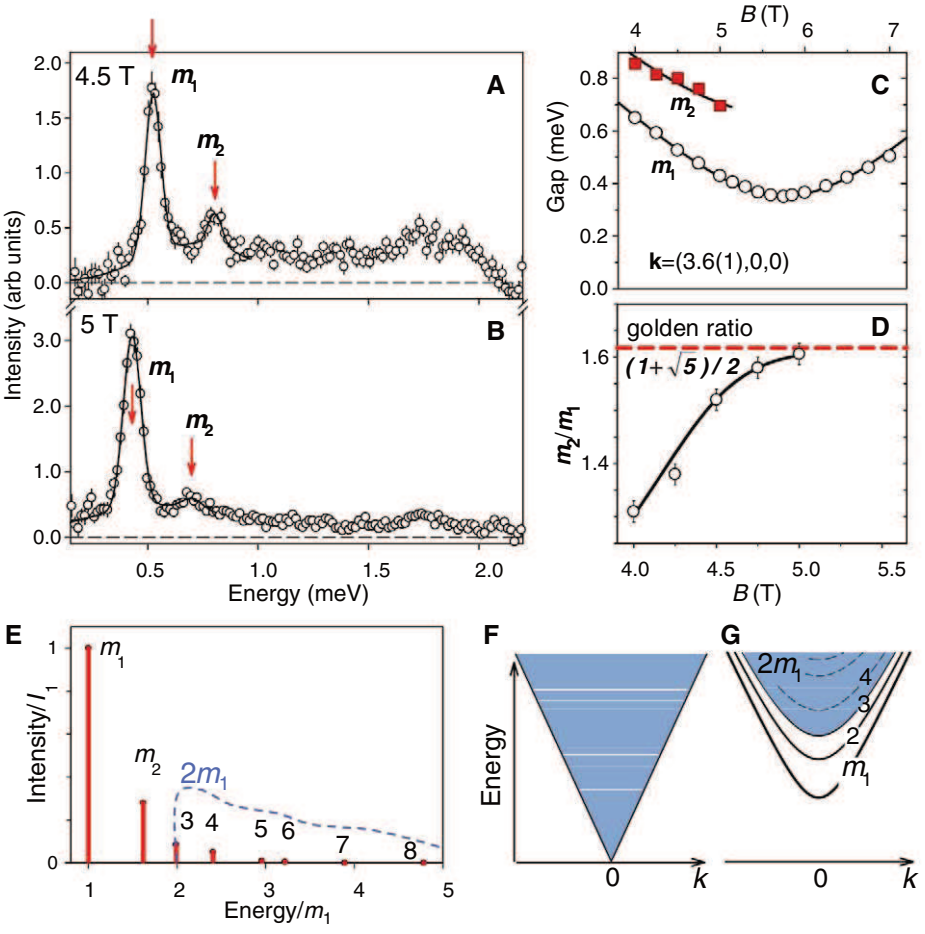


**Fig. 4.** (**A** and **B**) Energy scans at the zone center at 4.5 and 5 T observing two peaks, $\mathbf{m}_1$ and $\mathbf{m}_2$, at low energies. (**C**) Softening of the two energy gaps near the critical field (above ~5 T the $\mathbf{m}_2$ peak could no longer be resolved). Points come from data as in Fig. 2, B to D; lines are guides to the eye. The incomplete gap softening is attributed to the interchain couplings as described in the text. (**D**) The ratio $\mathbf{m}_2/\mathbf{m}_1$ approaches the $E_8$ golden ratio (dashed line) just below the critical field. (**E**) Expected line shape in the dominant dynamical correlations at the zone center $S^{zz}(k = 0,\omega)$ for the case shown in (G) [vertical bars are quasiparticle weights (*7*) relative to $\mathbf{m}_1$]: two prominent modes followed by the $2\mathbf{m}_1$ continuum (schematic dashed line), in strong resemblance to observed data in (A) and (B). (**F**) Gapless continuum of critical kinks (shaded area) predicted for the critical Ising chain. (**G**) $E_8$ spectrum expected for finite $h_z$. Lines indicate bound states; shaded area is the $2\mathbf{m}_1$ continuum.


### References and Notes

1. F. H. L. Essler, R. M. Konik, http://arxiv.org/abs/cond-mat/0412421 (2004).
2. A. B. Zamolodchikov, *Int. J. Mod. Phys. A* **4**, 4235 (1989).
3. B. Lake, D. A. Tennant, S. E. Nagler, *Phys. Rev. Lett.* **85**, 832 (2000).
4. M. Kenzelmann, Y. Chen, C. Broholm, D. H. Reich, Y. Qiu, *Phys. Rev. Lett.* **93**, 017204 (2004).
5. Ch. Rüegg *et al.*, *Phys. Rev. Lett.* **100**, 205701 (2008).
6. B. M. McCoy, T. T. Wu, *Phys. Rev. D* **18**, 1259 (1978).
7. G. Delfino, G. Mussardo, *Nucl. Phys. B* **455**, 724 (1995).
8. G. Delfino, G. Mussardo, P. Simonetti, *Nucl. Phys. B* **473**, 469 (1996).
9. P. Fonseca, A. Zamolodchikov, http://arxiv.org/abs/hep-th/0612304 (2006).
10. S. Sachdev, *Quantum Phase Transitions* (Cambridge Univ. Press, Cambridge, 1999).
11. A. O. Gogolin, A. A. Nersesyan, A. M. Tsvelik, *Bosonization and Strongly Correlated Systems* (Cambridge Univ. Press, Cambridge, 1998).
12. D. Vogan, *Not. AMS* **54**, 1022 (2007).
13. P. Pfeuty, *Ann. Phys.* **57**, 79 (1970).
14. C. Heid *et al.*, *J. Magn. Magn. Mater.* **151**, 123 (1995).
15. S. Kobayashi *et al.*, *Phys. Rev. B* **60**, 3331 (1999).
16. I. Maartense, I. Yaeger, B. M. Wanklyn, *Solid State Commun.* **21**, 93 (1977).
17. D. Prabhakaran, F. R. Wondre, A. T. Boothroyd, *J. Cryst. Growth* **250**, 72 (2003).
18. See supporting material on *Science* Online.
19. H. M. Rønnow *et al.*, *Science* **308**, 389 (2005).
20. D. Bitko, T. F. Rosenbaum, G. Aeppli, *Phys. Rev. Lett.* **77**, 940 (1996).
21. S. T. Carr, A. M. Tsvelik, *Phys. Rev. Lett.* **90**, 177206 (2003).
22. S. B. Rutkevich, *J. Stat. Phys.* **131**, 917 (2008).
23. S. Lee, R. K. Kaul, L. Balents, http://arxiv.org/abs/0911.0038.
24. The higher-energy particles $\mathbf{m}_3$ to $\mathbf{m}_8$ are expected to produce much smaller features in the total scattering line shape, as they carry a much reduced weight and are overlapping or are very close to the lower-boundary onset of the continuum scattering (see Fig. 4E).
25. The small offset between the estimated 1D and 3D critical fields is attributed to the interchain couplings, which strengthen the magnetic order. We note that a more precise quantitative comparison with the $E_8$ model would require extension of the theory to include how the mass ratio $\mathbf{m}_2/\mathbf{m}_1$ depends on the interchain wave vector $\mathbf{q}_\perp$, as the data in Fig. 4D were collected slightly away from the 3D Bragg peak positions; the already good agreement with the long-wavelength prediction expected to be valid near the 3D Bragg wave vector may suggest that the mass ratio dispersion is probably a small effect at the measured wave vectors.
26. T. Senthil *et al.*, *Science* **303**, 1490 (2004).
27. The 3D magnetic ordering wave vector has a finite component in the interchain direction due to antiferromagnetic couplings between chains.
28. We thank G. Mussardo, S. T. Carr, A. M. Tsvelik, M. Greiter, and in particular F. H. L. Essler and L. Balents for very useful discussions. Work at Oxford, Bristol, and ISIS was supported by the Engineering and Physical Sciences Research Council (UK) and at HZB by the European Commission under the 6th Framework Programme through the Key Action: Strengthening the European Research Area, Research Infrastructures, contract RII3-CT-2003-505925 (NMI3).

### Supporting Online Material

www.sciencemag.org/cgi/content/full/327/5962/177/DC1
Materials and Methods
References

3 August 2009; accepted 5 November 2009
10.1126/science.1180085

# Nematic Electronic Structure in the "Parent" State of the Iron-Based Superconductor $Ca(Fe_{1-x}Co_x)_2As_2$

T.-M. Chuang,[1,2]* M. P. Allan,[1,3]* Jinho Lee,[1,4] Yang Xie,[1] Ni Ni,[5,6] S. L. Bud'ko,[5,6] G. S. Boebinger,[2] P. C. Canfield,[5,6] J. C. Davis[1,3,4,7]†

The mechanism of high-temperature superconductivity in the newly discovered iron-based superconductors is unresolved. We use spectroscopic imaging–scanning tunneling microscopy to study the electronic structure of a representative compound $CaFe_{1.94}Co_{0.06}As_2$ in the "parent" state from which this superconductivity emerges. Static, unidirectional electronic nanostructures of dimension eight times the inter–iron-atom distance $a_{Fe\text{-}Fe}$ and aligned along the crystal $a$ axis are observed. In contrast, the delocalized electronic states detectable by quasiparticle interference imaging are dispersive along the $b$ axis only and are consistent with a nematic $\alpha_2$ band with an apparent band folding having wave vector $\vec{\mathbf{q}} \cong \pm 2\pi/8a_{Fe\text{-}Fe}$ along the $a$ axis. All these effects rotate through 90 degrees at orthorhombic twin boundaries, indicating that they are bulk properties. As none of these phenomena are expected merely due to crystal symmetry, underdoped ferropnictides may exhibit a more complex electronic nematic state than originally expected.

The ferropnictide (*1*–*6*) and cuprate high-temperature superconductors exhibit several apparent similarities. These include, for example, commensurate antiferromagnetism (AF) in the parent compounds, the quasi–two-dimensional nature of the $CuO_2$ and FeAs superconducting planes, and the importance of the transition-metal–atom $d$ states. One consequence of strong electronic correlations in the cuprates is the potential for smectic ("striped") or nematic electronic liquid crystal states (*7*–*10*). Neutron scattering provides clear evidence for magnetic "stripes" in some cuprates (*10*), whereas spectroscopic imaging–scanning tunneling microscopy (SI-STM) provides imaging evidence for electronic nematicity in the cuprate "pseudogap" states (*11*, *12*). There are proposals that such electronic phenomena may be critical to high-temperature superconductivity in cuprates (*9*, *10*). If similar phenomena existed in the parent state of ferropnictides, it could alter perceptions of the potential mechanism of high-temperature superconductivity in those systems.

Members of the $AEFe_2As_2$ (where $AE$ = Ca, Sr, or Ba) ferropnictide family typically exhibit a phase diagram as shown in Fig. 1A. Doping is achieved by either cation substitution outside the FeAs layer or transition-metal–atom substitution within this layer. The parent compounds are antiferromagnetic with a phase-transition temperature $T_{AF}$ between 134 and 220 K (*13*). $T_{AF}$ diminishes with increasing doping (blue curve), and the superconductivity occurs within a "dome" (green curve). The antiferromagnetic transition is always intertwined with a structural transition from tetragonal to orthorhombic crystal symmetry (Fig. 1A). The $a$ axis unit cell length becomes typically ~1% longer than that of the $b$ axis at temperature $T_S$, just above (or at) the antiferromagnetic transition (red curve). In this unusual AF state, each Fe atom along the $b$ axis has parallel spins, whereas those aligned along the $a$ axis have antiparallel spins (Fig. 1A). Inelastic neutron scattering studies show that the magnetic excitation structure can exhibit strong 180° ($C_2$) symmetry such that nearest-neighbor exchange constants along the $a$ and $b$ axes, $J_{1a}$ and $J_{1b}$, are dramatically different in magnitude (*14*, *15*), despite such minute lattice distortions.

This combination of commensurate AF with a tiny periodic moment, large exchange anisotropy with minute orthorhombic lattice distortion, and a high $T_{AF}$ for such an antiferromagnetic state has motivated a search for new explanations for the phases and magnetic phenomenology of underdoped ferropnictides. A plausible account of the underdoped magnetic ground state can be found in local spin models (*16*–*18*). Yet even within such relatively simple pictures of the magnetism, unidirectional magnetic nanodomains, separated by magnetic twin or antiphase boundaries (*19*), should exist. Electronic nematicity is anticipated because of the orthorhombic crystal symmetry (*18*, *20*). Moreover, functional renormalization group theory shows that a Pomeranchuk instability toward a $C_2$ symmetry nematic electronic structure is possible (*21*). A microscopic proposal to explain the simultaneous lattice and magnetic phase transitions and all of their peculiarities is that nematic orbital-ordering occurs in the $d_{xz}$ and $d_{yz}$ orbitals of Fe (*22*–*25*).

Thus, our objective is to examine the spatial arrangements in the electronic structure of the parent state of ferropnictides by imaging simultaneously their real space ($\vec{\mathbf{r}}$-space) and momentum space ($\vec{\mathbf{k}}$-space) electronic characteristics. SI-STM can be a powerful technique to achieve such electronic structure imaging; it has already revealed the structure and arrangement of ferropnictide vortices (*26*). Measurement of the STM tip-sample differential tunneling conductance $dI/dV(\vec{\mathbf{r}},V) \equiv g(\vec{\mathbf{r}},E=eV)$ at locations $\vec{\mathbf{r}}$ and sample-bias voltage $V$ (here, $E$ is the electron energy, and $e$ is a single electron charge) yields an image proportional to the local density of electronic states $LDOS(\vec{\mathbf{r}},E)$. Elements of the $\vec{\mathbf{k}}$-space electronic structure can then be determined by using Fourier transform scanning tunneling spectroscopy, because the spatial modulations in $g(\vec{\mathbf{r}},E)$ due to scattering interference of quasiparticles are detectable in $g(\vec{\mathbf{q}},E)$, which is the Fourier transform of $g(\vec{\mathbf{r}},E)$ (here, $\vec{\mathbf{q}}$ is the wave vector reciprocal to $\vec{\mathbf{r}}$).

However, the poor morphology of the cleaved surface of many ferropnictides (*27*–*31*) has made it challenging to achieve large–field-of-view (FOV), atomically registered $g(\vec{\mathbf{r}},E)$ imaging that is necessary to examine the FeAs-layer electronic structure with SI-STM. To avoid such cleave-surface pathologies, we explored the cryo-cleave characteristics of several different ferropnictide 122 compounds and eventually discovered that $Ca(Fe_{1-x}Co_x)_2As_2$ can be cleaved to reveal large, perfectly flat, debris-free and stable surfaces with excellent atomic resolution (Fig. 1B).

$Ca(Fe_{1-x}Co_x)_2As_2$ is well-representative of the ferropnictide 122 compounds (*6*, *32*–*34*). $CaFe_2As_2$ exhibits simultaneous structural and magnetic phase transitions (*32*, *33*) at 170 K. Angle-resolved photoemission spectroscopy (ARPES) reveals its Fermi surface arrangement in good agreement with reports from related compounds (*34*), and inelastic neutron scattering detects the reduction of symmetry in the magnetic excitation spectrum to $C_2$ (*14*, *15*). These observations make $Ca(Fe_{1-x}Co_x)_2As_2$ an excellent material in which to explore the nematic electronic structure of the underdoped ferropnictide state that is "parent" to the superconductivity.

For this study, we used $Ca(Fe_{1-x}Co_x)_2As_2$ samples with $x \sim 3.0 \pm 0.5\%$. The samples were inserted into the SI-STM system and cleaved in cryogenic ultrahigh vacuum; all data were acquired at 4.3 K. Figure 1B shows the typical surface conditions achieved in our experiments. This ~71-nm square FOV is believed to be the As-terminated FeAs plane (*30*, *31*) with an unknown distribution of Ca atoms (and, thus, an unknown degree of charge transfer at that plane). The plane is atomically flat but with a 1 × 2 surface reconstruction (blue and red arrows in Fig. 1B inset) at ~45° to both the $a$ and $b$ axes. The inset to Fig. 1B is a 4.2-nm square topograph

[1]Laboratory of Atomic and Solid State Physics, Department of Physics, Cornell University, Ithaca, NY 14853, USA. [2]National High Magnetic Field Laboratory, Department of Physics, Florida State University, Tallahassee, FL 32310, USA. [3]School of Physics and Astronomy, University of Saint Andrews, Saint Andrews, Fife KY16 9SS, UK. [4]Condensed Matter Physics and Materials Science Department, Brookhaven National Laboratory, Upton, NY 11973, USA. [5]Ames Laboratory, U.S. Department of Energy (DOE), Iowa State University, Ames, IA 50011, USA. [6]Department of Physics and Astronomy, Iowa State University, Ames, IA 50011, USA. [7]Department of Physics and Astronomy, University of British Columbia, Vancouver, British Columbia, Canada.

*These authors contributed equally to this work.
†To whom correspondence should be addressed. E-mail: jcdavis@ccmr.cornell.edu

of this surface in which the individual atoms on the reconstruction rows can be seen (red arrows). This 1 × 2 reconstruction is not a bulk property (*27*, *29*, *31*) but rather a surface condition whose effects must be avoided in SI-STM studies of the FeAs-plane electronic structure. In our studies, the orientation of the orthorhombic *a* and *b* axes can be determined from the topography (figs. S1 and S2).

Detailed examination of high-quality topographs of these surfaces reveals the first surprising fact. Figure 1B is typical; it appears to show faint unidirectional structures aligned along the *a* axis (orange arrows). Figure 2A shows that, when two identical atomically registered topographs measured at ±50 meV are subtracted (to cancel the signals of the surface reconstruction and topographic disorder that are independent of the sign of the tunnel bias), unidirectional nanostructures aligned along the *a* axis are seen. Because topographs represent a logarithmic measure of the integrated density of states, these data indicate the existence of some form of static electronic nanostructure. To get a clearer picture of any such electronic nanostructures, we image the energy-resolved $LDOS(\vec{\mathbf{r}},E)$ in the same FOV (fig. S3). Remarkably, electronic nanostructures aligned with the *a* axis and spatially equivalent to those in Fig. 2A are detected in all low-energy $LDOS(\vec{\mathbf{r}},E)$ images (fig. S3). To determine if these phenomena indicate static or dispersive states, one must integrate the $LDOS(\vec{\mathbf{r}},E)$ over energy. Thus, we image directly the net tunnel current *I* because

$$I(\vec{\mathbf{r}},E) = \int_0^E g(\vec{\mathbf{r}},E')dE' \qquad (1)$$

Figure 2B is an image of $I(\vec{\mathbf{r}},E = 50\ \text{meV})$; it reveals the same electronic nanostructures and thereby demonstrates that they must be static over this energy range. Moreover, autocorrelation analysis of such images (Fig. 2, A and B, insets) shows that the static structures throughout the image are all aligned with the *a* axis and are self-similar with a characteristic dimension of eight inter–iron-atom distances, ~$8a_{\text{Fe-Fe}}$. The spatially averaged density-of-states $DOS(E)$ spectrum (Fig. 2C, inset) consists of a metallic density-of-

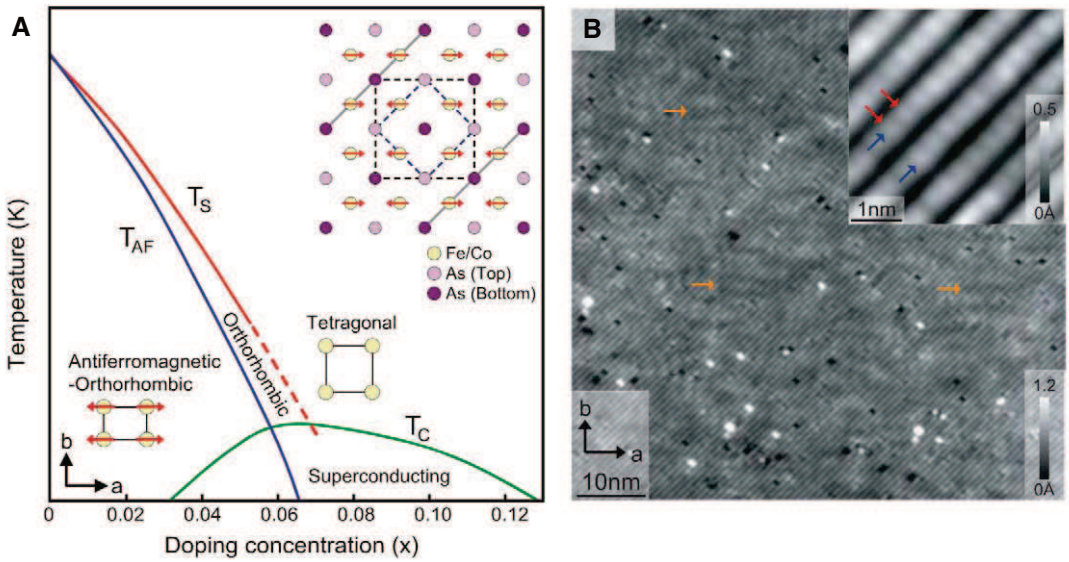


**Fig. 1.** (**A**) Schematic phase diagram of $AE(Fe_{1-x}Co_x)_2As_2$ (here *AE* = Ca, Sr, or Ba) as function of doping concentration (*x*) (*6*, *13*, *32*, *33*). Red, blue, and green curves show the transition temperature for structure ($T_S$), antiferromagnetism ($T_{AF}$), and superconductivity ($T_C$), respectively. The red arrows indicate the spin orientation for each Fe atom in the antiferromagnetic-orthorhombic phase. (Upper right) FeAs layer showing the unit cell in tetragonal (blue dashed lines) and orthorhombic (black dashed lines) phases. The orientation and periodicity of the surface reconstruction in the topographic images in (B) is indicated by gray lines. (**B**) Constant-current topographic image of $Ca(Fe_{1-x}Co_x)_2As_2$ taken at $V_0 = -50$ mV and $I_z = 10$ pA on a 71.0-nm square FOV. (Inset) A high-resolution topograph in a smaller FOV (4.2-nm square) taken at $V_0 = -5$ mV and $I_z = 100$ pA. The red and blue arrows indicate the atoms of 1 × 2 configuration. The orange arrows indicate the first indications of unidirectional *a* axis–oriented electronic nanostructures.

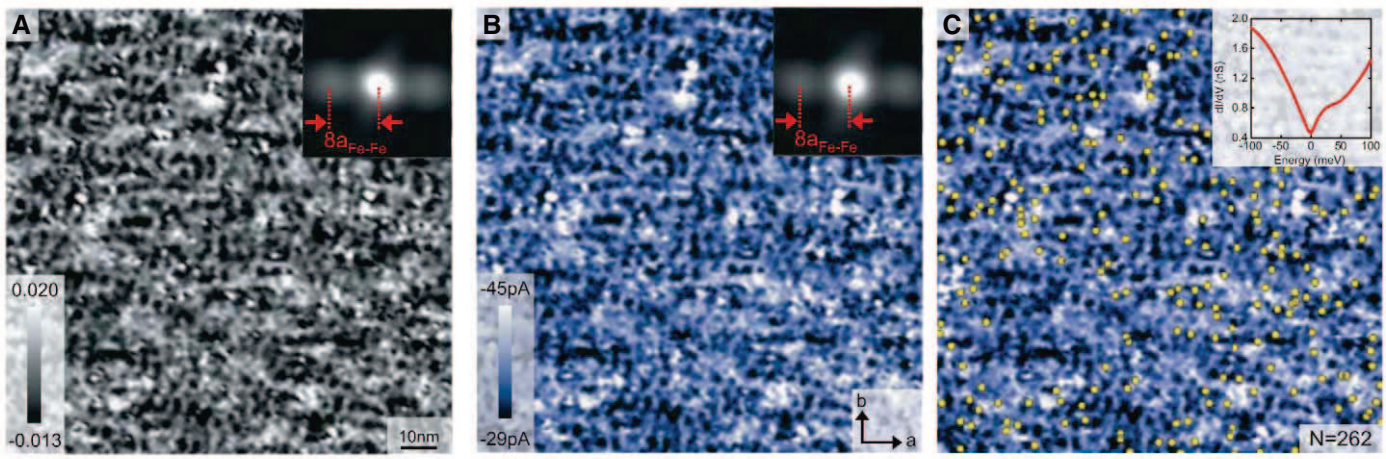


**Fig. 2.** (**A**) Difference between two atomically registered topographs *z*(+50 mV) − *z*(−50 mV) (where *z* is the tip-sample distance), acquired in the same 61.3-nm square FOV at $I_z$ = 10 pA. (Inset) Autocorrelation analysis of this image; the centers of self-similarity peaks (red dotted lines) are separated by ~$8a_{\text{Fe-Fe}}$. (**B**) The current map $I(\vec{\mathbf{r}},E = +50\ \text{meV})$ in the same FOV as (A). (Inset) Autocorrelation analysis of this image; the centers of self-similarity peaks (red dotted lines) are separated by ~$8a_{\text{Fe-Fe}}$. (**C**) The current map $I(\vec{\mathbf{r}},E = +50\ \text{meV})$ in the same FOV as in (A) and (B). The atomic-scale impurity state locations as determined from conductance mapping at 150 meV are shown as 262 yellow dots. If they represent the Co dopant atoms, they exhibit only ~15% of the density expected in the top FeAs layer, based on the average measured Co density of the whole sample. (Inset) A typical conductance spectrum exhibits a mixed metallic and "pseudogap-like" shape.

states $DOS(E = 0)$ with a V-shaped "pseudogap" spectrum superimposed. The cobalt dopant-atom locations should, in theory (*35*), be detectable as atomic-scale local conductance maxima between +100 and +200 meV. The locations of atomic-scale impurity states imaged in this energy range are shown in Fig. 2C as yellow dots overlaid on the same $I(\vec{\mathbf{r}}, E = 50\ \text{meV})$ map; the normalized cross-correlation between this $I$ map and dopant locations can be as high as 0.22. Thus, some degree of dopant-atom pinning of the unidirectional static electronic nanostructure seems to be occurring.

From these data, static, self-similar, electronic nanostructures of dimension ~$8a_{\text{Fe-Fe}}$ that are aligned in a unidirectional fashion along the $a$ axis (AF axis) and correlated in their locations with dopant atoms appear to exist in underdoped $Ca(Fe_{1-x}Co_x)_2As_2$. If this is correct, the $\vec{\mathbf{k}}$-space electronic structure should exhibit (i) $C_2$ symmetry with dispersive excitations along the $b$ axis and (ii) a $\vec{\mathbf{q}} \cong 2\pi/8a_{\text{Fe-Fe}}$ band folding along the $a$ axis. To test this picture, we determine the simultaneous $\vec{\mathbf{k}}$-space electronic structure through quasiparticle interference (QPI) imaging. Important to the demonstration of ferropnictide QPI here was the development of large-FOV, flat, stable surfaces of $Ca(Fe_{1-x}Co_x)_2As_2$. In fig. S4 (*36*), we show the unprocessed $g(\vec{\mathbf{r}}, E)$ data measured in a 40-nm square FOV of such a surface, over an energy range from $E = -20$ to +25 meV. The wavelength of conductance modulations is long and increases continuously with increasing energy, but only along the vertical axis of these images (*36*). The resulting $g(\vec{\mathbf{q}}, E)$ are shown in Fig. 3, A to J, and figs. S4 and S5. Their dispersion is seen in the evolution between Fig. 3, A and J; it evolves along one axis only. This means that the scattering interference modulations are strongly unidirectional, which should occur if the $\vec{\mathbf{k}}$-space band supporting them is nematic. Finally, not one, but three parallel sets of dispersive peaks exist in all of these QPI data (e.g., vertical arrows below Fig. 3J).

To further analyze these data, we consider the relative orientation of the dispersive QPI modulations to the crystal axes (Fig. 3K). The QPI modulations are at 45° to the surface reconstruction and exhibit $\vec{\mathbf{q}}$-vector magnitudes smaller than those of any crystal or surface periodicity; thus, these QPI signals are not influenced by the surface reconstruction. In Fig. 3L, we show that the three sets of $\vec{\mathbf{q}}$ vectors disperse on $\vec{\mathbf{q}}(E)$ trajectories identical to each other up to a displacement by $\vec{\mathbf{q}} \cong \pm 2\pi/8a_{\text{Fe-Fe}}$. This is what would be expected from a band folding due to a ~$8a_{\text{Fe-Fe}}$ periodic reconstruction of the $\vec{\mathbf{r}}$-space electronic structure along the $a$ axis.

The ARPES-measured dispersion of the $\alpha_2$ band (*34*) is shown in fig. S6 (*36*). When the $\vec{\mathbf{k}} = \pm\vec{\mathbf{q}}/2$ (here, $\vec{\mathbf{k}}$ is a momentum-space wave vector) points taken from QPI data in Fig. 3L are overlaid centered on its Γ point (Γ is at the center of the Brillouin zone), they appear to be in good agreement. Thus, the observed QPI data are consistent with scattering between states in the $\alpha_2$ band, but a version of this band actually exhibits $C_2$ symmetry plus an additional $\vec{\mathbf{q}} \cong \pm 2\pi/8a_{\text{Fe-Fe}}$ folding.

A final test of the validity of this emerging picture of static, $a$-axis–oriented, ~$8a_{\text{Fe-Fe}}$ electronic nanostructures generating a $C_2$-symmetric,

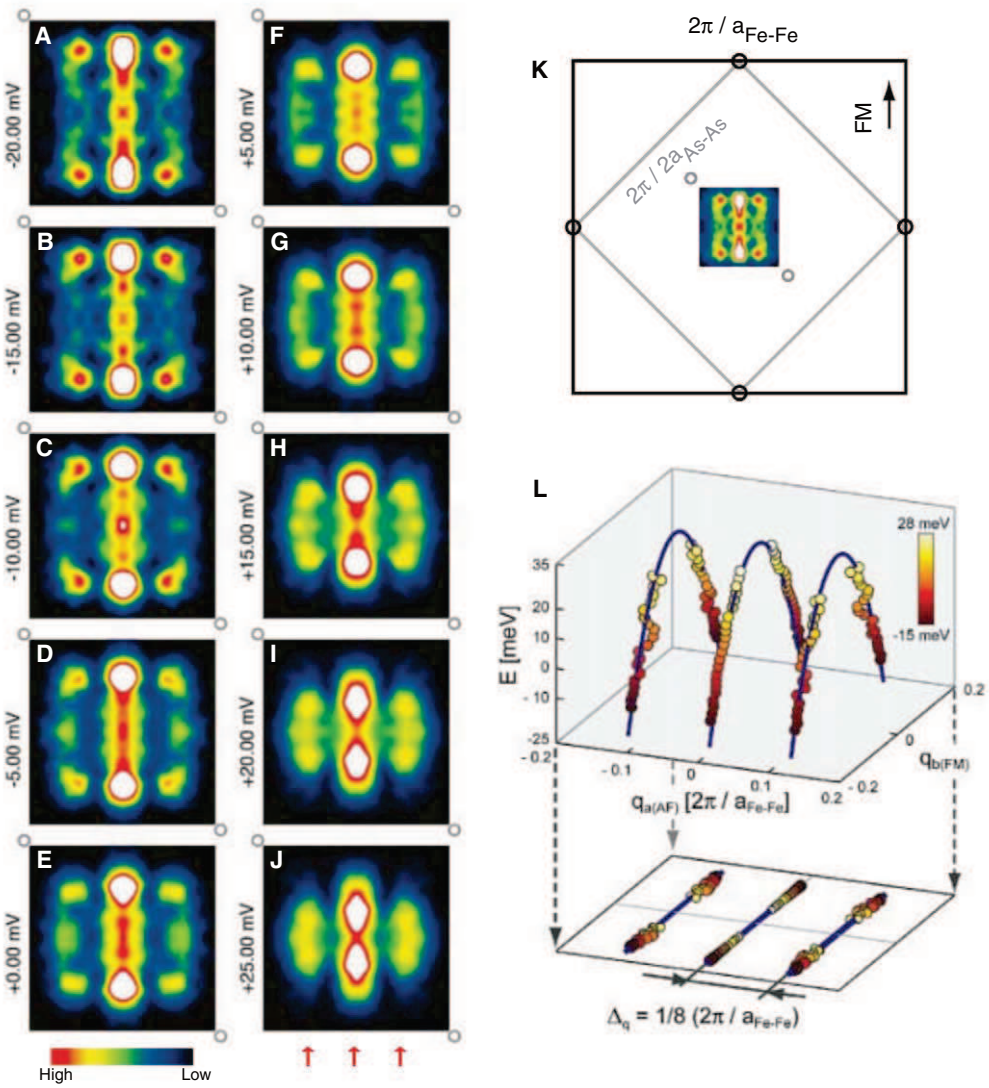


**Fig. 3.** (**A** to **J**) The Fourier transforms $g(\vec{\mathbf{q}}, E)$ of the $g(\vec{\mathbf{r}}, E)$ images in fig. S4 reveal the highly $C_2$-symmetric structure of the QPI patterns. The data shown here are from a larger 94-nm square FOV. Six dispersing peaks are clearly visible. The two center peaks disperse in a hole-like fashion along the $b$ axis only. Pairs of side peaks mimic their dispersion at $\vec{\mathbf{q}} \approx \pm 1/8(2\pi/a_{\text{Fe-Fe}})$. The open circles at two corners of each image represent the $\vec{\mathbf{q}}$-space locations of the 1 × 2 reconstruction. Red arrows indicate the three parallel dispersion trajectories. (**K**) Overview of the different directions and length scales in $\vec{\mathbf{q}}$ space. The dispersing QPI vectors are short compared with the $2\pi/a_{\text{Fe-Fe}}$ box that spans all scattering vectors in the first Fe-Fe Brillouin zone (the large black box). The small gray box indicates the first As-As reciprocal unit cell. FM indicates the $b$ axis direction along which spin correlations are ferromagnetic. (**L**) The hole-like dispersion of QPI, plotted in $\vec{\mathbf{q}}_b, \vec{\mathbf{q}}_a, E$ space. Circles mark the positions of the six dispersion peaks extracted from each $g(\vec{\mathbf{q}}, E)$ image; the blue lines are the parabolic fit for QPI. Projections to the $(\vec{\mathbf{q}}_b, \vec{\mathbf{q}}_a)$ plane emphasize how unidirectional the dispersions are along the $b$ axis. The side peaks are at ~$\pm 1/8(2\pi/a_{\text{Fe-Fe}})$, suggesting an intimate relation between the unidirectional QPI modulations and unidirectional static electronic structure in Fig. 2.

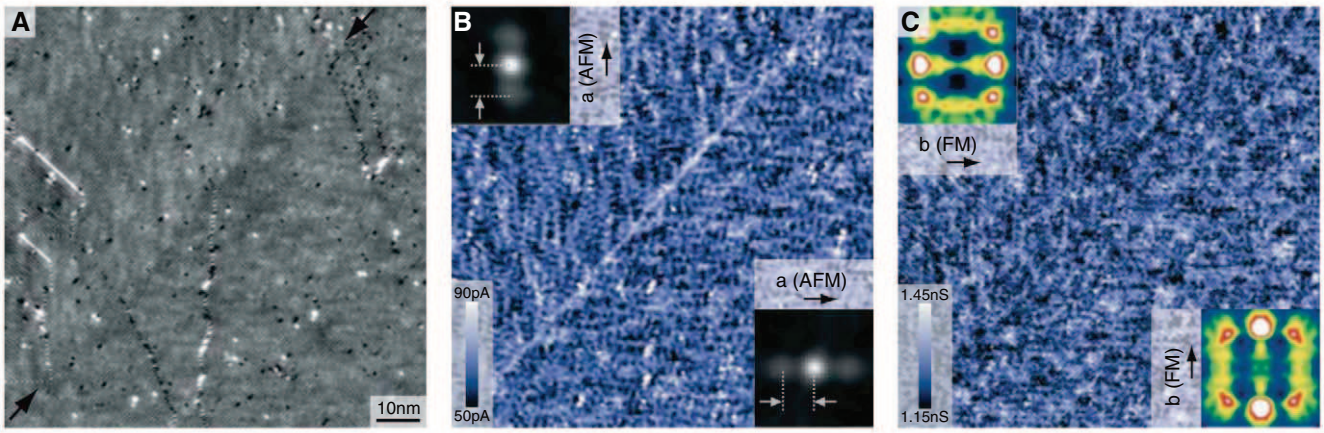


**Fig. 4.** (**A**) A 96.0-nm FOV topographic image (junction resistance = 500 megohm, $V_0 = -50$ mV) measured simultaneously with the $g(\vec{\mathbf{r}},E)$ and $I(\vec{\mathbf{r}},E)$ data of (B) and (C). The orthorhombic twin boundary visible in (B) and (C) is marked with black arrows. Slight deviations in the angle of the surface-reconstruction reveal the orthogonal orthorhombic axes of the two crystal domains (*36*). (**B**) The current image, $I(\vec{\mathbf{r}},E = 50\ \text{meV})$ in the same FOV as (A). The static unidirectional domains of Fig. 2 clearly change directionality by 90° across the twin boundary. (Insets) Autocorrelations; center of self-similarity peaks (gray dotted lines) are separated by ~$8a_{\text{Fe-Fe}}$. (**C**) The conductance image $g(\vec{\mathbf{r}},E = -10\ \text{meV})$ in the same FOV. (Insets) Fourier-transforms in the respective domains demonstrate that the QPI dispersions exhibit a 90° rotation across the twin boundary.

quasi-folded band along the $b$ axis would be to detect the effect of an orthorhombic twin boundary. In Fig. 4A, we show a 96-nm square topograph through which a twin boundary passes diagonally (*36*). Figure 4B depicts the $I$ map taken simultaneously with Fig. 4A, along with the autocorrelations of this map on each side of the twin boundary. In both the raw data and the autocorrelations, the static ~$8a_{\text{Fe-Fe}}$ $a$-axis–oriented domains rotate through 90°. In Fig. 4C, we show the $g(\vec{\mathbf{r}},E = -10\ \text{meV})$ taken simultaneously along with the two $g(\vec{\mathbf{q}},E = -10\ \text{meV})$ measured on each side of the twin boundary. Again, the $C_2$-symmetric $b$ axis QPI modulations rotate through 90°. This rules out effects of both the surface reconstruction and the distribution of Ca atoms remaining on that surface (neither of which rotates at the twin boundary) as the cause of the observed electronic nematicity. Instead, we conclude that all the unidirectional electronic phenomena (both in $\vec{\mathbf{r}}$ space and $\vec{\mathbf{k}}$ space) detected here are bulk electronic characteristics of the orthorhombic antiferromagnetic state. Hence, a related conclusion is that $C_4$-symmetric photoemission data in this state must represent the average over a strongly $C_2$-symmetric electronic structure in different orthorhombic domains.

Our SI-STM studies indicate that the electronic structure of underdoped $Ca(Fe_{1-x}Co_x)_2As_2$ supports a variety of unexpected phenomena, including (i) the existence of unidirectional electronic nanostructures, which are highly self-similar with dimension ~$8a_{\text{Fe-Fe}}$ and possibly pinned by Co dopant atoms, and (ii) $b$-axis dispersive QPI modulations, consistent with a nematic version of the $\alpha_2$ band and with an additional apparent $\vec{\mathbf{q}} \cong \pm 2\pi/8a_{\text{Fe-Fe}}$ band folding. As none of these effects are expected merely due to the crystal symmetry, the underdoped ferropnictide parent state from which superconductivity emerges appears to be a more complex electronic nematic than originally expected. These new perceptions of its electronic structure should inform revised theories for the mechanism of the high-temperature superconductivity.

### References and Notes


1. Y. Kamihara, T. Watanabe, M. Hirano, H. Hosono, *J. Am. Chem. Soc.* **130**, 3296 (2008).
2. X. H. Chen *et al.*, *Nature* **453**, 761 (2008).
3. C. Wang *et al.*, *Europhys. Lett.* **83**, 67006 (2008).
4. M. Rotter, M. Tegel, D. Johrendt, *Phys. Rev. Lett.* **101**, 107006 (2008).
5. A. S. Sefat *et al.*, *Phys. Rev. Lett.* **101**, 117004 (2008).
6. N. Ni *et al.*, *Phys. Rev. B* **78**, 014523 (2008).
7. J. Zaanen, O. Gunnarsson, *Phys. Rev. B* **40**, 7391 (1989).
8. S. A. Kivelson, E. Fradkin, V. J. Emery, *Nature* **393**, 550 (1998).
9. S. Sachdev, *Rev. Mod. Phys.* **75**, 913 (2003).
10. V. J. Emery, S. A. Kivelson, J. M. Tranquada, *Proc. Natl. Acad. Sci. U.S.A.* **96**, 8814 (1999).
11. Y. Kohsaka *et al.*, *Science* **315**, 1380 (2007); published online 7 February 2007 (10.1126/science.1138584).
12. Y. Kohsaka *et al.*, *Nature* **454**, 1072 (2008).
13. H. Hosono, *Physica C* **469**, 314 (2009).
14. J. Zhao *et al.*, *Nat. Phys.* **5**, 555 (2009).
15. S. O. Diallo *et al.*, *Phys. Rev. Lett.* **102**, 187206 (2009).
16. T. Yildirim, *Phys. Rev. Lett.* **101**, 057010 (2008).
17. Q. Si, E. Abrahams, *Phys. Rev. Lett.* **101**, 076401 (2008).
18. C. Fang, H. Yao, W.-F. Tsai, J. Hu, S. A. Kivelson, *Phys. Rev. B* **77**, 224509 (2008).
19. I. I. Mazin, M. D. Johannes, *Nat. Phys.* **5**, 141 (2009).
20. C. Xu, Y. Qi, S. Sachdev, *Phys. Rev. B* **78**, 134507 (2008).
21. H. Zhai, F. Wang, D.-H. Lee, *Phys. Rev. B* **80**, 064517 (2009).
22. F. Krüger, S. Kumar, J. Zaanen, J. van den Brink, *Phys. Rev. B* **79**, 054504 (2009).
23. R. R. P. Singh, http://arxiv.org/abs/0903.4408 (2009).
24. C.-C. Lee, W.-G. Yin, W. Ku, http://arxiv.org/abs/0905.2957 (2009).
25. W.-C. Lee, C. Wu, *Phys. Rev. Lett.* **103**, 176101 (2009).
26. Y. Yin *et al.*, *Phys. Rev. Lett.* **102**, 097002 (2009).
27. M. C. Boyer *et al.*, http://arxiv.org/abs/0806.4400 (2008).
28. F. Massee *et al.*, *Phys. Rev. B* **79**, 220517 (2009).
29. D. Hsieh *et al.*, http://arxiv.org/abs/0812.2289 (2008).
30. V. B. Nascimento *et al.*, *Phys. Rev. Lett.* **103**, 076104 (2009).
31. F. C. Niestemski *et al.*, http://arxiv.org/abs/0906.2761 (2009).
32. A. I. Goldman *et al.*, *Phys. Rev. B* **78**, 100506 (2008).
33. S.-H. Baek *et al.*, *Phys. Rev. B* **79**, 052504 (2009).
34. T. Kondo *et al.*, http://arxiv.org/abs/0905.0271 (2009).
35. A. F. Kemper, C. Cao, P. J. Hirschfeld, H.-P. Cheng, *Phys. Rev. B* **80**, 104511 (2009).
36. Materials and methods are available as supporting material on *Science* Online.


37. We thank F. Baumberger, P. J. Hirschfeld, J. E. Hoffman, A. Kaminski, D.-H. Lee, G. Luke, E.-A. Kim, M. Lawler, A. P. Mackenzie, I. I. Mazin, M. Norman, S. Pan, G. Sawatzky, and S. Uchida for helpful discussions and communications. These studies are supported by the Center for Emergent Superconductivity, a DOE Energy Frontier Research Center headquartered at Brookhaven National Laboratory. Work at the Ames Laboratory was supported by the DOE, Basic Energy Sciences under Contract no. DE-AC02-07CH11358. Support for this work was provided by NSF/DMR-0654118 through the National High Magnetic Field Lab (to T.-M.C.); the Cornell Center for Materials Research under NSF/DMR-0520404 (to Y.X.); and the U.K. Engineering and Physical Sciences Research Council and the Scottish Funding Council (to M.P.A.). J.C.D. acknowledges gratefully the hospitality and support of the Physics and Astronomy Department at the University of British Columbia, Vancouver, BC, Canada.


### Supporting Online Material

www.sciencemag.org/cgi/content/full/327/5962/181/DC1
Materials and Methods
SOM Text
Figs. S1 to S7
References

25 August 2009; accepted 13 November 2009
10.1126/science.1181083

# Energy-Conversion Properties of Vapor-Liquid-Solid–Grown Silicon Wire-Array Photocathodes

Shannon W. Boettcher, Joshua M. Spurgeon, Morgan C. Putnam, Emily L. Warren, Daniel B. Turner-Evans, Michael D. Kelzenberg, James R. Maiolo, Harry A. Atwater,* Nathan S. Lewis*

Silicon wire arrays, though attractive materials for use in photovoltaics and as photocathodes for hydrogen generation, have to date exhibited poor performance. Using a copper-catalyzed, vapor-liquid-solid–growth process, $SiCl_4$ and $BCl_3$ were used to grow ordered arrays of crystalline p-type silicon (p-Si) microwires on $p^+$-Si(111) substrates. When these wire arrays were used as photocathodes in contact with an aqueous methyl viologen$^{2+/+}$ electrolyte, energy-conversion efficiencies of up to 3% were observed for monochromatic 808-nanometer light at fluxes comparable to solar illumination, despite an external quantum yield at short circuit of only 0.2. Internal quantum yields were at least 0.7, demonstrating that the measured photocurrents were limited by light absorption in the wire arrays, which filled only 4% of the incident optical plane in our test devices. The inherent performance of these wires thus conceptually allows the development of efficient photovoltaic and photoelectrochemical energy-conversion devices based on a radial junction platform.

Highly purified planar crystalline Si provides the basis for high-efficiency photovoltaics and has shown promise as a photocathode material for the production of $H_2$ from water and sunlight (*1*). In this planar geometry, efficient devices require the use of high-purity Si to obtain minority-carrier diffusion lengths that are comparable to the long optical absorption depth (~200 μm) associated with the indirect band gap of Si (*2*). Semiconductor wire arrays are an attractive alternative to this planar geometry because they can possess both long optical paths for efficient light absorption and short transport distances so as to ensure collection of the photogenerated charge carriers before they recombine (*2*–*13*). A wire-array geometry should thus allow for the use of semiconductors in which the collection length of photogenerated minority carriers is much shorter than the optical penetration depth. Indeed, device-physics modeling has predicted that wire-array structures using Si with a minority-carrier diffusion length of less than 10 μm can achieve solar energy–conversion efficiencies of greater than 15% (*2*).

To date, device efficiencies for radial-junction Si photovoltaics and photoelectrodes fabricated by use of potentially inexpensive techniques, such as vapor-liquid-solid (VLS)–growth processes (*14*), have been low. The highest reported efficiencies are for single-nanowire devices in which the performance was normalized to the active portion of the single wire, that is, excluding contacts and empty area (*8*, *9*). Up to 3.4% efficiency under solar simulation has been observed for a p-type/intrinsic/n-type (p-i-n) Si nanowire, with a low open-circuit voltage of 260 mV (*7*). Macroscopic VLS-grown Si wire-array devices have exhibited poor efficiencies (~0.1%) in both liquid-junction (*3*, *4*) and solid-state (*10*, *11*) configurations. A key question is whether higher performance, in accord with theoretical predictions, can be obtained with wire-array energy-conversion devices through improved control over the bulk impurities, surface defects, and doping.

To evaluate this possibility, we grew p-type Si wire arrays from $SiCl_4$ [10 standard cubic centimeters per minute (sccm)], $H_2$ (500 sccm), and dilute $BCl_3$ at 1000°C at atmospheric pressure for 20 to 30 min on $p^+$-Si(111) substrates. These substrates had been photolithographically patterned with 3-μm-diameter by 300-nm-thick Cu VLS-growth catalyst islands that were confined within a 300-nm-thick thermal Si oxide (*15*, *16*). The resulting wires were ~100 μm long, ~1.6 μm in diameter, and arranged on a square lattice with a 7-μm pitch, resulting in a packing fraction of ~4% (Fig. 1, A and B). The resistivity of the wires, as measured with single-wire four-point-probe methods (*9*), was varied by changing the $BCl_3$ flow rate. Wires grown from 0.25% $BCl_3$ in $H_2$ at a flow rate of 1 sccm had a resistivity of 0.05 ± 0.01 ohm cm, corresponding to a majority-carrier concentration near $7 \times 10^{17}$ $cm^{-3}$, and exhibited optimal photoelectrochemical properties relative to wires with other doping levels. Before photoelectrochemical evaluation, the samples were etched with aqueous solutions of $FeCl_3$, KOH, and HF, so as to remove the Cu catalyst, the outer ~50 nm of Si (including Cu contained at or near the surface), and the native oxide, respectively, without substantial etching of the patterned thermal oxide that surrounded the bases of the wires (Fig. 1, C and D).

The energy-conversion properties of the p-type silicon (p-Si) wire arrays were evaluated in an aqueous electrolyte containing the redox couple methyl viologen ($MV^{2+/+}$), whose conformal liquid contact allowed for testing without introducing difficulties associated with the production of rectifying, conformal solid-state junctions, transparent conductors, or metallic grid contacts. This redox system produces a high barrier height on p-Si (*3*, *17*) and enables the straightforward evaluation of any differences in the junction behavior between planar p-Si samples and p-Si wire-array electrodes. The comparison was performed in a three-electrode cell configuration in order to directly evaluate the performance of the photocathodes, to minimize resistive losses, and to allow quantification of the concentration and kinetic overpotentials that would be variables in two-electrode photoelectrochemical devices (Fig. 2). Monochromatic 808-nm light was used to minimize the optical absorption of the reduced form of the $MV^{2+/+}$ couple (*18*). This wavelength of light also has a relatively long optical-penetration depth of 11 μm in Si, which stresses the ability to collect photogenerated charge carriers produced deeply in the absorbing semiconductor.

A comparison between the current density versus potential (*J*-*E*) behavior of a planar, single-crystalline Czochralski-grown p-Si (0.7 ohm cm) sample and a p-Si wire array is shown in Fig. 3. Under 60 mW $cm^{-2}$ of 808 nm illumination (selected to produce a similar photon flux above the Si band gap as that obtained from broadband, 100 mW $cm^{-2}$, air mass 1.5 solar illumination), the planar electrodes typically yielded open-circuit voltages ($V_{oc}$) of 0.555 ±

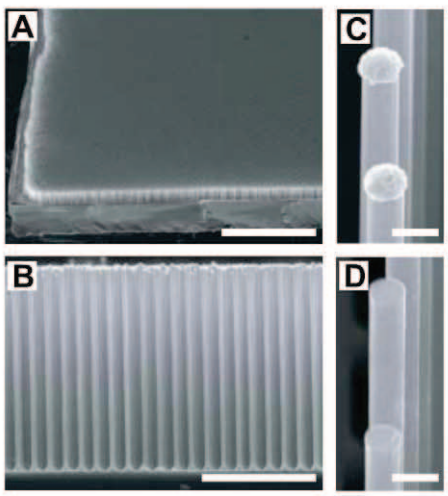


**Fig. 1.** (**A**) Scanning electron microscope image showing the p-Si wire arrays on a ~2-$cm^2$ wafer (scale bar, 600 μm). (**B**) Side view of a cleaved sample (scale bar, 50 μm). (**C**) Close-up showing the faceted wire and the copper catalyst tip before etching (scale bar, 2 μm). (**D**) Close-up showing the wire tops after etching with $FeCl_3$, KOH, and HF (scale bar, 2 μm).

Kavli Nanoscience Institute and Beckman Institute, 1200 East California Boulevard, California Institute of Technology, Pasadena, CA 91125, USA.

*To whom correspondence should be addressed. E-mail: nslewis@caltech.edu (N.S.L.); haa@caltech.edu (H.A.A.)

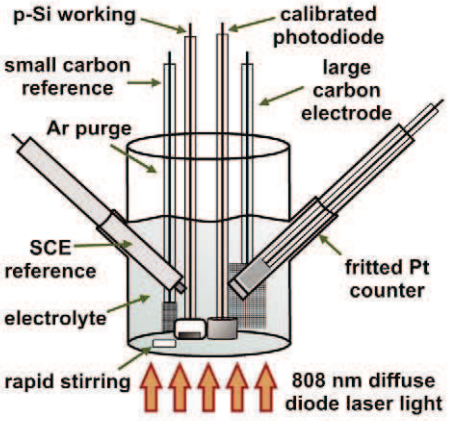


**Fig. 2.** Photoelectrochemical characterization was conducted in a glass cell configured so that the redox potential of the solution could be controlled versus a standard calomel reference electrode (SCE) and the incident light intensity could be measured in situ. The cell was filled with ~50 mL of aqueous electrolyte containing 0.5 M $K_2SO_4$ and 0.05 M methyl viologen dichloride ($MV^{2+}$) and buffered at pH = 2.9. The solution potential was driven to −0.60 V versus SCE by using the large carbon-cloth electrode as a working electrode and the frit-separated Pt mesh as a counter electrode, which turned the electrolyte deep purple-blue because of the formation of $MV^+$ radical (~ 3 mM). During photoelectrochemical characterization, the p-Si sample was used as the working electrode, the large carbon cloth as the counter electrode, and the small carbon cloth as the reference electrode.

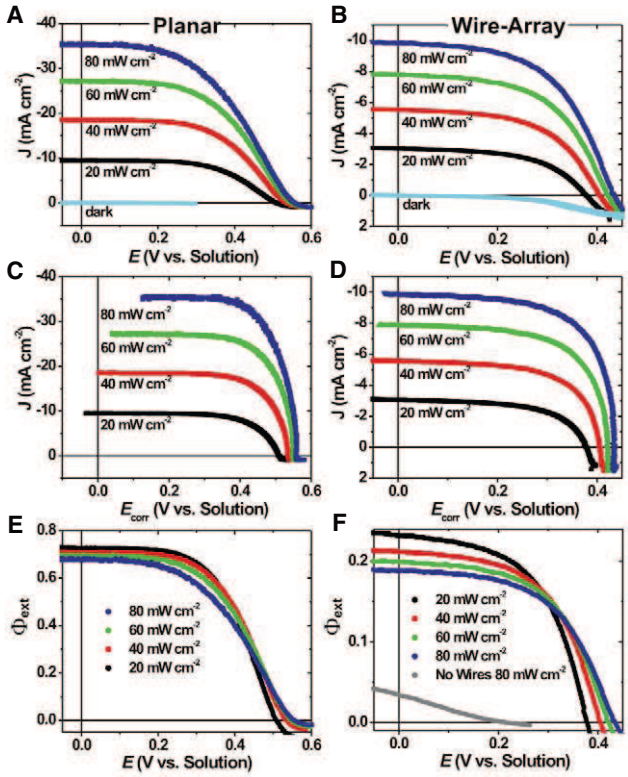


**Fig. 3.** Current-potential data as a function of 808-nm illumination intensity for (**A**) planar and (**B**) wire-array photoelectrodes. Solution absorbance is accounted for via the in situ measurement of the incident light intensity. In panels (**C**) and (**D**), the same data are displayed corrected for the solution effects, including uncompensated cell resistance (~20 ohms) and concentration overpotentials, so as to attain photoelectrode performance parameters inherent to the Si electrodes. The external quantum yield plotted in panels (**E**) and (**F**) was calculated on the basis of the incident light intensity, the sample area, and the measured photocurrent from panels (A) and (B), respectively. The performance of a wire-array sample in which the wires had been physically removed from the substrate confirmed that the $p^+$-Si substrate did not substantially contribute to the observed photoresponse.

0.015 V, short-circuit photocurrent densities ($J_{sc}$) of 27.9 ± 0.8 mA $cm^{-2}$, external quantum yields at short-circuit ($\Phi_{ext,sc}$) of 0.71 ± 0.02, fill factors (*ff*) of 0.51 ± 0.05, and photoelectrode energy-conversion efficiencies ($\eta_{808}$) of 12.9 ± 1.0% (across six devices; the uncertainty is reported as 1 SD). Correction for the concentration overpotential and uncompensated resistance losses (*15*, *19*) in the aqueous $MV^{2+/+}$ test electrolyte yielded the inherent photoelectrode properties under these conditions of $ff_{corr}$ = 0.68 ± 0.05 and $\eta_{808,corr}$ = 17.4 ± 1.0%. Under the same conditions, wire-array samples exhibited $V_{oc}$ = 0.41 ± 0.04 V, $J_{sc}$ = 7.7 ± 0.9 mA $cm^{-2}$, $\Phi_{ext,sc}$ = 0.20 ± 0.02, *ff* = 0.50 ± 0.10, and $\eta_{808}$ = 2.6 ± 0.4% (across six devices). For the specific wire-array electrode displayed in Fig. 3, $V_{oc}$ = 0.42 V, $J_{sc}$ = 7.9 mA $cm^{-2}$, $\Phi_{ext,sc}$ = 0.20, *ff* = 0.55, and $\eta_{808}$ = 3.0%. The inherent photoelectrode properties of this electrode were $ff_{corr}$ = 0.65 and $\eta_{808,corr}$ = 3.6%.

The $V_{oc}$ of a semiconductor junction is given by

$$V_{oc} = (nk_BT/q)\ ln\ (J_{ph}/\gamma J_o) \qquad (1)$$

where $n$ is the diode quality factor, $k_B$ is the Boltzmann constant, $T$ is the temperature (in Kelvin), $q$ is the (unsigned) charge on an electron, $J_{ph}$ is the photocurrent density, $J_o$ is the exchange current density, and γ is the ratio of the actual junction area to the projected surface area of the electrode, that is, the roughness factor (*2*, *6*). The planar p-Si samples exhibited a $V_{oc}$ that was near the bulk recombination limit of 0.60 V (at $J_{ph} = J_{sc}$ = 27 mA $cm^{-2}$), which was calculated from the value of $J_o$ produced by the known bulk properties and effective minority-carrier diffusion length of the p-Si sample investigated (*20*), attesting to the high quality of the semiconductor/liquid junction obtained in this test electrolyte system.

Equation 1 implies that for each 10-fold increase in γ, the reduced splitting in the quasi-Fermi levels when the photogenerated charge carriers are diluted over the larger junction area will decrease $V_{oc}$ at room temperature by at least 59 mV. Because γ ~ 10 for the wire-array samples fabricated here, the $V_{oc}$ is thus within ~50 mV of that expected on the basis of the behavior of the planar cells at similar $J_{sc}$ levels. This result suggests that these p-Si microwires are largely free of electronically deleterious defects or impurities that would lower the $V_{oc}$ substantially beyond that dictated by purely geometric considerations.

Optimized wire-array solar cells would exhibit a much higher $J_{sc}$ than the values observed in the test samples. To evaluate the reasons for the lower $J_{sc}$ values of the wire arrays relative to the planar Si sample, $\Phi_{ext}$ was measured for the electrodes as a function of angle (θ, where θ = 0° is normal incidence), using excitation with a laser spot (~1 $mm^2$) much smaller than the sample area (Fig. 4). At θ = 60°, at which the light path through the array was substantially increased relative to that for θ = 0°, $\Phi_{ext}$ approached 0.7. Accounting for reflection and residual absorption by the photo-inactive $p^+$ substrate, the internal quantum yield ($\Phi_{int}$) was thus near unity. This conclusion is consistent with the observation that $\Phi_{ext}$ = ~0.2 at normal incidence for the wire array even though the specific growth template produced wires that filled only 4% of the optical plane.

Under 100 mW $cm^{-2}$ of simulated solar illumination in the same electrolyte that did not contain $MV^+$ (so as to eliminate visible light absorption), these p-Si wire arrays exhibited $J_{sc}$ values of ~9 to 11 mA $cm^{-2}$ (*21*). The theoretical $J_{sc}$ limit for Si under such conditions is 43 mA $cm^{-2}$, and in practice optical reflection losses reduce this value to ~35 mA $cm^{-2}$. Hence, the $J_{sc}$ observed for the wire-array sample is larger, by a factor of ~6, than the $J_{sc}$ expected for complete light absorption and unity internal quantum yield by an array that captured only 4% of the incident photons (based on the geometric filling fraction of the optical plane). This observation indicates substantial internal light scattering and optical focusing into the Si regions of the wire arrays.

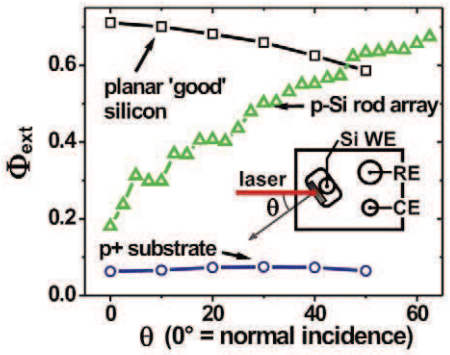


**Fig. 4.** Angle-resolved photocurrent measurements performed with a 633-nm He-Ne laser (power = 2.6 μW). Measurements were conducted in the absence of the $MV^+$ radical cation in order to avoid issues associated with oxygen sensitivity and solution absorbance (*29*). The uncertainties associated with the measurement of $\Phi_{ext}$ and θ were ±0.003 and ±0.5°, respectively. (Inset) Schematic of the cell, showing the rotating p-Si working electrode (WE) that was biased during measurement at −0.45 V versus SCE, the reference electrode (RE), and the counter electrode (CE).

Because in this work the internal quantum yields have been determined to approach unity, methods for achieving nearly complete light absorption [by increasing the wire-array packing fraction from the current value of ~4% or by improving optical trapping effects (*21*), for instance by placing dielectric scattering elements in between the wires] would thus be expected to produce a fourfold increase in the short-circuit photocurrent density to values comparable with or in excess of those observed for Si single crystals under the same conditions.

As shown in Fig. 3, the fill factor was similar for both the planar samples and the p-Si wire arrays. The *J-E* behavior of the planar sample indicates that with sufficient mass transport, either by active convection (as used here) or by passive means through the use of a thin-layer cell configuration (*22*), this specific test electrolyte allows for $J_{sc} > 35$ mA cm$^{-2}$ with low accompanying mass-transport–based overpotentials. Consistent with these observations, we found that increasing the concentration of $MV^{2+}$ to 0.1 M had little effect on the *J-E* behavior. However, in order to use wire arrays that produce increased photocurrent densities due to optimal light absorption at normal incidence, mass-transport limitations of redox species in the internal volume of the wire-array structure and unwanted optical absorption due to the ineffective removal of the colored $MV^+$ species within this volume must be minimized. Similar challenges have been overcome in the optimization of dye-sensitized nanocrystalline $TiO_2$ solar cells (*23*).

Provided that the optical absorption of the redox species can be minimized, improvements in $J_{sc}$ to 35 mA cm$^{-2}$, while retaining the open-circuit voltages and uncorrected fill factors displayed in Fig. 3B, would imply that photoelectrode efficiencies >8% are attainable under air mass 1.5 conditions (*24*). The importance of the observations reported here, however, is not whether optimized photoelectrochemical solar cells can be prepared by using this specific test electrolyte but rather that the inherent performance of these p-Si wire arrays in a radial junction geometry allows, conceptually, the development of efficient photovoltaic and/or photoelectrochemical energy-conversion devices based on a wire-array platform, provided that the device-related engineering issues are satisfactorily addressed.

The use of Cu as the VLS-growth catalyst (*25*), as opposed to Au (*3*, *4*, *8*, *10*), probably contributes to the relatively high inherent energy-conversion performance of these p-Si wire-array devices. Cu concentrations of less than $10^{18}$ cm$^{-3}$ appear to have little effect on the performance of planar Si solar cells (*26*). Apparently, the high diffusivity ($2.8 \times 10^{-7}$ cm$^2$ s$^{-1}$ at 300 K) and the large energy barrier for precipitate nucleation of Cu in p-Si allow for collection of Cu at surfaces and defects, thus leaving the bulk Si largely free of Cu (*27*). At the growth temperature (1000°C), the wires are presumably saturated (~$5 \times 10^{17}$ cm$^{-3}$) with Cu, but upon cooling Cu probably segregates to the wire surface, allowing for its subsequent removal via chemical etching before testing of the resulting devices. No Cu was detected on the etched wire samples by using surface-sensitive techniques such as x-ray photoelectron spectroscopy, although more detailed experiments are needed to quantify the location and removal of Cu impurities that might originate from the VLS catalyst (*28*).

Although Si wire arrays and dye-sensitized nanocrystalline $TiO_2$ photoelectrodes both have absorbers with high aspect ratios, the properties of these two systems are governed by different physical principles. Dye-sensitized nanocrystalline $TiO_2$ photoelectrochemical cells do not have an appreciable space-charge layer in the $TiO_2$, and charge-carrier separation after dye-based light absorption relies on diffusion, along with the asymmetric, slow interfacial charge-transfer kinetics of the $I_3^-/I^-$ redox couple that is uniquely effective in preventing electron-hole recombination in such systems. In contrast, charge-separation in the Si wire-array system is driven by an interfacial electric field in the space-charge region of the radial junction, and charge-carrier transport and recombination are governed by conventional device-physics principles implemented in a radial geometry (*2*). Thus, in addition to lacking a surface-bound dye for light absorption, Si wire arrays should be useful both as photoanodes and photocathodes in contact with a variety of aqueous and nonaqueous electrolytes that contain well-developed, kinetically facile, one-electron redox couples, as well as for photoelectrochemical $H_2$ evolution from water, given the integration of appropriate electrocatalysts (*1*).

## References and Notes


1. R. N. Dominey, N. S. Lewis, J. A. Bruce, D. C. Bookbinder, M. S. Wrighton, *J. Am. Chem. Soc.* **104**, 467 (1982).
2. B. M. Kayes, H. A. Atwater, N. S. Lewis, *J. Appl. Phys.* **97**, 114302 (2005).
3. A. P. Goodey, S. M. Eichfeld, K. K. Lew, J. M. Redwing, T. E. Mallouk, *J. Am. Chem. Soc.* **129**, 12344 (2007).
4. J. R. Maiolo 3rd *et al.*, *J. Am. Chem. Soc.* **129**, 12346 (2007).
5. E. C. Garnett, P. D. Yang, *J. Am. Chem. Soc.* **130**, 9224 (2008).
6. J. M. Spurgeon, H. A. Atwater, N. S. Lewis, *J. Phys. Chem. C* **112**, 6186 (2008).
7. B. Z. Tian *et al.*, *Nature* **449**, 885 (2007).
8. B. Tian, T. J. Kempa, C. M. Lieber, *Chem. Soc. Rev.* **38**, 16 (2009).
9. M. D. Kelzenberg *et al.*, *Nano Lett.* **8**, 710 (2008).
10. L. Tsakalakos *et al.*, *Appl. Phys. Lett.* **91**, 3 (2007).
11. T. Stelzner *et al.*, *Nanotechnology* **19**, 295203 (2008).
12. K. Peng *et al.*, *Small* **1**, 1062 (2005).
13. C. Colombo, M. Heiss, M. Gratzel, A. F. I. Morral, *Appl. Phys. Lett.* **94**, 3 (2009).
14. R. S. Wagner, W. C. Ellis, *Appl. Phys. Lett.* **4**, 89 (1964).
15. Materials and methods are available as supporting material on *Science* Online.
16. B. M. Kayes *et al.*, *Appl. Phys. Lett.* **91**, 103110 (2007).
17. D. C. Bookbinder, N. S. Lewis, M. G. Bradley, A. B. Bocarsly, M. S. Wrighton, *J. Am. Chem. Soc.* **101**, 7721 (1979).
18. J. F. Stargardt, F. M. Hawkridge, *Anal. Chim. Acta* **146**, 1 (1983).
19. T. W. Hamann, F. Gstrein, B. S. Brunschwig, N. S. Lewis, *J. Am. Chem. Soc.* **127**, 7815 (2005).
20. N. S. Lewis, *J. Electrochem. Soc.* **131**, 2496 (1984).
21. O. L. Muskens, J. G. m. Rivas, R. E. Algra, E. P. A. M. Bakkers, A. Lagendijk, *Nano Lett.* **8**, 2638 (2008).
22. J. F. Gibbons, G. W. Cogan, C. M. Gronet, N. S. Lewis, *Appl. Phys. Lett.* **45**, 1095 (1984).
23. M. Grätzel, *Nature* **414**, 338 (2001).
24. The efficiency is calculated as $J_{sc} * V_{oc} * ff$(100 mW cm$^{-2}$), where $J_{sc}$ is assumed to be 35 mA cm$^{-2}$, $V_{oc}$ = 0.42, and $ff$ = 0.55. These photoelectrode parameters are consistent with those estimated from air mass 1.5 illumination.
25. V. Schmidt, J. V. Wittemann, S. Senz, U. Gosele, *Adv. Mater.* **21**, 2681 (2009).
26. J. R. Davis *et al.*, *IEEE Trans. Electron. Dev.* **27**, 677 (1980).
27. A. A. Istratov, E. R. Weber, *J. Electrochem. Soc.* **149**, G21 (2002).
28. M. C. Putnam *et al.*, *Nano Lett.* **8**, 3109 (2008).
29. These current densities were measured in the absence of $MV^+$ radical cation. This configuration allows for testing in an optically transparent solution and hence measurement of accurate values for $J_{sc}$ under solar simulation. Under these conditions, the cell does not operate as a regenerative photovoltaic because the potentiostat drives oxygen evolution at the Pt counter (as opposed to $MV^+$ oxidation).


30. We acknowledge the Stanford Global Climate and Energy Project and the U.S. Department of Energy (grant DE-FG02-05ER15754) for financial support. S.W.B. thanks the Kavli Nanoscience Institute for a postdoctoral fellowship. L. O'Leary is thanked for her contributions. The authors have filed U.S. patent applications (20090020150 and 20090020853) related to this work.


## Supporting Online Material

www.sciencemag.org/cgi/content/full/327/5962/185/DC1
Materials and Methods
References

19 August 2009; accepted 10 November 2009
10.1126/science.1180783

# Two White Dwarfs with Oxygen-Rich Atmospheres

B. T. Gänsicke,[1]* D. Koester,[2] J. Girven,[1] T. R. Marsh,[1] D. Steeghs[1]

Stars with masses ranging from 7 to 10 times the mass of the Sun end their lives either as massive white dwarfs or weak type II supernovae, but there are only limited observational constraints on either evolutionary channel. Here we report the detection of two white dwarfs with large photospheric oxygen abundances, implying that they are bare oxygen-neon cores and that they may have descended from the most massive progenitors that avoid core collapse.

White dwarfs represent the end points of stellar evolution for the overwhelming majority of all stars. Most white dwarfs in the galaxy have carbon-oxygen (CO) core compositions, being descendants of low- to intermediate-mass stars that underwent hydrogen (H) and helium (He) core burning. Stars with initial masses $M$ between 7 and 10 solar masses ($M_\odot$) will reach sufficiently high core temperatures to proceed to C burning, and either produce oxygen-neon (ONe)–core white dwarfs or undergo a core-collapse supernova (type II supernova, or SN II) via electron capture on the products of C burning (*1*). Knowledge about the exact outcome of stellar evolution in this mass range depends critically on a detailed understanding of mass loss (*2*), the relevant nuclear reaction rates, and the efficiency of convective mixing in the stellar cores (*3*). Some observational constraints on stellar models come from analysis of SN II progenitors (*4*), which suggests a lower limit on the progenitor masses of $8^{+1.0}_{-1.5} M_\odot$. A linear extrapolation of the observed relation between the masses of white dwarfs and their progenitor stars (*5*) up to the maximum mass of white dwarfs (or Chandrasekhar mass) leads to a broadly consistent result.

Information about the core compositions of white dwarfs, in particular of those descending from stars with the highest possible masses, would help to test and improve the theory of stellar evolution. Unfortunately, almost all white dwarfs have H and/or He envelopes that, although low in mass, are sufficiently thick to shield the core from direct view. Asteroseismology has the potential to unveil their core composition (*6*), but observational studies attempting to exploit this potential remain ambiguous [see, for example, the case of GD358 (*3*, *7*, *8*)]. Core material can be directly detected in the photospheres of a small number of stars (*9*) that underwent a very late thermal pulse during their asymptotic giant branch (AGB) evolution, ejecting a large fraction of the envelope (*10*) and leaving a white dwarf with only a thin layer of He. Examples of H-deficient post-AGB stars are the hot PG1159 objects, white dwarfs with He-rich (DB) atmospheres, and the cool, C-rich (DQ) white dwarfs. The most extreme case known to date is 1H1504+65, which is H- and He-deficient, with a hot, naked CO surface (*11*).

Recently, the Sloan Digital Sky Survey (SDSS), through its comprehensive spectroscopic snapshot of the galactic stellar population, has revealed a small class of H-deficient white dwarfs (*12*). Their spectra are consistent with nearly pure C atmospheres (*13*). It has been suggested that these "hot" DQ white dwarfs represent the evolutionary link between objects such as PG1159 and 1H1504+65, the DB white dwarfs, and the cool DQ white dwarfs (*14*, *15*).

Until now, all known white dwarfs for which photospheric O and C abundances have been determined have had abundance ratios O/C ≤ 1. Some stellar models predict that the most-massive stars avoiding core collapse will result in ONe white dwarfs with very low C abundances (*16*). Should such a core lose its H envelope, an extremely O-rich spectrum would be expected. Here we present the results of a search for white dwarfs with large photospheric O abundances within the SDSS spectroscopic data release 7 (DR7) (*17*).

We selected all spectroscopic objects in DR7 that fall within the *ugriz* color space of the white dwarfs from (*18*). We then subjected these spectra to an automatic measurement of the equivalent widths [see (*19*) for details of the method] of the neutral O (OI) 616-nm and 778-nm multiplets, which are the strongest OI lines expected in a cool O-rich atmosphere. Another strong OI multiplet is located at 845 nm; however, this region can be affected by residuals from the night-sky line subtraction, and therefore we did not include it in our procedure. As an additional constraint, we required the spectra to have a signal-to-noise ratio ≥10 in the regions around the two OI lines, resulting in the analysis of 25,639 SDSS spectra in total (*20*).

We found 1000 spectra with a formal 99.99% (4σ) detection of both OI lines, and visual inspection of these spectra showed that 998 were erroneously flagged by our automated routine because of poor data quality. Only two objects with genuine OI 616-nm and 778-nm absorption, SDSS J092208.19+292810.9 and SDSS J110239.69+205439.4, survived our scrutiny (Table 1). Both have high proper motions, 0.275″ year$^{-1}$ and 0.163″ year$^{-1}$, respectively (*21*), consistent with them being nearby low-luminosity blue stars. Aside from the OI 616-nm and 778-nm absorption lines, the spectrum of SDSS 0922+2928 (Fig. 1) is typical of a cool DQ white dwarf, with strong $C_2$ Swan bands in the blue, superimposed by a number of atomic C lines. In contrast, SDSS 1102+2054 is a unique white dwarf (*22*) with a photospheric spectrum totally dominated by absorption lines of OI (Fig. 1). The only other noticeable features are some weak lines of atomic CI as well as Hα and Hβ.

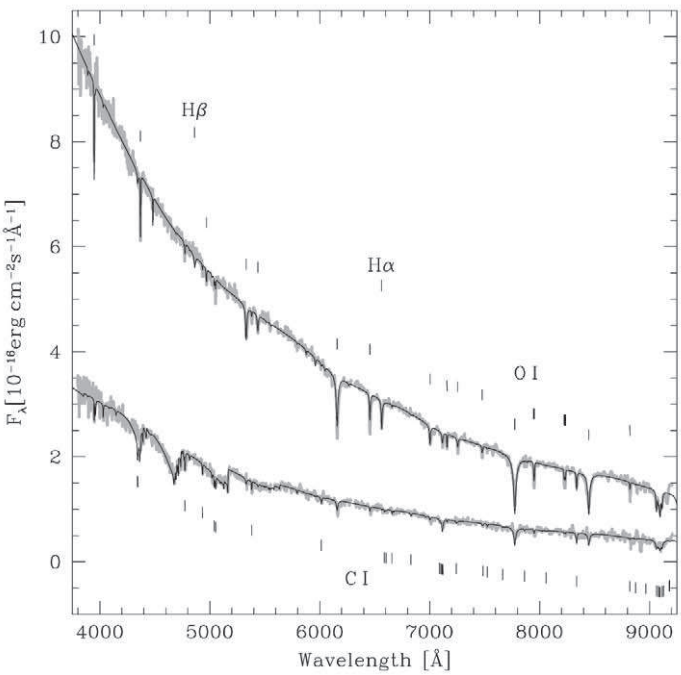


**Fig. 1.** SDSS spectroscopy. The observed spectra of SDSS 0922+2928 (bottom) and SDSS 1102+2054 (top) are shown as thick gray lines. Superimposed as thin black lines are models for $T_{eff}$ = 10,000 K and log($g$) = 8 (bottom) and $T_{eff}$ = 10,500 K and log($g$) = 8 (top). The wavelengths of the strongest OI and CI absorption lines, as well as of Hα and Hβ, are indicated by tick marks. $F_\lambda$ is the power received at Earth per unit area and wavelength interval.

[1]Department of Physics, University of Warwick, Coventry CV4 7AL, UK. [2]Institut für Theoretische Physik und Astrophysik, University of Kiel, 24098 Kiel, Germany.

*To whom correspondence should be addressed. E-mail: Boris.Gaensicke@warwick.ac.uk

We determined the effective temperatures of the two white dwarfs by fitting their SDSS *ugriz* photometry with two grids of theoretical atmosphere models: one for a pure He composition [supporting online material (SOM) text, section 1], and one including H, C, and O as well (SOM text, section 2). The white dwarf temperatures and chemical abundances determined from these fits depend only mildly on the assumed surface gravity log(*g*), and, because their masses are not constrained by the available observations, we fixed $M = 0.6\ M_{\odot}$, corresponding to the canonical value of log(*g*) = 8 [(*23*), SOM text, section 2].

Independent of the details of the atmospheric composition, the photometry suggests that both white dwarfs have temperatures in the range from 8000 to 9000 K (Table 2). The implied distances depend strongly on the assumed surface gravity via the radius; here we used the mass-radius relation from (*24*). We used the effective temperatures (and assumed surface gravity) to calculate synthetic spectra for a final determination of atmospheric abundances from the absorption lines in the SDSS spectroscopy (SOM text, section 2).

For SDSS 1102+2054, we adopted an effective temperature $T_{\rm eff}$ = 8150 K and log(*g*) = 8 and iterated the abundances of H, C, and O until we obtained a reasonable fit to the line strengths. Because this was not possible for all O lines, we concentrated on the strong lines at 778 and 845 nm, which originate from the lowest-lying levels of all optical lines. These lines depend only weakly on temperature and are best suited for a determination of abundances. The best compromise was achieved for the abundances shown in Table 3.

However, for this model, the carbon lines near 712 and 834 nm, Hα, and many OI lines from higher levels are much too broad, indicating too high a pressure in the atmosphere. In addition, OI lines from the higher levels are much too weak. The most likely solution to this discrepancy is to assume a higher temperature, which increases the strength of the high-excitation lines as compared with the strong multiplets (SOM text, section. 2). A reasonable compromise was achieved with $T_{\rm eff}$ = 10,500 K, log(*g*) = 8 (Table 3). The remaining differences in the absorption lines between the model and what was observed are probably within the uncertainties of the atomic data and, in particular, the van der Waals broadening constants (SOM text, section 2).

This model, however, is in marked disagreement with the temperature that was derived from the SDSS photometry. One plausible cause for the discrepancy between the temperatures determined from our fits to the photometry and those to the spectroscopy are uncertainties in the ultraviolet opacities of an atmosphere of such peculiar composition, which strongly affect the slope of the optical continuum [(*14*), SOM text, section 1].

The atmospheric parameters of SDSS 1102+2054 thus remain somewhat uncertain. Nevertheless, when varying the parameters within the range demanded by photometry, line strengths, and widths, the C and O abundances did not change by more than factors of ~3. Thus, the O/C abundance ratio in SDSS 1102+2054 is clearly much larger than 1, which makes this star unique among the many thousands of known white dwarfs.

According to the photometry, the effective temperature for the two white dwarfs cannot be very different; therefore, the C abundance in SDSS 0922+2928 must be higher in order to produce the strong $C_2$ Swan bands. On the other hand, the H abundance must be lower, because no Balmer lines are visible. We fixed the H/He ratio at $10^{-5}$, which is the upper limit allowed by Hβ. Further reduction did not substantially influence the models, because the major electron donors are C and O. Using $T_{\rm eff}$ = 8270 K from the fit to the photometry, and assuming log(*g*) = 8.0, we obtained a good fit to the spectrum with the O abundance decreased by $10^{0.2}$ and a C abundance increased by $\sim 10^{0.6}$ with respect to SDSS 1102+2054 (Table 3). Therefore, O/C > 1 also in SDSS 0922+2928. With the exception of the strong OI multiplets at 778 and 845 nm, most of the higher-excitation OI lines and the CI lines show the same problem as in SDSS 1102+2054: They are too weak and too broad. This is again much improved at a hotter temperature, for example, 10,000 K, which is, however, in conflict with the photometry (SOM text, section 1).

The low H abundance suggests that SDSS 0922+2928 and SDSS 1102+2054, similar to the other classes of H-deficient white dwarfs, underwent a late shell flash, leaving a He-dominated atmosphere. At the low temperatures of these stars, the He convection zone extends sufficiently deep to dredge core material up into the atmospheres (*25*, *26*). Given the large age of the two stars (>500 million years), gravitational diffusion will unavoidably lead to a larger concentration of C in the envelope. The only plausible explanation for the observed O/C abundance ratio is that these two white dwarfs have, overall, very low C mass fractions and hence represent naked ONe cores. As such, they are distinct from 1H1504+65 and the "hot" DQ white dwarfs.

Most stellar models that produce ONe cores predict a layer of CO surrounding the core that should be sufficiently thick to avoid upward diffusion of large amounts of O. However, a sequence of stellar evolution calculations approaching the mass boundary of stars forming ONe white dwarfs and those undergoing electron-capture SN II shows that the mass of the CO layer decreases with increasing initial stellar mass (*16*, *27*, *28*). Thus, SDSS 0922+2928 and SDSS 1102+2054 may have descended from the most massive stars avoiding core collapse, in which case they would be expected to be very massive themselves. Our current data are insufficient to provide any unambiguous measure of the masses of SDSS 0922+2928 and SDSS 1102+2054; however, their C/He abundance is at the top of the range observed in the C-rich sequence of cool DQ (*23*, *29*) white dwarfs, some of which have parallax measurements that imply that they are of high mass.

**Table 1.** Equatorial coordinates, magnitudes, and proper motions (p.m.). RA, right ascension; Dec, declination.

| | SDSS 0922+2928 | SDSS 1102+2054 |
|---|---|---|
| RA (2000) | 09 22 08.19 | 11 02 39.69 |
| Dec (2000) | +29 28 10.9 | +20 54 39.4 |
| *u* | 18.77 ± 0.02 | 17.58 ± 0.02 |
| *g* | 18.52 ± 0.02 | 17.24 ± 0.01 |
| *r* | 18.47 ± 0.02 | 17.26 ± 0.01 |
| *i* | 18.58 ± 0.02 | 17.34 ± 0.01 |
| *z* | 18.71 ± 0.03 | 17.46 ± 0.02 |
| p.m. | 0.275″ year$^{-1}$ | 0.163″ year$^{-1}$ |

**Table 2.** Atmospheric parameters for a surface gravity of log(*g*) = 8.

| System | $T_{\rm eff}$ (K) | | Distance (pc) | |
|---|---|---|---|---|
| | Pure He | With metals | Pure He | With metals |
| SDSS 0922+2928 | 8720 ± 260 | 8270 ± 320 | 141 ± 6 | 122 ± 7 |
| SDSS 1102+2054 | 8820 ± 110 | 8150 ± 150 | 81 ± 2 | 67 ± 2 |

**Table 3.** Photospheric abundances (by number).

| System [$T_{\rm eff}$/log(*g*)] | log(H/He) | log(C/He) | log(O/He) | log(O/C) |
|---|---|---|---|---|
| SDSS 1102+2054 (8150/8.0) | −3.2 | −3.2 | −1.8 | 1.4 |
| SDSS 1102+2054 (10500/8.0) | −4.0 | −3.6 | −1.8 | 1.8 |
| SDSS 0922+2928 (8270/8.0) | −5.0 | −2.6 | −2.0 | 0.6 |

We explored spectral models of SDSS 1102+2054 with the abundances kept fixed as in Table 3, but adopting surface gravities of $\log(g) = 8.5$ and 9.0, which correspond to masses of 0.9 $M_\odot$ and 1.2 $M_\odot$ (SOM text, section 2). Broadly similar fits to the absorption lines can be achieved for higher surface gravities, if the temperature is increased by 1000 to 2000 K as well. For $\log(g) = 9.0$, the strongest O I lines become somewhat too broad as compared with the observations, and we conclude that the currently available data are consistent with masses of up to ~1 $M_\odot$.

Initial models of the evolution of intermediate-mass stars predict that ONe cores should also contain substantial amounts of Mg. Updated nuclear reaction rates have lead to a marked downward revision of the Mg abundances (*30*). For SDSS 1102+2054, which has the better-quality spectrum of the two white dwarfs presented here, we can place an upper limit on the Mg abundance of $\log[\mathrm{Mg/He}] < -6.1$ from the absence of the Mg II 448-nm line.


**References and Notes**

1. K. Nomoto, *Astrophys. J.* **277**, 791 (1984).
2. A. Heger, C. L. Fryer, S. E. Woosley, N. Langer, D. H. Hartmann, *Astrophys. J.* **591**, 288 (2003).
3. O. Straniero, I. Domínguez, G. Imbriani, L. Piersanti, *Astrophys. J.* **583**, 878 (2003).
4. S. J. Smartt, J. J. Eldridge, R. M. Crockett, J. R. Maund, *Mon. Not. R. Astron. Soc.* **395**, 1409 (2009).
5. K. A. Williams, M. Bolte, D. Koester, *Astrophys. J.* **693**, 355 (2009).
6. A. H. Córsico, E. García-Berro, L. G. Althaus, J. Isern, *Astron. Astrophys.* **427**, 923 (2004).
7. T. S. Metcalfe, D. E. Winget, P. Charbonneau, *Astrophys. J.* **557**, 1021 (2001).
8. G. Fontaine, P. Brassard, *Astrophys. J.* **581**, L33 (2002).
9. K. Werner, F. Herwig, *Publ. Astron. Soc. Pac.* **118**, 183 (2006).
10. F. Herwig, T. Blöcker, N. Langer, T. Driebe, *Astron. Astrophys.* **349**, L5 (1999).
11. K. Werner, T. Rauch, M. A. Barstow, J. W. Kruk, *Astron. Astrophys.* **421**, 1169 (2004).
12. J. Liebert *et al.*, *Astrophys. J.* **126**, 2521 (2003).
13. P. Dufour, J. Liebert, G. Fontaine, N. Behara, *Nature* **450**, 522 (2007).
14. P. Dufour, G. Fontaine, J. Liebert, G. D. Schmidt, N. Behara, *Astrophys. J.* **683**, 978 (2008).
15. L. G. Althaus, E. García-Berro, A. H. Córsico, M. M. Miller Bertolami, A. D. Romero, *Astrophys. J.* **693**, L23 (2009).
16. I. J. Iben, C. Ritossa, E. Garcia-Berro, *Astrophys. J.* **489**, 772 (1997).
17. K. N. Abazajian *et al.*, *Astrophys. J. Suppl.* **182**, 543 (2009).
18. D. J. Eisenstein *et al.*, *Astrophys. J. Suppl.* **167**, 40 (2006).
19. B. T. Gänsicke, T. R. Marsh, J. Southworth, *Mon. Not. R. Astron. Soc.* **380**, L35 (2007).
20. We inspected a representative subset of all the DR7 spectra in our sample and estimate that our analysis comprised ≅ 6000 genuine white dwarfs. Applying the same color constraints used in our query on DR7 to the DR4 white dwarf catalog (*18*) left ≅ 2400 objects, which implies that using DR7 more than doubles the available candidate sample.
21. S. Lépine, M. M. Shara, *Astrophys. J.* **129**, 1483 (2005).
22. We specifically did not restrict our search to objects classified as "stars" by the SDSS processing pipeline, because very unusual objects may be misidentified by the SDSS spectroscopic classification algorithm. Within DR7, the algorithm correctly identified SDSS 0922+2928 as a star but left SDSS 1102+2054 as an object of unknown type.
23. P. Dufour, P. Bergeron, G. Fontaine, *Astrophys. J.* **627**, 404 (2005).
24. M. A. Wood, *White Dwarfs*, D. Koester, K. Werner, Eds., no. 443 in *Lecture Notes in Physics* (Springer, Heidelberg, Germany, 1995), pp. 41–45.
25. D. Koester, V. Weidemann, E.-M. Zeidler, *Astron. Astrophys.* **116**, 147 (1982).
26. C. Pelletier, G. Fontaine, F. Wesemael, G. Michaud, G. Wegner, *Astrophys. J.* **307**, 242 (1986).
27. E. Garcia-Berro, I. Iben, *Astrophys. J.* **434**, 306 (1994).
28. E. Garcia-Berro, C. Ritossa, I. J. Iben, *Astrophys. J.* **485**, 765 (1997).
29. D. Koester, S. Knist, *Astron. Astrophys.* **454**, 951 (2006).
30. J. Gutiérrez, R. Canal, E. García-Berro, *Astron. Astrophys.* **435**, 231 (2005).


31. J.G. is supported by a Science and Technology Facilities Council (STFC) studentship. B.T.G., T.R.M., and D.S. are supported by an STFC rolling grant. We thank D. Townsley for useful discussions.


**Supporting Online Material**

www.sciencemag.org/cgi/content/full/1180228/DC1
SOM Text
Figs. S1 and S2
References


5 August 2009; accepted 30 October 2009
Published online 12 November 2009;
10.1126/science.1180228
Include this information when citing this paper.


# E-Type Asteroid (2867) Steins as Imaged by OSIRIS on Board Rosetta


**H. U. Keller,[1]* C. Barbieri,[2] D. Koschny,[3] P. Lamy,[4] H. Rickman,[5,20] R. Rodrigo,[6] H. Sierks,[1] M. F. A'Hearn,[7] F. Angrilli,[2] M. A. Barucci,[8] J.-L. Bertaux,[9] G. Cremonese,[2] V. Da Deppo,[21] B. Davidsson,[10] M. De Cecco,[2] S. Debei,[2] S. Fornasier,[8] M. Fulle,[11] O. Groussin,[4] P. J. Gutierrez,[6] S. F. Hviid,[1] W.-H. Ip,[12] L. Jorda,[4] J. Knollenberg,[13] J. R. Kramm,[1] E. Kührt,[13] M. Küppers,[14] L.-M. Lara,[6] M. Lazzarin,[2] J. Lopez Moreno,[6] F. Marzari,[2] H. Michalik,[15] G. Naletto,[2] L. Sabau,[16] N. Thomas,[17] K.-P. Wenzel,[3] I. Bertini,[6] S. Besse,[4] F. Ferri,[2] M. Kaasalainen,[18] S. Lowry,[19] S. Marchi,[2] S. Mottola,[13] W. Sabolo,[6] S. E. Schröder,[1] S. Spjuth,[1] P. Vernazza[3]**



The European Space Agency's Rosetta mission encountered the main-belt asteroid (2867) Steins while on its way to rendezvous with comet 67P/Churyumov-Gerasimenko. Images taken with the OSIRIS (optical, spectroscopic, and infrared remote imaging system) cameras on board Rosetta show that Steins is an oblate body with an effective spherical diameter of 5.3 kilometers. Its surface does not show color variations. The morphology of Steins is dominated by linear faults and a large 2.1-kilometer-diameter crater near its south pole. Crater counts reveal a distinct lack of small craters. Steins is not solid rock but a rubble pile and has a conical appearance that is probably the result of reshaping due to Yarkovsky-O'Keefe-Radzievskii-Paddack (YORP) spin-up. The OSIRIS images constitute direct evidence for the YORP effect on a main-belt asteroid.


The European Space Agency's (ESA) Rosetta mission was launched in 2004 to rendezvous with comet 67P/Churyumov-Gerasimenko in 2014. It passed the asteroid (2867) Steins with a relative velocity of 8.6 km $s^{-1}$ on 5 September 2008. Closest approach (CA) took place at 18:38:20 UTC at a distance of 803 km, chosen such that the spacecraft could keep the instruments continuously pointed toward the asteroid. Early in the approach, the solar phase angle (Sun–object–observer) was 38°. It decreased to a minimum of 0.27° (opposition) 2 min before CA. It increased again to 51° at CA, and finally to 141° at the end of observations. The scientific camera system OSIRIS consists of a narrow-angle camera (NAC) and a wide-angle camera (WAC) (*1*). The NAC (with five times higher resolving power) unfortunately stopped its automatic operation at a distance of 5200 km, 10 min before CA. Thus the highest-resolution images of the surface of Steins were taken by the WAC.

The shape of Steins resembles that of a brilliant cut diamond. The last NAC image, taken at 31° before reaching minimum phase angle, and the best WAC image, near CA at 61.5° phase angle, show a very similar outline (Fig. 1). The surface of Steins is mostly covered by shallow craters, often with subdued, ambiguous rims. Some of the larger craters are pitted with smaller ones. The overall crater shape and depth-to-diameter ratio (~0.12) are consistent with degradation


[1]Max Planck Institute for Solar System Research, Katlenburg-Lindau, Germany. [2]University of Padova, Padova, Italy. [3]European Space and Technology Centre, Noordwijk, Netherlands. [4]Laboratoire d'Astrophysique de Marseille, Université de Provence, Marseille, France. [5]Institute för Astronomi och Rymdfysik, Uppsala, Sweden. [6]Instituto de Astrofísica de Andalucía–Consejo Superior de Investigaciones Científicas, Granada, Spain. [7]University of Maryland, College Park, MD 20742, USA. [8]Observatoire de Paris, Meudon, France. [9]Services d'Aéronomie de CNRS, Verrières le Buisson, France. [10]Department of Physics and Astronomy, Uppsala University, Uppsala, Sweden. [11]International School for Advanced Studies, Trieste, Italy. [12]National Central University, Jhongli City, Taiwan. [13]German Aerospace Center, Berlin, Germany. [14]European Space Astronomy Centre (ESAC), Madrid, Spain. [15]Institute of Computer and Network Engineering, Braunschweig, Germany. [16]Instituto Nacional de Técnica Aérospacial, Torrejon de Ardoz, Spain. [17]Physikalisches Institut der Universität Bern, Switzerland. [18]Tampere University of Technology, Tampere, Finland. [19]University of Kent, Canterbury, UK. [20]Polish Academy of Sciences Space Research Center, Warsaw, Poland. [21]Consiglio Nazionale delle Ricerche-Istituto Nazionale per la Fisica della Materia, Luxor, Padova, Italy.

*To whom correspondence should be addressed. E-mail: keller@linmpi.mpg.de

caused by ejecta blanketing and regolith disturbance by impact seismic shaking (*2*). A large, 2.1-km-diameter crater is located near the south pole. A series of circular indentations and irregular ridges in an almost linear arrangement extending northward from this crater features prominently on the side that was visible during CA (Fig. 1). Chains of pits (or crater-like indentations) were also observed on other asteroids visited by spacecraft (*3*, *4*), but not to the global extent seen on Steins. Chance formation of a chain (catena) of seven craters of roughly similar size is highly improbable. Instead, this feature may be linked to the impact that caused the large crater. It indicates partial drainage of loose surface material into a fracture within stronger, deeper material, possibly marking pre-existing physical inhomogeneities (*5*). Therefore, we do not consider the seven pits of the catena to be impact craters. Another elongated feature (groove), surrounded by small pits and craters, is visible in NAC images (Fig. 1). This groove is located along a meridian approximately opposite to the catena.

We identified and counted impact craters in near-CA WAC images using different methods, from visual inspection to contrast-enhancing filtering, and we obtained consistent counts for craters as small as 3 pixels across (corresponding to 240 m). From the resulting cumulative distribution of crater sizes (Fig. 2), we estimated the cratering age (*6*) based on the impactor population derived for asteroids in the main belt (*7*). Corresponding crater sizes were derived from scaling laws based on hydrocode simulations [(NSL) (*8*)] or laboratory experiments [(HSL) (*9*)]. The crater-erasing rate was obtained by scaling a model for the asteroid Gaspra (*6*). An age of 154 ± 35 million years (My) old, based on NSL, fits the distribution for craters larger than 0.5 km in diameter. Cratering ages based on HSL are typically up to a factor of 10 older (*10*), and depend on the asteroid tensile strength. We found ages of 0.4 ± 0.2 and 1.6 ± 0.5 billion years (Gy) for $10^5$ and $10^6$ dyne $cm^{-2}$, respectively. The surface of Steins is not saturated with craters like the surfaces of Ida and Mathilde (*6*). The fall-off in the distribution for crater sizes below 0.5-km diameter shows that smaller craters are underrepresented, similarly to what was found for the asteroid Eros. The NSL age that is most representative for the small craters is only 32 ± 4 My (72 ± 10 and 240 ± 30 My for HSL), possibly because the small craters were erased recently, compared with the age of the large craters. According to Asphaugh (*11*), the diameter of the largest undegraded crater on an asteroid is close to the critical diameter that is associated with an impact that "resets" the surface, that is, erases all traces of earlier craters. We then attribute the deficiency in small craters to surface reshaping (through landslides) due to spin-up by the YORP effect. YORP can modify the rotation rate and spin-axis orientation of small asteroids and has been identified as an important process driving their physical and dynamical evolution (*12*). The derived ages are younger than the collisional lifetime of 2.2 Gy that is expected for a main-belt asteroid of Steins's size (*13*).

Approximately 60% of the surface of Steins was resolved during the fly-by. We modeled the asteroid's shape (Fig. 3), based on limb positions from 1 NAC and 61 WAC images and the simultaneous inversion of a set of 28 light curves taken from Earth and during approach (*14*). Steins's overall dimensions are 6.67 × 5.81 × 4.47 $km^3$ and its spherical equivalent radius is 2.65 km. Its shape is best approximated by an oblate spheroid rotating about its short axis with a mean equatorial radius of 3.1 km and mean polar radius of 2.2 km. The pole direction is defined by right ascension = 91.6° and declination = –68.2°, resulting in an obliquity of 169.5°, that is, close to perpendicular to the ecliptic plane and retrograde rotation with a sidereal period of 6.04679 ± 0.00002 hours (*15*).

The disk-integrated geometric albedo of Steins at a wavelength of 632 nm, which was directly calculated from the radiance of the image obtained at the lowest phase angle (0.36°), is 0.40 ± 0.01. This value is consistent with Earth-based determinations (*14*, *16*) and the high albedos of other E-type asteroids. The slope of the phase curve for phase angles between 5° and 30° is 0.024 magnitude/degree. The parameters in the International Astronomical Union (IAU) H-G photometric system (*17*) are H = 12.90 and G = 0.45. We used more than 100 WAC images covering the range of wavelengths from 296 to 632 nm and phase angles between 0° and 132° to characterize the disk-resolved photometry following Hapke's model (*18*). A relatively large mean slope angle θ indicates a surface roughness higher than that typical for C- or S-type asteroids, but similar to that estimated for the asteroid 951 Gaspra (*19*). Radar observations of E-type asteroids also reveal an enhanced surface roughness (*20*). Steins's integrated geometric albedo is 0.41 ± 0.016 and its Bond

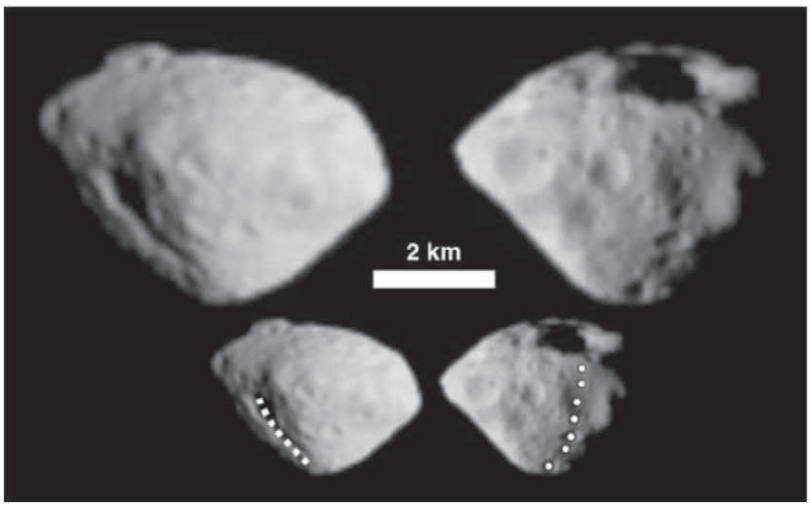


**Fig. 1.** The WAC image (top right) taken around CA at a phase angle of 61.5° shows the surface of Steins at a resolution of 80 m/pixel. The NAC image (top left) taken 10 min before CA has a slightly lower resolution of 100 m/pixel. The scale is given by the 2-km bar. The difference in viewing angle between the images is 91°, so they show opposite sides of the body. Celestial north is up. A large crater is visible near the south pole; Steins's rotation is retrograde and therefore its north pole points toward the celestial south according to IAU rules. The positions of the catena with the seven pits (bottom right image) and of the large fault on the opposite side (bottom left image) are indicated on the small annotated image copies. [Source: ESA copyright 2008 MPS for OSIRIS Team MPS/UPD/LAM/IAA/RSSD/INTA/UPM/DASP/IDA]

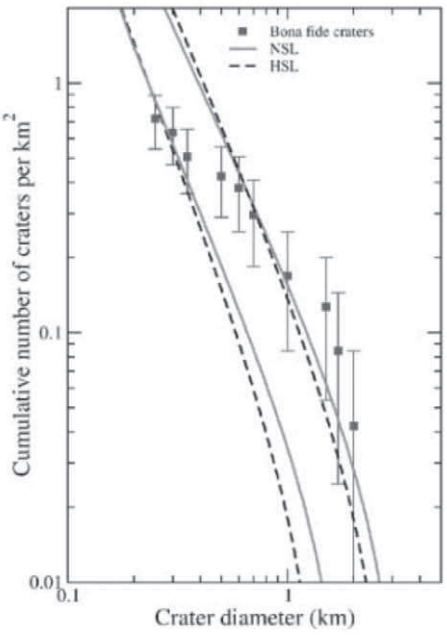


**Fig. 2.** The cumulative distribution of craters with diameter larger than 3 pixels (~240 m) visible in the WAC images around CA. The seven pits of the catena are excluded. Error bars are estimated on the basis of Poisson statistics. The pair of solid and dashed lines on the right represent best-fit models based on NSL and HSL, respectively, for craters >0.5 km. The pair on the left represents fits for craters <0.4 km.

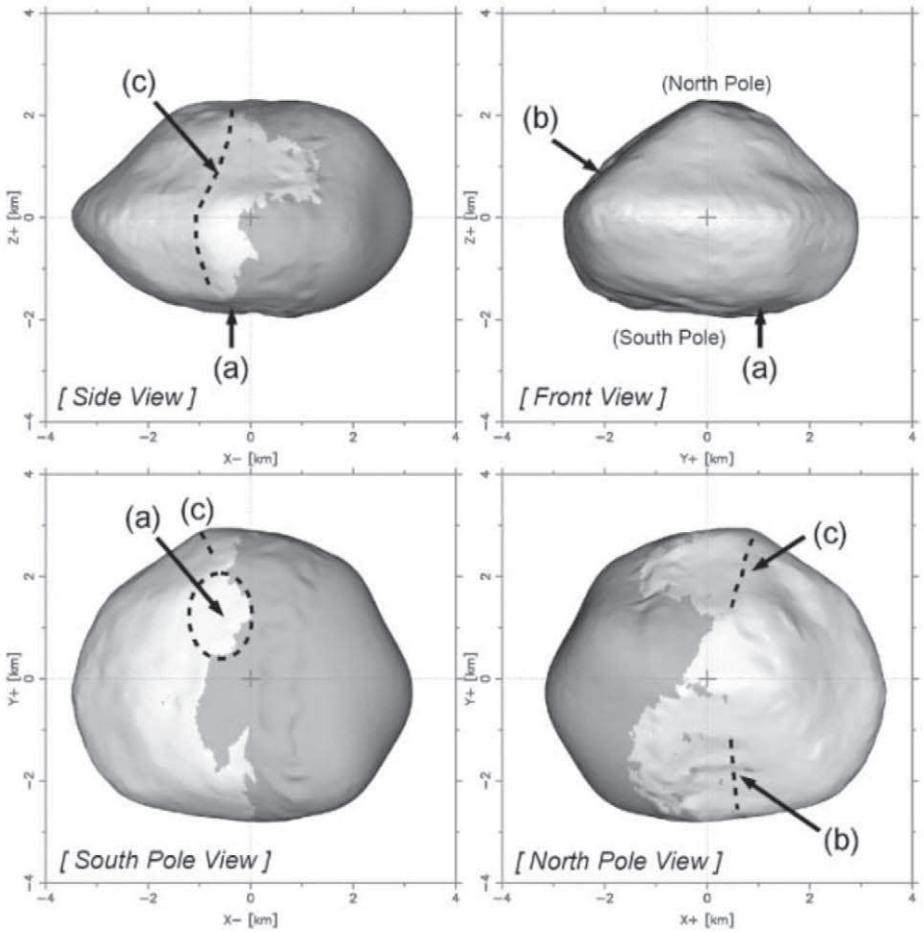


**Fig. 3.** The shape of asteroid (2867) Steins, reconstructed from limb positions, is illustrated by two equatorial views (top panels) and two polar views (bottom panels). Craters are not modeled. The north pole is up. The polar views show the shape looking down on the south (left) and north pole (right). Bright terrain represents surface visible in at least one image used to construct the shape model. The shape of the dark terrain is constrained by light curve analysis. The features indicated are labeled as follows: (a) large crater, (b) meridianal fault visible in the NAC image, and (c) catena with seven pits. Details visible on the dark terrain are artifacts from the model merging process.

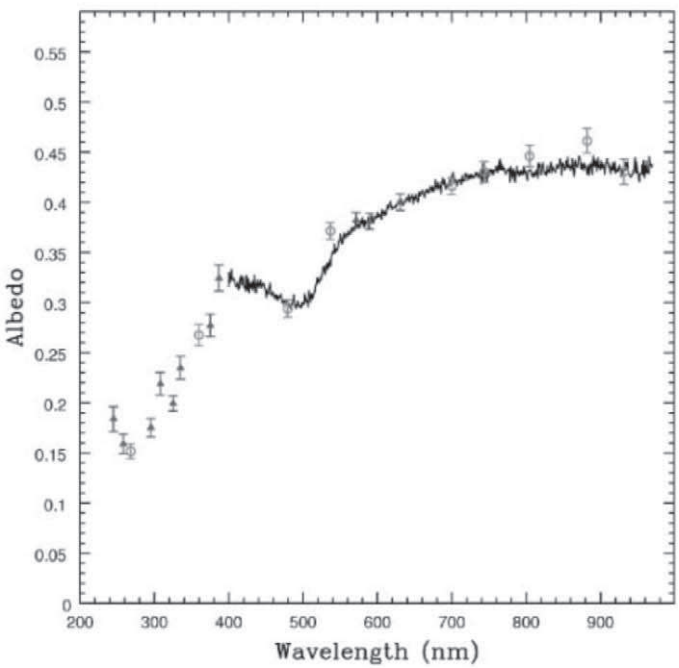


**Fig. 4.** Spectrum of Steins derived from images with 11 filters of the OSIRIS WAC (triangles) and with 9 filters of the NAC (circles). A ground-based spectrum (*24*) scaled to match at 632 nm is shown for comparison.

albedo is 0.22 ± 0.01, both calculated at 632 nm from the Hapke parameters.

The spectrum of Steins derived from OSIRIS multicolor photometry (Fig. 4) is in agreement with ground-based observations. It is slightly reddish, and phase reddening is observed over the wavelength range from 296 to 632 nm (for filter wavelengths, see Fig. 4). The spectrum shows a steep drop in the previously unexplored wavelength range below 400 nm, which is typical for low–iron content minerals (*21*). The surface composition of E-type asteroids is dominated by iron-free or iron-poor silicates such as enstatite, forsterite, or feldspar (*22*). Three different subgroups of E-type asteroids are identified by their spectral properties (*23*, *24*). The OSIRIS data confirm that Steins is a member of subtype E[II] (*24*, *25*) with a characteristic strong absorption feature at 490 nm of uncertain origin, tentatively attributed to sulfides (*23*, *26*, *27*). E-type asteroids are commonly thought to be parent bodies of enstatite meteorites, in particular of aubrites. Aubrites are highly reduced achondrites, composed of large white crystals of Fe-poor, Mg-rich orthopyroxene, or enstatite ($Mg_2Si_2O_6$), and they contain variable amounts of metallic Fe, Ni, sulfides such as troilite and oldhamite, and rare minerals. Aubrites are breccias of igneous cumulates that are not derived from shock melts but formed in an environment with temperatures higher than 1000°C (*28*).

No surface color variegation larger than 1% was detected in a principal component analysis based on six NAC images through different filters. This contrasts with previous asteroid encounters, all of which found color variegation (*4*). This uniformity suggests that Steins is compositionally homogenous and that its regolith does not display signs of space weathering (*29*) over time scales shorter than 150 My, which is the minimum age of the large craters.

Other eye-catching features on Steins are the equatorial bulge and the relatively smooth, roughly rotationally symmetric northern hemisphere, which are clearly visible in the images (Fig. 1) and in the derived shape model (Fig. 3). The shape of the northern hemisphere is reminiscent of that of the near-Earth asteroid 1999 KW4 (*30*, *31*), which has been attributed to spin-up by the YORP effect. The typical time scale associated with YORP is 250 My for a 5-km main-belt asteroid (*32*). Whereas the current rotation period of 6 hours is too long to induce shape changes, Steins's evolution may have been dominated by YORP torques in the past. A plausible scenario is that Steins was spun up by YORP, leading to material sliding toward the equator to form the typical cone shape (*33*). Such reshaping requires that Steins has a rubble pile structure, consistent with the presence of the large impact crater on the south pole. Small craters have accumulated after YORP reshaping.

The presence of the large crater at the south pole provides information about the physical properties of the interior of Steins. The specific energy of the impactor, inferred by assuming a

solid impactor and appropriate scaling (*9*), is about $6 \times 10^6$ erg $g^{-1}$. This is considerably larger than the energy required for shattering a solid rock Steins [$10^4$ to $10^6$ erg $g^{-1}$ (*34*)]. The ratio of the crater diameter (2.1 km) to the effective asteroid diameter (5.3 km) is 0.4, which is not particularly high. This ratio is lower than those recorded on Ida (0.44), Mathilde (0.62), and Vesta (0.87); however, it is high for an asteroid of Steins's size. The implication for Steins is that the attenuation of seismic waves is relatively strong, placing it in the same range as Mathilde. The interior of Mathilde, a low-density C-type asteroid, is inferred to be porous (*34*). Steins, on the other hand, is not expected to be composed of porous, primitive aggregate material because of its taxonomic type and the existence of meteorite analogs of rocky composition. Thus, before the big impact occurred, Steins was not a monolith but strongly fractured; it may even have been a rubble pile. The big impact must have converted Steins into a rubble pile, consistent with the requirement for YORP reshaping. The relative scarceness of small craters also points in this direction. Its igneous composition argues for an origin from the interior of a much larger differentiated parent body.

**References and Notes**


1. H. U. Keller *et al.*, *Space Sci. Rev.* **128**, 433 (2007).
2. J. E. Richardson Jr., H. Melosh, R. Greenberg, D. O'Brien, *Icarus* **179**, 325 (2005).
3. M. J. S. Belton *et al.*, *Science* **265**, 1543 (1994).
4. C. R Chapman, in *Asteroids III*, W. F. Bottke, P. Paolicchi, R. P. Binzel, A. Cellino, Eds. (Univ. of Arizona Press, Tucson, AZ, 2002), pp. 315–329.
5. D. C. Richardson *et al.*, in *Asteroids III*, W. F. Bottke, P. Paolicchi, R. P. Binzel, A. Cellino, Eds. (Univ. of Arizona Press, Tucson, AZ, 2002), pp. 501–515.
6. D. P. O'Brien, R. Greenberg, J. Richardson, *Icarus* **183**, 79 (2006).
7. W. F. Bottke Jr. *et al.*, *Icarus* **179**, 63 (2005).
8. M. C. Nolan, E. Asphaug, H. J. Melosh, R. Greenberg, *Icarus* **124**, 359 (1996).
9. K. A. Holsapple, K. R. Housen, *Icarus* **191**, 586 (2007).
10. P. Michel, D. P. O'Brien, S. Abe, N. Hirata, *Icarus* **200**, 503 (2009).
11. E. Asphaug, *Meteorit. Planet. Sci.* **43**, 1075 (2008).
12. D. Vokrouhlický, D. Nesvorný, W. F. Bottke, *Nature* **425**, 147 (2003).
13. S. Marchi, P. Paolicchi, M. Lazzarin, S. Magrin, *Astron. J.* **131**, 1138 (2006).
14. P. Lamy *et al.*, *Astron. Astrophys.* **487**, 1179 (2008).
15. P. Lamy *et al.*, *Astron. Astrophys.* **487**, 1187 (2008).
16. S. Fornasier, I. Belskaya, M. Fulchignoni, M. A. Barucci, C. Barbieri, *Astron. Astrophys.* **449**, L9 (2006).
17. E. Bowell, *Asteroids* **II**, 524 (1989).
18. B. Hapke, *Icarus* **157**, 523 (2002).
19. B. Clark *et al.*, *Icarus* **155**, 189 (2002).
20. L. A. M. Benner *et al.*, *Icarus* **198**, 294 (2008).
21. A. R. Hendrix, F. Vilas, *Astron. J.* **132**, 1396 (2006).
22. M. J. Gaffey *et al.*, *Icarus* **100**, 95 (1992).
23. B. E. Clark *et al.*, *J. Geophys. Res.* **109**, E12S03 (2004).
24. S. Fornasier, A. Migliorini, E. Dotto, M. Barucci, *Icarus* **196**, 119 (2008).
25. M. A. Barucci *et al.*, *Astron. Astrophys.* **430**, 313 (2005).
26. S. Fornasier, M. Lazzarin, *Icarus* **152**, 127 (2001).
27. T. H. Burbine *et al.*, *Meteorit. Planet. Sci.* **37**, 1233 (2002).
28. T. J. McCoy *et al.*, *Meteorit. Planet. Sci.* **34**, 735 (1999).
29. M. Lazzarin *et al.*, *Astrophys. J.* **647**, L179 (2006).
30. D. J. Scheeres *et al.*, *Science* **314**, 1280 (2006).
31. S. J. Ostro *et al.*, *Science* **314**, 1276 (2006).
32. D. P. Rubincam, *Icarus* **148**, 2 (2000).
33. K. J. Walsh, D. C. Richardson, P. Michel, *Nature* **454**, 188 (2008).
34. K. A. Holsapple, *Planet. Space Sci.* **57**, 127 (2009).


35. OSIRIS was built by a European consortium and is part of the Rosetta spacecraft, provided by the European Space Agency (ESA). We thank the Rosetta Science Operations Centre and the Rosetta Mission Operations Centre for their support. We acknowledge the funding of the national space agencies Agenzie Spaziale Italiana, Centre National d'Etudes Spatiales, Deutsches Zentrum für Luft- und Raumfahrt (contract number 50 QP 9703/8), Swedish National Space Board, the Spanish Space Program (Ministerio de Educación y Ciencia), and the ESA.

23 July 2009; accepted 9 November 2009
10.1126/science.1179559


# Iron Partitioning and Density Changes of Pyrolite in Earth's Lower Mantle


**Tetsuo Irifune,[1]* Toru Shinmei,[1] Catherine A. McCammon,[2] Nobuyoshi Miyajima,[2] David C. Rubie,[2] Daniel J. Frost[2]**



**Phase transitions and the chemical composition of minerals in Earth's interior influence geophysical interpretations of its deep structure and dynamics. A pressure-induced spin transition in olivine has been suggested to influence iron partitioning and depletion, resulting in a distinct layered structure in Earth's lower mantle. For a more realistic mantle composition (pyrolite), we observed a considerable change in the iron-magnesium partition coefficient at about 40 gigapascals that is explained by a spin transition at much lower pressures. However, only a small depletion of iron is observed in the major high-pressure phase (magnesium silicate perovskite), which may be explained by preferential retention of the iron ion $Fe^{3+}$. Changes in mineral proportions or density are not associated with the change in partition coefficient. The observed density profile agrees well with seismological models, which suggests that pyrolite is a good model composition for the upper to middle parts of the lower mantle.**


The evolution of the structure and dynamics of Earth's interior is influenced primarily by its composition. Based on geophysical interpretations, the lower mantle is typically considered relatively homogenous; however, recent seismological studies have demonstrated that there are some minor discontinuous changes in seismic velocities in the upper to middle parts of the lower mantle (*1*–*3*). Some of these changes are attributed to the presence of subducted slabs (*1*, *2*) or to unresolved phase transitions in mantle materials, including electron spin transitions in Fe-bearing minerals (*1*, *4*). To resolve the origin of these seismic discontinuities, precise observations of phase transitions and associated changes in chemical compositions, densities, and elastic wave velocities of mantle materials are needed.

Pyrolite is a hypothetical representative bulk composition for the mantle. Experimental studies of phase transitions and composition changes in this material have been made at high pressures and temperatures using both the multianvil apparatus (*5*–*8*) and the laser-heated diamond anvil cell (LHDAC) (*9*, *10*). The major phases in the pyrolite model for the lower mantle are orthorhombic Mg-silicate perovskite (Mg-Pv), magnesiowüstite (Mw, also known as ferropericlase), and cubic Ca-silicate perovskite (Ca-Pv). Majorite garnet (*5*) and post-perovskite (*11*) are known to be present as major high-pressure phases in the uppermost and lowermost portions of the lower mantle, respectively.

Understanding the nature of Fe partitioning between the two major phases, Mg-Pv and Mw, under lower mantle conditions may provide important clues for interpreting seismic discontinuities. $Fe^{2+}$ has been known to preferentially partition into Mw relative to Mg-Pv in the simple $MgO$-$FeO$-$SiO_2$ system (*12*). Recent multianvil experiments on more complex mixtures of pyrolite and peridotite—the dominant rock type of the upper mantle—demonstrated that the Fe-Mg partition coefficient between Mg-Pv and Mw [$K_D = (Fe/Mg)_{Mg\text{-}Pv}/(Fe/Mg)_{Mw}$] increases considerably with pressure and approaches unity as a result of Fe enrichment in Mg-Pv (*5*, *6*, *8*, *13*). This is attributed to a coupled substitution of $Mg^{2+}$ and $Si^{4+}$ by $Fe^{3+}$ and $Al^{3+}$ in Mg-Pv (*6*, *13*, *14*) due to the progressive transformation of majorite garnet to the perovskite structure under the pressures and temperatures of the uppermost lower mantle (*5*, *6*). In contrast, LHDAC studies showed substantially smaller values of $K_D$ = ~0.4 to 0.5 under the pressure and temperature conditions of the entire lower mantle (*9*, *10*).

To determine the phase and density changes in pyrolite, we conducted in situ synchrotron-based x-ray diffraction measurements at pressures up to 47 GPa and at temperatures of 1873 to 2073 K along a typical adiabatic geotherm (*15*) using a multianvil apparatus with sintered diamond anvils (*16*). The chemical compositions of the coexisting


[1]Geodynamics Research Center, Ehime University, Matsuyama 790-8577, Japan. [2]Bayerisches Geoinstitut, Universitaet Bayreuth, D-95440 Bayreuth, Germany.

*To whom correspondence should be addressed. E-mail: irifune@dpc.ehime-u.ac.jp

phases were determined by electron microprobe analyses on the recovered samples (fig. S1). Mössbauer and electron energy-loss spectroscopy (EELS) measurements were also made on some run products to evaluate the Fe valence states in Mg-Pv and Mw (*16*).

The Fe and Al contents of Mg-Pv increase with increasing pressure to 30 GPa, whereas the Mg and Si contents of Mg-Pv decrease concomitantly (Fig. 1 and table S1). Both Mg and Fe in Mw were found to decrease with increasing pressure in this range, whereas other cations increase (e.g., Al, Cr, Si, Na, and Ni). The chemical compositions of both Mg-Pv and Mw remain virtually constant at pressures between 30 and 40 GPa. At higher pressures, however, the compositional changes trend in the opposite direction in Mg-Pv (i.e., Mg and Si increase while Fe and Al decrease). A considerable enrichment of Fe in Mw is also observed at pressures above 40 GPa.

Based on this chemical data, $K_D$ increases with increasing pressure up to about 28 GPa (Fig. 2), which is interpreted in terms of the coupled substitution mechanism in Mg-Pv. The $K_D$ value stays almost constant (~0.85) at pressures between 28 and 40 GPa. In this pressure range, virtually no changes in either phase assemblage or chemical compositions of the individual phases are observed. However, $K_D$ notably decreases with higher pressures down to ~0.5, approaching the values observed in earlier LHDAC experiments on similar compositions (*9*, *10*). Thus, the high $K_D$ values observed in multianvil experiments below 30 GPa can be reconciled with the relatively low values obtained in LHDAC studies because of the substantial decrease of $K_D$ at pressures above ~40 GPa.

Recent experimental and theoretical studies (*4*, *17*–*20*) have demonstrated that an electronic high-spin to low-spin transition of $Fe^{2+}$ occurs in Mw over a wide pressure range between ~35 GPa and ~80 GPa in the lower mantle. Because the effective ionic radius of $Fe^{2+}$ in the low-spin state is smaller than that of $Mg^{2+}$, an enrichment of Fe in Mw relative to Mg-Pv is expected to accompany the spin transition in Mw. It is unclear whether such transitions occur in Mg-Pv in the corresponding pressure range, which would presumably influence this enrichment (*19*, *21*–*24*). The notable increase in the Fe content of Mw at the expense of Fe in Mg-Pv (Fig. 1), and hence the resulting decrease in $K_D$ (Fig. 2), may thus be attributed to the commencement of the spin transition in Mw at pressures near 40 GPa. This could be effectively completed by pressures of ~70 to 80 GPa, when the $K_D$ values constrained by LHDAC experiments and some theoretical predictions are taken into account (*9*, *10*, *18*–*20*).

Some LHDAC studies demonstrated a decrease in $K_D$ in San Carlos olivine with a composition of $(Mg_{0.9}Fe_{0.1})_2SiO_4$ at pressures ~70 GPa (*25*, *26*) (Fig. 2), which was interpreted as the commencement of the spin transition. However, considering the uncertainties associated with the $K_D$ values (~0.02 to 0.1) determined using LHDAC (*25*–*27*), it is difficult to see a clear trend in the variation of $K_D$ attributable to the spin transition (Fig. 2). In fact, a recent LHDAC study with careful examination of chemical heterogeneity in the sample actually shows an increase of $K_D$ (*28*). Thus, it is not clear whether the observed decrease in $K_D$ at ~70 GPa (*25*, *26*) is related to the spin transition in Mw, which may start at considerably lower pressures near 40 GPa, as suggested in our study. Alternatively, the discrepancy in the possible commencement of the spin transition could be due to a compositional effect, because pyrolite has a more complex chemical composition.

The valence state of Fe has also been shown to influence $K_D$, as is the case for the increase from 23 to 28 GPa, where the enrichment of $Fe^{3+}$ occurs in Mg-Pv (*14*). To examine the possible changes in $Fe^{2+}/Fe^{3+}$ ratios in Mw and Mg-Pv with increasing pressure, EELS and Mössbauer measurements were made on two samples recovered from the runs at 28.7 GPa and 44.2 GPa. The EELS measurements show that Fe in Mw in both of these samples is almost entirely $Fe^{2+}$, with the $Fe^{3+}/(Fe^{2+} + Fe^{3+})$ value being less than ~0.02 (±0.05) (Fig. 3, A and D). Thus, we propose that the increase of Fe in Mw (Fig. 1) is due to the increase of $Fe^{2+}$ in this phase with increasing pressure above ~40 GPa. The $Fe^{3+}/(Fe^{2+} + Fe^{3+})$ values for Mg-Pv at 28.7 GPa and 44.2 GPa are 0.66 (±0.06) and 0.67 (±0.08) (Fig. 3, B and E), respectively, whereas those based on Mössbauer measurements are 0.52 (±0.10) and 0.52 (±0.16) (Fig. 3, C and F). Although there was only a small sample volume available for the Mössbauer measurements, these values agree reasonably well with those estimated from literature values (*14*). Thus, Mg-Pv has a nearly constant $Fe^{3+}/(Fe^{2+} + Fe^{3+})$ value between 0.52 and 0.67 at these pressures, suggesting that both $Fe^{2+}$ and $Fe^{3+}$ were removed from Mg-Pv in similar proportions at pressures above ~40 GPa. It has been shown that $Fe^{2+}$ preferentially partitions into Mw in this pressure range, but $Fe^{3+}$ may also have been removed from Mg-Pv in association with the slightly decreasing $Al^{3+}$ content of this phase with increasing pressure (Fig. 1). The slight decrease of $Al^{3+}$ in Mg-Pv may be attributed to the formation of a small amount of an Al-rich phase or its possible enrichment in fine-grained Ca-Pv, although we did not see any evidence for the presence of additional phases in either in situ

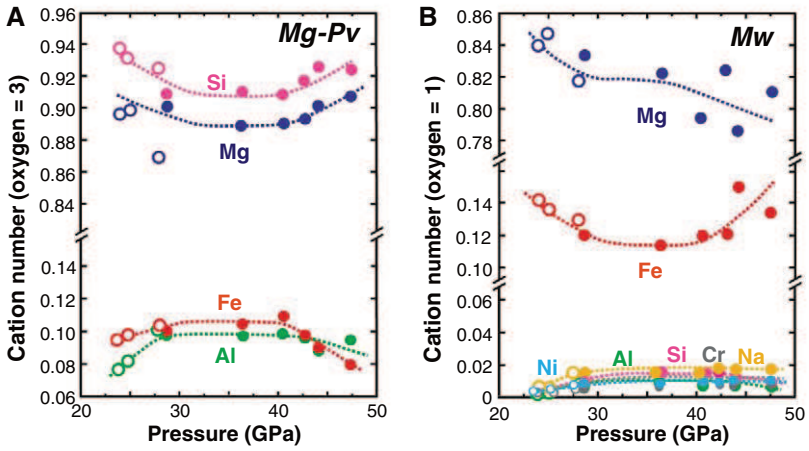


**Fig. 1.** Variations of chemical compositions of Mg-Pv (**A**) and Mw (**B**) in pyrolite as a function of pressure combined with results from an earlier study using the same starting material (*5*). The number of oxygen atoms is fixed to 3 and 1 for Mg-Pv and Mw, respectively. Filled circles are results of the present study; open circles are from (*5*).

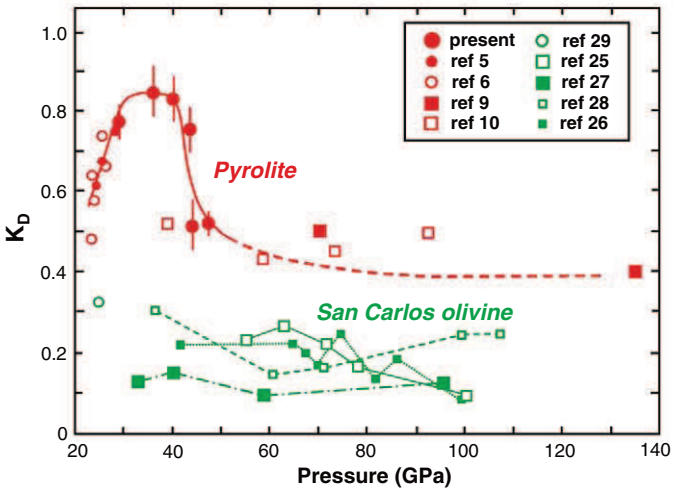


**Fig. 2.** Variations of the Fe-Mg $K_D$ between Mg-Pv and Mw in pyrolite or peridotite composition (red symbols) as a function of pressure (*5*, *6*, *9*, *10*). The solid line is based on data from multianvil studies; the line is dashed when only LHDAC data are available. Values determined or estimated for San Carlos olivine compositions (green symbols) are shown for comparison (*25*–*29*). Circles denote the results based on multianvil experiments; squares are those obtained using LHDAC.

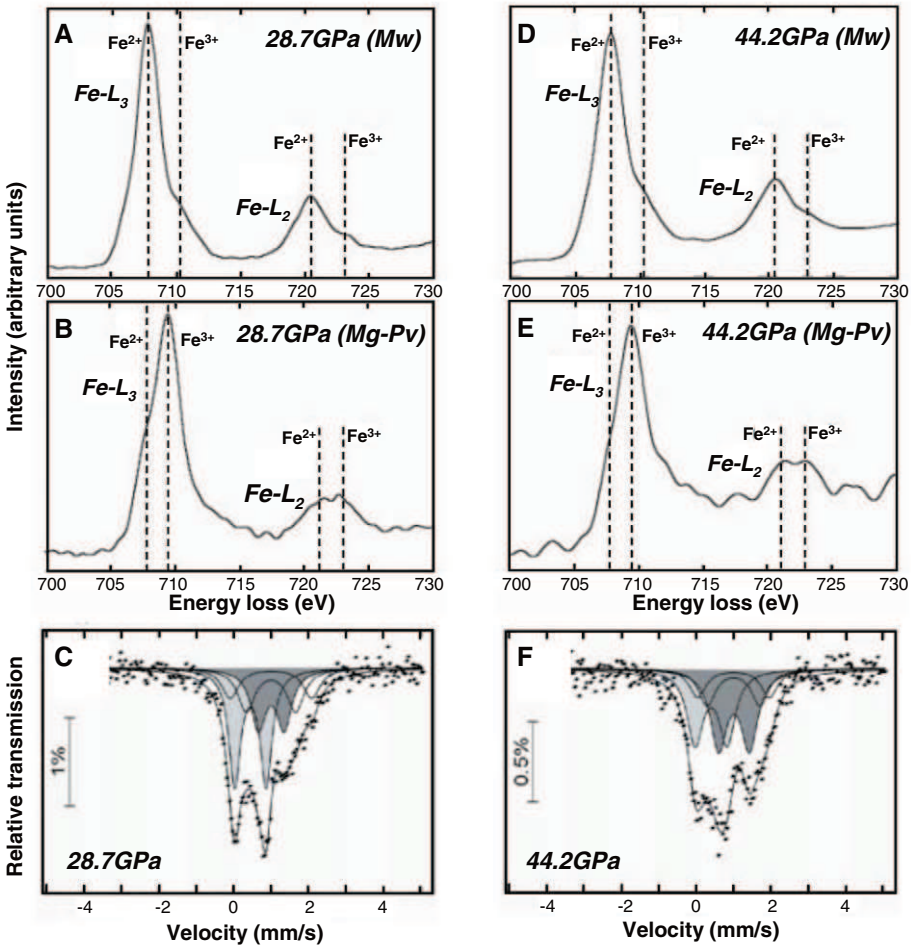


**Fig. 3.** Fe $L_{2,3}$-edge energy-loss near-edge structure spectra based on EELS measurements of a run product at 28.7 GPa for Mw (**A**) and Mg-Pv (**B**), and the Mössbauer spectrum for the same sample (**C**). The corresponding spectra for 44.2 GPa are shown in (**D**), (**E**), and (**F**), respectively. For the Mössbauer spectra, the doublets corresponding to $Fe^{3+}$ in Mg-Pv and $Fe^{2+}$ in Mw are shaded light gray and dark gray, respectively; the remaining doublets correspond to $Fe^{2+}$ in Mg-Pv.

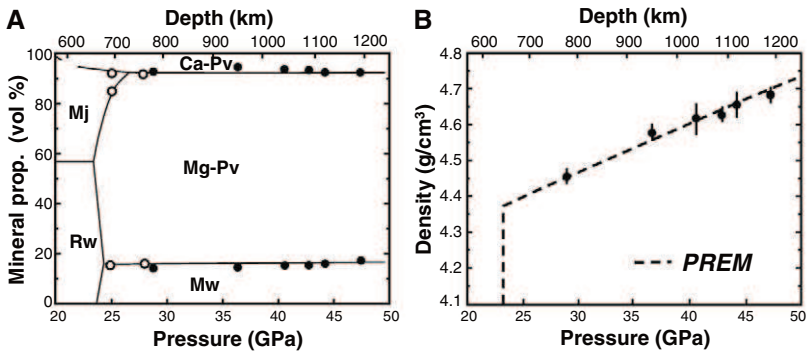


**Fig. 4.** Proportion of mineral phases in pyrolite with pressure (**A**). In addition to the lower mantle phases (Mw, Mg-Pv, and Ca-Pv), majorite garnet (Mj) and ringwoodite (Rw) are shown. Filled circles were computed using data from this study; open circles are from (*5*). Density changes in pyrolite, based on unit-cell volumes and chemical compositions of the coexisting phases (**B**), are compared with that of the Preliminary Reference Earth Model (PREM) (*30*).

x-ray diffraction measurements or scanning electron microscopy (fig. S1) observations.

It has been shown that Mg-Pv becomes essentially Fe-free when all Fe in Mw is in the low-spin state at pressures greater than ~80 GPa (*4*, *25*), but these values are only valid for $Fe^{2+}$ in the simple MgO-FeO-$SiO_2$ system. A certain amount of Fe will be retained in Mg-Pv in pyrolite even when the spin transition causes a depletion of $Fe^{2+}$ in Mg-Pv because of the presence of a considerable amount of $Al_2O_3$ (4 to 5 weight percent) in this phase (table S1). The effect of the spin transition in Mw on the viscosity of Mg-Pv should also be smaller than expected (*4*, *25*) because of the relatively small depletion of total Fe in Mg-Pv in the deeper part of the lower mantle.

Based on observed chemical compositions and unit-cell volumes of the coexisting phases, the volume proportions of Mg-Pv, Mw, and Ca-Pv do not change with pressure (Fig. 4A). Consistent with an earlier study using the quench method at pressures up to 28 GPa (*5*), the volume proportions remain at ~75%, 18%, and 7%, respectively. The density of pyrolite along a typical adiabatic geotherm, calculated using directly determined unit-cell volumes of individual phases and chemical composition data (*16*), is in excellent agreement with the seismological model (Fig. 4B). Thus, pyrolite is a reasonable model composition for the lower mantle.

### References and Notes


1. H. Kawakatsu, F. Niu, *Nature* **371**, 301 (1994).
2. S. Kaneshima, G. Helffrich, *Science* **283**, 1888 (1999).
3. R. D. van der Hilst, H. Karason, *Science* **283**, 1885 (1999).
4. J. Badro *et al.*, *Science* **300**, 789 (2003).
5. T. Irifune, *Nature* **370**, 131 (1994).
6. B. J. Wood, *Earth Planet. Sci. Lett.* **174**, 341 (2000).
7. K. Hirose, *J. Geophys. Res.* **107**, 2078 (2002).
8. N. Nishiyama, T. Yagi, *J. Geophys. Res.* **108**, 2255 (2003).
9. S. E. Kesson, J. D. Fitz Gerald, J. M. Shelley, *Nature* **393**, 252 (1998).
10. M. Murakami, K. Hirose, N. Sata, Y. Ohishi, *Geophys. Res. Lett.* **32**, L03304 (2005).
11. M. Murakami, K. Hirose, K. Kawamura, N. Sata, Y. Ohishi, *Science* **304**, 855 (2004).
12. E. Ito, E. Takahashi, *J. Geophys. Res.* **94**, 10637 (1989).
13. B. J. Wood, D. C. Rubie, *Science* **273**, 1522 (1996).
14. D. J. Frost, F. Langenhorst, *Earth Planet. Sci. Lett.* **199**, 227 (2002).
15. J. M. Brown, T. J. Shankland, *Geophys. J. R. Astron. Soc.* **66**, 579 (1981).
16. Materials and methods are available as supporting material on *Science* Online.
17. J. F. Lin *et al.*, *Nature* **436**, 377 (2005).
18. T. Tsuchiya, R. M. Wentzcovitch, C. R. S. da Silva, S. de Gironcoli, *Phys. Rev. Lett.* **96**, 198501 (2006).
19. J. F. Lin, T. Tsuchiya, *Phys. Earth Planet. Inter.* **170**, 248 (2008).
20. I. Kantor *et al.*, *Phys. Rev. B* **80**, 014204 (2009).
21. J. Badro *et al.*, *Science* **305**, 383 (2004).
22. J. Li *et al.*, *Proc. Natl. Acad. Sci. U.S.A.* **101**, 14027 (2004).
23. J. M. Jackson *et al.*, *Am. Mineral.* **90**, 199 (2005).
24. C. McCammon *et al.*, *Nat. Geoscience* **1**, 684 (2008).
25. A.-L. Auzende *et al.*, *Earth Planet. Sci. Lett.* **269**, 164 (2008).
26. T. Sakai *et al.*, *Am. Mineral.* **94**, 921 (2009).
27. Y. Kobayashi *et al.*, *Geophys. Res. Lett.* **32**, L19301 (2005).
28. R. Sinmyo *et al.*, *J. Geophys. Res.* **113**, B11204 (2008).
29. T. Katsura, E. Ito, *Geophys. Res. Lett.* **23**, 2005 (1996).
30. A. M. Dziewonski, D. L. Anderson, *Phys. Earth Planet. Sci.* **25**, 297 (1981).


31. We thank K. Funakoshi, Y. Tange, N. Nishiyama, T. Sanehira, and T. Tsuchiya for technical assistance at SPring-8 and for helpful discussions. T.I. thanks the Alexander von Humboldt Foundation and Bayerisches Geoinstitut for support during this study. Parts of this work were supported by a Grant-in-Aid for Scientific Research and Joint Research Project to T.I. from the Japan Society for the Promotion of Science (JSPS).


### Supporting Online Material

www.sciencemag.org/cgi/content/full/science.1181443/DC1
Materials and Methods
Fig. S1
Table S1
References


2 September 2009; accepted 13 November 2009
Published online 3 December 2009;
10.1126/science.1181443
Include this information when citing this paper.

# Reefs as Cradles of Evolution and Sources of Biodiversity in the Phanerozoic

Wolfgang Kiessling,[1]* Carl Simpson,[1] Michael Foote[2]

Large-scale biodiversity gradients among environments and habitats are usually attributed to a complex array of ecological and evolutionary factors. We tested the evolutionary component of such gradients by compiling the environments of the geologically oldest occurrences of marine genera and using sampling standardization to assess if originations tended to be clustered in particular environments. Shallow, tropical environments and carbonate substrates all tend to have harbored high origination rates. Diversity within these environments tended to be preferentially generated in reefs, probably because of their habitat complexity. Reefs were also prolific at exporting diversity to other environments, which might be a consequence of low-diversity habitats being more susceptible to invasions.

Systematic differences in evolutionary patterns are well documented among marine environments. On the largest environmental scales these differences are manifested in onshore-offshore patterns, where higher taxa tend to have originated preferentially in nearshore environments and expanded offshore later in their evolutionary history (*1*, *2*), and tropical-extratropical patterns, where more origination took place in the tropics and tropical genera expanded toward extratropical latitudes (*3*). Both patterns suggest that shallow-water and tropical marine environments are not only evolutionary cradles, but are also more prolific at exporting diversity than deeper-water and extratropical habitats and thus represent net sources of biodiversity. The underlying mechanisms of these patterns presumably involve physical disturbance regimes, energy availability, and biotic interactions (*2*, *4*, *5*).

Using fossil occurrence data of benthic marine invertebrate genera from the Paleobiology Database [PaleoDB, (*6*)], we tested the cradle and source hypotheses for biogenic reefs. These largely shallow-water and tropical ecosystems are known for their amazing biodiversity (*7*), but it is disputed whether diversity is mainly generated within reefs (*8*–*12*) or if reefs rather act as ecological attractors for and evolutionary refuges of biodiversity that originated elsewhere (*13*–*15*).

We examined the environments of the geologically oldest occurrences of marine genera and compared sets of (i) reef (R) and nonreefal (NR) ecosystems, (ii) calcium carbonate (C) versus terrigenous clastic (siliciclastic, S) substrates, (iii) tropical (T) versus extratropical (ET) latitudes, and (iv) shallow- (SH) versus deep-water (DP) habitats, applying definitions in (*16*). To reduce the influence of taxonomic errors, we only referred to classified genera for which a species was identified (*17*), and we minimized stratigraphic errors by using only the species occurrences that were firmly assigned to 1 of 74 geological time intervals [supporting online material (SOM)]. If the oldest appearance of a genus fell into several environments, we randomly chose one occurrence and applied resampling to achieve an overall estimate of the most likely environment of origin. Because some environments are genuinely rare or undersampled in particular intervals, we performed subsampling to test if the number of origins was randomly distributed among environments in a uniform subset. We also analyzed the relative proportions of originating taxa that dispersed to other environments during their stratigraphic range.

Of the 6615 benthic invertebrate genera that span more than one geological interval and for which an environment of origin can be assigned, 1426 genera originated in reef environments. This proportion (21.6%) is impressive when considering that only 16.7% of all benthic occurrences in the PaleoDB are from reefs. Probably because of a bias in the taxonomic description of ancient reefs toward the occurrence of reef-building organisms, the proportion of reef originations is much greater for corals and sponges than for reef dwellers such as bivalves and gastropods (Fig. 1). The originations in C, T, and SH are similarly greater than expected by the distribution of sampling (Table 1), but because the relation between sampling and observed originations is nonlinear, sampling standardization is needed to assess the true effect of environmental setting on origination probability.

Subsampling analysis demonstrates that reefs are important evolutionary cradles independent of their preferred habitat in shallow, low-latitude, calcium carbonate environments (Fig. 2). Although the R-NR comparison yields an intermediate origination preference between T-ET and SH-DP, we emphasize that the R-NR pattern is based on a comparison of low-latitude reefs with only those nonreef environments that were also low latitude, carbonate, and shallow water. Per-genus origination probabilities are about 45% greater in reefs than outside reefs. This pattern applies to individual higher taxa as well: The higher probability of reefal origination seen in the raw data is maintained in corals (Fig. 1, Anthozoa), and the sparse reefal originations in bivalves and gastropods are higher than outside reefs when sampling is made uniform (fig. S5).

The C-S, T-ET, and SH-DP comparisons are based on all data and on data excluding reefs. These imply that C, T, and SH are notable

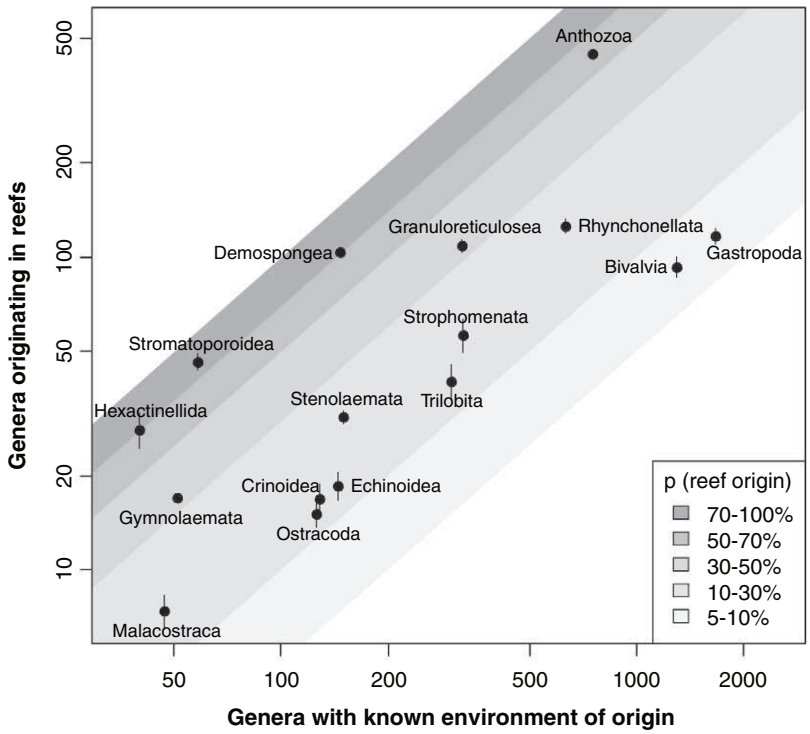


**Fig. 1.** Phanerozoic originations of marine benthic genera in reefs for the most common classes recorded in the Paleobiology Database. Error bars represent two times the standard deviation of 50 resampling trials of raw data.

[1]Museum für Naturkunde, Leibniz Institute for Research on Evolution and Biodiversity at the Humboldt University Berlin, 10115 Berlin, Germany. [2]Department of the Geophysical Sciences, University of Chicago, Chicago, IL 60637, USA.

*To whom correspondence should be addressed. E-mail: wolfgang.kiessling@mfn-berlin.de

centers of originations independent of reefs, although the SH-DP gradient drops significantly when reefs are excluded. In nonreefal ecosystems, shallow-water environments represent the most important evolutionary cradle, followed by carbonate environments and tropical latitudes. The strong SH-DP signal is somewhat surprising given previous suggestions that the onshore-offshore gradient would only pertain to higher taxonomic levels (*2*). The gradient might be biased by the much better sampling of the spectrum of shallow-water habitats, which cannot be counterbalanced completely by subsampling (SOM). Our results agree with analyses suggesting that particular biologic groups had preferred tropical origins (*3*), although the overall origination preference is comparatively small.

To test if particular environments have also been sources of biodiversity for other environments, we computed the proportions of genera that originated in one environment and are subsequently found in another one. The proportions of these exporters were generally greater for genera originating in R, C, T, and SH than those originating in NR, S, ET, and DP (Fig. 3). The pattern is most prominent in reefs, which have thus been the most significant net exporters of biodiversity. Reefs were ~25% more likely to have exported diversity in the Phanerozoic to nonreefs than were nonreefs to reefs. This is in marked contrast to the SH-DP pair, for which shallow-water environments show a pronounced cradle signal but exported only slightly more of their new genera to deep-water environments than they imported. Offshore-onshore migrations thus may have been proportionally more common than usually assumed (*18*). The T-ET pattern is consistent with the out-of-the-tropics model (*3*), but out-of-the-reefs and out-of-the-carbonates models are equally applicable over the entire Phanerozoic.

**Table 1.** Global proportions of originations and sampling in raw data and their 95% confidence intervals.

| | R/(R+NR)* | C/(C+S) | T/(T+ET) | SH/(SH+DP) |
|---|---|---|---|---|
| Originations | 0.22 ± 0.010 | 0.53 ± 0.011 | 0.51 ± 0.011 | 0.72 ± 0.011 |
| Occurrences | 0.17 ± 0.002 | 0.47 ± 0.002 | 0.48 ± 0.002 | 0.68 ± 0.002 |

*R and NR exclude plankton and nekton.

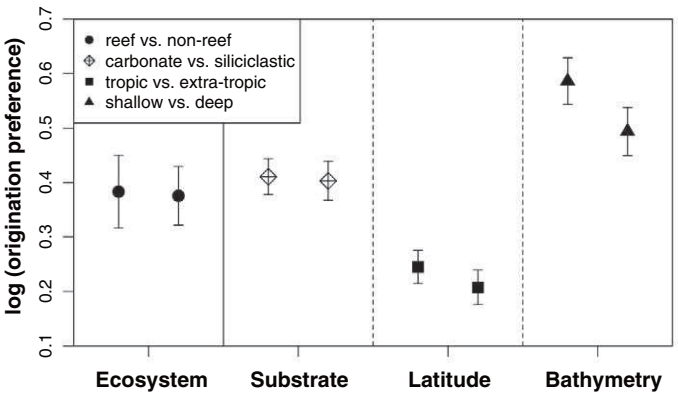


**Fig. 2.** Sampling-standardized logged origination preferences in pairs of habitats. Ecosystem stands for benthic originations in low-latitude, shallow-water reefs (R) compared with originations in low-latitude, shallow, and nonreef carbonates (NR). Points refer to <30° (left) and <45° paleolatitude (right). The left points in lithology, latitude, and bathymetry comprise all data, whereas the right points exclude reef data. Lithology compares originations on or in carbonate substrates (C) and siliciclastic substrates (S). Latitude weighs tropical (T, < 30° paleolatitude) originations against extratropical (ET) originations. Bathymetry evaluates originations in shallow water (SH, above the storm-weather wave base) versus deeper water (DP). Origination preference is calculated by the risk ratio of per-genus originations in respective habitats (SOM). Error bars represent 95% confidence intervals. All values are significantly above zero, indicating that reefs, carbonates, the tropics, and shallow-water environments represent more important evolutionary cradles than their counterparts.

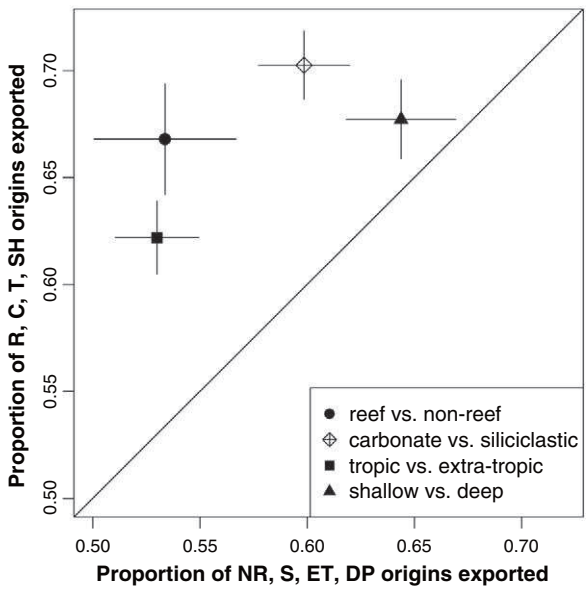


**Fig. 3.** Sampling-standardized balance of exported and imported diversity in environmental pairs. The plot depicts the proportions of genera originating in R, C, T, and SH that migrate into NR, S, ET, and DP and the proportions of genera originating in NR, S, ET, and DP migrating into R, C, T, and SH. Data for S-C, T-ET, and SH-DP exclude reefs. Error bars indicate 95% confidence intervals.

The strength of the cradle and the source effects varied through the Phanerozoic. Standardized per-genus origination rates were much higher in reefs, carbonates, and tropical latitudes in the Paleozoic than later on (fig. S8). Therefore, either these environments have lost some of their potential to be evolutionary cradles, or their counterparts have increased their potential. The foreign trading balance is less variable (fig. S9). On even finer time scales, the reefal cradle is not clearly related to rebounds from mass extinctions (fig. S10), perhaps because reef ecosystems need to be restructured by organisms before they can act as evolutionary motors.

Our results might be affected by taphonomic biases, geographic aggregation of data, and different stratigraphic ranges of genera. However, none of these potential biases is strong enough to affect the basic results. Sampling probabilities are similar among environments (table S2), geographic clustering does not differ significantly between R and NR (table S3), results are robust with different subsampling methods (figs. S3 and S4), and the slightly different stratigraphic ranges of genera in respective habitats do not substantially influence the source effect (fig. S7).

That a pronounced evolutionary role of reefs is evident even when we explicitly control for correlated factors suggests that an additional ecological aspect must be sought to supplement the energy and disturbance hypotheses, which are usually advocated to explain environmental gradients in evolution. The most likely factor is habitat complexity, expressed in topographic complexity that is generated by the three-dimensional growth of reefs, and ecological complexity generated the many biotic interactions in even low-diversity reefs (*19*). Topographic complexity is known to provide ecological opportunities for species packing of marine fishes (*20*, *21*), and reefal habitat complexity has been suggested to drive the diversification of teleost fishes (*12*). Taphonomic biases inhibit the direct test of a cradle effect for reef fishes, because even undoubted coral reef fish assemblages are usually recovered from off-reef sediments (*22*).

Habitat complexity can only control maximum standing diversity, and there is no evidence that reef diversity increased profoundly over the Phanerozoic (*23*). Without extinctions, we would thus probably not see the pronounced cradle signal in our data.

Indeed, extinction probabilities are as concentrated in reefs as are originations (fig. S13), such that enhanced evolutionary turnover rates might be a reasonable explanation for the reefal cradle, with high origination rates keeping reefs from turning into a museum. This would also explain the stronger cradle signal in the Paleozoic than later on, because turnover rates were generally higher (*24*, *25*). The role of evolutionary turnover has separated reefs from other topographically complex ecosystems such as rocky shores (*26*).

The observation that those settings that tended to have higher rates of origination also tended to export proportionally more taxa to other settings might be a consequence of diversity gradients. Despite conflicting experimental results [reviewed by (*27*)], some theoretical work predicts that high diversity forms a barrier against species invasions by lowering niche opportunities (*28*). This barrier could apply equally to locally evolved genera as well as invaders (*29*), but, compared with immigrants, taxa evolving in a high-diversity regime should more readily occupy vacant niche space that is generated by extinctions. Our study supports the contention that large-scale gradients in biodiversity are at least partially governed by evolutionary history and are not simply due to ecological factors that control standing diversity.

### References and Notes


1. D. Jablonski, J. J. Sepkoski Jr., D. J. Bottjer, P. M. Sheehan, *Science* **222**, 1123 (1983).
2. D. Jablonski, *J. Exp. Zool.* **304B**, 504 (2005).
3. D. Jablonski, K. Roy, J. W. Valentine, *Science* **314**, 102 (2006).
4. M. R. Willig, D. M. Kaufman, R. D. Stevens, *Annu. Rev. Ecol. Evol. Syst.* **34**, 273 (2003).
5. J. W. Valentine, D. Jablonski, A. Z. Krug, K. Roy, *Paleobiology* **34**, 169 (2008).
6. See http://paleodb.org. Data were downloaded on 20 July 2009.
7. M. L. Reaka-Kudla, in *Biodiversity II: Understanding and Protecting Our Natural Resources*, M. L. Reaka-Kudla, D. E. Wilson, E. O. Wilson, Eds. (Joseph Henry Press, Washington, DC, 1997), pp. 83–108.
8. F. G. Stehli, J. W. Wells, *Syst. Zool.* **20**, 115 (1971).
9. N. Knowlton, J. B. C. Jackson, *Trends Ecol. Evol.* **9**, 7 (1994).
10. A. J. Kohn, in *Marine Biodiversity: Patterns and Processes*, R. F. G. Ormond, J. D. Gage, M. V. Angel, Eds. (Cambridge Univ. Press, Cambridge, 1997), pp. 201–215.
11. J. C. Briggs, *J. Biogeogr.* **32**, 1517 (2005).
12. M. E. Alfaro, F. Santini, C. D. Brock, *Evolution* **61**, 2104 (2007).
13. B. R. Rosen, in *Fossils and Climate*, P. Brenchley, Ed. (Wiley, Chichester, UK, 1984), pp. 201–260.
14. J. M. Pandolfi, *J. Biogeogr.* **19**, 593 (1992).
15. C. C. Wallace, B. R. Rosen, *Proc. Biol. Sci.* **273**, 975 (2006).
16. W. Kiessling, M. Aberhan, *Paleobiology* **33**, 414 (2007).
17. P. J. Wagner, M. Aberhan, A. Hendy, W. Kiessling, *Proc. Biol. Sci.* **274**, 439 (2007).
18. A. Lindner, S. D. Cairns, C. W. Cunningham, R. DeSalle, *PLoS ONE* **3**, e2429 (2008).
19. P. W. Glynn, *Ecosystems* **7**, 358 (2004).
20. B. Gratwicke, M. R. Speight, *Mar. Ecol. Prog. Ser.* **292**, 301 (2005).
21. M. Lingo, S. Szedlmayer, *Environ. Biol. Fishes* **76**, 71 (2006).
22. D. R. Bellwood, *Coral Reefs* **15**, 11 (1996).
23. W. Kiessling, *Nature* **433**, 410 (2005).
24. D. M. Raup, J. J. Sepkoski Jr., *Science* **215**, 1501 (1982).
25. J. Alroy, *Proc. Natl. Acad. Sci. U.S.A.* **105**, 11536 (2008).
26. S. T. Williams, D. G. Reid, *Evolution* **58**, 2227 (2004).
27. J. M. Levine, C. M. D'Antonio, *Oikos* **87**, 15 (1999).
28. K. Shea, P. Chesson, *Trends Ecol. Evol.* **17**, 170 (2002).
29. M. A. McPeek, *Am. Nat.* **172**, E270 (2008).


30. This work was supported by the Deutsche Forschungsgemeinschaft (grant KI 806/5–1) and the VolkswagenStiftung. We thank U. Merkel for contributing substantially to the reef occurrence data. This is Paleobiology Database publication #105.


### Supporting Online Material

www.sciencemag.org/cgi/content/full/1182241/DC1
Materials and Methods
SOM Text
Figs. S1 to S14
Tables S1 to S4
References

21 September 2009; accepted 20 November 2009
10.1126/science.1182241

# Therapeutic Silencing of MicroRNA-122 in Primates with Chronic Hepatitis C Virus Infection

**Robert E. Lanford,[1]* Elisabeth S. Hildebrandt-Eriksen,[2]* Andreas Petri,[2]* Robert Persson,[2] Morten Lindow,[2] Martin E. Munk,[2] Sakari Kauppinen,[2,3]* Henrik Ørum[2]†**

**The liver-expressed microRNA-122 (miR-122) is essential for hepatitis C virus (HCV) RNA accumulation in cultured liver cells, but its potential as a target for antiviral intervention has not been assessed. We found that treatment of chronically infected chimpanzees with a locked nucleic acid (LNA)–modified oligonucleotide (SPC3649) complementary to miR-122 leads to long-lasting suppression of HCV viremia, with no evidence of viral resistance or side effects in the treated animals. Furthermore, transcriptome and histological analyses of liver biopsies demonstrated derepression of target mRNAs with miR-122 seed sites, down-regulation of interferon-regulated genes, and improvement of HCV-induced liver pathology. The prolonged virological response to SPC3649 treatment without HCV rebound holds promise of a new antiviral therapy with a high barrier to resistance.**

Hepatitis C virus (HCV) infection is a leading cause of liver disease worldwide, with more than 170 million infected individuals at greatly increased risk of liver failure and hepatocellular carcinoma. The current standard anti-HCV therapy, which combines pegylated interferon-α (IFN-α) with ribavirin, provides sustained clearance of HCV in only about 50% of patients and is often associated with serious side effects (*1*, *2*). Therapies that target essential host functions for HCV may provide a high barrier to resistance, and thus could present an effective approach for the development of new HCV antiviral drugs. MicroRNA-122 (miR-122) is a highly abundant, liver-expressed microRNA that binds to two closely spaced target sites in the 5′ noncoding region (NCR) of the HCV genome, resulting in up-regulation of viral RNA levels (*3*, *4*). Interaction of miR-122 with the HCV genome is essential for accumulation of viral RNA in cultured liver cells, and both target sites are required for modulation of HCV RNA abundance (*3*–*5*).

[1]Department of Virology and Immunology and Southwest National Primate Research Center, Southwest Foundation for Biomedical Research, San Antonio, TX 78227, USA. [2]Santaris Pharma, Kogle Allé 6, DK-2970 Hørsholm, Denmark. [3]Copenhagen Institute of Technology, Aalborg University, Lautrupvang 15, DK-2750 Ballerup, Denmark.

*These authors contributed equally to this work.
†To whom correspondence should be addressed. E-mail: hoe@santaris.com

Previously, we reported on potent and specific miR-122 silencing in vivo using a locked nucleic acid (LNA)–modified phosphorothioate oligonucleotide (SPC3649) complementary to the 5′ end of miR-122, which led to long-lasting decrease of serum cholesterol in mice and African green monkeys (*6*). Here, we investigated the potential of miR-122 antagonism by SPC3649 as a new anti-HCV therapy in chronically infected chimpanzees (genotype 1). Baseline measurements were obtained from four chimpanzees for 4 weeks, the last two of which included an intravenous (i.v.) placebo dose of saline. Two animals each were assigned to the high- and low-dose groups (5 mg $kg^{-1}$ and 1 mg $kg^{-1}$, respectively) and were treated with i.v. injections of SPC3649 on a weekly basis for 12 weeks (Fig. 1A), followed by a treatment-free period of 17 weeks. In the high-dose group, a significant decline of HCV RNA in the serum was detected 3 weeks after the onset of SPC3649 dosing, with a maximum decrease of 2.6 orders of magnitude in HCV RNA levels 2 weeks after end of treatment (Fig. 1A). Analysis of HCV RNA levels in the liver showed a decrease of 2.3 orders of magnitude in the high-dose animals. One low-dose animal achieved a viral decline of 1.3 orders of magnitude; the other experienced fluctuations in HCV RNA levels during dosing that made evaluation of the degree of suppression difficult (Fig. 1A).

We next assessed the in vivo antagonism of miR-122 in chimpanzee liver biopsies. Mature miR-122 was detected in the baseline samples (week –4) from all animals, whereas SPC3649 was detected in RNA samples obtained during treatment and up to 8 weeks after the last dose in the high-dose animals. This coincided with sequestration of miR-122 in a heteroduplex with

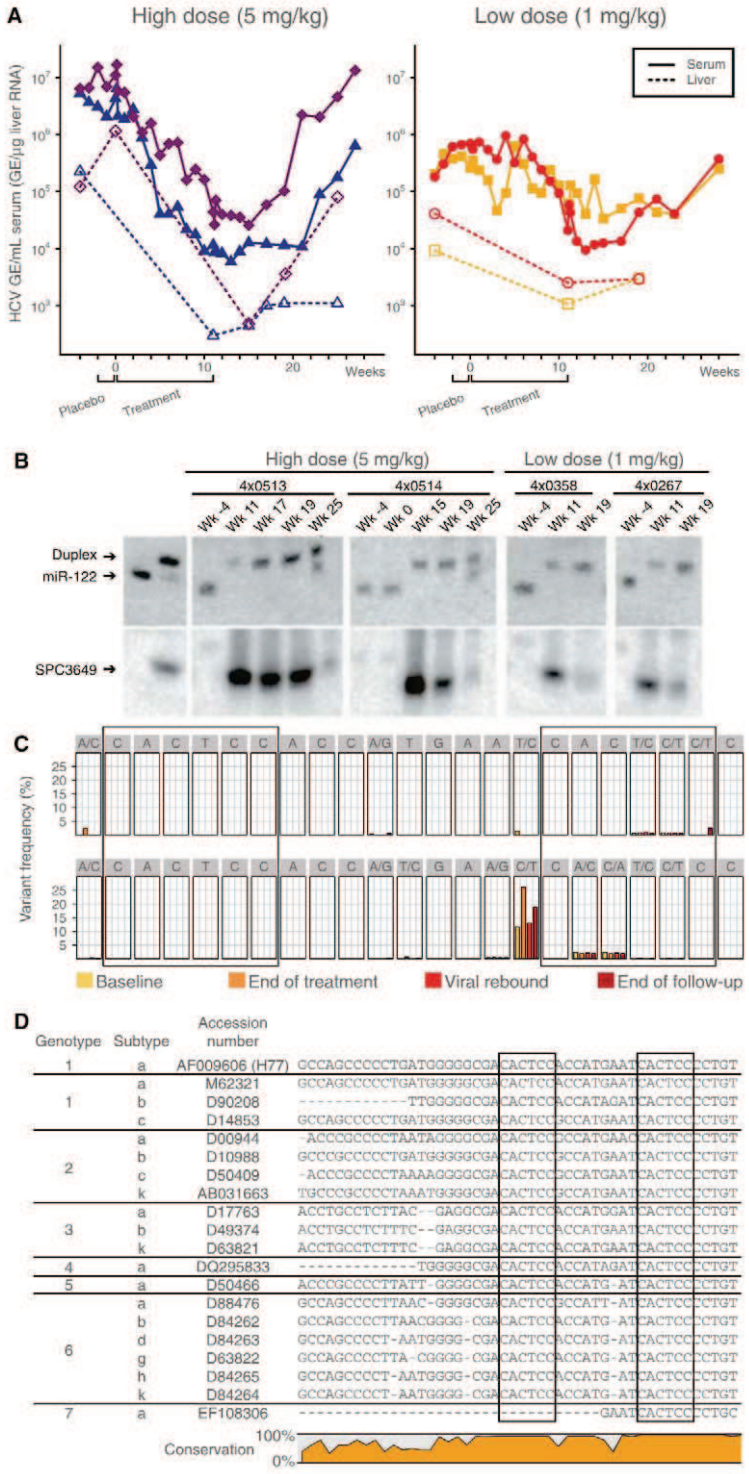


**Fig. 1.** Silencing of miR-122 by SPC3649 in chimpanzees with chronic hepatitis C virus infection. (**A**) Analysis of HCV RNA levels in HCV-infected chimpanzees during the study. The HCV titers are shown as genomic equivalents (GE) for the high-dose animals (4x0513, blue triangles; 4x0514, magenta diamonds) and low-dose animals (4x0267, orange squares; 4x0358, red dots) in serum (GE/ml, solid lines) and liver (GE/μg liver RNA, dashed lines). The placebo and active treatment periods are indicated below. (**B**) Northern blot analysis of RNA from chimpanzee liver biopsies using LNA-modified probes detecting free and sequestered miR-122 (upper panel) and SPC3649 (lower panel). The first two lanes are positive controls for free miR-122 and preformed miR-122:SPC3649 heteroduplexes, respectively. (**C**) Detection of sequence variants in the miR-122 seed sites (boxed) by deep sequencing of the HCV 5′ NCR from the high-dose animals at four time points: baseline, end of treatment, viral rebound, and end of the follow-up period. (**D**) The two miR-122 seed sites (boxed) in the HCV 5′ NCR are conserved in all HCV genotypes and subtypes (see Supporting Online Material for details).

SPC3649, as detected by a shifted band on Northern blots (Fig. 1B) (*6*). Quantification of miR-122 levels by real-time reverse transcription polymerase chain reaction showed a factor of >300 decrease in free miR-122 levels for the high-dose animals (fig. S1). Free SPC3649 was markedly reduced in the liver at week 25 in the high-dose animals, accompanied with detection of free miR-122 alongside the miR-122:SPC3649 heteroduplex band (Fig. 1B). These findings demonstrate efficient delivery of SPC3649 to the chimpanzee liver, resulting in potent and sustained antagonism of miR-122. The reason for the reduced response in the low-dose group was not apparent from the Northern data, because no miR-122 was detected at the end of dosing. It is possible that low levels of miR-122 undetectable by Northern blot could still be sufficient to support HCV RNA accumulation in these animals. A recent report on markedly decreased miR-122 levels in interferon nonresponder patients with chronic HCV infection supports the notion that even low levels of miR-122 could facilitate HCV abundance in vivo (*7*).

Two lines of evidence imply that no viral resistance to therapy occurred during treatment with SPC3649. First, no rebound in viremia was observed during the 12-week dosing phase; HCV RNA levels were still an order of magnitude below baseline 16 weeks after dosing (4x0513, Fig. 1A). Second, deep sequencing of the HCV 5′ NCR from the two high-dose animals—which yielded between 73,000 and 214,000 reads each at four time points (baseline, end of treatment, viral rebound, and end of the follow-up period)—showed no enrichment of adaptive mutations in the miR-122 seed sites (Fig. 1C and fig. S2). This is consistent with the fact that both miR-122 sites are conserved in all HCV genotypes and subtypes (Fig. 1D and figs. S3 to S9). The lack of viral resistance during SPC3649 therapy is in stark contrast to what has been observed with direct acting antivirals in HCV-infected chimpanzees. Within 2 days of dosing with a nonnucleoside polymerase inhibitor, 67% of the HCV clones already possessed known resistance mutations, with 10% of the clones having two resistance mutations, which triggered a rapid rebound in viremia (*8*).

We next investigated the effect of miR-122 antagonism on the chimpanzee liver transcriptome by expression profiling of the liver biopsies performed after SPC3649 treatment relative to baseline samples. Liver mRNAs with miR-122 seed match sites in the 3′ untranslated regions (UTRs) showed a significant tendency to be derepressed in both high-dose animals and the responding low-dose animal relative to transcripts without miR-122 sites (Fig. 2A, $P = 7.3 \times 10^{-4}$, $1.0 \times 10^{-3}$, and $2.2 \times 10^{-10}$ for 8-mer seed sites, respectively, Kolmogorov-Smirnov test; see also fig. S10). A total of 259 mRNAs with 8-mer miR-122 seed sites were identified by this approach (table S1). By contrast, no significant target mRNA derepression was observed in the weakly responding low-dose animal (Fig. 2A).

We also examined the expression data for changes related to prolonged decrease in viral RNA during SPC3649 therapy. A supervised analysis of chimpanzee interferon-regulated genes (IRGs) (*9*, *10*) revealed that the reduction in viremia was clearly associated with down-regulation of most IRGs in the high-dose animals and the responding low-dose animal (Fig. 2B and table S2). This correlated with the measured serum levels of the chemokine IP-10 (CXCL10), a highly induced IRG in HCV infections, which thereby provides a readily accessible biomarker of the hepatic IFN response during SPC3649 therapy (Fig. 2C). Together, these data imply that the endogenous IFN pathway in the liver is rapidly normalized in response to inhibition of HCV RNA accumulation even when therapy does not completely eradicate detectable viral RNA. Nonresponders to IFN-α–based HCV therapy have increased hepatic levels of IRG transcripts and serum IP-10 protein levels (*11*–*17*), reflecting a maximally induced and nonresponsive hepatic IFN response. The chimpanzee appears to be an extreme representative of this phenotype in human HCV patients, designated as IFN null-responders (*18*). Thus, our finding that treatment with SPC3649 results in normalization of IRG levels suggests that this therapy could be used to convert IFN null-responders to responders by reducing the viral load, thereby permitting the endogenous IFN pathway to reset to responsiveness.

Antagonism of miR-122 in chimpanzees by SPC3649 led to markedly lowered serum cholesterol in the high-dose group (Fig. 2D), similar to observations in mice and in African green monkeys (*6*, *19*). One of the high-dose animals had a maximum decline of 44% at week 14, whereas the other animal showed a 29% decrease in cholesterol at the same time point. Pronounced decreases were observed in both low-density lipoprotein (LDL) (25 to 54%) and apolipoprotein apo-B, its primary lipoprotein component (23 to 42%) (fig. S12). In contrast to our previous findings in monkeys, where decreases in high-density lipoprotein (HDL) and its major apolipoprotein apo-A1 were more pronounced relative to LDL and apo-B (*7*), the observed changes in HDL or apo-A1 in chimpanzees were more variable (fig. S13). Thus, it is possible that the cholesterol-lowering effect of miR-122 antagonism is different in chimpanzees and may better reflect the expected response in humans.

To assess the safety of miR-122 antagonism after prolonged treatment with SPC3649, we monitored an extensive set of clinical chemistries and correlated them with plasma levels of the compound. The peak plasma concentrations ($C_{max}$) were dose-proportional and similar after first and last dose, ranging from 6.1 to 6.3 μg/ml for the low-dose animals and from 17.7 to 30.6 μg/ml for the high-dose animals (Table 1). The terminal plasma half-life was about 20 days in the high-dose animals. The plasma trough levels at the high dose ranged from 31 to 67 ng/ml and were maintained at this level for 4 weeks after the last dose (Fig. 3A). Complete blood counts, blood chemistries, coagulation markers, urinalysis, and complement activation were determined throughout the study, as were lymphocyte subsets, circulating cytokine-chemokine profiles, and additional safety parameters (table S3). No SPC3649-related abnormalities were observed for any of the measurements (Fig. 3, B and C, figs. S14 and S15,

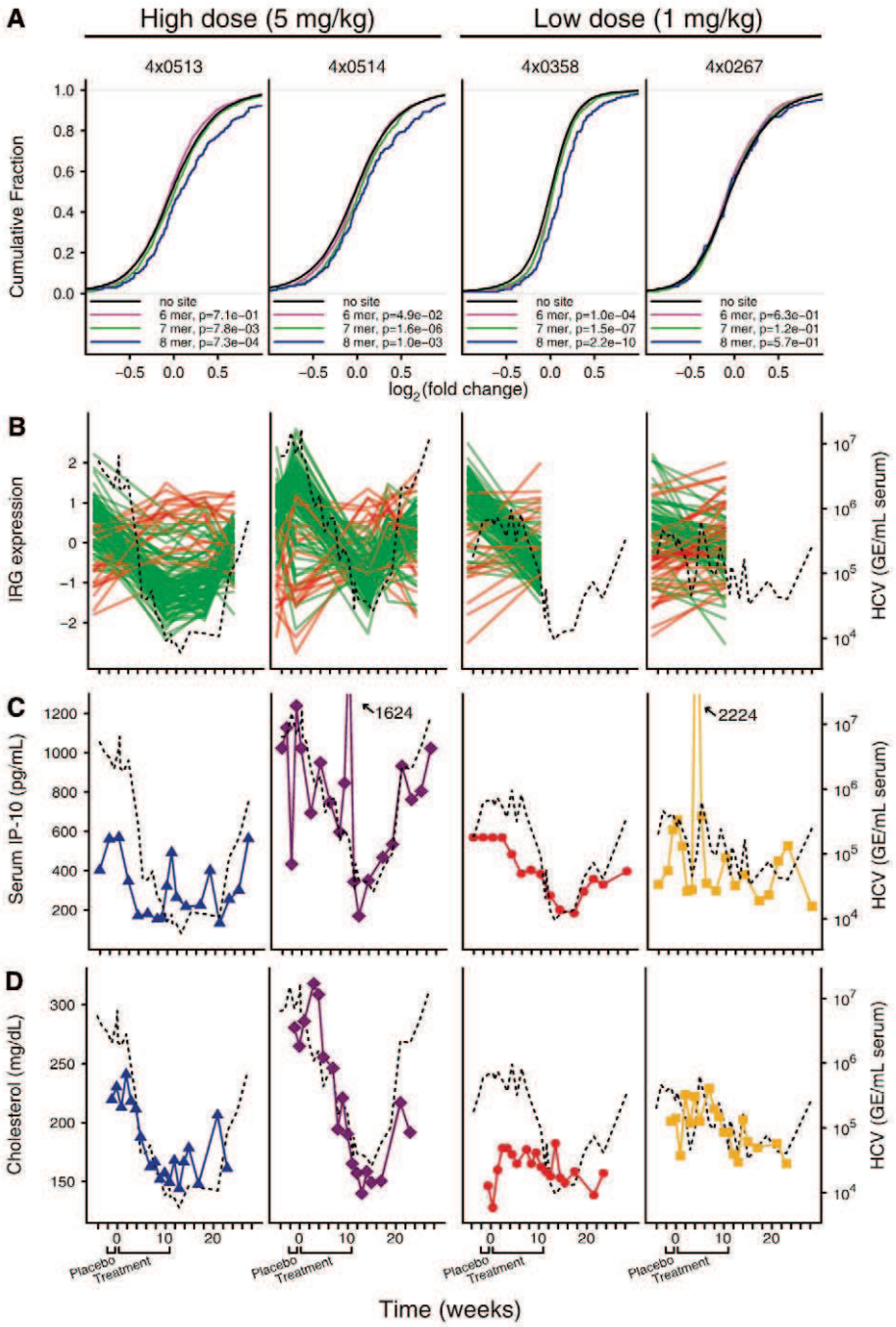


**Fig. 2.** Functional antagonism of miR-122 by SPC3649 in HCV-infected chimpanzees. (**A**) Assessment of liver transcriptome changes after SPC3649 treatment in each animal by microarray expression profiling of liver biopsies. The liver mRNA 3′ UTRs were analyzed for the presence of different types of canonical miR-122 seed match sites. The cumulative fraction plots show the distribution of $\log_2$ fold changes between the baseline and end of treatment samples for each seed match type; a Kolmogorov-Smirnov test was used to compare the three miR-122 seed match types to mRNAs with no seed sites in the 3′ UTR. (**B**) Expression profiles of interferon-regulated genes (green lines correspond to IRGs with decreased expression from baseline to end of treatment; red lines indicate IRGs showing an increase) and serum HCV RNA levels (black dashed line) in HCV-infected chimpanzees during the study. (**C**) Serum IP-10 levels (color coding and plot symbols as in Fig. 1A) and serum HCV titer (dashed black line) in HCV-infected chimpanzees during the study. (**D**) Serum cholesterol levels (color coding and plot symbols as in Fig. 1A) and serum HCV RNA levels (dashed black line) in HCV-infected chimpanzees during the study.

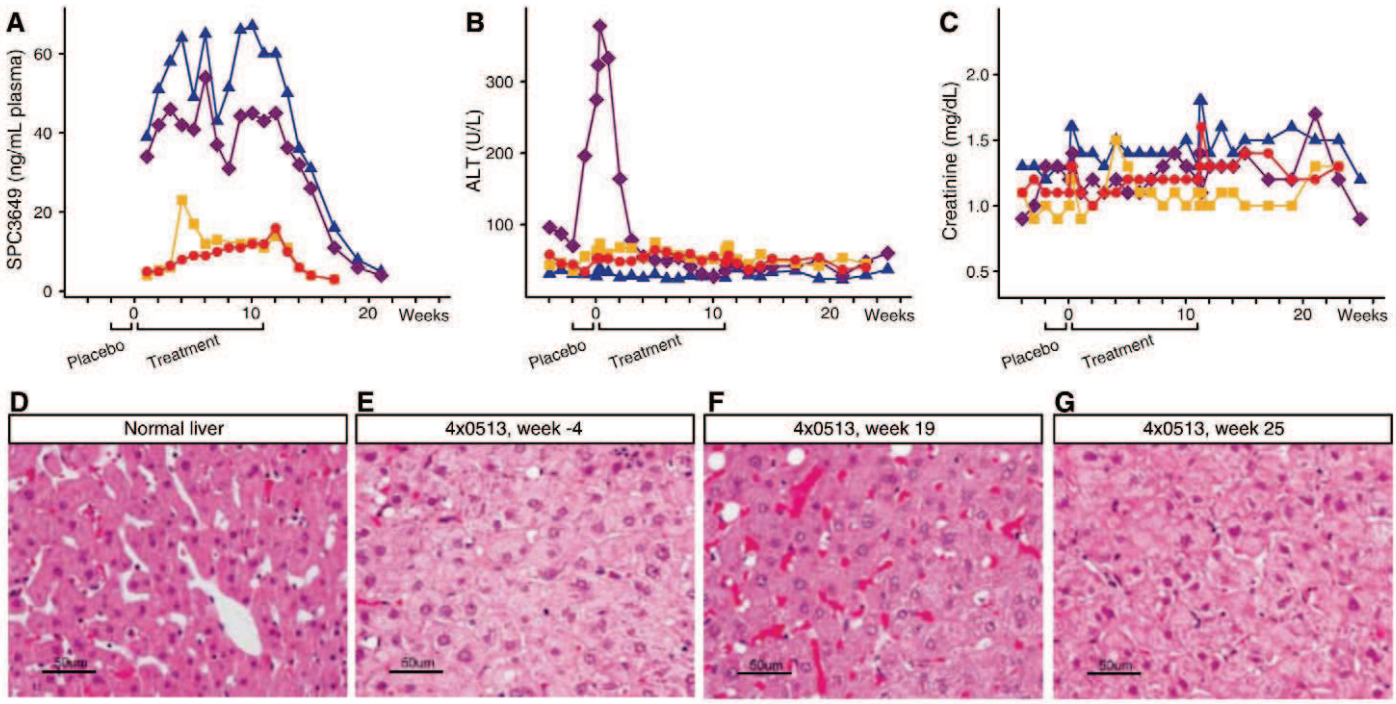


**Fig. 3.** Treatment of HCV-infected chimpanzees with SPC3649 was well tolerated. (**A**) Plasma trough levels of SPC3649. (**B** and **C**) Alanine aminotransferase (ALT) levels (B) and creatinine levels (C) in HCV-infected chimpanzees during the study. (**D** to **G**) Photomicrographs of hematoxylin and eosin–stained sections from biopsies of a normal chimpanzee liver (D) and animal 4x0513 at week −4 (E), week 19 (F), and week 25 (G), respectively.

**Table 1.** Pharmacokinetic properties of SPC3649 in chimpanzee plasma. $C_{max}$, maximum observed plasma concentration; $AUC_{inf}$, area under concentration versus time curve from time 0 to infinity; $V_z$, apparent volume of distribution during the terminal phase; Cl, total body clearance. Data are from week 11.

| Animal | $C_{max}$ (μg ml$^{-1}$) | $AUC_{inf}$ (hour · μg ml$^{-1}$) | Terminal half-life (days) | $V_z$ (liter kg$^{-1}$) | Cl (ml hour$^{-1}$ kg$^{-1}$) |
|---|---|---|---|---|---|
| 4x0267 | 6.3 | 25.0 | 21.4 | 29.6 | 40.0 |
| 4x0358 | 6.1 | 22.2 | 21.0 | 32.8 | 45.0 |
| 4x0513 | 30.6 | 169 | 17.2 | 17.6 | 29.6 |
| 4x0514 | 17.7 | 106 | 22.6 | 37.0 | 47.3 |

and table S3). A spike in alanine aminotransferase (ALT) was observed in one high-dose animal (4x0514), but this commenced prior to the first dose and resolved in the early dosing phase (Fig. 3B). Notably, during therapy ALT was reduced to normal levels, likely due to reduction in the viral load, and was again elevated at the end of the follow-up period when viremia returned to baseline. Histology examinations of the baseline liver biopsies from the high-dose animals revealed HCV-specific changes, including mild hepatocellular swelling with disruption of hepatocellular sinuses and cords (Fig. 3, D to G, and fig. S16). Improved liver histology was observed in both high-dose animals after treatment at week 19, indicating a response to prolonged suppression of viremia and normalization of the IFN pathway.

Our results show that antagonism of miR-122 by the LNA oligonucleotide SPC3649 leads to marked suppression of viremia in chronically HCV-infected chimpanzees, thus implying that miR-122 is essential for accumulation of HCV RNA in vivo. The good PK properties, safety profile, and high stability of SPC3649 in vivo, combined with the prolonged suppression of viremia beyond treatment, suggest that less frequent dosing could be used after viral suppression is attained. SPC3649 therapy provided a high barrier to resistance, as shown by the lack of rebound in viremia during the 12-week treatment and the lack of adaptive mutations in the two miR-122 seed sites of HCV 5′ NCR. Conservation of both miR-122 seed sites in all HCV genotypes and subtypes suggests that such therapy will be genotype-independent. Finally, this study demonstrates the feasibility and safety of prolonged administration of a LNA oligonucleotide drug that antagonizes the function of a specific microRNA in a highly relevant disease model.

### References and Notes

1. F. V. Chisari, *Nature* **436**, 930 (2005).
2. J. J. Feld, J. H. Hoofnagle, *Nature* **436**, 967 (2005).
3. C. L. Jopling, M. K. Yi, A. M. Lancaster, S. M. Lemon, P. Sarnow, *Science* **309**, 1577 (2005).
4. C. L. Jopling, S. Schütz, P. Sarnow, *Cell Host Microbe* **4**, 77 (2008).
5. G. Randall *et al.*, *Proc. Natl. Acad. Sci. U.S.A.* **104**, 12884 (2007).
6. J. Elmén *et al.*, *Nature* **452**, 896 (2008).
7. M. Sarasin-Filipowicz, J. Krol, I. Markiewicz, M. H. Heim, W. Filipowicz, *Nat. Med.* **15**, 31 (2009).
8. C. M. Chen *et al.*, *Antimicrob. Agents Chemother.* **51**, 4290 (2007).
9. R. E. Lanford *et al.*, *Hepatology* **46**, 999 (2007).
10. R. E. Lanford *et al.*, *Hepatology* **43**, 961 (2006).
11. L. M. Chen *et al.*, *Gastroenterology* **128**, 1437 (2005).
12. M. Lagging *et al.*; DITTO-HCV Study Group, *Hepatology* **44**, 1617 (2006).
13. M. Diago *et al.*, *Gut* **55**, 374 (2006).
14. D. Butera *et al.*, *Blood* **106**, 1175 (2005).
15. A. I. Romero *et al.*, *J. Infect. Dis.* **194**, 895 (2006).
16. M. Sarasin-Filipowicz *et al.*, *Proc. Natl. Acad. Sci. U.S.A.* **105**, 7034 (2008).
17. J. J. Feld *et al.*, *Hepatology* **46**, 1548 (2007).
18. C. B. Bigger *et al.*, *J. Virol.* **78**, 13779 (2004).
19. J. Elmén *et al.*, *Nucleic Acids Res.* **36**, 1153 (2008).
20. We thank D. Chavez, B. Guerra, and H. Lee for excellent technical assistance; K. Brasky for veterinary support; L. Giavedoni for immunological analyses; P. Giclas for complement analyses; and E. Dick for pathology examinations. Supported by a grant from the Danish National Advanced Technology Foundation (S.K.); the primate studies performed at the Southwest National Primate Research Center are supported by NIH base grant P51 RR13986 and by the National Center for Research Resources (Research Facilities Improvement Program grant C06 RR 12087). The expression microarray data have been deposited in the ArrayExpress repository under accession number E-MEXP-2375. The GEO accession number for the sequencing data is GSE18919. E.S.H-E., A.P., and S.K. have a pending patent on the method of treatment.

### Supporting Online Material

www.sciencemag.org/cgi/content/full/1178178/DC1
Materials and Methods
Figs. S1 to S16
Tables S1 to S4
References

24 June 2009; accepted 30 October 2009
Published online 3 December 2009;
10.1126/science.1178178
Include this information when citing this paper.

# Topology Links RNA Secondary Structure with Global Conformation, Dynamics, and Adaptation

**Maximillian H. Bailor, Xiaoyan Sun, Hashim M. Al-Hashimi***

Thermodynamic rules that link RNA sequences to secondary structure are well established, but the link between secondary structure and three-dimensional global conformation remains poorly understood. We constructed comprehensive three-dimensional maps depicting the orientation of A-form helices across RNA junctions in the Protein Data Bank and rationalized our findings with modeling and nuclear magnetic resonance spectroscopy. We show that the secondary structures of junctions encode readily computable topological constraints that accurately predict the three-dimensional orientation of helices across all two-way junctions. Our results suggest that RNA global conformation is largely defined by topological constraints encoded at the secondary structural level and that tertiary contacts and intermolecular interactions serve to stabilize specific conformers within the topologically allowed ensemble.

The ability to predict and rationally manipulate the atomic structures of biomolecules is an overarching aim that is anticipated to advance drug discovery and bioengineering applications. The problem is particularly challenging for highly flexible RNAs, which adopt wide-ranging conformations in response to cellular cues and changes in physicochemical conditions (*1*–*4*). The thermodynamic principles that relate RNA primary sequence to secondary structure are well established and are routinely used in secondary structure prediction (*5*–*7*). However, current approaches for predicting three-dimensional (3D) structures of RNA ignore flexibility and conformational adaptation, and strongly rely on homology modeling for identifying long-range contacts rather than on principles that are encoded at the secondary structural level (*8*, *9*).

RNA global conformation is largely defined by the orientation of A-form helices that are linked by flexible pivot points, ~70% of which are two-way junctions such as bulges and internal loops (*1*–*3*, *10*, *11*) (Fig. 1A). By combining domain-elongation nuclear magnetic resonance (NMR) spectroscopy (*12*) and molecular dynamics (MD) simulations (*13*), we recently constructed ensembles of atomic-resolution structures for the transactivation response element (TAR) RNA (*14*) from human immunodeficiency virus type 1 (HIV-1) and type 2 (HIV-2) with time scale sensitivity extending from picoseconds to milliseconds. The ensembles revealed 3D rigid-body collective movements of A-form helices across trinucleotide (HIV-1) and dinucleotide (HIV-2) bulges, which are depicted in 3D maps in which the twist angles about the two helices ($\alpha_h$ and $\gamma_h$) and an interhelical bend angle ($\beta_h$) are specified for each conformer in the ensemble (Fig. 1). In both HIV-1 and HIV-2 TAR, the helices sample <5% of possible orientations and trace out a spatially nonrandom trajectory in which the two helices twist in a correlated manner while bending (Fig. 1B, in blue). Increasing the bulge length from two to three nucleotides resulted in an increase in the sampled interhelical orientations and a decrease in the correlations between the twist angles (*13*) (Fig. 1B, in blue). Seven distinct ligand-bound HIV-1 TAR conformations were represented in this narrow spatially anisotropic distribution, indicating that ligands induce structural adaptation by capturing preexisting conformations (*13*). Despite its persistent occurrence in TAR, the physical basis for this spatially anisotropic interhelical confinement remains unknown.

To explore the generality of the anisotropic interhelical confinement, we devised an approach to measure and compare interhelical angles across any type of two-way junction (*15*). Building on a previous convention (*16*), we designate two-way junctions $H_iS_XH_jS_Y$ in

Department of Chemistry and Biophysics, University of Michigan, Ann Arbor, MI 48109, USA.

*To whom correspondence should be addressed. E-mail: hashimi@umich.edu

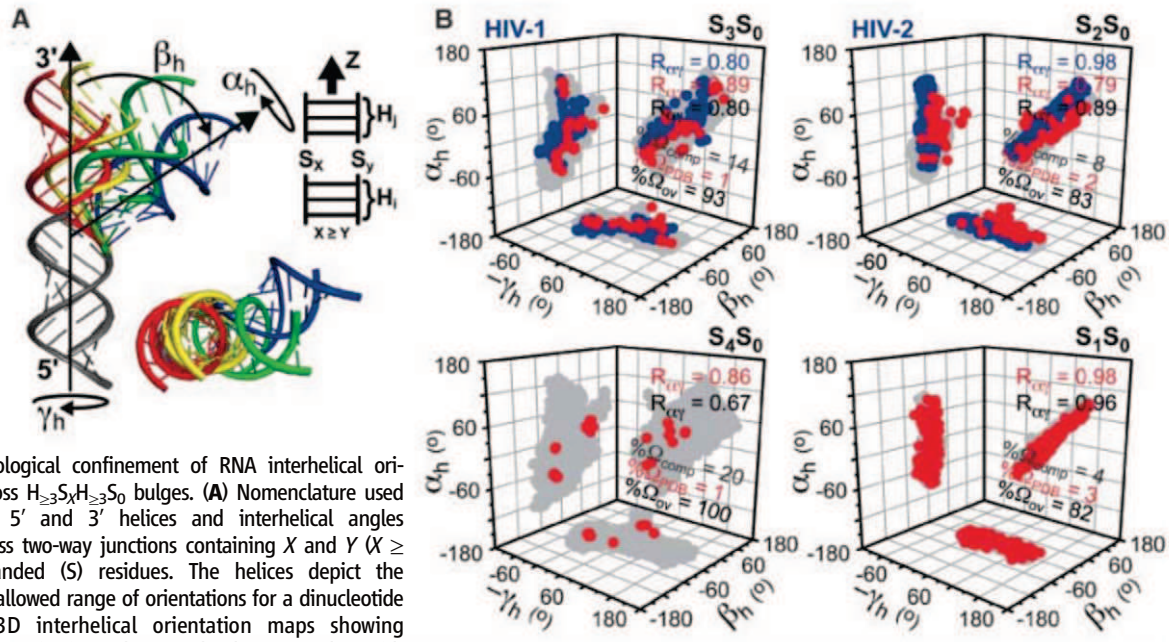


**Fig. 1.** Topological confinement of RNA interhelical orientations across $H_{\geq 3}S_XH_{\geq 3}S_0$ bulges. (**A**) Nomenclature used to designate 5′ and 3′ helices and interhelical angles ($\alpha_h\beta_h\gamma_h$) across two-way junctions containing *X* and *Y* (*X* ≥ *Y*) single-stranded (S) residues. The helices depict the topologically allowed range of orientations for a dinucleotide bulge. (**B**) 3D interhelical orientation maps showing individual 2D projections along each plane, together with the associated correlation coefficients (*R*) between the interhelical twist angles for bulges that are four ($S_4S_0$), three ($S_3S_0$, HIV-1 TAR), two ($S_2S_0$, HIV-2 TAR), and one ($S_1S_0$) nucleotide long. The NMR-MD, PDB-derived, and topologically computed interhelical distributions are shown in blue, red, and gray, respectively. There are a total of 751, 275, 148, and 21 PDB-derived entries for $S_1S_0$-, $S_2S_0$-, $S_3S_0$-, and $S_4S_0$-type junctions, respectively. The percentage of 3D interhelical orientations sampled by the PDB-derived and topologically computed distributions ($\Omega_{PDB}$ and $\Omega_{comp}$, respectively) is indicated, along with the fraction of the PDB-derived orientations that falls within 10° of the topologically allowed distribution ($\Omega_{ov}$).

which $i$ and $j$ specify the length of 5′ and 3′ helices, respectively, and in which $X$ and $Y$ ($X \geq Y$) specify the number of single-stranded residues in the 5′ and 3′ strands, respectively (Fig. 1A). We measured interhelical angles for all $H_{\geq 3}S_XH_{\geq 3}S_Y$ junctions (table S1) in the Protein Data Bank (PDB) (*17*), referred to hereafter as $S_XS_Y$. Similar results were obtained for $H_{\geq 4}S_XH_{\geq 4}S_Y$ junctions (fig. S1 and table S1). Strikingly, the interhelical orientations observed for all 148 trinucleotide and 275 dinucleotide bulges—which feature 15 and 10 unique sequences, respectively, in free and protein- or ligand-bound contexts—are also confined to narrow anisotropic distributions (Fig. 1B, in red) that sample <5% of possible orientations. The distributions fall close within the distribution observed for HIV-1 and HIV-2 TAR and feature similar variations with bulge length (Fig. 1B).

We investigated whether the anisotropic interhelical confinement observed across bulges arises from simple topological forces that restrict the allowed range of interhelical orientations. To this end, we computed the allowed interhelical orientations across bulges of varying lengths subject to two trivial constraints: (i) Helices cannot sterically clash, and (ii) the distance between O3′($i$) and P($i$ + 1) in the 3′ and 5′ helices, respectively, cannot exceed the average bulge linker length (4.9 Å per nucleotide) (*15*). Remarkably, the topologically allowed interhelical orientations quantitatively reproduce the PDB-derived and TAR dynamic distributions and

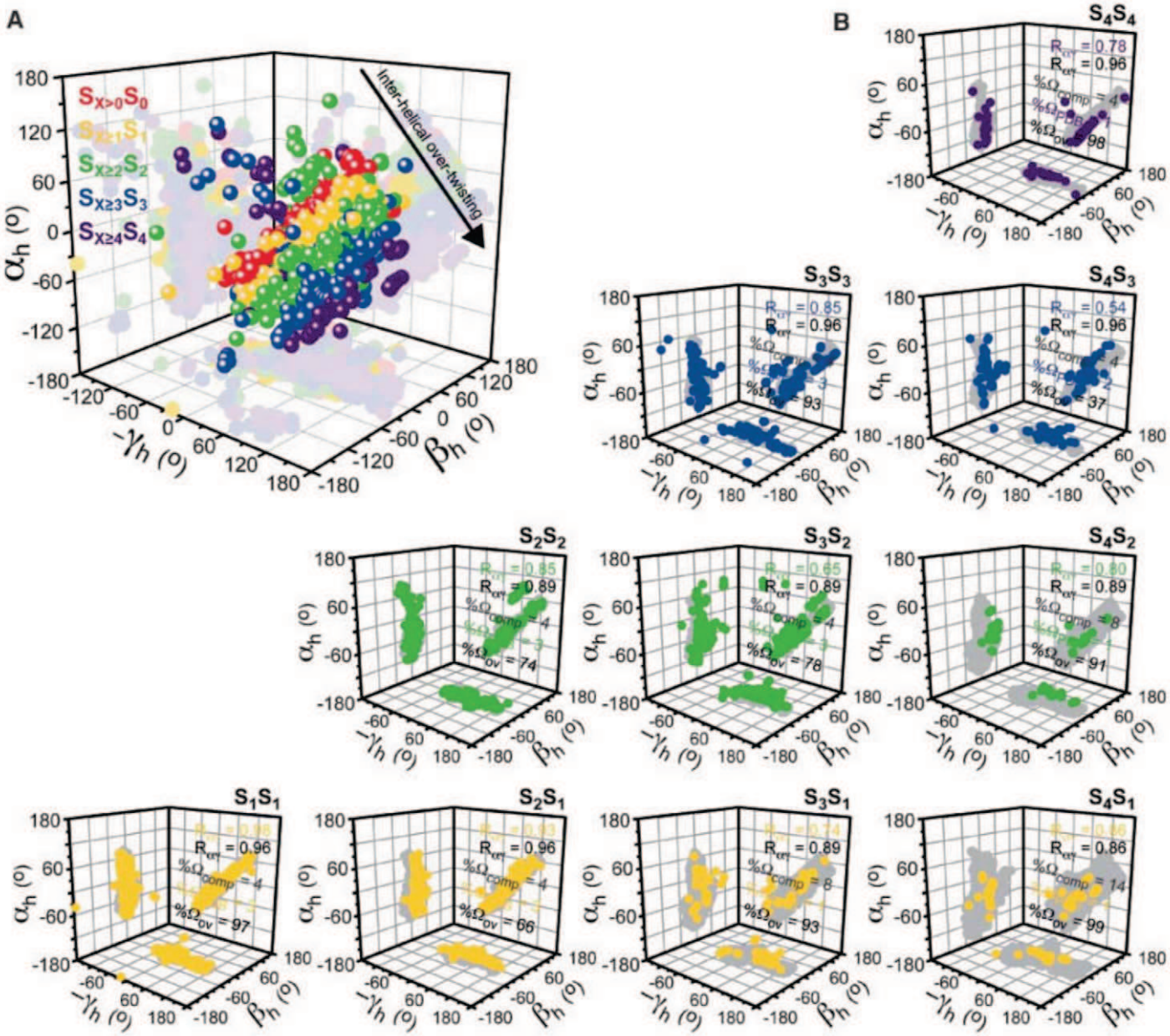


**Fig. 2.** Topological confinement of RNA interhelical orientations across $H_{\geq 3}S_XH_{\geq 3}S_Y$ internal loops. 3D interhelical orientation maps show individual 2D projections along each plane, together with the associated correlation coefficients ($R$) between the interhelical twist angles for different types of internal loops. (**A**) PDB-derived interhelical distributions for various families of $Y$-junctions. (**B**) PDB-derived and topologically computed interhelical distributions for different types of internal loops are shown in color and gray, respectively. There are a total of [374, 471, 133, 130], [230, 309, 32], [455, 155], and [104] PDB-derived entries for [$S_1S_1$, $S_2S_1$, $S_3S_1$, $S_4S_1$]-type, [$S_2S_2$, $S_3S_2$, $S_4S_2$]-type, [$S_3S_3$, $S_4S_3$]-type, and [$S_4S_4$]-type junctions, respectively. The percentage of interhelical orientations sampled by the PDB-derived and topologically computed distributions ($\Omega_{PDB}$ and $\Omega_{comp}$, respectively) is indicated, along with the fraction of the PDB-derived orientations that falls within 10° of the topologically allowed distribution ($\Omega_{ov}$).

their variation with bulge length (Fig. 1B, in gray). The allowed interhelical orientations sample only 4 to 20% of possible 3D orientations, yet they account for 82 to 100% of the PDB-derived orientations (Fig. 1B). For bulges ≤4 nucleotides long, the confinement is dominated by connectivity constraints (excludes 73 to 90% of orientations) rather than steric constraints (excludes ~49% of orientations). The connectivity constraints decrease gradually with bulge length and are inconsequential at seven nucleotides. In contrast, steric constraints are independent of helix length (fig. S2A). However, because of the strong anisotropy of the interhelical distributions and 34° helical pitch, changing the length of a helix can lead to large (34° per base pair) changes in the relative twist angles of neighboring helices (fig. S2B).

The spatially anisotropic interhelical confinement extends to symmetric and asymmetric internal loops (Fig. 2). The PDB-derived internal loop distributions are strikingly similar to those observed for bulges with one exception: They feature a systematic shift in the $\alpha_h$ and $\gamma_h$ twist angles of ~17° and thus an interhelical overtwisting ($\alpha_h + \gamma_h$) of ~34° with each *Y* increment. The *Y* value specifies the number of nucleotides in the shorter strand (Fig. 1A) and therefore the maximum number of noncanonical base pairs that can insert between helices at the junction (Fig. 2A). Thus, the *Y*-dependent variations in $\alpha_h$ and $\gamma_h$ are as expected if residues at the junction preferentially adopt a looped-in stacked conformation that maintains the helical pitch of ~33° (Fig. 2A).

By correcting the interhelical twist angles ($\alpha_h$ and $\gamma_h$) in the bulge computed topological distributions to account for maximum noncanonical base pairing at the junction (*15*), we were able to quantitatively reproduce the interhelical distributions observed for all symmetric and asymmetric internal loops (Fig. 2B, in gray). It is remarkable that even though the topologically computed distributions for the 14 different junction types (Fig. 1B and Fig. 2) sample only 4 to 20% (on average 7%) of possible 3D orientations, they accommodate ~90% of the interhelical orientations observed in the PDB. Major outliers are junctions that exceed our assumed average interhelical length and can readily be accommodated using a distribution of lengths. The topological constraints are also expected to increase with increasing RNA size as a result of growing self-avoidance constraints, leading to further definition of RNA global architecture.

Our results suggest that tertiary contacts and intermolecular interactions serve to selectively stabilize specific conformers from within a narrow topologically allowed ensemble. To gain insights into the conformational selection rules, we used NMR spectroscopy to structurally characterize HIV-1 TAR (Fig. 3A) when bound to five aminoglycoside small molecules (Fig. 3B) that differ in charge, shape, and size and that bind TAR with dissociation constants ($K_d$) in the micromolar range (*18*). Small molecules preferentially bind RNA interhelical junctions and thus provide an ideal framework for exploring the rules of global structural adaptation (*19*, *20*).

The chemically similar neomycin B (NeoB) and paromomycin (Par) induced similar chemical shift perturbations in NMR spectra of uniformly $^{13}C/^{15}N$-labeled TAR that were particularly pronounced in and around the bulge (Fig. 3, A and C). Likewise, similar perturbations were observed for the chemically similar tobromycin (Tob) and kanamycin B (KanB), which differed from those of NeoB and Par, whereas unique perturbations were observed for ribostamycin (Rib) (Fig. 3, A and C). Thus, the aminoglyco-

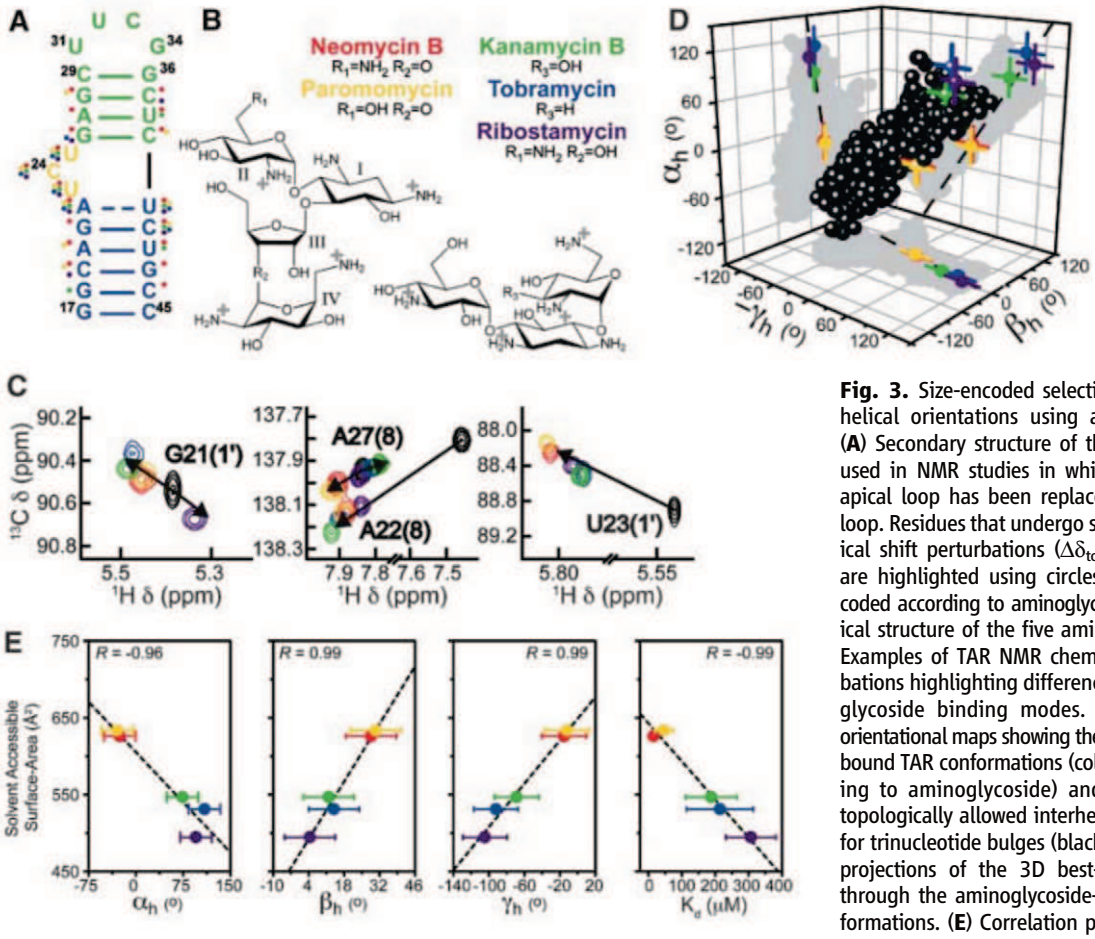


**Fig. 3.** Size-encoded selection of TAR interhelical orientations using aminoglycosides. (**A**) Secondary structure of the TAR construct used in NMR studies in which the wild-type apical loop has been replaced with a UUCG loop. Residues that undergo substantial chemical shift perturbations ($\Delta\delta_{total}$ > 0.30 ppm) are highlighted using circles that are color-coded according to aminoglycoside. (**B**) Chemical structure of the five aminoglycosides. (**C**) Examples of TAR NMR chemical shift perturbations highlighting differences in the aminoglycoside binding modes. (**D**) Interhelical orientational maps showing the aminoglycoside-bound TAR conformations (color-coded according to aminoglycoside) and the computed topologically allowed interhelical orientations for trinucleotide bulges (black). Shown are 2D projections of the 3D best-fit straight line through the aminoglycoside-bound TAR conformations. (**E**) Correlation plots between the solvent-accessible surface area (SAS) of the aminoglycosides versus the bound TAR interhelical angles (left three panels) and the dissociation constant ($K_d$, right panel). Points are color-coded according to aminoglycoside. The best-fit line is shown in each case along with the correlation coefficient (*R*).

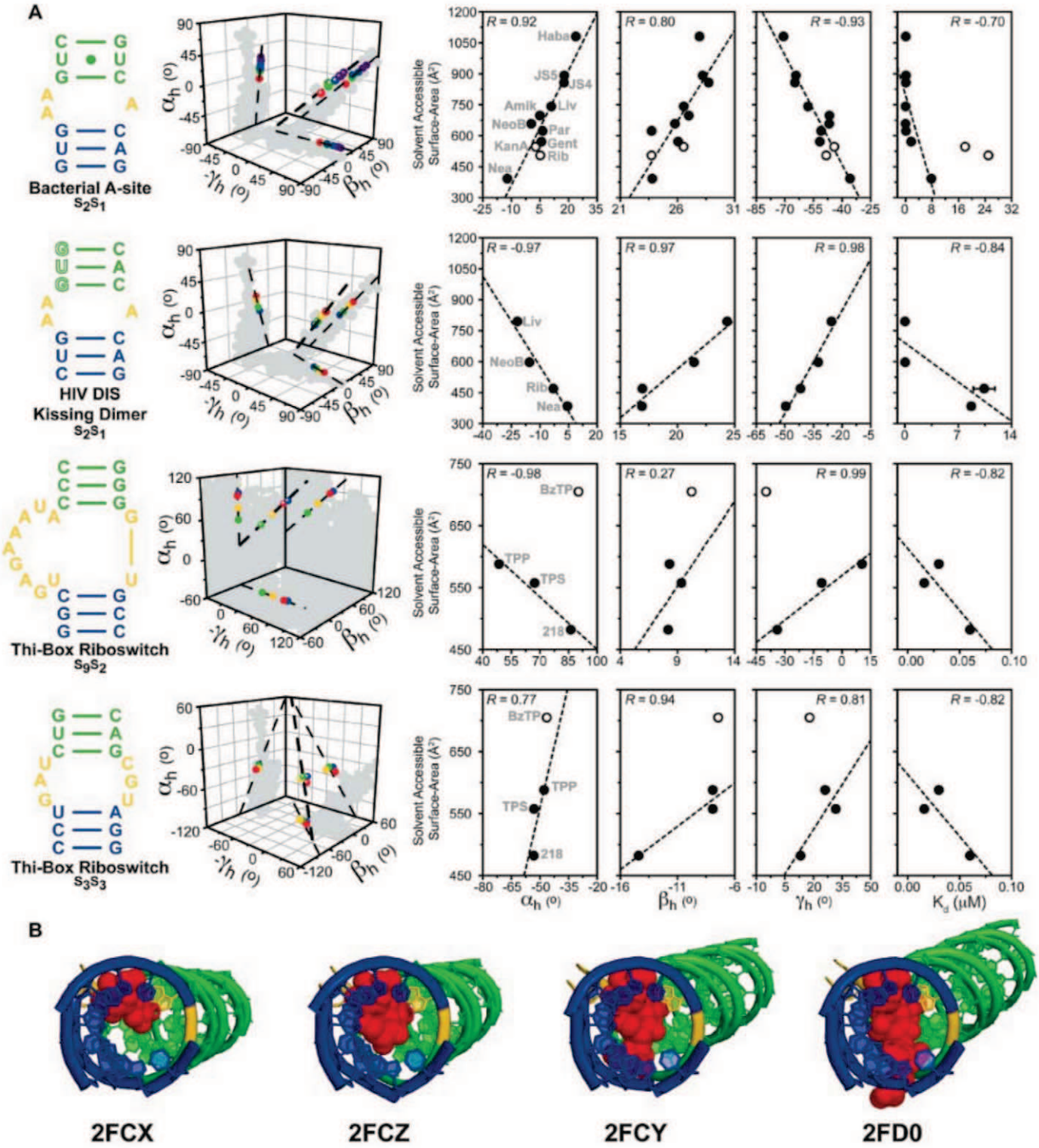


**Fig. 4.** Generalized size-encoded RNA conformational selection using small molecules. (**A**) Interhelical orientation maps depicting small-molecule bound RNA interhelical orientations color-coded according to small-molecule SAS (range: red, 400 Å$^2$; purple, 1100 Å$^2$) and the junction-allowed topological distribution (in gray) for diverse RNA two-way junctions (shown and labeled at the left) including aminoglycosides and derivatives bound to A-site RNA (1J7T, 2BE0, 2BEE, 2ESI, 2ES), 2ET3, 2ET4, 2ET5, 2ET8, 2G5Q, 2PWT), HIV kissing dimers (2FCX, 2FCY, 2FCZ, 2FD0), and thiamine phosphate analogs bound to *E. coli* Thi-Box (2HOJ, 2HOK, 2HOL, 2HOM, 2HOO, 2HOP). Shown at the right are correlation plots between the small-molecule SAS and bound RNA interhelical angles ($\alpha_h\beta_h\gamma_h$) and $K_d$. Outliers shown in open symbols represent cases in which more than one small molecule is bound to the RNA or in which added functional groups protrude out in solution and do not directly contact the RNA. (**B**) A representative series of x-ray structures of two-way RNA junctions bound to small molecules of increasing size. The specific example is of the dimerization initiation site kissing dimer bound to aminoglycosides (PDB accession 2FCX, 2FCY, 2FCZ, 2FD0). The aminoglycosides are shown in red; residues in the junction are in yellow.

sides bind distinct TAR conformations and/or interact differently with a common TAR structure. Using an order tensor analysis (*21*) of NMR residual dipolar couplings (*22*) (fig. S3 and tables S2 and S3), we determined the relative orientation of the TAR helices in each aminoglycoside complex. Results confirmed that NeoB and Par, Tob and KanB, and Rib bind and stabilize different TAR conformations within the trinucleotide bulge-encoded distribution (Fig. 3D).

The aminoglycoside-bound TAR conformations trace a linear conformational pathway along the bulge-encoded distribution (Fig. 3D). Remarkably, the specific position of a bound TAR conformation along the pathway is quantitatively encoded by the aminoglycoside size. We observe a strong correlation between all three TAR interhelical angles and the aminoglycoside solvent-accessible surface area (SAS), with the larger aminoglycosides favoring more bent and twisted conformations (Fig. 3E). A correlation is also observed between the aminoglycoside SAS and the NMR-derived binding affinities (fig. S3C), with tighter binding resulting in more bent conformations (Fig. 3E). Thus, changing the size of aminoglycosides allows selective and tunable capture of distinct TAR interhelical orientations spanning a total of ~160° in $\alpha_h\beta_h\gamma_h$ space.

Analysis of all RNA structures bound to three or more small molecules in the PDB revealed that the trends observed for TAR are a general feature of RNA small-molecule structural adaptation. For a variety of small-molecule bound RNA junctions (fig. S4A) with known x-ray crystal structures (*23*–*31*), small molecules capture interhelical orientations that trace linear pathways along the junction-encoded topological distribution (Fig. 4A and fig. S5). In all cases, increasing the small-molecule size results in increased interhelical bending and correlated clockwise or anticlockwise helical twisting. The size-encoded relations observed in A-site constructs containing an $S_2S_1$-type junction (Fig. 4A) are preserved in the larger ribosome context (fig. S4B). Interestingly, reversing the directionality of the A-site sequence, as occurs in the dimerization initiation site, leads to a flip in the clockwise versus anticlockwise sense of the twist angles (Fig. 4A). Large variations in interhelical angles are also observed for $S_9S_2$- and $S_3S_3$-type junctions in the *Escherichia coli* thiamine pyrophosphate (Thi-Box) riboswitch when bound to thiamine phosphate analogs that differ in size but otherwise have identical charge (*30*) (Fig. 4A and fig. S4). Conversely, the variations are trivial for eukaryotic thiamine pyrophosphate (TPP) riboswitch $S_9S_2$- and $S_3S_3$-type junctions when bound to thiamine phosphate analogs that have similar size (*31*) (fig. S5). In general, weaker correlations are observed with other properties of small molecules such as charge (fig. S6).

What is the molecular basis for size-encoded RNA conformational selection? The x-ray structures of RNA complexes show that the junctions are enlarged by variable levels of interhelical bending and twisting so as to accommodate small molecules of different sizes with optimal packing (Fig. 4B and fig. S7). The strong correlations observed between interhelical bending and twisting are similar to those observed for highly topologically confined junctions (e.g., $S_1S_0$, Fig. 1B) and likely reflect added topological constraints arising from insertion of the small molecules within the junctions. Thus, topological constraints define both RNA global conformation and dynamic adaptation, and the rational manipulation of RNA structure, and possibly activity, with the use of small molecules appears to be within reach.

### References and Notes


1. A. Serganov, D. J. Patel, *Nat. Rev. Genet.* **8**, 776 (2007).
2. H. M. Al-Hashimi, N. G. Walter, *Curr. Opin. Struct. Biol.* **18**, 321 (2008).
3. J. A. Cruz, E. Westhof, *Cell* **136**, 604 (2009).
4. H. Schwalbe, J. Buck, B. Furtig, J. Noeske, J. Wohnert, *Angew. Chem. Int. Ed.* **46**, 1212 (2007).
5. D. H. Mathews, D. H. Turner, *Curr. Opin. Struct. Biol.* **16**, 270 (2006).
6. B. A. Shapiro, Y. G. Yingling, W. Kasprzak, E. Bindewald, *Curr. Opin. Struct. Biol.* **17**, 157 (2007).
7. M. Zuker, *Nucleic Acids Res.* **31**, 3406 (2003).
8. M. Parisien, F. Major, *Nature* **452**, 51 (2008).
9. R. Das, D. Baker, *Proc. Natl. Acad. Sci. U.S.A.* **104**, 14664 (2007).
10. D. M. Lilley, *Q. Rev. Biophys.* **33**, 109 (2000).
11. E. Bindewald, R. Hayes, Y. G. Yingling, W. Kasprzak, B. A. Shapiro, *Nucleic Acids Res.* **36**, D392 (2008).
12. Q. Zhang, A. C. Stelzer, C. K. Fisher, H. M. Al-Hashimi, *Nature* **450**, 1263 (2007).
13. A. T. Frank, A. C. Stelzer, H. M. Al-Hashimi, I. Andricioaei, *Nucleic Acids Res.* **37**, 3670 (2009).
14. J. D. Puglisi, R. Tan, B. J. Calnan, A. D. Frankel, J. R. Williamson, *Science* **257**, 76 (1992).
15. See supporting material on *Science* Online.
16. D. M. Lilley *et al.*, *Nucleic Acids Res.* **23**, 3363 (1995).
17. H. M. Berman *et al.*, *Acta Crystallogr.* **D58**, 899 (2002).
18. K. F. Blount, Y. Tor, K. Hamasaki, A. Ueno, *Nucleic Acids Res.* **31**, 5490 (2003).
19. J. R. Thomas, P. J. Hergenrother, *Chem. Rev.* **108**, 1171 (2008).
20. T. Hermann, D. J. Patel, *Science* **287**, 820 (2000).
21. C. Musselman *et al.*, *J. Biomol. NMR* **36**, 235 (2006).
22. N. Tjandra, A. Bax, *Science* **278**, 1111 (1997).
23. B. Francois *et al.*, *Nucleic Acids Res.* **33**, 5677 (2005).
24. Q. Vicens, E. Westhof, *Structure* **9**, 647 (2001).
25. J. Kondo *et al.*, *ChemMedChem* **2**, 1631 (2007).
26. J. Kondo, B. François, R. J. Russell, J. B. Murray, E. Westhof, *Biochimie* **88**, 1027 (2006).
27. B. Francois *et al.*, *Angew. Chem. Int. Ed.* **43**, 6735 (2004).
28. E. Ennifar *et al.*, *Nucleic Acids Res.* **34**, 2328 (2006).
29. S. Freisz, K. Lang, R. Micura, P. Dumas, E. Ennifar, *Angew. Chem. Int. Ed.* **47**, 4110 (2008).
30. T. E. Edwards, A. R. Ferre-D'Amare, *Structure* **14**, 1459 (2006).
31. S. Thore, M. Leibundgut, N. Ban, *Science* **312**, 1208 (2006).


32. We thank C. Brooks for stimulating discussions and A. Kurochkin for NMR expertise. We acknowledge the Michigan Economic Development Cooperation and the Michigan Technology Tri-Corridor for the support of the purchase of a 600-MHz spectrometer and the W. F. Keck Foundation, NSF, and NIH for funds for the purchase of a 800-MHz spectrometer. Supported by NIH grant R01 AI066975-01.


### Supporting Online Material

www.sciencemag.org/cgi/content/full/327/5962/202/DC1
Materials and Methods
Figs. S1 to S7
Tables S1 to S3
References

25 August 2009; accepted 12 November 2009
10.1126/science.1181085

# Structure of an RNA Polymerase II–TFIIB Complex and the Transcription Initiation Mechanism

**Xin Liu, David A. Bushnell, Dong Wang, Guillermo Calero,* Roger D. Kornberg†**

**Previous x-ray crystal structures have given insight into the mechanism of transcription and the role of general transcription factors in the initiation of the process. A structure of an RNA polymerase II–general transcription factor TFIIB complex at 4.5 angstrom resolution revealed the amino-terminal region of TFIIB, including a loop termed the "B finger," reaching into the active center of the polymerase where it may interact with both DNA and RNA, but this structure showed little of the carboxyl-terminal region. A new crystal structure of the same complex at 3.8 angstrom resolution obtained under different solution conditions is complementary with the previous one, revealing the carboxyl-terminal region of TFIIB, located above the polymerase active center cleft, but showing none of the B finger. In the new structure, the linker between the amino- and carboxyl-terminal regions can also be seen, snaking down from above the cleft toward the active center. The two structures, taken together with others previously obtained, dispel long-standing mysteries of the transcription initiation process.**

Cellular RNA polymerases require protein cofactors for promoter recognition and the initiation of transcription. In bacteria, this requirement is met by a single protein, the σ factor (*1*). By contrast, RNA polymerase II (Pol II) of eukaryotes depends on five "general" factors, comprising some 30 polypeptides, for promoter-dependent transcription. The general

factors, known as TFIIB, -D, -E, -F, and -H, assemble with the polymerase and promoter DNA in a complex of ~2 MD at every round of the initiation of transcription. Promoters containing a TATA box may be transcribed with only the TATA-binding protein (TBP) subunit of TFIID, whereas TATA-less promoters require the TBP-associated factor (TAF) subunits of TFIID as well. TFIIB and TBP/TFIID are primarily responsible for promoter recognition; indeed, TFIIB and TBP are alone sufficient for Pol II transcription of a negatively supercoiled promoter in vitro (*2*). In the absence of supercoiling, TFIIE and TFIIH are required to introduce negative superhelical strain and unwind promoter DNA for the initiation of transcription. Structural studies of Pol II, both alone and as an actively transcribing complex, have revealed a large conformational change between the "closed" complex containing entirely double-stranded promoter DNA and the "open" complex containing an unwound region ("transcription bubble"). The promoter DNA is straight in the closed complex, but in the open complex it bends about 90° and descends some 30 Å into the central polymerase cleft. The mechanism of this large conformational change has remained unclear. The general factors are believed to assist and to remain associated throughout the process, but after initiation, they are released and the polymerase escapes from the promoter. The challenge is to understand how protein-protein interactions can be formed during the assembly of the transcription initiation complex and then reversed during promoter escape.

Biochemical and genetic studies have implicated TFIIB in start site selection and in the stabilization of the initial transcript. A previous structure of a Pol II–TFIIB complex, obtained from crystals grown in the presence of 800 mM ammonium sulfate, revealed the N-terminal region of TFIIB but little of the cyclin repeats that make up the C-terminal "core" of the protein (*3*). A notable finding was a loop, termed the "B finger," reaching into the Pol II active center. As the B finger would clash with nascent RNA beyond about five residues, it might be involved in the decision between abortive transcription (release of a short nascent transcript and reinitiation) and promoter escape. We now report a substantially different structure of the Pol II–TFIIB complex, obtained from crystals grown from solution containing 1.2 M sodium–potassium phosphate. The structure was solved by molecular replacement with a model of Pol II in the "clamp-closed" conformation. A difference ($F_o - F_c$) map between the Pol II–TFIIB structure determined here and that of Pol II alone revealed the zinc ribbon domain in the N-terminal region of TFIIB, and additional electron density attributable to the linker and C-terminal core domains of TFIIB, but no density due to the B finger (Fig. 1). The zinc ribbon domain was in essentially the same conformation as in the previous cocrystal structure (*3*), and was in the same location, in contact with the "dock" domain of Pol II.

A homology model of the yeast TFIIB core was constructed from the published human TFIIB core structure (*4*, *5*) and was manually placed in the $F_o - F_c$ map (Fig. 1B), resulting in a good fit of the first cyclin repeat, consisting of a five-helix bundle (BH1 to BH5). The location of the cyclin repeat was confirmed by a match to anomalous signals from Se-Met at four sites (Fig. 1B: M135, M168, M172 and M210) and was manually adjusted for a best fit to the anomalous signals. An additional α helix (BH0) was then built connected to BH1 and was validated by anomalous signals from Se-Met at one intrinsic (M104) and one mutant (L110M) site (Fig. 1B). The rest of the linker domain was built with the aid of anomalous signals from Se-Met at two additional mutant sites (S83M and R95M).

Mutations in the B finger (F66M, D69M, N72M, D75M, and V79M) gave no Se-Met anomalous signals, indicating a high degree of mobility of the B finger. The disordered region (residues 67 to 80) corresponds to the tip of the B finger, and an analogous region in bacterial σ factor ($\sigma_3$-$\sigma_4$ linker or $\sigma_{3.2}$) is also partially disordered at a comparable resolution (*6*). Residues of the linker domain adjacent to the disordered region are located at the ends of the previous B-finger electron density (fig. S1), showing consistency with the previous results and suggesting that the B finger, although mobile, projects into the Pol II active center as previously observed.

The N-terminal half of the linker domain winds past loops of Rpb1 and Rpb2 including the "lid," "rudder," and "fork loop 1" (Fig. 2A). Turn regions connecting on the N-terminal side to the B finger and on the C-terminal side to the other half of the linker (BH0 helix) contain conserved glycines and prolines (fig. S2). The BH0 helix is the most exposed part of the linker, lying on the surface of the Rpb1 clamp (Fig. 2B). The association of the linker domain with Rpb1 and Rpb2 loops and clamp may contribute to the stabilization of the loop conformations and to clamp closure (the loops are disordered in the structure of Pol II alone).

The TFIIB core domain is located above the Pol II cleft, about 50 Å from the N-terminal zinc-ribbon domain (Fig. 1A). The first cyclin repeat interacts with both the "protrusion" and the "wall" of Rpb2 (Fig. 2B), consistent with previous cross-linking and FeBABE cleavage mapping results (*7*, *8*). A large part of the protrusion is ordered by this interaction (fig. S3), but due to the presence of β strands and loops, a model of the ordered region could not be built. Interaction of BH2 with the top of the wall (fig. S3) may explain why yeast TFIIB is specific for yeast Pol II (*9*). A mutation (C149Y) in the BH2-wall interaction interface (fig. S3B) causes a shift of the transcription start site at *ADH1* in yeast (*10*). There was no evidence of the second cyclin repeat in the electron density map, presumably due to motion in absence of TBP and promoter DNA, which may be pronounced for yeast TFIIB because it contains a long inter-repeat linker (*11*) (fig. S2). The two cyclin repeats may perform distinctive roles, because a TFIIB-like protein, which interacts with Pol II and is required for transcription of sliced leader RNA in the human parasite *Trypanosoma brucei*, shows sequence homology to the first but not the second cyclin repeat (*12*). A recent publication that shows a structure of the Pol II–TFIIB complex at 4.3 Å

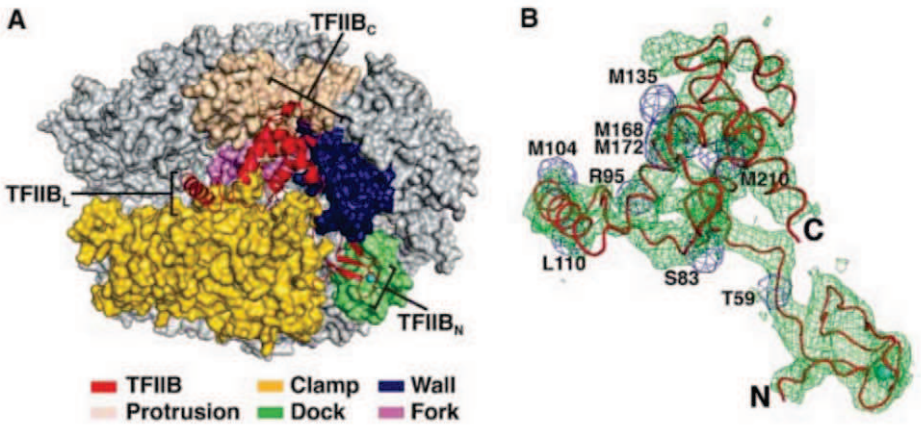


**Fig. 1.** Structure of Pol II–TFIIB complex. (**A**) "Top" view of Pol II in a surface representation, with previously identified domains in the colors indicated, and with TFIIB in ribbon representation. TFIIB zinc ribbon (TFIIB$_N$), linker (TFIIB$_L$), and first cyclin repeat (TFIIB$_C$) are indicated. (**B**) Difference ($F_o - F_c$) electron density map between Pol II–TFIIB and Pol II alone, contoured at 2.0σ, shown in green mesh, and Se-Met anomalous peaks, contoured at 6 to 10σ, shown in blue mesh.

Department of Structural Biology, Stanford University School of Medicine, Stanford, CA 94305, USA.

*Present address: Department of Structural Biology, University of Pittsburgh School of Medicine, Pittsburgh, PA 15260, USA. †To whom correspondence should be addressed. E-mail: kornberg@stanford.edu.

resolution in general agrees with the structure reported here (*13*).

The topography of the Pol II–TFIIB complex is similar to that of a bacterial RNA polymerase–σ factor complex (*6*, *14*). As previously noted, the zinc ribbon and B finger interact with polymerase surfaces similar to those of the $\sigma_4$ domain and the $\sigma_3$-$\sigma_4$ linker. We now find that the TFIIB linker and core interact with polymerase surfaces similar to those of $\sigma_2$ and $\sigma_3$. There are similarities of the TFIIB and σ factor structures as well. The first cyclin repeat of TFIIB aligns with the $\sigma_3$ domain, in particular with the $\sigma_{3.1}$ helix (Fig. 3), which contacts DNA downstream of the −10 element of bacterial promoters, facilitating transcription bubble formation (*15*, *16*). The TFIIB core makes sequence-specific contacts with promoter DNA, both upstream ($BRE^u$) and downstream ($BRE^d$) of the TATA box (*17*, *18*), and the solvent-exposed BH0-BH1 region may interact with the DNA downstream of $BRE^d$, in a manner analogous to the $\sigma_{3.1}$ helix–DNA interaction. Thus, TFIIB may recapitulate two important functions of σ factor in the initiation of transcription: that of the $\sigma_3$-$\sigma_4$ linker, which contacts the start site, and that of the $\sigma_{3.1}$ helix, which fixes the upstream edge of the transcription bubble. TFIIB may also serve as a scaffold for binding other transcription factors that perform functions attributed to σ factor in bacteria. For example, some regions of the TFIIF subunit Tfg2, which shows sequence similarity to σ and has been suggested to perform analogous functions, have been placed by cryo–electron microscopy (cryo-EM) in locations near that of the first cyclin repeat of TFIIB shown here (fig. S4) (*19*).

The first cyclin repeat in the Pol II–TFIIB cocrystal structure could be aligned with the same repeat in a previous structure of C-terminal fragments of human TFIIB and TBP bound to TATA box DNA (fig. S5). Docking the structures resulted in a model of a "minimal" pre-initiation complex (Fig. 4, A and B). The second cyclin repeat in the model interacts with the Rpb2 protrusion and Rpb12, consistent with cross-linking and FeBABE cleavage mapping studies (*7*, *8*). When the TATA box DNA fragment in the model was extended with straight B-form DNA, to simulate the "closed" form of the promoter, only minor adjustments were needed, to avoid steric clashes with the clamp [Fig. 4, A and B; see supporting online material (SOM)]. The DNA follows a path above the central cleft leading to the polymerase active center. The structure of the closed promoter complex could be modified with the nucleic acid region of a transcribing complex (*20*–*23*) to model an open promoter complex (Fig. 4C and fig. S6; see SOM). Extension of the template strand upstream of the transcription bubble in this model leads through a "tunnel" formed by TFIIB and Pol II to the location of duplex DNA in the closed promoter model (dashed cyan line in Fig. 4C; location of tunnel indicated in Fig. 4D).

The formation of the template-strand tunnel by TFIIB gives insight into the closed-to-open promoter transition. It suggests a straightforward mechanism for the process. Transient promoter melting may be captured by interaction of the template strand with the tunnel. The orientation and proximity of the promoter DNA to the upstream end of the tunnel provide a pathway whereby progressive melting and short-range interactions can lead, sequentially, to a large conformational change.

Biochemical studies in a mammalian system have demonstrated transcription bubble formation beginning about 20 base pairs (bp) downstream of the TATA box and extending, as transcription proceeds, to a bubble size of 18 bp and transcript length of about seven residues, upon which the upstream 8 bp of the bubble reanneal ("bubble collapse") (*24*–*26*). The template single strand between the growing DNA-RNA hybrid and the TFIIB tunnel presumably loops out, or "scrunches," as previously described (dashed orange line in Fig. 4D) (*27*, *28*). Bubble collapse involves the region passing through the TFIIB tunnel (dashed cyan line in Fig. 4D), as well as the scrunched strand. Following the reannealing of 8 bp, the upstream edge of the bubble is located adjacent to the Rpb1 rudder and lid, as observed in the structure of a transcribing complex. The open promoter model thus accounts for bubble expansion and collapse.

Biochemical studies have further demonstrated a role for the B finger in bubble collapse and promoter escape (*24*, *29*). Interaction with the B finger has been shown by the stabilizing effect of TFIIB on a five-residue transcribing complex (*3*). Mutation of the B finger eliminates a pause in transcription at seven residues, observed with a "premelted" DNA template (*24*). The B finger may play multiple roles, both stabilizing a five-residue transcribing complex and clashing with RNA in a seven-residue complex. These roles of the B finger may relate to the alternative states revealed by crystallography, one with a well-localized B finger but no linker or cyclin repeat,

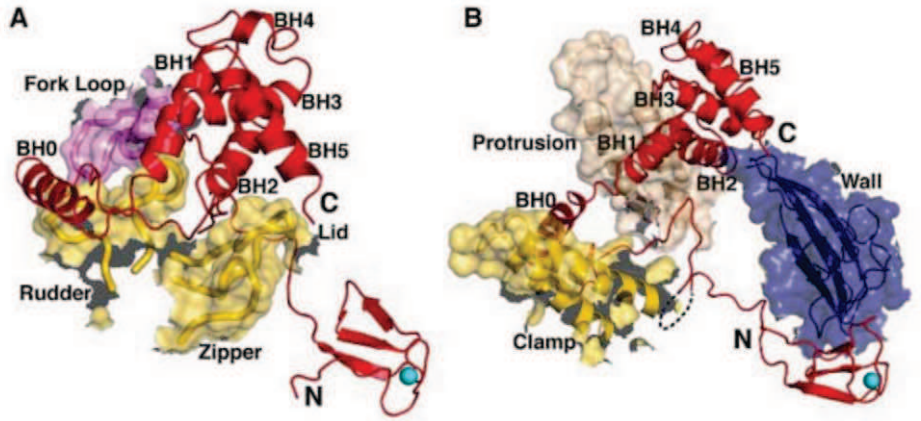


**Fig. 2.** Structure of TFIIB and Pol II–TFIIB interactions. (**A**) Expanded view from Fig. 1A, with Pol II fork loop 1, rudder, lid, and zipper shown in both transparent surface and ribbon representation, and with TFIIB helices labeled. (**B**) Same as (A) rotated 45° around the *x* axis, except with parts of Pol II clamp, protrusion, and wall shown in both transparent surface and ribbon representation. The B finger from the previous cocrystal structure is shown as a dashed black line.

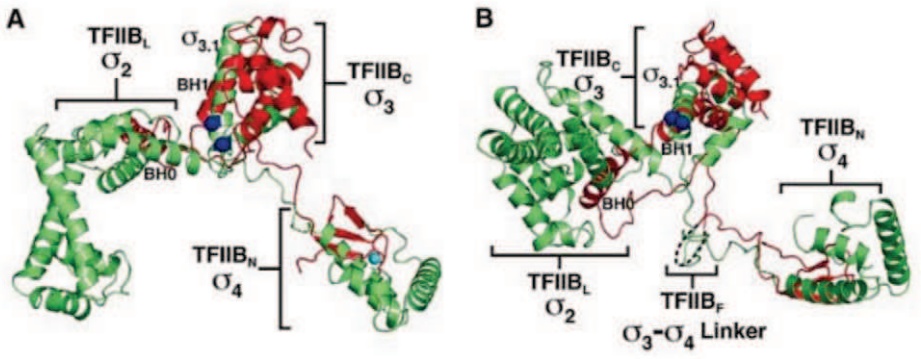


**Fig. 3.** Comparison of TFIIB and bacterial σ factor structures. (**A**) Superposition of TFIIB (red) and σ factor (green) structures. Conserved residues H455 and E458 of σ factors that bind to the −10 element and mark the start of transcription bubble formation are highlighted as blue spheres. Corresponding domains from TFIIB and σ factor are labeled. (**B**) Same as (A) rotated 45° around the *x* axis. The B finger ($TFIIB_F$) from the previous cocrystal structure is shown as a dashed black line.

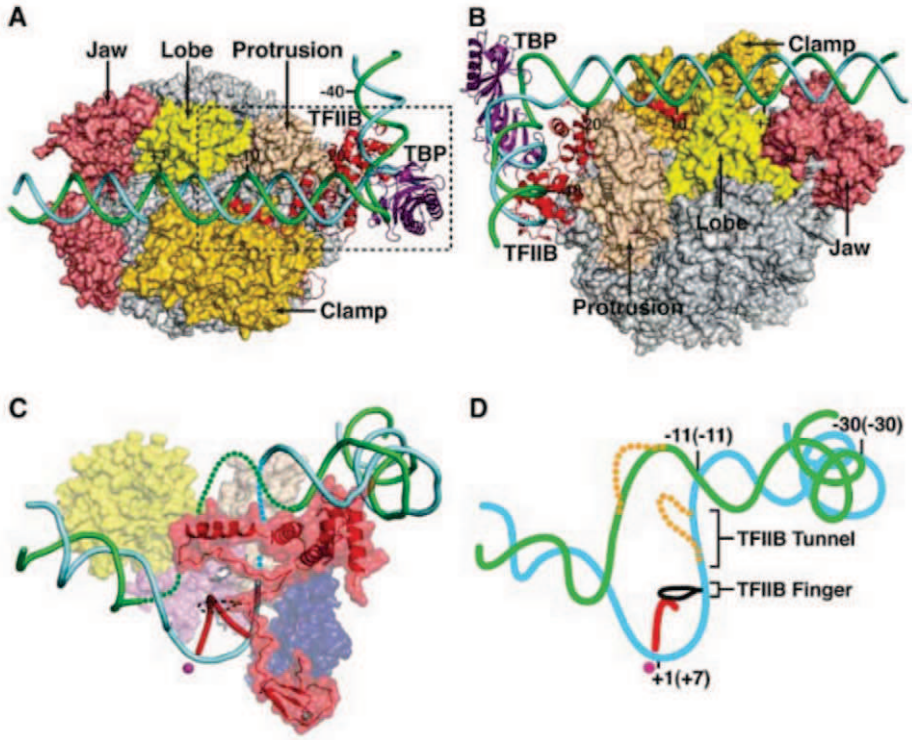


**Fig. 4.** Models of promoter complexes. (**A**) Model of closed promoter complex based on the alignment in fig. S4, viewed as in Fig. 1A rotated 45° around the *y* axis. Yeast $TFIIB_C$ and the second cyclin repeat of human $TFIIB_C$ are shown in red and $TBP_C$ is shown in purple. DNA upstream and downstream of the TATA box was extended with B-form double helix. A slight distortion was introduced in the template strand to avoid clashes with the Pol II clamp. Template and nontemplate strands are shown in cyan and green. (**B**) Same as (A) rotated 180° about *y* axis and 120° about the *x* axis. (**C**) Model of the open promoter complex. Expected path of the template strand, connecting the upstream edge of the transcription bubble seen in the structure of a transcribing complex (*24*) with duplex promoter DNA from the closed promoter complex, is shown as a dashed cyan line. Possible path of the nontemplate strand is shown as a dashed green line. View is of the dashed boxed area in fig. S6A, rotated 45° around the *x* axis. The Pol II clamp has been removed for clarity. TFIIB is shown as a red transparent surface with the location of the B finger represented by a black dashed line. The nascent RNA transcript and active-site $Mg^{2+}$ are shown as a red ribbon and a magenta sphere. (**D**) Cartoon of transcription initiation complex, based on the nucleic acid structure in (C), with template DNA positions at the start of transcription indicated, and those after synthesis of a seven-residue transcript in parentheses. The "scrunched" template strands resulting from synthesis of the seven-residue transcript are shown as dashed orange lines.

and the alternative containing a well-localized linker and cyclin repeat but no B finger. These states are evidently similar in energy and may interconvert during the initiation of transcription: Initiation occurs in the state depicted in the open promoter model, with the template strand bound by the linker and cyclin repeat; upon reaching about five residues in length, the nascent transcript contacts the B finger, forming a stable complex (*3*), tipping the balance between states, flipping from that reported here to that obtained previously, in which the linker and cyclin repeat are mobile and the B finger is observed; extension of the transcript beyond seven residues results in a clash with the B finger, displacing it as well, thereby completing the process of promoter escape. The requirement for disruption of protein-protein interactions that would seem to impede promoter escape is solved by substituting one set of contacts (B finger–Pol II and B finger–RNA) for another (linker–Pol II and cyclin repeat–Pol II). Disruption of TFIIB–Pol II interaction occurs sequentially. Meanwhile, the TFIIB tunnel maintains the transcription bubble until the DNA-RNA hybrid is long enough to persist on its own. The stability conferred upon the open promoter complex by the TFIIB tunnel is ultimately replaced by the stability of an RNA-DNA hybrid. The entire process of transcription initiation, from initial promoter melting to promoter escape, may be explained in this way.

### References and Notes


1. C. A. Gross *et al.*, *Cold Spring Harb. Symp. Quant. Biol.* **63**, 141 (1998).
2. J. D. Parvin, P. A. Sharp, *Cell* **73**, 533 (1993).
3. D. A. Bushnell, K. D. Westover, R. E. Davis, R. D. Kornberg, *Science* **303**, 983 (2004).
4. F. T. Tsai, P. B. Sigler, *EMBO J.* **19**, 25 (2000).
5. D. B. Nikolov *et al.*, *Nature* **377**, 119 (1995).
6. K. S. Murakami, S. Masuda, S. A. Darst, *Science* **296**, 1280 (2002).
7. H. T. Chen, S. Hahn, *Cell* **119**, 169 (2004).
8. H. T. Chen, L. Warfield, S. Hahn, *Nat. Struct. Mol. Biol.* **14**, 696 (2007).
9. S. P. Shaw, J. Wingfield, M. J. Dorsey, J. Ma, *Mol. Cell. Biol.* **16**, 3651 (1996).
10. W. H. Wu, I. Pinto, B. S. Chen, M. Hampsey, *Genetics* **153**, 643 (1999).
11. F. Hayashi *et al.*, *Biochemistry* **37**, 7941 (1998).
12. B. Schimanski, J. Brandenburg, T. N. Nguyen, M. J. Caimano, A. Günzl, *Nucleic Acids Res.* **34**, 1676 (2006).
13. D. Kostrewa *et al.*, *Nature* **462**, 323 (2009).
14. D. G. Vassylyev *et al.*, *Nature* **417**, 712 (2002).
15. K. S. Murakami, S. A. Darst, *Curr. Opin. Struct. Biol.* **13**, 31 (2003).
16. K. S. Murakami, S. Masuda, E. A. Campbell, O. Muzzin, S. A. Darst, *Science* **296**, 1285 (2002).
17. T. Lagrange, A. N. Kapanidis, H. Tang, D. Reinberg, R. H. Ebright, *Genes Dev.* **12**, 34 (1998).
18. W. Deng, S. G. Roberts, *Genes Dev.* **19**, 2418 (2005).
19. W. H. Chung *et al.*, *Mol. Cell* **12**, 1003 (2003).
20. A. L. Gnatt, P. Cramer, J. Fu, D. A. Bushnell, R. D. Kornberg, *Science* **292**, 1876 (2001).
21. K. D. Westover, D. A. Bushnell, R. D. Kornberg, *Cell* **119**, 481 (2004).
22. K. D. Westover, D. A. Bushnell, R. D. Kornberg, *Science* **303**, 1014 (2004).
23. N. Korzheva *et al.*, *Science* **289**, 619 (2000).
24. M. Pal, A. S. Ponticelli, D. S. Luse, *Mol. Cell* **19**, 101 (2005).
25. F. C. Holstege, U. Fiedler, H. T. Timmers, *EMBO J.* **16**, 7468 (1997).
26. C. Giardina, J. T. Lis, *Science* **261**, 759 (1993).
27. A. Revyakin, C. Liu, R. H. Ebright, T. R. Strick, *Science* **314**, 1139 (2006).
28. A. N. Kapanidis *et al.*, *Science* **314**, 1144 (2006).
29. K. Tran, J. D. Gralla, *J. Biol. Chem.* **283**, 15665 (2008).


30. This research was supported by NIH grants GM049985 and AI21144 to R.D.K. X.L. was supported by the Jane Coffin Childs Memorial Fund fellowship. D.W. was supported by the NIH Pathway to Independence Award (K99 GM085136). Portions of this research were carried out at the Stanford Synchrotron Radiation Laboratory (SSRL), a national user facility operated by Stanford University on behalf of the U.S. Department of Energy, Office of Basic Energy Sciences. The SSRL Structural Molecular Biology Program is supported by the Department of Energy, Office of Biological and Environmental Research, and by the NIH, National Center for Research Resources, Biomedical Technology Program, and the National Institute of General Medical Sciences. The Advanced Light Source is supported by the Director, Office of Science, Office of Basic Energy Sciences, of the U.S. Department of Energy under contract DE-AC02-05CH11231. Use of the Advanced Photon Source was supported by the U.S. Department of Energy, Office of Science, Office of Basic Energy Sciences, under contract DE-AC02-06CH11357. Coordinates and structure factors have been deposited at the Protein Data Bank under accession code 3K7A.


### Supporting Online Material

www.sciencemag.org/cgi/content/full/1182015/DC1
Materials and Methods
SOM Text
Figs. S1 to S6
Table S1
References


16 September 2009; accepted 3 November 2009
Published online 12 November 2009;
10.1126/science.1182015
Include this information when citing this paper.

# A Transient Niche Regulates the Specification of *Drosophila* Intestinal Stem Cells

Divya Mathur,[1] Alyssa Bost,[1] Ian Driver,[2] Benjamin Ohlstein[1]*

Stem cell niches are locations where stem cells reside and self-renew. Although studies have shown how niches maintain stem cell fate during tissue homeostasis, less is known about their roles in establishing stem cells. The adult *Drosophila* midgut is maintained by intestinal stem cells (ISCs); however, how they are established is unknown. Here, we show that an ISC progenitor generates a niche cell via Notch signaling. This niche uses the bone morphogenetic protein 2/4 homolog, decapentaplegic, to allow progenitors to divide in an undifferentiated state and subsequently breaks down and dies, resulting in the specification of ISCs in the adult midgut. Our results demonstrate a paradigm for stem cell–niche biology, where progenitors generate transient niches that determine stem cell fate and may give insights into stem cell specification in other tissues.

Intercellular factors regulate stem cell proliferation and maintenance in stem cell niches in the *Drosophila* ovary (*1*) and testis (*2*, *3*), as well as in mammalian systems, such as the hematopoietic system (*4*–*6*), skin (*7*), and neural cells (*8*). These niches, which are generally fixed stromal locations, signal to prevent stem cell differentiation (*9*, *10*). However, even though the role of niches in the maintenance of tissue homeostasis has been well examined, relatively little is known about their function in establishing stem cell lineages during organogenesis.

The lineage of intestinal stem cells (ISCs) in the adult *Drosophila* midgut (*11*, *12*) can be tracked to determine how progenitors establish different intestinal cells during development. Adult midgut progenitors (AMPs) from the three larval stages generate all epithelial cells in the adult midgut, including ISCs, enterocytes, and enteroendocrine cells (table S1) (*13*, *14*). In the first two instars (L1 and L2), AMPs proliferate and disperse throughout the midgut. Dispersal stops by the third instar (L3), when AMPs proliferate and form clusters known as midgut imaginal islands. During metamorphosis, when the larval gut histolyses, the islands merge and generate the adult midgut epithelium, including ISCs, enterocytes, and enteroendocrine cells (fig. S1). Here we analyze the mechanism by which these cells are established from this pool of AMPs.

Because Notch signaling determines stem cell–daughter identity in the adult midgut (*11*, *12*, *15*), we asked if it plays a similar role during larval intestinal development. We examined the expression of the Notch ligand, Delta (Dl), which is expressed in adult ISCs, and the Notch reporter, *Gbe*$^{+}$*Su(H)LacZ*, which marks ISC daughters, called enteroblasts (table S1), in the process of differentiation. We identified enteroendocrine cells by staining for the nuclear protein Prospero, and we distinguished enterocytes by their polyploid nuclei with 4′,6′-diamidino-2-phenylindole (DAPI) staining (*11*, *12*, *15*). In late L1 (*16*), AMPs could be identified as single Dl-positive cells dispersed throughout the midgut, although no Notch activity could be detected at this time by staining for *Gbe*$^{+}$*Su(H)LacZ* (Fig. 1A). Toward the late L2, when AMP islands contained two cells, one cell was Dl-positive, and the other was *lacZ*-positive (Fig. 1B). Because it has been shown that all cells in an AMP island arise from a founder AMP (*14*), the first AMP division after the dispersion phase must be asymmetric, from which one daughter became a *lacZ*-positive cell.

[1]Department of Genetics and Development, Columbia University Medical Center, New York, NY 10032, USA. [2]The Integrated Program in Cellular, Molecular, Structural and Genetic Studies, Columbia University Medical Center, New York, NY 10032, USA.

*To whom correspondence should be addressed. E-mail: bo2160@columbia.edu

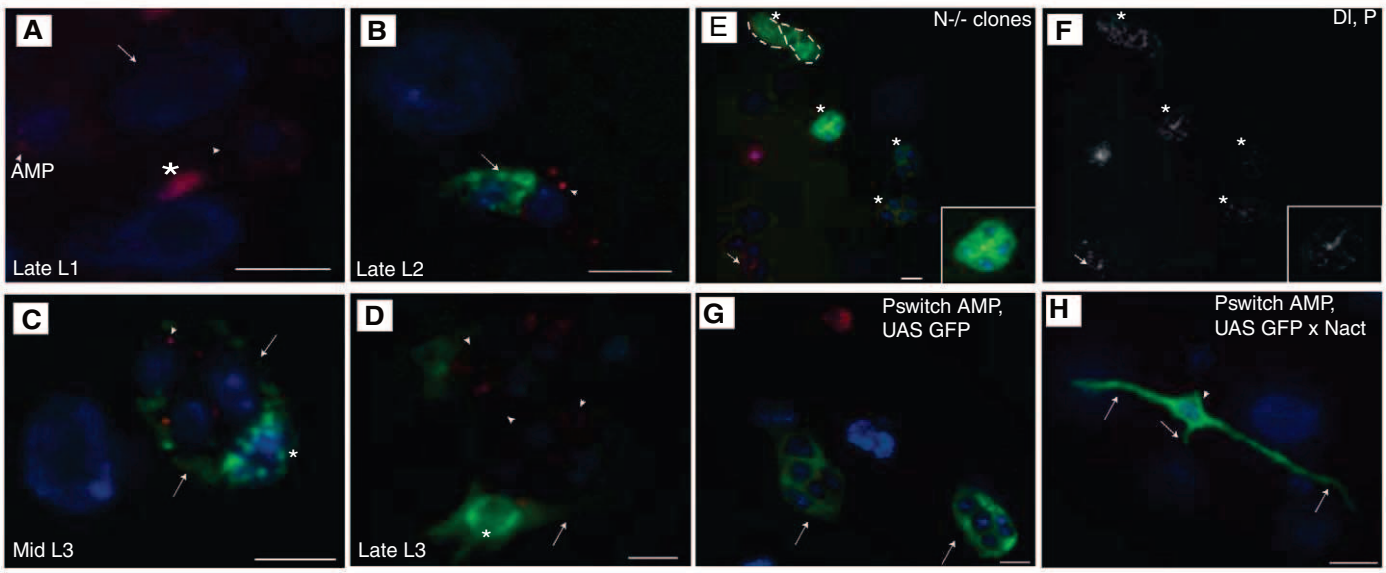


**Fig. 1.** Characterization of AMP islands during larval development. (**A**) During late L1, AMPs exist as single, Dl-positive cells (arrowheads). Larval enterocytes are polyploid (arrow), and enteroendocrine cells are Prospero-positive (asterisk). (**B**) By late L2, an AMP island contains one Dl-positive AMP (arrowhead), and another cell that is *Gbe*$^{+}$*Su(H)lacZ*-positive (arrow). (**C**) The *Gbe*$^{+}$*Su(H)lacZ*-positive cell (asterisk) extends processes (arrows) around AMPs, throughout mid L3 and (**D**) late L3, and islands contain multiple Delta-positive AMPs (arrowheads). (A to D) DAPI, nuclear blue; Dl, cytoplasmic red; Prospero, nuclear red; and β-galactosidase, green. (**E** and **F**) Notch mutant MARCM clones (green, asterisk) lack a discernible PC [(inset in (E)]. Sometimes, mutant clones merge with each other (dashed line). They also have increased Dl staining at the membranes [inset in (F)], whereas WT islands (arrow) have predominantly vesicular Dl. (**G**) Pswitch$^{AMP}$ UAS-GFP (green), expressed in all cells of an AMP island (late L3 shown) used to (**H**) ectopically express N$^{act}$ at early L1, results in differentiation into a PC-like cell (green) with long extensions (arrows) when analyzed at late L3. (E, G, and H) DAPI, nuclear blue; Dl, cytoplasmic red; Prospero, nuclear red; and GFP, green. Scale bars, 10 μm.

Thereafter, as the island grew, all newly generated AMPs expressed Dl but were *lacZ*-negative (Fig. 1, C and D).

We observed that by mid L3, the *Gbe*$^{+}$*Su(H)lacZ*-positive cell extended processes that encased all AMPs in the island (Fig. 1C). The *lacZ*-positive cells were similar to those described more than 50 years ago by El Shatoury and Waddington, who called them peripheral cells (PCs) (table S1); however, the function of these cells was not determined (*17*). As the island grew, the PC processes extended even further (Fig. 1D). Additionally, the PC nucleus appeared to be larger than AMP nuclei and often had a bent shape (Fig. 1C). The PC processes could also be outlined by staining for the *Drosophila* β-catenin homolog Armadillo (Arm) and appeared to extend loosely around AMP clusters, which were tightly packed as indicated by Arm expression between AMPs (fig. S2). Although in most islands there was only one PC, by late L3 ~20% of the islands ($n$ = 328) had a second PC, which was at the opposite end from the first one (fig. S2). We made MARCM (mosaic analysis of a repressible cell marker) clones to elucidate the origin of the second PC. In clusters where two PCs were present, our clonal analyses indicated that the second one was generated by AMPs, and, therefore, PCs did not undergo any divisions (fig. S3).

Because AMPs express Dl and PCs express *Gbe*$^{+}$*Su(H)lacZ*, we investigated the role of Notch signaling in the generation of a PC. Loss-of-function clones of *Notch* induced in early L1 larvae and analyzed at late L3 lacked a discernible PC, suggesting that Notch signaling is required for PC generation (Fig. 1, E and F). Furthermore, *Notch* mutant islands tended to merge together, indicating that PCs may be required to keep islands separated throughout the midgut (Fig. 1E). However, the lack of a PC did not seem to affect AMP divisions, implying that the activity of known AMP proliferation signals, the epidermal growth factor receptor ligands (*14*) emanating from the overlying muscle and surrounding AMPs, was not affected. In a screen to identify cell-type–specific, RU-486 (mifepristone)–inducible GAL4 lines (Pswitch) (*16*, *18*) expressed in the larval midgut, we found one that was specifically expressed in the midgut in AMP islands (Pswitch$^{AMP}$) (Fig. 1G). Pswitch$^{AMP}$ was recombined with UAS—mCD8::GFP (GFP, green fluorescent protein), which localizes to cell membranes, and used to induce expression of activated Notch (N$^{act}$) in AMPs of early L1 larvae. N$^{act}$ expression directed AMPs to differentiate into cells that morphologically resembled PCs, as indicated by their long processes (Fig. 1H). Moreover, these processes lacked directionality, suggesting that they are normally attracted by an unknown signal secreted by AMPs. These experiments suggest that Notch signaling in AMPs is both necessary and sufficient for PC generation.

From our Pswitch screen, we also identified a GAL4 line that was expressed specifically in PCs throughout the larval midgut (Fig. 2A and fig. S4A) and enteroblasts in the adult posterior midgut (fig. S4B). When we recombined this GAL4 line (Pswitch$^{PC}$) with UAS-mCD8::GFP, we were able to clearly visualize the long processes that encase AMP islands. Furthermore, Pswitch$^{PC}$-mediated expression of actin5C-GFP showed that the cytoskeleton of these processes was actin-rich (fig. S5).

Pswitch$^{PC}$ UAS-GFP was used to trace the development of PCs and AMPs into the early hours of metamorphosis, when the adult midgut is formed (*19*). At 0 hours after puparium formation (APF), AMP islands with surrounding PCs could be detected (Fig. 2B). However, between 2 and 3 hours APF, PC processes appeared to open up and spread out, AMPs began to be released from the islands (Fig. 2, C and D), and two pools of AMPs emerged. The larger pool consisted of AMPs that expressed both GFP, like that seen with enteroblasts in the adult midgut, and Pdm1, a marker for adult (*20*)

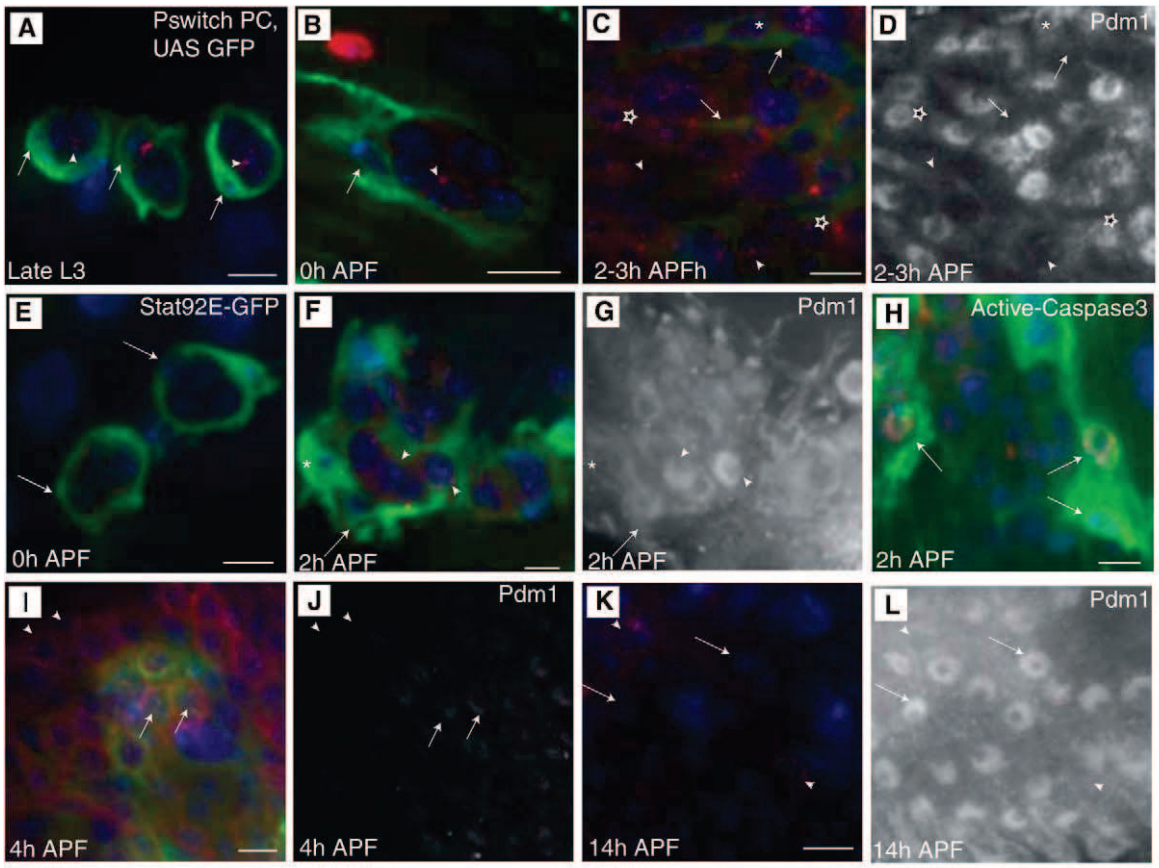


**Fig. 2.** Developmental fate of AMPs and PCs during metamorphosis. (**A**) Pswitch$^{PC}$ UAS-GFP labels PCs (arrows) surrounding Dl-positive AMPs (arrowheads) during late L3 and (**B**) 0 hours APF. (**C** and **D**) Between 2 and 3 hours APF, PC (asterisk) extensions appear to spread out (arrows), and most AMPs (stars) express GFP and Pdm1, indicating differentiation into enterocytes. A smaller AMP population (arrowheads) remains Pdm1-negative, whereas some cells are Delta-positive. (**E**) Stat92E-GFP is expressed only in PCs (arrows) at 0 hours APF. (**F** and **G**) At 2 hours APF, PC (asterisk) processes break apart (arrow) and AMPs express Pdm1 (arrowheads). (**H**) PCs stain positive for active caspase-3 (arrows). (**I** and **J**) At 4 hours APF, Pswitch$^{PC}$ UAS-GFP expression is diminished in differentiating AMPs. Most Pdm1-positive cells accumulate membrane-bound Dl (arrows). Pdm1-negative cells with vesicular Dl (arrowheads) are present at this stage. (**K** and **L**) By 14h APF, Pdm1–positive cells lose GFP and Dl expression (arrows), whereas Pdm1-negative cells are Dl-positive (arrowheads). (A to C, F, I, and K) GFP, green; Dl, cytoplasmic red; Prospero, nuclear red; and DAPI, nuclear blue. (D, G, and L) Pdm1, nuclear grayscale, unmerged. (H) GFP, green; active caspase-3, nuclear red; and DAPI, nuclear blue. Scale bars, 10 μm.

and larval enterocytes (fig. S6), indicating that these AMPs were differentiating into enterocytes. Intermingled within these differentiating AMPs were fewer AMPs consisting of cells negative for both GFP and Pdm1 expression, some of which expressed Dl, similar to the expression pattern of ISCs in the adult midgut. However, because both PCs and differentiating AMPs were GFP-positive at this stage, we followed the expression of Stat92E-GFP, a GFP reporter for JAK/STAT (JAK, Janus kinase; STAT, signal transducers and activators of transcription) signaling (*21*), as a marker that we identified was expressed specifically in PCs in the larval and pupal midguts (Fig. 2E). At 2 hours APF, we observed breakdown of processes in Stat92E-GFP–positive PCs (Fig. 2, F and G). Consistent with this fragmentation, PC nuclei stained positive for active caspase-3, indicating that these cells were undergoing programmed cell death (Fig. 2H). By 4 hours APF, they were no longer visible in the pupal midgut (fig. S7). Following PC breakdown (after 4 hours APF), most AMPs continued to differentiate into Pdm1-positive cells and started losing their enteroblast-like Pswitch$^{PC}$ expression. They accumulated membrane-bound Dl, suggesting that they were no longer able to traffic Dl into endocytic vesicles, which is essential for Dl-Notch signaling (Fig. 2, I and J) (*22*). By 14 hours APF, Pdm1-positive cells in the pupal gut were no longer Dl-positive, whereas all cells with vesicular Dl remained Pdm1-negative. Based on Dl expression in these Pdm1 negative cells, they probably correspond to the ISCs of the adult midgut (Fig. 2, K and L). The number of these cells at this stage (767 ± 142.7, $n$ = 4 guts) correlated approximately with the number of islands in late L3 (820 ± 91.1, $n$ = 10 guts), suggesting that, on average, one AMP from each island becomes a future ISC. In support of this hypothesis, these numbers also correspond with the number of ISCs (~1000) previously reported to be present in an adult midgut (*11*).

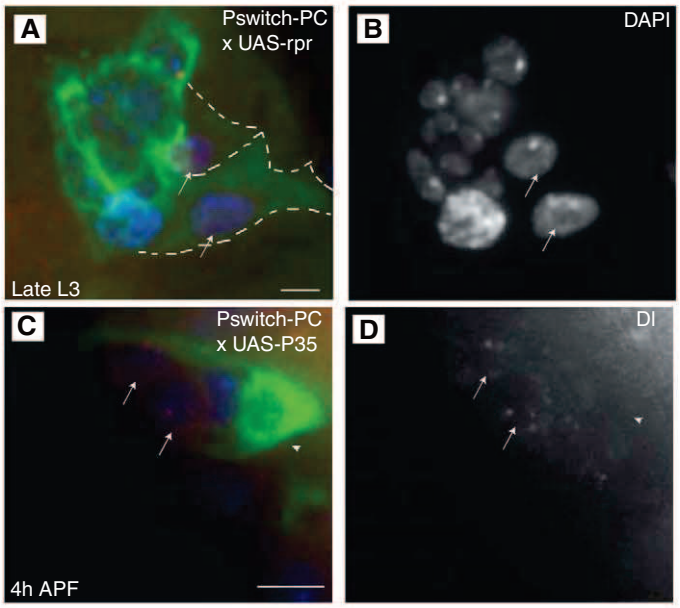


**Fig. 3.** The PC acts as a niche that regulates AMP differentiation. (**A** and **B**) Pswitch$^{PC}$ UAS-GFP–mediated expression of *UAS-reaper* at early L3 results in differentiation of AMPs into polyploid, GFP-positive, Pdm1-positive, enterocyte-like cells with a large cytoplasm (arrows indicate PDM1-positive, polyploid nuclei; dashed lines denote enterocyte-like cells). DAPI, blue; GFP, green; and Pdm1, red, nuclear. (**C** and **D**) (Dl channel) Pswitch$^{PC}$, UAS-GFP–driven expression of UAS-P35 results in prolonged PC survival (arrowhead) and delayed AMP differentiation (arrows). DAPI, nuclear blue; GFP, green; Dl, cytoplasmic red; and Prospero, nuclear red. Scale bars, 10 μm.

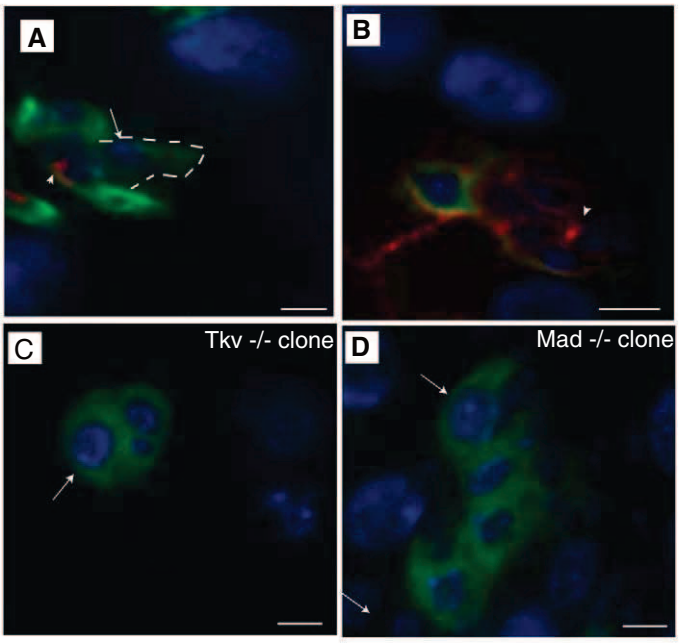


**Fig. 4.** PCs signal via the Dpp pathway to prevent AMP differentiation. (**A** and **B**) Pswitch$^{PC}$ UAS-GFP–driven expression of *dpp* RNAi results in (A) AMP differentiation into GFP-positive, polyploid, enterocyte-like cells (arrow, dashed line) that dissociate from other AMPs, indicated by diminished Arm staining, as compared with the Arm expression (arrowhead) between GFP-negative, undifferentiated AMPs. (B) Arm is expressed between cells in islands with GFP UAS-GFP-negative AMPs (arrowhead). MARCM clones of (**C**) *tkv* and (**D**) *Mad* result in differentiation of AMPs into polyploid enterocyte-like cells (arrows). (A to D) GFP, green; DAPI, nuclear blue. (A and B) Arm, red. Scale bars, 10 μm.

The observation that the breakdown of PC processes during metamorphosis correlates with the appearance of Pdm1-positive cells in AMP islands suggests that PCs may regulate AMP differentiation and establishment of ISCs. To determine the function of PCs, we crossed Pswitch$^{PC}$ UAS-GFP to a programmed cell death–inducing line, *UAS-reaper*, and fed larvae RU-486 at early L3 to induce *reaper* expression in PCs. By mid L3, PC nuclei stained for active caspase-3, indicating that these cells were dying (fig. S8). Subsequently, by late L3, AMPs differentiated into polyploid enterocyte-like cells, as established by positive staining for GFP, Pdm1, and DAPI (Fig. 3, A and B). This result suggests that PCs are required for maintaining AMPs in an undifferentiated state until the onset of metamorphosis. In further support of this hypothesis, at 4 hours APF, when PCs have normally disappeared and AMPs have scattered throughout the midgut, Pswitch$^{PC}$ UAS-GFP–induced expression of the cell death–blocking line, *UAS-p35*, delayed the disappearance of PCs and differentiation of AMPs (Fig. 3, C and D). Consequently, PC-encased AMP islands with multiple Dl-positive cells could be detected at this stage, further suggesting that the loss of PCs is required for directing AMPs to generate ISCs and differentiated cells in the adult midgut.

These experiments demonstrate that in the larval midgut, the PC acts as a niche for AMPs to keep them undifferentiated until metamorphosis. Stem cell niches in the *Drosophila* ovary and testis send molecular signals to stem cells to keep them undifferentiated (*23*–*25*). Because both these niches use bone morphogenetic protein signaling to maintain stem cells, we tested the relevance of this pathway in maintaining the differentiation state of AMPs. *Decapentaplegic* (*Dpp*) RNA interference (RNAi) induced specifically in PCs using Pswitch$^{PC}$ UAS-GFP resulted in the appearance of positive, polyploid cells in the islands, which started to break away from other AMPs in the island, as indicated by a decrease in Arm staining between the cells (Fig. 4, A and B). Similar to differentiating enteroblasts, these cells also expressed GFP, suggesting that a Dpp signal from the PC maintains AMPs in an un-

differentiated state. However, these differentiating cells were Pdm1-negative, suggesting that other signals that repress differentiation are present. In accordance with the *dpp* RNAi results, loss-of-function MARCM clones of a Dpp receptor, *thickveins* (*tkv*) (*26*), and a downstream effector molecule, mothers against decapentaplegic (Mad) (*27*), both resulted in premature differentiation of AMPs into large, polyploid, enterocyte-like cells (Fig. 4, C and D) compared with wild-type (WT) MARCM clones (fig. S9).

Our studies suggest how stem cells might be determined during intestinal organogenesis (fig. S10). After symmetric divisions and dispersal during early larval development, a founder AMP undergoes an asymmetric division and signals via the Notch pathway to direct its first daughter to become a PC that acts as a niche, where the AMP and its subsequent daughters can remain undifferentiated in response to a Dpp signal from the PC, and proliferate to form AMP islands. During metamorphosis, the PC breaks down, allowing AMPs in the island to respond to Notch signaling and differentiate into enterocytes. However, one AMP per island, on average, remains undifferentiated and becomes a future ISC. The mechanism that allows this AMP to stay undifferentiated remains to be determined.

Unlike other characterized niches, where a stem or progenitor cell moves away from its niche to differentiate (*1*, *7*, *28*), the PC niche is a holding pen, which does not allow its cells to escape or to differentiate until the niche breaks down. The transition to a functionally homeostatic adult niche that maintains ISCs would require a separate step. Our observations indicate a paradigm that other stem cell systems may also use: The progenitor cell divides to form both niche and stem cells. Such a mechanism that lends greater autonomy to stem cells might exist in other epithelial cell populations during development or tissue homeostasis.

### References and Notes


1. T. Xie, A. C. Spradling, *Science* **290**, 328 (2000).
2. A. A. Kiger, D. L. Jones, C. Schulz, M. B. Rogers, M. T. Fuller, *Science* **294**, 2542 (2001).
3. N. Tulina, E. Matunis, *Science* **294**, 2546 (2001).
4. J. Zhang *et al*., *Nature* **425**, 836 (2003).
5. O. H. Yilmaz, M. J. Kiel, S. J. Morrison, *Blood* **107**, 924 (2006).
6. L. M. Calvi *et al*., *Nature* **425**, 841 (2003).
7. T. Tumbar *et al*., *Science* **303**, 359 (2004); published online 11 December 2003 (10.1126/science.1092436).
8. F. Doetsch, *Curr. Opin. Genet. Dev.* **13**, 543 (2003).
9. R. Schofield, *Blood Cells* **4**, 7 (1978).
10. B. Ohlstein, T. Kai, E. Decotto, A. Spradling, *Curr. Opin. Cell Biol.* **16**, 693 (2004).
11. B. Ohlstein, A. Spradling, *Nature* **439**, 470 (2006).
12. C. A. Micchelli, N. Perrimon, *Nature* **439**, 475 (2006).
13. V. J. Hartenstein, Y. N. Jan, *Rouxs Arch. Dev. Biol.* **201**, 194 (1992).
14. H. Jiang, B. A. Edgar, *Development* **136**, 483 (2009).
15. B. Ohlstein, A. Spradling, *Science* **315**, 988 (2007).
16. Materials and methods are available as supporting material on *Science* Online.
17. H. H. El Shatoury, C. H. Waddington, *J. Embryol. Exp. Morphol.* **5**, 9 (1957).
18. L. Nicholson *et al*., *Genetics* **178**, 215 (2008).
19. C. W. Robertson, *J. Morphol.* **59**, 351 (1936).
20. W. C. Lee, K. Beebe, L. Sudmeier, C. A. Micchelli, *Development* **136**, 2255 (2009).
21. E. A. Bach *et al*., *Gene Expr. Patterns* **7**, 323 (2007).
22. A. Chitnis, *Dev. Dyn.* **235**, 886 (2006).
23. A. A. Shivdasani, P. W. Ingham, *Curr. Biol.* **13**, 2065 (2003).
24. T. Xie, A. C. Spradling, *Cell* **94**, 251 (1998).
25. E. Kawase, M. D. Wong, B. C. Ding, T. Xie, *Development* **131**, 1365 (2004).
26. T. J. Brummel *et al*., *Cell* **78**, 251 (1994).
27. J. J. Sekelsky, S. J. Newfeld, L. A. Raftery, E. H. Chartoff, W. M. Gelbart, *Genetics* **139**, 1347 (1995).
28. Y. M. Yamashita, D. L. Jones, M. T. Fuller, *Science* **301**, 1547 (2003).


29. We thank J. Wolken and S. Selway for technical assistance with the Pswitch screen; members of the *Drosophila* community for sending fly stocks; Developmental Studies Hybridoma Bank for antibodies; E. Matunis, M. Buszczak, and J. Wilhelm for helpful discussions; and anonymous reviewers for comments. B.O. is the recipient of the 2009 Searle Scholars Award, the Charles Bohmfalk Research Award, and an NIH grant (R01 DK082456-01).


### Supporting Online Material

www.sciencemag.org/cgi/content/full/327/5962/210/DC1
Materials and Methods
Figs. S1 to S10
Table S1
References

15 September 2009; accepted 25 November 2009
10.1126/science.1181958

# Essential Role of the Histone Methyltransferase G9a in Cocaine-Induced Plasticity

**Ian Maze,[1] Herbert E. Covington III,[1] David M. Dietz,[1] Quincey LaPlant,[1,2] William Renthal,[2] Scott J. Russo,[1] Max Mechanic,[2] Ezekiell Mouzon,[1] Rachael L. Neve,[3] Stephen J. Haggarty,[4,5] Yanhua Ren,[1] Srihari C. Sampath,[6] Yasmin L. Hurd,[1] Paul Greengard,[7] Alexander Tarakhovsky,[6] Anne Schaefer,[7] Eric J. Nestler[1]***

Cocaine-induced alterations in gene expression cause changes in neuronal morphology and behavior that may underlie cocaine addiction. In mice, we identified an essential role for histone 3 lysine 9 (H3K9) dimethylation and the lysine dimethyltransferase G9a in cocaine-induced structural and behavioral plasticity. Repeated cocaine administration reduced global levels of H3K9 dimethylation in the nucleus accumbens. This reduction in histone methylation was mediated through the repression of G9a in this brain region, which was regulated by the cocaine-induced transcription factor ΔFosB. Using conditional mutagenesis and viral-mediated gene transfer, we found that G9a down-regulation increased the dendritic spine plasticity of nucleus accumbens neurons and enhanced the preference for cocaine, thereby establishing a crucial role for histone methylation in the long-term actions of cocaine.

Repeated cocaine exposure is characterized by persistent changes in gene expression and altered neuronal morphology within the rodent nucleus accumbens (NAc), a key component of the brain's reward circuitry (*1*, *2*). Chromatin remodeling is important in aberrant transcriptional changes in this brain region that may underlie aspects of cocaine addiction (*3*–*9*). Cocaine regulation of chromatin structure in the NAc results, in part, from direct cocaine-induced modifications of the chromatin enzymatic machinery, leading to changes in histone acetylation and phosphorylation (*4*, *7*–*9*); however, roles for enzymes controlling histone methylation have not yet been investigated.

A recent genome-wide promoter analysis using chromatin immunoprecipitation coupled to microarrays (ChIP-Chip) identified altered patterns of repressive histone H3 lysine 9 (H3K9) and 27 (H3K27) methylation at specific gene promoters in the NAc after repeated cocaine treatment (*6*). In mice, we therefore profiled numerous lysine methyltransferases (KMTs) and demethylases (KDMs) that are known to control H3K9 or H3K27 methylation (Fig. 1A). Only two enzymes, G9a and G9a-like protein (GLP), displayed persistent transcriptional regulation 24 hours after repeated cocaine administration, when the expression of both genes was significantly down-regulated. Because G9a and GLP specifically catalyze the dimethylation of H3K9 (H3K9me2), their down-regulation by cocaine is consistent with decreased global levels of euchromatic H3K9me2 observed at this time point (Fig. 1B). In contrast, global levels of heterochromatic H3K27 meth-

[1]Fishberg Department of Neuroscience, Mount Sinai School of Medicine, New York, NY, USA. [2]Departments of Psychiatry and Neuroscience, University of Texas Southwestern Medical Center, Dallas, TX, USA. [3]Department of Brain and Cognitive Sciences, Massachusetts Institute of Technology, Cambridge, MA, USA. [4]Psychiatric and Neurodevelopmental Genetics Unit and Molecular Neurogenetics Unit, Center for Human Genetic Research, Massachusetts General Hospital, Boston, MA, USA. [5]Stanley Center for Psychiatric Research, Broad Institute of Harvard and Massachusetts Institute of Technology, Cambridge, MA, USA. [6]Laboratory of Lymphocyte Signaling, The Rockefeller University, New York, NY, USA. [7]Laboratory of Molecular and Cellular Neuroscience, The Rockefeller University, New York, NY, USA.

*To whom correspondence should be addressed. E-mail: eric.nestler@mssm.edu

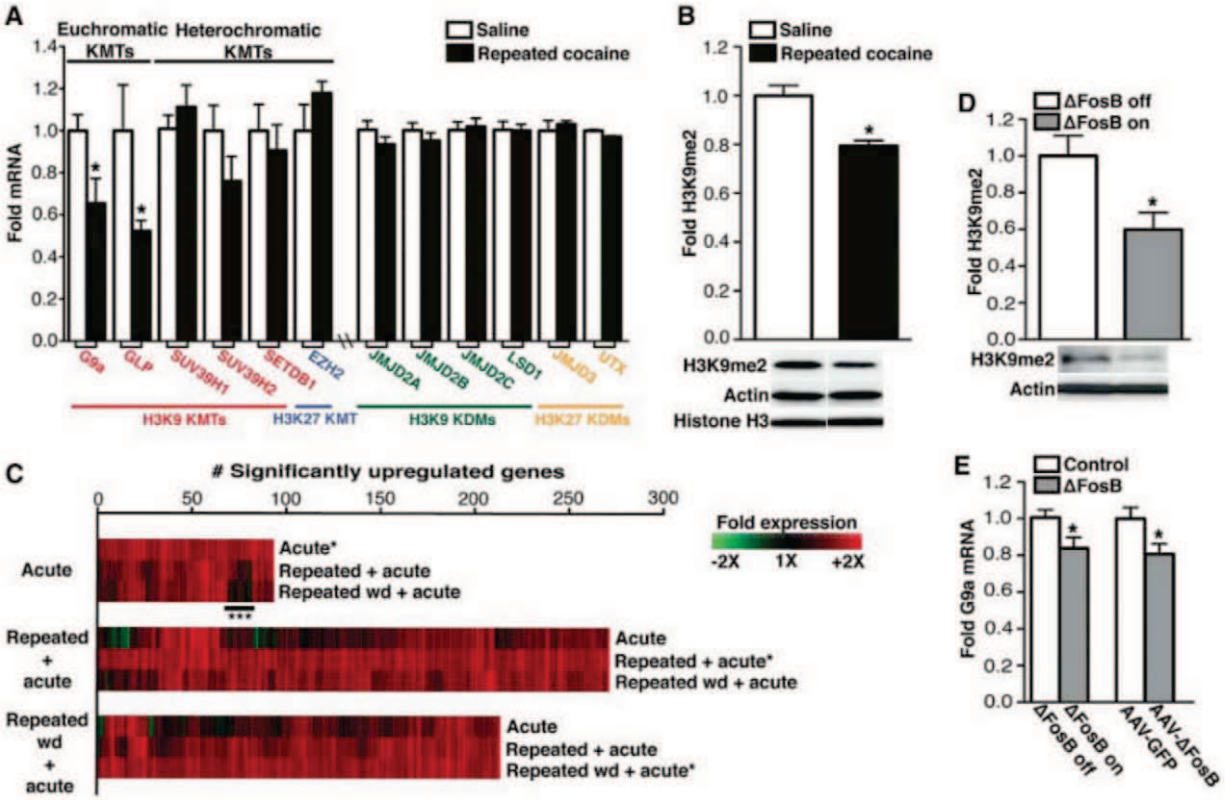


**Fig. 1.** Repeated cocaine administration represses G9a expression in the NAc through a ΔFosB-dependent mechanism. (**A**) mRNA expression of H3K9/K27 KMTs and KDMs in the NAc 24 hours after repeated cocaine. (**B**) H3K9me2 levels in NAc 24 hours after repeated cocaine. (**C**) Analysis of gene expression after acute or repeated cocaine. Heat maps (*) show genes up-regulated in NAc 1 hour after a cocaine challenge in naïve animals (acute), in animals treated repeatedly with cocaine (repeated + acute), or in animals after 168 hours of withdrawal from repeated cocaine (repeated wd + acute). Associated heat maps show how genes were affected under the other two conditions. Desensitized transcriptional responses after repeated cocaine are indicated (***). (**D**) H3K9me2 levels in the NAc from NSE-*tTA* x tetOP-*ΔFosB* mice on (ΔFosB off) or off (ΔFosB on) doxycycline 1 hour after repeated cocaine. (**E**) G9a mRNA expression in the NAc from NSE-*tTA* x tetOP-*ΔFosB* mice on (ΔFosB off) and off (ΔFosB on) doxycycline and from mice infected with AAV-GFP or AAV-ΔFosB. Data are presented as mean ± SEM. For statistical analyses, see the full figure legends in the supporting online text.

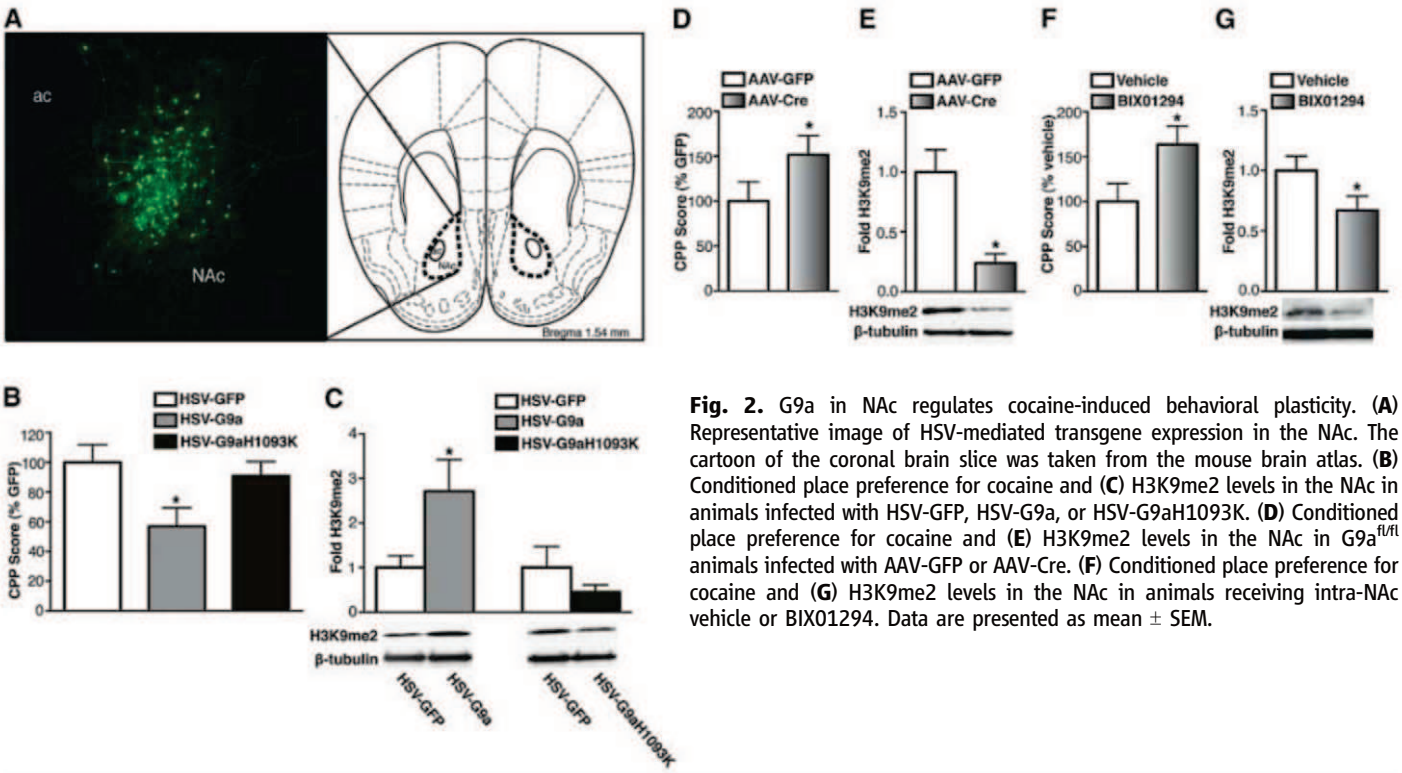


**Fig. 2.** G9a in NAc regulates cocaine-induced behavioral plasticity. (**A**) Representative image of HSV-mediated transgene expression in the NAc. The cartoon of the coronal brain slice was taken from the mouse brain atlas. (**B**) Conditioned place preference for cocaine and (**C**) H3K9me2 levels in the NAc in animals infected with HSV-GFP, HSV-G9a, or HSV-G9aH1093K. (**D**) Conditioned place preference for cocaine and (**E**) H3K9me2 levels in the NAc in G9a$^{fl/fl}$ animals infected with AAV-GFP or AAV-Cre. (**F**) Conditioned place preference for cocaine and (**G**) H3K9me2 levels in the NAc in animals receiving intra-NAc vehicle or BIX01294. Data are presented as mean ± SEM.

ylation remained unaltered by repeated cocaine exposure (fig. S1). Because of its high levels of catalytic activity both in vitro and in vivo (*10*), we set out to further investigate the functional significance of G9a repression after repeated cocaine exposure in the NAc. Levels of G9a protein, like levels of its mRNA, were significantly reduced 24 hours after repeated cocaine administration (fig. S2). Although G9a mRNA expression was reduced by 35% in the NAc, immunohistochemical analysis revealed a more modest 15% reduction in G9a protein levels, which is consistent with the observed 21% decrease in H3K9me2 after repeated cocaine administration (Fig. 1B). G9a mRNA expression was also down-regulated in this brain region by 20% after repeated self-administration of cocaine (fig. S3).

To identify whether changes in euchromatic H3K9me2 correlate with genome-wide alterations in gene expression in the NAc, we employed microarray analyses to examine gene expression profiles induced by a challenge dose of cocaine in mice with or without a history of prior cocaine exposure (see the gene lists in tables S1 to S3). Animals that had received repeated cocaine displayed dramatically increased gene expression 1 hour after a cocaine challenge, in comparison to acutely treated animals (Fig. 1C). This increased gene expression still occurred in response to a cocaine challenge given after 1 week of withdrawal from repeated cocaine. Consistent with previous reports, a small percentage of genes (~10%) displayed desensitized transcriptional responses after repeated cocaine administration (Fig. 1C and table S1) (*5*). To directly investigate the role of G9a down-regulation in the enhanced gene expression observed after repeated cocaine exposure, mice received intra-NAc injections of herpes simplex virus (HSV) vectors expressing either green fluorescent protein (GFP) or G9a and were treated with saline or repeated cocaine to determine whether G9a overexpression was sufficient to block the repeated cocaine–induced enhancement of gene expression. From a set of 12 randomly selected genes displaying heightened levels of expression after repeated cocaine, we observed that G9a significantly reduced the enhanced expression of 50% of these genes (table S4).

To identify upstream transcriptional events that mediate the repeated cocaine–induced repression of G9a expression, we investigated a possible role for ΔFosB, a highly stable splice product of the immediate early gene *fosB*. ΔFosB accumulates in the NAc after repeated exposure to cocaine, where it has been linked to increased cocaine reward (*11*). ΔFosB can act as either a transcriptional activator or repressor, depending on the target gene involved (*3*, *5*, *6*, *12*). Using bi-transgenic NSE-*tTA* x tetOP-Δ*FosB* mice, wherein ΔFosB expression can be induced selectively in the NAc and dorsal striatum of adult animals (*13*), we examined the impact of ΔFosB expression on cocaine regulation of H3K9me2 and KMTs in the NAc. ΔFosB overexpression was sufficient to reduce levels of both H3K9me2 (Fig. 1D) and G9a expression (Fig. 1E), thereby mimicking the effects of repeated cocaine. In contrast, ΔFosB did not reduce GLP expression in this brain region and had no effect on SUV39H1 and EZH2, the principal trimethylating enzymes for H3K9 and H3K27, respectively (fig. S4). To confirm these data using an independent ΔFosB overexpression system, wild-type adult mice received bilateral intra-NAc injections of adenoassociated virus (AAV) vectors expressing either GFP or ΔFosB. Viral-mediated overexpression of ΔFosB decreased levels of G9a expression in this brain region (Fig. 1E).

Such pronounced and specific regulation of G9a prompted us to investigate whether altering G9a expression specifically in NAc neurons regulates behavioral responses to cocaine. Wild-type mice received intra-NAc injections of HSV vectors expressing GFP or G9a and were then analyzed with an unbiased cocaine-conditioned place-preference paradigm, which provides an indirect measure of drug reward. Viral overexpression of G9a in NAc neurons was con-

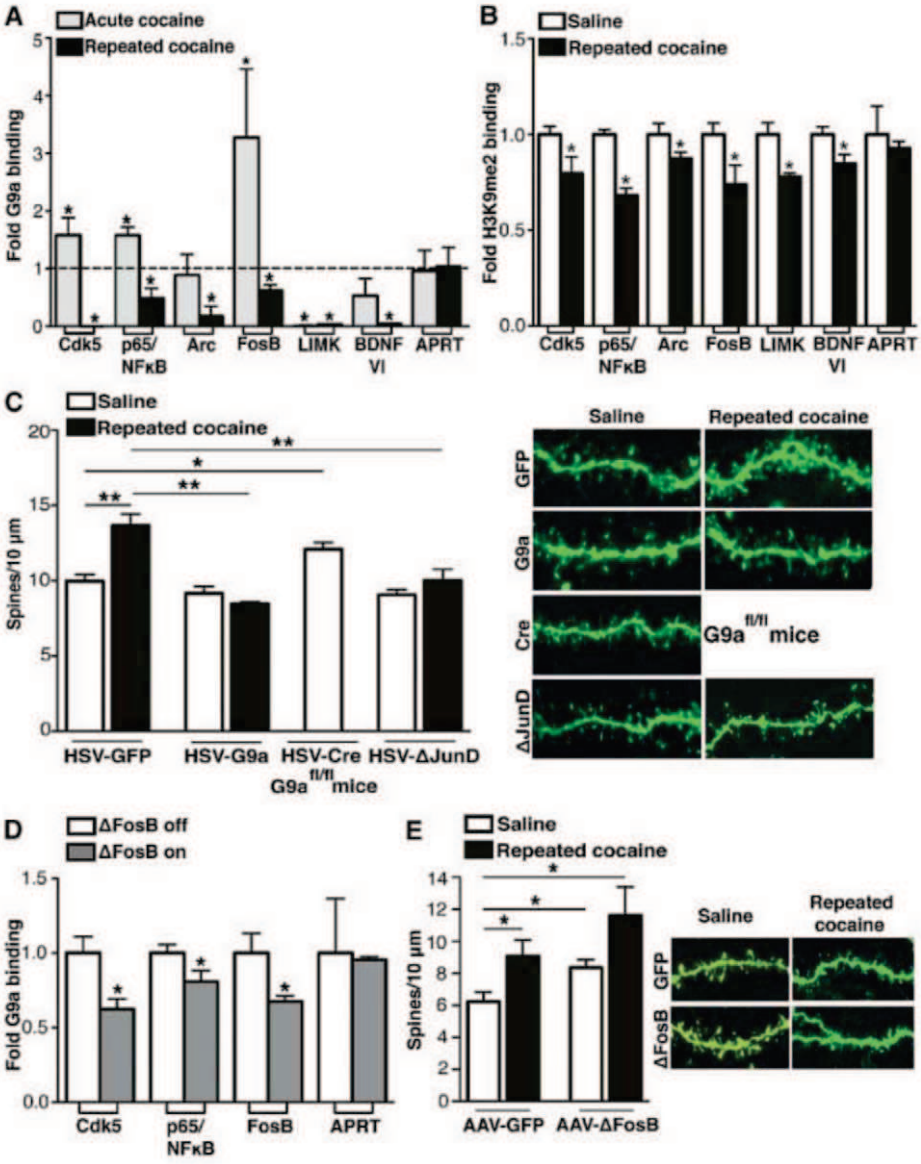


**Fig. 3.** G9a in the NAc regulates cocaine-induced dendritic spine plasticity. (**A**) Quantitative G9a ChIP in the NAc from animals treated acutely or repeatedly with cocaine, at 1 or 24 hours, respectively. Adenine phosphoribosyltransferase (APRT) was used as a negative control. Data are presented as the relative fold difference from saline controls. (**B**) Quantitative H3K9me2 ChIP in the NAc from repeated cocaine–treated animals at 24 hours, presented as the relative fold difference from saline controls. (**C**) Dendritic spine analysis of animals infected with HSV-GFP, HSV-G9a, or HSV-ΔJunD after repeated cocaine, and dendritic spines in G9a$^{fl/fl}$ mice after HSV-Cre infection. (**D**) Quantitative G9a ChIP in the NAc from NSE-*tTA* x tetOP-Δ*FosB* mice on (ΔFosB off) and off (ΔFosB on) doxycycline. (**E**) Dendritic spine analysis in animals infected with AAV-GFP or AAV-ΔFosB after repeated cocaine. Data are presented as mean ± SEM.

firmed after behavioral testing (Fig. 2A). G9a overexpression significantly decreased the preference for cocaine in comparison to that seen in animals overexpressing GFP (Fig. 2B) and increased H3K9me2 levels in the NAc (Fig. 2C). Overexpression of a catalytically dead mutant of G9a (G9aH1093K) (*14*) did not affect cocaine preference (Fig. 2B) and had no effect on H3K9me2 levels in this brain region (Fig. 2C).

To further study the role of G9a in the behavioral effects of cocaine, and more specifically to mimic the repeated cocaine–induced repression of G9a expression in the NAc, adult $G9a^{fl/fl}$ mice (*14*) received intra-NAc injections of AAV vectors expressing Cre recombinase or GFP as a control. AAV-Cre knockdown of G9a in the NAc, which was confirmed immunohistochemically (fig. S5), significantly increased the effects of cocaine in place-conditioning experiments and decreased H3K9me2 levels in the NAc (Fig. 2, D and E). A commercially available pharmacological inhibitor of G9a and GLP, BIX01294 (*15*, *16*), was used to ascertain whether enzyme inhibition similarly affects behavioral responses to cocaine. Indeed, pharmacological inhibition of G9a and GLP significantly increased the preference for cocaine and decreased H3K9me2 in the NAc (Fig. 2, F and G).

Repeated administration of cocaine increases the density of dendritic spines on NAc medium spiny neurons (*17*), a process associated with functional changes at excitatory glutamatergic synapses onto these neurons (*18*, *19*) and sensitized behavioral responses to the drug (*17*, *20*). We thus hypothesized that down-regulation of G9a activity in the NAc by repeated cocaine exposure might mediate cocaine's ability to regulate the dendritic spine density of NAc neurons. Using ChIP with an antibody to G9a, we identified several putative G9a gene targets in the NAc, each of which has previously been implicated in cocaine-induced dendritic plasticity (Fig. 3A) (*20*–*26*). We found that repeated cocaine administration significantly decreased G9a binding, as well as levels of H3K9me2, at these gene promoters (Fig. 3B). In contrast, acute cocaine administration rapidly recruited G9a to some of these same gene promoters, which is consistent with increased G9a expression observed in the NAc 1 hour after an acute dose of cocaine (fig. S6). Although G9a binding at specific gene promoters correlates with changes in its expression, it remains unclear whether such events are mediated by altered global levels of G9a in the NAc and/or by differences in G9a recruitment after acute versus repeated cocaine administration.

Based on G9a's regulation of numerous plasticity-related genes in the NAc, we directly examined whether maintenance of G9a expression in this brain region after repeated cocaine treatment was sufficient to block cocaine-induced dendritic spine formation. Using a cocaine treatment protocol previously demonstrated to promote dendritic spine induction in the NAc (*20*), we examined spine density in animals injected with either HSV-GFP or HSV-G9a. In agreement with previous findings, we observed a significant increase in dendritic spine density in the NAc after cocaine treatment, an effect that was blocked completely by G9a overexpression (Fig. 3C). G9a overexpression alone was not sufficient to decrease NAc dendritic spine density in the absence of cocaine. To complement these data, $G9a^{fl/fl}$ mice received intra-NAc injections of HSV-Cre, and spine density was quantified and compared to that in animals receiving HSV-GFP in the absence of cocaine. Knockdown of G9a expression significantly increased spine density on NAc medium spiny neurons (Fig. 3C).

Given the evidence that G9a down-regulation in the NAc after repeated cocaine treatment is mediated by ΔFosB, we next examined whether this transcription factor is likewise involved in the regulation of NAc dendritic spines. Although ΔFosB has not previously been linked causally to such dendritic plasticity, several of its targets, including Cdk5 and nuclear factor–κB subunits, have been so implicated (*20*–*23*); and ΔFosB's persistent expression in NAc neurons correlates with increased dendritic spine density after repeated cocaine treatment (*27*). First, we found that induction of ΔFosB in bi-transgenic mice in the absence of cocaine, which down-regulated G9a and H3K9me2 expression (Fig. 1D, E), decreased G9a binding to numerous plasticity-related genes, many of which have also been shown to be direct targets of ΔFosB itself (Fig. 3D) (*3*, *6*). We next showed that viral overexpression of ΔFosB in the NAc significantly increased dendritic spine density under basal conditions, similar to that observed after repeated cocaine administration (Fig. 3E). Conversely, overexpression in the NAc of ΔJunD, a dominant negative mutant protein that antagonizes ΔFosB transcriptional activity, blocked the ability of repeated cocaine to increase dendritic spine formation in the NAc (Fig. 3C).

Our observation that ΔFosB regulates G9a expression in the NAc and that ΔFosB and G9a regulate some of the same target genes led us to examine other interactions between ΔFosB and G9a. After acute cocaine administration, when G9a levels were increased, binding of G9a to the *fosB* gene was increased, whereas after repeated cocaine administration, when G9a expression was suppressed, G9a binding to the *fosB* gene was decreased (Fig. 3A). Such decreased G9a binding after repeated cocaine was not observed for c-*fos,* where G9a binding is increased by repeated cocaine (fig. S7). This is consistent with the fact that, unlike *fosB*, c-*fos* is repressed, not induced, by chronic psychostimulant exposure (*5*). ΔFosB overexpression in bi-transgenic mice was sufficient to significantly decrease G9a binding to the *fosb* gene (Fig. 3D). Furthermore, G9a overexpression was sufficient to reduce increased ΔFosB expression after repeated cocaine administration (table S4). These data suggest an autoregulatory loop whereby G9a initially limits the induction of ΔFosB under acute cocaine administration. However, as ΔFosB accumulates with repeated drug exposure, it represses G9a and thereby potentiates its own further induction.

We have demonstrated that histone lysine methylation in the NAc is critically involved in regulating neuronal gene expression in response to cocaine. Repression of G9a and H3K9me2 after repeated cocaine administration promotes cocaine preference, in part through the transcriptional activation of numerous genes known to regulate aberrant forms of dendritic plasticity. Gaining a better understanding of the genes being regulated through such mechanisms will improve our knowledge of the complex biological basis of drug addiction and could aid in the development of more effective treatments for addictive disorders.

### References and Notes


1. T. E. Robinson, B. Kolb, *Neuropharmacology* **47** (suppl. 1), 33 (2004).
2. S. E. Hyman, R. C. Malenka, E. J. Nestler, *Annu. Rev. Neurosci.* **29**, 565 (2006).
3. A. Kumar *et al.*, *Neuron* **48**, 303 (2005).
4. W. Renthal *et al.*, *Neuron* **56**, 517 (2007).
5. W. Renthal *et al.*, *J. Neurosci.* **28**, 7344 (2008).
6. W. Renthal *et al.*, *Neuron* **62**, 335 (2009).
7. A. Stipanovich *et al.*, *Nature* **453**, 879 (2008).
8. E. Borrelli, E. J. Nestler, C. D. Allis, P. Sassone-Corsi, *Neuron* **60**, 961 (2008).
9. K. Brami-Cherrier, E. Roze, J. A. Girault, S. Betuing, J. Caboche, *J. Neurochem.* **108**, 1323 (2009).
10. M. Tachibana, K. Sugimoto, T. Fukushima, Y. Shinkai, *J. Biol. Chem.* **276**, 25309 (2001).
11. E. J. Nestler, *Philos. Trans. R. Soc. London Ser. B* **363**, 3245 (2008).
12. C. A. McClung, E. J. Nestler, *Nat. Neurosci.* **6**, 1208 (2003).
13. M. B. Kelz *et al.*, *Nature* **401**, 272 (1999).
14. S. C. Sampath *et al.*, *Mol. Cell* **27**, 596 (2007).
15. S. Kubicek *et al.*, *Mol. Cell* **25**, 473 (2007).
16. Y. Chang *et al.*, *Nat. Struct. Mol. Biol.* **16**, 312 (2009).
17. T. E. Robinson, B. Kolb, *J. Neurosci.* **17**, 8491 (1997).
18. M. A. Ungless, J. L. Whistler, R. C. Malenka, A. Bonci, *Nature* **411**, 583 (2001).
19. M. J. Thomas, R. C. Malenka, *Philos. Trans. R. Soc. London Ser. B* **358**, 815 (2003).
20. S. J. Russo *et al.*, *J. Neurosci.* **29**, 3529 (2009).
21. J. A. Bibb *et al.*, *Nature* **410**, 376 (2001).
22. S. D. Norrholm *et al.*, *Neuroscience* **116**, 19 (2003).
23. S. Pulipparacharuvil *et al.*, *Neuron* **59**, 621 (2008).
24. H. Ujike, M. Takaki, M. Kodama, S. Kuroda, *Ann. N.Y. Acad. Sci.* **965**, 55 (2002).
25. S. Toda, H. W. Shen, J. Peters, S. Cagle, P. W. Kalivas, *J. Neurosci.* **26**, 1579 (2006).
26. D. L. Graham *et al.*, *Nat. Neurosci.* **10**, 1029 (2007).
27. K. W. Lee *et al.*, *Proc. Natl. Acad. Sci. U.S.A.* **103**, 3399 (2006).


28. This work was supported by grants from the National Institute on Drug Abuse: P01 DA08227 and R01 DA07359 (E.J.N.) and P0110044 (P.G.). E.J.N. certifies that none of the materials included in the manuscript have been previously published or are under consideration elsewhere, including on the Internet. All work involving the use of animals was conducted in accordance with institutional and Institutional Animal Care and Use Committee guidelines at both the University of Texas Southwestern Medical Center and Mount Sinai School of Medicine.


### Supporting Online Material

www.sciencemag.org/cgi/content/full/327/5962/213/DC1
Materials and Methods
Fig. S1 to S8
Tables S1 to S5
References


21 July 2009; accepted 27 October 2009
10.1126/science.1179438

# Overexpression of Alpha2A-Adrenergic Receptors Contributes to Type 2 Diabetes

Anders H. Rosengren,[1] Ramunas Jokubka,[1]* Damon Tojjar,[1]* Charlotte Granhall,[1] Ola Hansson,[1] Dai-Qing Li,[2] Vini Nagaraj,[1] Thomas M. Reinbothe,[1] Jonatan Tuncel,[3] Lena Eliasson,[1] Leif Groop,[1] Patrik Rorsman,[4] Albert Salehi,[1] Valeriya Lyssenko,[1] Holger Luthman,[1] Erik Renström[1]†

Several common genetic variations have been associated with type 2 diabetes, but the exact disease mechanisms are still poorly elucidated. Using congenic strains from the diabetic Goto-Kakizaki rat, we identified a 1.4-megabase genomic locus that was linked to impaired insulin granule docking at the plasma membrane and reduced β cell exocytosis. In this locus, *Adra2a*, encoding the alpha2A-adrenergic receptor [alpha(2A)AR], was significantly overexpressed. Alpha(2A)AR mediates adrenergic suppression of insulin secretion. Pharmacological receptor antagonism, silencing of receptor expression, or blockade of downstream effectors rescued insulin secretion in congenic islets. Furthermore, we identified a single-nucleotide polymorphism in the human *ADRA2A* gene for which risk allele carriers exhibited overexpression of alpha(2A)AR, reduced insulin secretion, and increased type 2 diabetes risk. Human pancreatic islets from risk allele carriers exhibited reduced granule docking and secreted less insulin in response to glucose; both effects were counteracted by pharmacological alpha(2A)AR antagonists.

Reduced secretory capacity of pancreatic β cells and insulin resistance constitute the central features of type 2 diabetes (T2D). Recently, a more comprehensive picture of the common genetic variations that predispose to T2D has emerged (*1*–*3*), but the cellular disease mechanisms remain largely undefined. One strategy to dissect complex polygenic disorders like T2D is to use inbred animal models. The Goto-Kakizaki (GK) rat displays many of the hallmarks of T2D and is well characterized genetically (*4*). The major diabetes susceptibility locus in the GK rat is the 52-Mb locus *Niddm1* on rat chromosome 1 (*5*). A 16-Mb portion of *Niddm1*, *Niddm1i*, confers defective insulin secretion without insulin resistance (*6*) and is homologous to a region on human chromosome 10 that is associated with T2D (*7*) and includes *TCF7L2*, the strongest candidate gene for T2D to date (*8*).

In congenic strains harboring different parts of GK-derived *Niddm1i* on the genetic background of normoglycemic F344 rats, two distinct regions within *Niddm1i* have been identified that confer impaired glucose metabolism and aberrant β cell exocytosis, respectively (*9*). The latter "dysexocytotic" 4.5-Mb locus with 26 known genes is fully contained in the congenic strain N1I12, which was further dissected here by generation of the congenic strains N1I5 and N1I11 that have reduced extent of GK genotype in the locus (Fig. 1A) (*10*).

Glucose-stimulated insulin secretion (GSIS), measured in batch-incubated islets, was normal in N1I11 islets. By contrast, N1I5 islets had a 35% reduction in GSIS compared with N1I11 ($P < 0.001$) and control islets ($P < 0.001$) (Fig. 1B). Pancreatic β cells release insulin through $Ca^{2+}$-induced exocytosis, which can be monitored as increases in cell capacitance. The exocytotic response to a depolarization train stimulus amounted to 134 ± 18 fF in N1I11 β cells, similar to control cells (120 ± 11 fF) (Fig. 1C). However, N1I5 β cells displayed a ~50% reduction of exocytosis (69 ± 9 fF; $P < 0.01$ versus N1I11), equal to N1I12 β cells, demonstrating that the full dysexocytotic phenotype of N1I12 rats is retained in the N1I5 strain. Also, when exocytosis was evoked by intracellular dialysis of a $Ca^{2+}$ buffer (free $[Ca^{2+}]_i \sim 1.5$ μM), it was significantly reduced in N1I5 (Fig. 1D and fig. S1), suggesting a late-stage defect, distal to elevation of cytosolic $[Ca^{2+}]_i$. This was corroborated by ratiometric fura-2 measurements of intracellular $[Ca^{2+}]_i$ that produced similar results in both strains when the islets were stimulated with either 5 or 20 mM glucose or high $K^+$ (60 mM) (Fig. 1E and fig. S2).

Insulin-containing secretory granules exist in different functional pools and are recruited from a large reserve to dock the plasma membrane, where they become release-competent (*11*, *12*). Interestingly, insulin granule distribution differed between N1I5 and N1I11 β cells. In N1I11 cells, 3.3 ± 0.3% of the insulin granules were docked, compared with only 1.8 ± 0.2% in N1I5 cells (Fig. 1F and fig. S3). These observations suggest major differences in the secretory machineries of the two strains. These are not secondary to hyperglycemia, as the animals investigated had no overt diabetes. Instead, the impaired β cell exocytosis in N1I5 seems to be caused by the additional 1.4-Mb GK-derived genetic segment (see Fig. 1A).

The segment contains five known protein-coding genes: *Pdcd4*, *Lysmd3*, *Shoc2*, *Adra2a*, and *ENSRNOG00000036577* (fig. S4). Expression analysis revealed a 59% up-regulation of *Adra2a* mRNA in pancreatic islets from N1I5 compared with N1I11 ($P < 0.01$) but no differences for the other genes (Fig. 1G). This was paralleled by a 90% increase in alpha2A-adrenergic receptor [alpha(2A)AR] protein in both islets ($P < 0.001$) (Fig. 1H and fig. S5A) and brain ($P < 0.01$) (fig. S5B) in N1I5 relative to N1I11 (see also fig. S6).

The alpha(2A)AR is known to mediate adrenaline-mediated suppression of insulin secretion. Accordingly, *Adra2a* knockout mice present with enhanced insulin secretion (*13*), and animals with β cell–specific overexpression of *Adra2a* are glucose-intolerant (*14*), but the receptor has not previously been implicated in the pathogenesis of type 2 diabetes. We hypothesized that naturally occurring genetic variations in the GK genome could cause glucose intolerance by alpha(2A)AR overexpression in N1I5 and investigated this possibility by in vivo intraperitoneal glucose tolerance tests (IPGTT) (Fig. 1I). Already in the fasting state, N1I5 rats had reduced plasma insulin compared with N1I11 ($P < 0.05$). Five minutes after a challenge, N1I5 rats displayed significantly elevated glucose levels compared with N1I11 ($P < 0.05$), which were paralleled by a pronounced reduction in insulin ($P < 0.05$ at 15 min). There was no difference in insulin sensitivity between the strains ($k = 0.9 \pm 0.1$ and $1.0 \pm 0.2$ $min^{-1}$ for N1I11 and N1I5, respectively). Treatment with the alpha(2A)AR agonist clonidine reduced insulin levels and impaired glucose tolerance in both strains. Interestingly, treatment with the antagonist yohimbine largely obliterated the differences between the strains and significantly lowered plasma glucose concentrations in N1I5 ($P < 0.001$ at 5 min) while increasing plasma insulin levels by as much as 156% ($P < 0.01$ at 15 min).

These findings echoed those observed in vitro. Insulin release was reduced in N1I5 islets at 8.3, 16.7, and 20 mM glucose (Fig. 2A). In the presence of yohimbine, GSIS was similar in N1I5 and N1I11 at all glucose concentrations. At 20 mM glucose, yohimbine increased GSIS by 30% in N1I11 islets, whereas secretion was enhanced by as much as 90% in N1I5 ($P < 0.001$). The strong inhibitory effect of clonidine on GSIS was also demonstrated in both strains (see also fig. S7). Next, silencing of *Adra2a* by RNA interference (Fig. 2B and fig. S8) (*10*) prevented clonidine-mediated suppression of GSIS (Fig. 2C). Interestingly, GSIS was enhanced by more than 55% in N1I5 islets after *Adra2a* silencing, to levels similar to those observed in N1I11 islets under the same condition. The reversal of the secretory defect was evident also at the single β cell level ($P < 0.05$) (Fig. 2D).

[1]Lund University Diabetes Centre, Malmö, SE-20502 Malmö, Sweden. [2]Key Laboratory of Hormones and Development, Ministry of Health, China, Tianjin Metabolic Diseases Hospital, Tianjin Medical University, China. [3]Section for Medical Inflammation Research, Department of Medical Biochemistry and Biophysics, Karolinska Institutet, SE-17177 Stockholm, Sweden. [4]Oxford Centre for Diabetes Endocrinology and Metabolism, University of Oxford, Churchill Hospital, Oxford, UK.

*These authors contributed equally to this work.
†To whom correspondence should be addressed. E-mail: erik.renstrom@med.lu.se

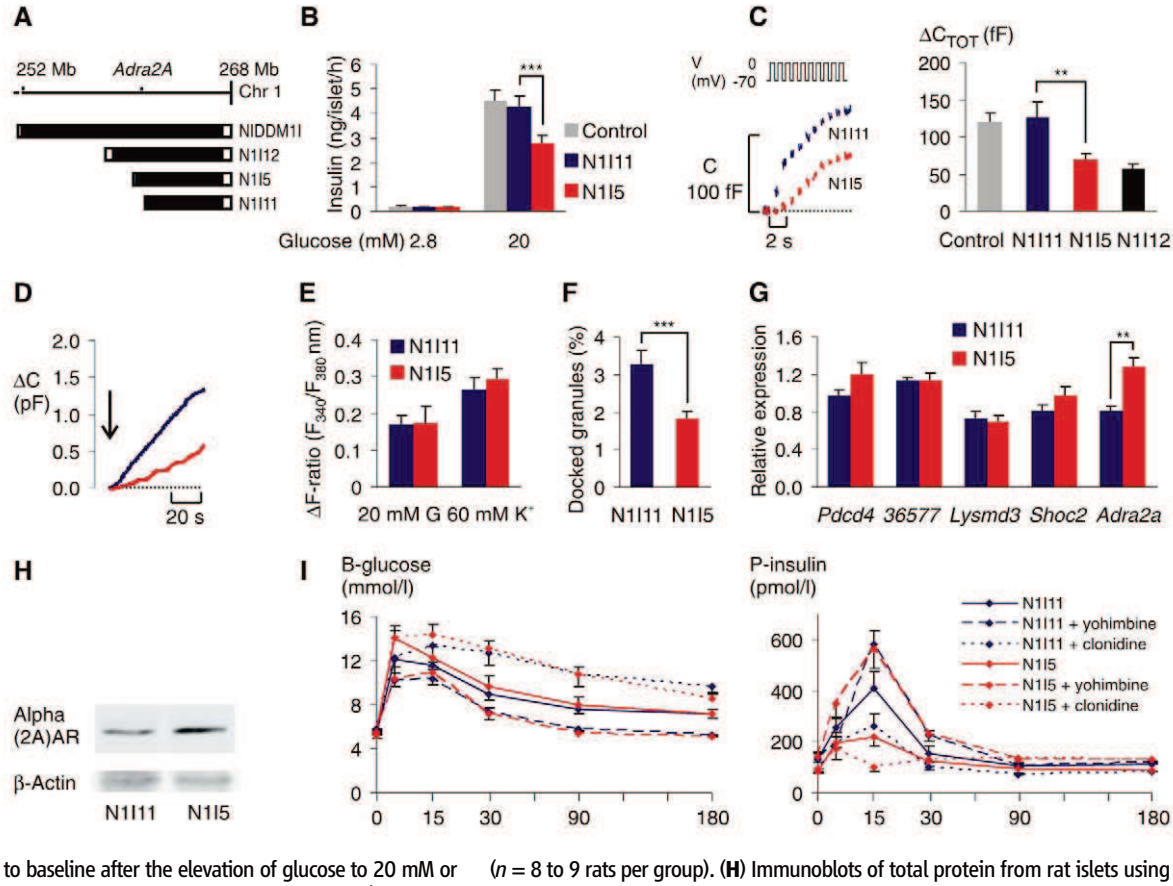


**Fig. 1.** Characterization of congenic rat strains. (**A**) Solid bars show known GK-derived genetic segments; open ends designate intervals containing the recombinant end points. (**B**) Insulin secretion from control, N1I11, and N1I5 islets ($n$ = 5 to 9 batches per strain). (**C**) Increases in cell capacitance (ΔC) in N1I11 and N1I5 β cells after 10 depolarizations. The histogram shows total exocytosis evoked by the train stimulus ($\Delta C_{TOT}$) ($n$ = 12, 8, 11, and 21 cells from control, N1I11, N1I5, and N1I12, respectively. (**D**) ΔC evoked by intracellular infusion of a $Ca^{2+}$-containing solution in N1I11 (blue) and N1I5 (red) β cells). The arrow indicates the establishment of the standard whole-cell configuration. (**E**) Maximal change in fluorescence ($F$) ratio ($\Delta F$ ratio) relative to baseline after the elevation of glucose to 20 mM or KCl to 60 mM ($n$ = 9 to 11 islets for glucose, and $n$ = 5 islets for $K^+$). (**F**) The percentage of rat β cell granules docked at the plasma membrane ($n$ = 25 cells per strain). (**G**) Islet mRNA expression of indicated genes normalized to *Hprt* ($n$ = 8 to 9 rats per group). (**H**) Immunoblots of total protein from rat islets using polyclonal alpha(2A)AR antisera. (**I**) Glucose and insulin levels during IPGTT with or without yohimbine or clonidine as indicated ($n$ = 7 to 20 rats per group). Time scale expanded at 0 to 30 min. *$P$ < 0.05; **$P$ < 0.01; ***$P$ < 0.001.

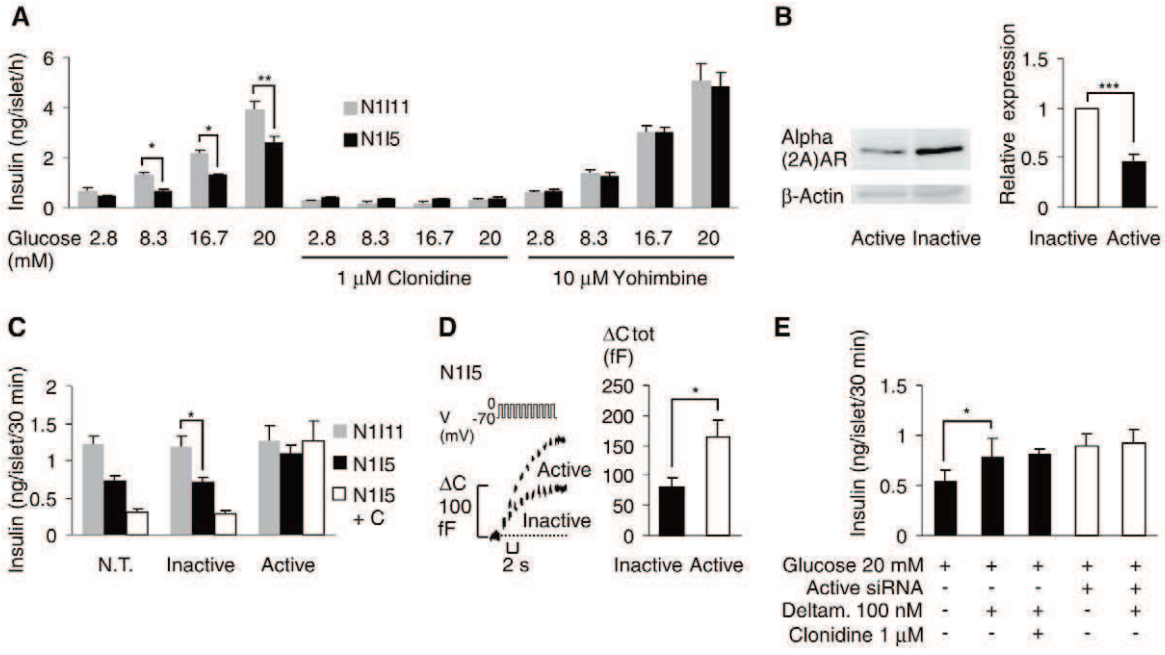


**Fig. 2.** Analysis of alpha(2A)AR signaling in rat pancreatic islets. (**A**) Insulin secretion from N1I11 and N1I5 islets at different glucose concentrations with or without clonidine or yohimbine as indicated ($n$ = 3 to 8 batches per group). (**B**) Immunoblots of total protein from N1I5 islets transfected with small interfering RNA (siRNA) active against *Adra2a* or inactive siRNA. The histogram shows average alpha(2A) AR signal normalized for β-actin. Data from four blots. (**C**) Insulin secretion at 20 mM glucose from islets that are nontransfected (N.T.) or transfected with inactive or active siRNA [$n$ = 6 to 13 batches per transfection condition for N1I11, N1I5, or N1I5 with 1 μM clonidine (C)]. (**D**) Depolarization-evoked capacitance increase in N1I5 β cells transfected with inactive or active siRNA. Average total exocytosis ($\Delta C_{TOT}$) from 7 to 9 cells per group. (**E**) Insulin release from N1I5 islets at 20 mM glucose with active siRNA, deltamethrin, or clonidine as indicated ($n$ = 4 to 6 batches per group). *$P$ < 0.05; **$P$ < 0.01; ***$P$ < 0.001.

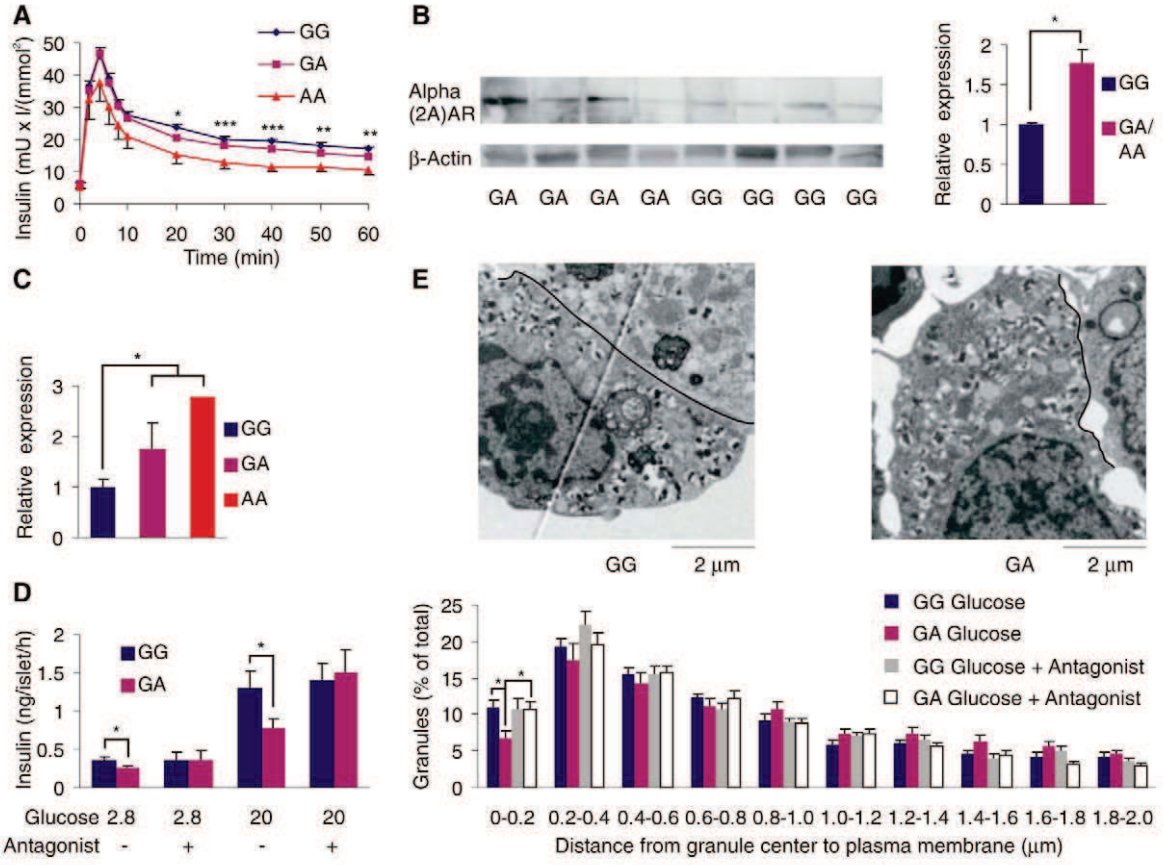


**Fig. 3.** Association of *ADRA2A* rs553668 with insulin secretion in humans. (**A**) Effects of rs553668 genotype on insulin secretion during IVGTT in 799 individuals. Data are means ± SEM. *P* values were obtained using an additive model. (**B**) Immunoblots of total protein from human islets from eight individuals using polyclonal alpha(2A)AR antisera. The histogram shows average alpha(2A)AR signal normalized for β-actin from four blots from a total of 11 GG, 7 GA, and 1 AA carriers. (**C**) Islet *ADRA2A* mRNA expression in 24 GG, 7 GA, and 1 AA carriers. $P < 0.05$ for GG versus GA/AA, or $P < 0.05$ for linear regression of expression versus number of risk alleles. (**D**) Islet insulin secretion at 2.8 or 20 mM glucose with or without alpha(2A)AR antagonist. (**E**) Electron micrographs of human islet sections from GG and GA carriers at 20 mM glucose without alpha(2A)AR antagonist showing β cells with insulin granules, recognized by the central dense core and surrounding halo. The border to adjacent cells is indicated. The histogram shows the distribution of insulin granules located in 0.2-μm concentric shells in the first 2 μm below the plasma membrane after incubation at 20 mM glucose with or without alpha(2A)AR antagonist. Total granule numbers per section did not differ between GG (104 ± 9) and GA (93 ± 15) [*n* for (D) and (E) is specified in (*10*)]. **P* < 0.05; ***P* < 0.01; ****P* < 0.001.

The alpha(2A)AR couples to inhibitory heterotrimeric GTP–binding proteins ($G_i$ proteins). Inactivation of $G_i$ by pertussis toxin reversed the exocytotic defect in both islets and single β cells from N1I5 (fig. S9). Pertussis toxin was effective even in the absence of adrenaline, suggestive of tonic activity in the alpha(2A)AR/$G_i$ signaling system. This is in line with previous findings in Noc2 knockout mice (*15*). $G_i$ proteins inhibit exocytosis distal to the elevation of $[Ca^{2+}]_i$ (*16*) by decreasing cyclic adenosine monophosphate (cAMP) production, but activation of the protein phosphatase 2B/calcineurin has also been proposed to contribute to the effect (*17*, *18*). Interestingly, in all capacitance recordings, cytosolic cAMP was clamped at 0.1 mM, and impaired cAMP production accordingly cannot be the sole explanation for reduced exocytosis in N1I5. In fact, cAMP levels did not differ between the strains at 2.8 or 20 mM glucose (fig. S10). However, 5 min after addition of clonidine, cAMP was significantly lower in N1I5 islets compared with N1I1, as expected if alpha(2A)AR is overexpressed. In the absence of receptor stimulation, additional mechanisms for suppression of insulin secretion must be in operation. The previously suggested role of calcineurin was corroborated by incubation with the calcineurin inhibitor deltamethrin that increased GSIS in N1I5 islets by almost the same magnitude (45%; $P < 0.05$) as silencing of the receptor (Fig. 2E), while the inhibitor was ineffective in *Adra2a*-silenced islets. A near-identical enhancement of GSIS was obtained using FK506, another blocker of calcineurin, while the inactive deltamethrin analog perimethrin did not improve GSIS (fig. S11). Interestingly, calcineurin, in concert with protein kinases A and C, has been suggested to affect functional granule distribution and exocytosis (*19*, *20*). Taken together, our data demonstrate that genetically encoded overexpression of *Adra2a* impairs β cell exocytosis at a late stage and that inappropriately activated calcineurin plays a prominent role by interfering with granule recruitment.

The *Niddm1i* locus is species-conserved, and we therefore genotyped 19 single-nucleotide polymorphisms (SNPs) covering 1 Mb up- or downstream of the human *ADRA2A* gene in 935 individuals well characterized for insulin secretion (fig. S12 and table S1) (*10*). Notably, the minor allele (A) of rs553668, located in the 3′ UTR region of *ADRA2A*, was associated with impaired insulin secretion (additive model). The impact was prominent, with a significant effect both on acute insulin response and late-phase insulin secretion at 20 to 60 min during the intravenous glucose tolerance test (IVGTT) (Fig. 3A and Table 1). Some of the other SNPs were also associated with impaired insulin secretion (table S2). Based on this, five SNPs, rs553668, rs7911129, rs1971596, rs602618, and rs2203616, were replicated in a larger cohort with 4935 individuals, which verified the importance of genetic variation in rs553668 for insulin secretion capacity. The SNP was associated with reduced fasting insulin as well as decreased insulin secretion at 30 and 120 min in response to oral glucose (Table 1). Moreover, in a case-control material with 3740 nondiabetics and 2830 diabetics, rs553668 was associated with increased risk of T2D [recessive effect; odds ratio (OR) 1.42, confidence interval (CI) 1.01 to 1.99, $P = 0.04$]. When focusing on individuals with low body mass index (BMI) (<24) or low C-peptide levels (<0.6), the increased T2D risk was evident also among heterozygous subjects [OR 1.31 (CI 1.03 to 1.68), $P = 0.02$, and OR 1.28 (CI 1.02 to 1.61), $P = 0.03$, respectively, using an additive model]. The results for rs553668 were significant also when correcting for the genotype for *TCF7L2* rs7903146, located 1.9 Mb downstream of *ADRA2A*. *ADRA2A* rs553668 has previously been associated with increased stress sensitivity

**Table 1.** Effects of *ADRA2A* rs553668 on metabolic parameters in the human study populations. Serum insulin (S-insulin) levels are expressed as the corrected insulin response (mU × l/mmol$^2$), and plasma glucose (P-glucose) is in mmol/l. Parameters analyzed by linear regression. Data are means ± SD. HOMA-IR, homeostasis model assessment of insulin resistance; ISI, insulin sensitivity index.

| Study | Phenotype | Genotypes | | | *P* |
|---|---|---|---|---|---|
| | | GG | GA | AA | |
| Botnia IVGTT ($n$ = 799 individuals) | Age (years) | 45 ± 13 | 45 ± 13 | 43 ± 11 | |
| | BMI (kg/m$^2$) | 25.5 ± 4.0 | 25.4 ± 4.0 | 24.0 ± 2.3 | |
| | Fasting P-glucose | 5.92 ± 1.80 | 5.91 ± 1.82 | 6.06 ± 1.97 | 0.8 |
| | Fasting S-insulin | 6.31 ± 3.96 | 6.08 ± 3.01 | 5.18 ± 2.48 | 0.3 |
| | S-insulin 30 min | 20.1 ± 12.5 | 17.9 ± 9.6 | 12.9 ± 5.4 | 0.0009 |
| | S-insulin 60 min | 17.0 ± 13.4 | 14.7 ± 9.7 | 10.3 ± 6.3 | 0.001 |
| | Acute insulin response | 36.3 ± 21.2 | 34.2 ± 18.8 | 27.0 ± 14.4 | 0.04 |
| | $k$ (min$^{-1}$) | 1.39 ± 0.46 | 1.36 ± 0.51 | 1.41 ± 0.67 | 0.8 |
| Botnia PPP ($n$ = 4681 individuals) | Age (years) | 48 ± 15 | 48 ± 15 | 48 ± 15 | |
| | BMI (kg/m$^2$) | 26.4 ± 4.3 | 26.0 ± 4.1 | 26.0 ± 4.2 | |
| | Fasting P-glucose | 5.26 ± 0.56 | 5.26 ± 0.55 | 5.22 ± 0.57 | 0.7 |
| | Fasting S-insulin | 6.84 ± 6.13 | 6.20 ± 4.00 | 6.03 ± 3.95 | 0.0004 |
| | S-insulin 30 min | 60.2 ± 39.6 | 58.6 ± 38.0 | 54.1 ± 27.6 | 0.03 |
| | Systolic BP (mm Hg) | 131 ± 19 | 131 ± 18 | 131 ± 20 | 0.9 |
| | Diastolic BP (mm Hg) | 79.9 ± 10.3 | 79.5 ± 10.8 | 78.7 ± 10.6 | 0.04 |
| | HOMA-IR | 0.127 ± 0.103 | 0.119 ± 0.0.076 | 0.115 ± 0.071 | 0.3 |
| | ISI | 168 ± 106 | 171 ± 108 | 168 ± 85 | 0.3 |

and blood pressure in humans (*21*–*23*). In our cohort, it associated with lower blood pressure, which is in agreement with current views on the physiology of alpha(2A)AR (*24*) (Table 1).

*ADRA2A* overexpression in islets from carriers of the risk A allele for rs553668 was verified on both the transcript and the protein level (Fig. 3, B and C). Pancreatic islets from risk allele carriers exhibited a 30% decrease in insulin secretion at basal glucose (2.8 mM; $P < 0.05$) and a 40% reduction when stimulated by 20 mM glucose ($P < 0.05$) (Fig. 3D). Intriguingly, risk carriers also exhibited a reduced number of docked insulin granules (Fig. 3E). These defects were corrected by alpha(2A)AR antagonism, which normalized insulin granule distribution and insulin secretion to levels identical to those in non–risk carriers. These results unanimously suggest that impaired insulin secretion in rs553668 risk allele carriers is the consequence of hyperactive alpha(2A)AR signaling.

In conclusion, the present data establish the exact mechanism of reduced insulin secretion and increased T2D risk associated with *ADRA2A* rs553668. Alpha(2A)AR has also been implicated in the control of blood pressure and adipocyte function (*24*, *25*). It is tempting to speculate that *ADRA2A* could be a common culprit for several components of the metabolic syndrome and T2D. The present findings open up a route for specific diagnosis and therapy tailored to the individual patient.

### References and Notes


1. R. Sladek *et al.*, *Nature* **445**, 881 (2007).
2. R. Saxena *et al.*, *Science* **316**, 1331 (2007).
3. E. Zeggini *et al.*, *Nat. Genet.* **40**, 638 (2008).
4. Y. Goto, M. Kakizaki, N. Masaki, *Tohoku J. Exp. Med.* **119**, 85 (1976).
5. J. Galli *et al.*, *Diabetes* **48**, 2463 (1999).
6. J. M. Lin *et al.*, *Diabetes* **50**, 2737 (2001).
7. R. Duggirala *et al.*, *Am. J. Hum. Genet.* **64**, 1127 (1999).
8. S. F. Grant *et al.*, *Nat. Genet.* **38**, 320 (2006).
9. C. Granhall, A. H. Rosengren, E. Renstrom, H. Luthman, *Diabetes* **55**, 3494 (2006).
10. Materials and methods are available as supporting material on *Science* Online.
11. S. Daniel, M. Noda, S. G. Straub, G. W. Sharp, *Diabetes* **48**, 1686 (1999).
12. L. Eliasson *et al.*, *J. Physiol.* **586**, 3313 (2008).
13. V. Fagerholm *et al.*, *Eur. J. Pharmacol.* **505**, 243 (2004).
14. J. C. Devedjian *et al.*, *Diabetologia* **43**, 899 (2000).
15. M. Matsumoto *et al.*, *Proc. Natl. Acad. Sci. U.S.A.* **101**, 8313 (2004).
16. P. Rorsman *et al.*, *Nature* **349**, 77 (1991).
17. M. Hoy *et al.*, *Eur. J. Pharmacol.* **466**, 213 (2003).
18. E. Renstrom, W. G. Ding, K. Bokvist, P. Rorsman, *Neuron* **17**, 513 (1996).
19. E. Renstrom, L. Eliasson, P. Rorsman, *J. Physiol.* **502**, 105 (1997).
20. G. Nagy *et al.*, *Neuron* **41**, 417 (2004).
21. J. C. Finley Jr. *et al.*, *J. Appl. Physiol.* **96**, 2231 (2004).
22. L. P. Svetkey *et al.*, *Hypertension* **27**, 1210 (1996).
23. K. M. Small, K. M. Brown, C. A. Seman, C. T. Theiss, S. B. Liggett, *Proc. Natl. Acad. Sci. U.S.A.* **103**, 5472 (2006).
24. M. Philipp, M. Brede, L. Hein, *Am. J. Physiol. Regul. Integr. Comp. Physiol.* **283**, R287 (2002).
25. J. Galitzky, D. Larrouy, M. Berlan, M. Lafontan, *J. Pharmacol. Exp. Ther.* **252**, 312 (1990).


26. We thank I. Lundquist and T. Andersson for help with the in vivo and fura-2 data, and B.-M. Nilsson and M. Neptin for technical assistance. Supported by project grants from the Swedish Research Council, the European Foundation for the Study of Diabetes, the Novo Nordisk and Albert Påhlsson foundations (E.R), Kungliga Fysiografiska Sällskapet (A.R.), The Nordic Centre of Excellence in Disease Genetics (NCoEDG) (R.J.), a Linnaeus grant to the Lund University Diabetes Centre, and the Knut and Alice Wallenberg Foundation. Access to human pancreatic islets was granted by J. Taneera in collaboration with the Nordic Network for Clinical Islet Transplantation (NNCIT), O. Korsgren, Uppsala University.


### Supporting Online Material

www.sciencemag.org/cgi/content/full/1176827/DC1
Materials and Methods
Figs. S1 to S12
Tables S1 to S3
References


26 May 2009; accepted 29 October 2009
Published online 19 November 2009;
10.1126/science.1176827
Include this information when citing this paper.

## Peptide Synthesizer

The Sonata XT peptide synthesizer is designed for 0.5 mmol to 200 mmol synthesis scales (up to 400 g of resin). It features a single glass reaction vessel in multiple sizes (200 mL, 500 mL, 1.2 L, 2 L, 3.2 L, and 4.2 L), 20 amino acid bottles (500 mL or 1 L), and seven solvent bottle positions. Flexible software makes it easy to scale up any protocol. The Sonata XT can be used for batch or continuous flow syntheses and features timed or volumetric deliveries and multiple mixing modes (nitrogen bubbling, vortex, and recirculation), which can be performed separately or in combination. It also features two separate waste streams to minimize disposal costs and automated cleavage. It is good-manufacturing-practices compliant.

Protein Technologies For info: 520-629-9626 | www.peptideinstruments.com

## Cross-linking Immunoprecipitation Kit

The Pierce Crosslink Immunoprecipitation (IP) Kit extends the functionality of protein A/G-based IP reactions by adding cross-linking chemistry to the procedure. The kit features an improved protocol and buffers that result in a high yield of functional antigens using small amounts of antibody (2–10 µg). The irreversible attachment of the antibody and mild elution procedures not only minimize antibody contamination in the eluted sample but also allow the resin to be reused multiple times. The kit offers convenient sample handling using spin columns that eliminate resin loss and enable more efficient separation. The procedure can be easily scaled up and works with a wide variety of antibody subclasses and species.

Thermo Fisher Scientific

For info: 815-968-0747 | www.thermo.com/pierce

## CE Genetic Analyzers

Two lines of capillary electrophoresis (CE) genetic analyzers have been introduced. The 3500 Dx Series is intended for clinical use and will initially be launched in specific countries within the European Union. The analyzer is intended for use by trained operators in the analysis of human DNA or RNA for the detection of genetic changes that may lead to disease presence or susceptibility. It is the first CE system to comply with the European Union In Vitro Diagnostic Medical Devices Directive 98/79/EC. The 3500 Series Genetic Analyzers, for research use only, enable researchers to run up to 1,100 sequencing or 1,200 genotyping samples per day. It features novel consumable designs, incorporating the ability to track key information with radio frequency identification tags, new optical and thermal system designs, and redesigned data collection and analysis software, which enables easy generation of cost-effective analyses and high-quality data.

Applied Biosystems

For info: 650-638-5354 | www.appliedbiosystems.com

## Endothelial Colony Forming Cells

The Poietics ECFCs-Human Endothelial Colony Forming Cells are clonally expanded cells, isolated from human umbilical cord blood. They can be used to study many aspects of endothelial cell physiology and function, angiogenesis, and cardiovascular disease. Poietics ECFCs undergo rigorous qualification and authentication analyses during manufacturing to ensure consistency and uniformity of performance in culture.

Lonza Group

For info: +41-61-316-8798 | www.lonza.com

## Immersion Cooler

The FTS Flexi-Cool Immersion Cooler eliminates the inconvenience of handling dry ice or liquid nitrogen. The FTS Flexi-Cool features remote, refrigerated probes to provide reliable, rapid cooling to –100°C. The system's durable, heavy-duty refrigeration system is designed to provide years of trouble-free operation. Optional digital control with an RS-232 interface enables precise temperature control throughout the process as well as providing controlling capability and data collection from a remote location. It features a choice of three standard probes. Typical applications for the system include those involving reaction vessels, vapor trapping, laboratory dewars, differential scanning calorimeters, charge-coupled device cameras, and vapor sorption analyzers.

SP Industries

For info: 845-687-5315 | www.spindustries.com

Electronically submit your new product description or product literature information! Go to **www.sciencemag.org/products/newproducts.dtl** for more information.

Newly offered instrumentation, apparatus, and laboratory materials of interest to researchers in all disciplines in academic, industrial, and governmental organizations are featured in this space. Emphasis is given to purpose, chief characteristics, and availabilty of products and materials. Endorsement by *Science* or AAAS of any products or materials mentioned is not implied. Additional information may be obtained from the manufacturer or supplier.

## POSITIONS OPEN

McGill

**TENURE-TRACK POSITION**
**in Animal Behaviour, McGill University**

The Department of Biology at McGill University invites applications for a tenure-track position in animal behaviour. The new faculty member will complement a Department that has research strengths in ecology, conservation, evolution, behaviour, neuroethology, and molecular biology.

The successful applicant will be expected to conduct a vigorous program of independent, externally funded research and to contribute to teaching at both undergraduate and graduate levels.

Candidates must hold a Ph.D. or equivalent degree and postdoctoral experience demonstrating excellence in their respective fields. We anticipate that this position will be filled at the **ASSISTANT PROFESSOR** (tenure track) level, but applications from more established candidates may be considered for recruitment at the **ASSOCIATE** or **FULL PROFESSOR** rank. Competitive startup and equipment funding packages will be available.

Persons wishing to be considered for this position should forward electronically curriculum vitae, a statement of research interests, a statement of teaching interests, and PDF files of major publications to **e-mail: zabrina.kadkhodayan@mcgill.ca**. In the subject line, please enter Animal Behaviour Search and your name. Acceptable file formats are Microsoft Word and PDF. Also arrange to have three letters of reference submitted directly by e-mail to the same address.

The application deadline is 15 February 2010 or until position is filled.

*McGill University is committed to equity in employment and diversity. It welcomes applications from indigenous peoples, visible minorities, ethnic minorities, persons with disabilities, women, persons of minority sexual orientations and gender identities, and others who may contribute to further diversification. All qualified applicants are encouraged to apply; however, in accordance with Canadian immigration requirements, priority will be given to Canadian citizens and permanent residents of Canada.*

---

CAL POLY

**ANIMAL PHYSIOLOGIST, tenure-track position.** The Biological Sciences Department at California Polytechnic State University, San Luis Obispo is seeking a full-time, academic year Animal Physiologist beginning September 2010. For details, qualifications, and application instructions (online faculty application required), visit **website: http://www.calpolyjobs.org** and refer to **requisition #101984.** Review begin date: February 8, 2010. *Equal Employment Opportunity.*

---

The Department of Neuroscience at the University of Pennsylvania School of Medicine seeks candidates for an **ASSISTANT PROFESSOR** position in the tenure track. The successful applicant will have experience in the field of neuroscience with a focus on molecular or cellular approaches to study the development or function of neural systems. Applicants must have a Ph.D. degree and have demonstrated excellent qualifications in research and education. Teaching and an independently funded research program are expected.

Apply for this position online at **website: http://www.med.upenn.edu/apps/faculty_ad/index.php/g309/d2180**.

*The University of Pennsylvania is an Equal Opportunity, Affirmative Action Employer. Women and minority candidates are strongly encouraged to apply.*

## POSITIONS OPEN

UAB
THE UNIVERSITY OF ALABAMA AT BIRMINGHAM

**FACULTY POSITIONS, RESEARCH.** The Institute of Oral Health Research (IOHR) at the University of Alabama at Birmingham School of Dentistry seeks candidates for faculty positions in research. Candidates should possess a D.D.S./D.M.D./M.D. and/or a Ph.D. degree with preferably a documented history of funding and research productivity in the fields of craniofacial/developmental biology or tissue bioengineering/stem cells. Successful candidates will be expected to establish a major research program within the School of Dentistry and develop collaborative research partnerships within the broader UAB research community (**website: http://www.uab.edu**). Research facilities and startup packages for this appointment will be appropriate for the successful candidate. Partial support for this faculty position is provided by the National Institute of Dental and Craniofacial Research (NIDCR) under a P30 grant mechanism with funds from the American Recovery and Reinvestment Act of 2009. Candidates with research experience that complements the Center for Discoveries, Genomics and Therapeutics for Craniofacial Dental Diseases will be given preference.

UAB is a research intensive institution receiving over $430 million in funding in FY 2007. It has a long history of interdisciplinary research collaborations and includes a recently established Department of Genetics and a Center for BioMatrix Engineering and Regenerative Medicine. The University of Alabama at Birmingham is a comprehensive research university and medical center with over 2,000 full-time faculty and 17,000 students. UAB is ranked among the top tier research universities in federal grant support and the School of Dentistry is ranked eighth in NIDCR funds for 2008.

Salary, tenure status, and rank will be commensurate with experience. Applications will be accepted immediately, and will be considered until all positions are filled. Qualified applicants should send a letter indicating their interest, detailed curriculum vitae, description of research plans, and the names and contact information of a minimum of three references. Electronic submissions are encouraged and should be sent to **Dr. Mary MacDougall, e-mail: macdougall@uab.edu**, or mailed to: **Institute of Oral Health Research, University of Alabama at Birmingham, Suite SDB 702, 1530 3rd Avenue South, Birmingham, AL 35294-0007.**

*The Institute of Oral Health Research, The UAB School of Dentistry, and the University of Alabama at Birmingham are committed to building a culturally diverse work force and strongly encourage applications from women and individuals from underrepresented groups. UAB has an active NSF-supported ADVANCE program and a Dual Career Assistance Program to support and offer resources to help spouses and partners of newly recruited UAB faculty. UAB is an Affirmative Action/Equal Employment Opportunity Employer.*

---

**ASSISTANT/ASSOCIATE PROFESSOR/**
**FULL PROFESSOR**
**Neuroscience Faculty Position**
**University of New England**

For application and more information, please see our **website: http://www.une.edu/hr/jobs/index.cfm**.

Interested candidates should submit a resume and cover letter to **e-mail: imeng@une.edu**.

Please direct inquiries to **Dr. Ian Meng, Associate Professor, Department of Biomedical Sciences** (**e-mail: imeng@une.edu**). Review of applications will begin January 20, 2010.

**University of New England**
**Human Resource Department**
**11 Hills Beach Road**
**Biddeford, ME 04005**
**Fax: 207-602-5902**

*UNE is an Equal Opportunity/Affirmative Action Employer and strongly encourages candidates of diverse backgrounds.*

## Director of Chemistry, Therapeutics for Rare and Neglected Diseases (TRND) Program

**National Human Genome Research Institute**

The National Institutes of Health (NIH) is seeking a senior scientist to serve as the Director of Chemistry for the Therapeutics for Rare and Neglected Diseases (TRND) Program, a new effort administered by the National Human Genome Research Institute (NHGRI) and the NIH Office of Rare Diseases Research (ORDR). The goal of this Program is to discover and develop small molecules that are suitable for testing in humans and promising for treating individuals with rare and neglected diseases.

As an integral part of the TRND executive team, the Director of Chemistry will provide input on the overall strategy for TRND and lead the research operations of all functions of the Chemistry Section. The successful candidate will be a recognized leader with a proven track record in human drug development, with at least 15 years of relevant synthetic and analytical chemistry experience in the pharmaceutical industry. The candidate must have a Ph.D. in synthetic or medicinal chemistry, an excellent publication record and patent portfolio, should show fluency in structural and computational chemistry, and be cognizant of relevant state-of-the-art techniques and the utilization of specialized technical equipment. The candidate will have demonstrated ability to supervise a large group of chemists effectively and a history of providing outstanding mentorship. The candidate is also expected to be well versed in biology, pharmacology, drug metabolism and pharmacokinetics, as well as have a demonstrated history of effective and successful collaborations.

The TRND Program includes ongoing support for the Director of Chemistry and the scientific team that the Director is expected to build. Interested applicants should send their curriculum vitae, a three-page statement of interest in (and vision for) the Chemistry Section of TRND, and three letters of recommendation through our online application system, at http://research.nhgri.nih.gov/apply.

**Applications will be reviewed starting January 31, 2010 and will be accepted until the position is filled.**

Specific questions regarding the recruitment may be directed to Dr. Carole Bewley, Search Chair, at CaroleB@intra.niddk.nih.gov. Questions may also be directed to Dr. Melissa Ashlock at ashlockma@mail.nih.gov.

DHHS and NIH are Equal Opportunity Employers and encourage applications from women and minorities.

NATIONAL HUMAN GENOME RESEARCH INSTITUTE Division of Intramural Research
U.S. DEPARTMENT OF HEALTH AND HUMAN SERVICES | NATIONAL INSTITUTES OF HEALTH | genome.gov/DIR

## Scientific Director

**National Human Genome Research Institute**

The National Human Genome Research Institute (NHGRI), a major research component of the National Institutes of Health (NIH) and the Department of Health and Human Services (DHHS), seeks to identify an outstanding Scientific Director to lead its Division of Intramural Research (DIR; see genome.gov/DIR), located in Bethesda, Maryland. The NHGRI Scientific Director leads a basic and clinical research program that has consistently been at the forefront of scientific innovation, developing a variety of research approaches that have accelerated the understanding of the molecular basis of human disease. The Scientific Director is responsible for an annual budget exceeding $100 million and a staff of ~550. In addition to providing scientific and administrative leadership of this premier research enterprise, the Scientific Director is expected to be an internationally recognized and highly accomplished researcher in genetics and/or genomics.

This position offers a unique and exciting opportunity to develop and implement an overall vision for the NHGRI/DIR that is consistent with the mission and strategic objectives of the Institute. The Scientific Director is responsible for the recruitment and professional development of the NHGRI research faculty. S/he plays a key role in creating and maintaining a nurturing research environment that encourages creativity, collaboration among scientists from different disciplines, effective training of students and postdoctoral fellows, and efficient utilization of common resources. The ability to develop productive interactions among NHGRI investigators, other NIH Institutes, and the research community at large is critical, as is the ability to serve as a spokesperson for NHGRI/DIR research.

Applicants must have an M.D. and/or Ph.D or equivalent degree in the biomedical sciences, as well as a broad knowledge of the field of human genetics and genomics and a compelling vision for the future of the field, including clinical applications. S/he must have proven experience in directing and managing a scientific research program, with well-honed administrative and interpersonal skills to meet the demands of both research and program direction.

Salary is competitive and will be commensurate with the candidate's experience. A full Federal benefit package is available, including retirement, health and life insurance, long-term care insurance, annual and sick leave, and the Thrift Savings Plan (401K equivalent). Appropriate support for an ongoing independent research program will be provided.

Interested applicants should submit a cover letter that includes a brief description of research and administrative experience, a current curriculum vitae and bibliography, names and contact information of five references, and a brief written vision for leading the NHGRI/DIR. Questions about the position and applications themselves should be sent to Ms. Ellen Rolfes via email at ellenr@exchange.nih.gov. All information provided by the candidates will remain confidential and will not be released outside the NHGRI search process without a signed release from the candidate.

**Applications will be reviewed starting March 1st, 2010, and will be accepted until the position is filled.**

DHHS and NIH are Equal Opportunity Employers and encourage applications from women and minorities.

NATIONAL HUMAN GENOME RESEARCH INSTITUTE Division of Intramural Research
U.S. DEPARTMENT OF HEALTH AND HUMAN SERVICES | NATIONAL INSTITUTES OF HEALTH | genome.gov/DIR

**UNIVERSITY OF VIRGINIA HEALTH SYSTEM**
**Center for Membrane Biology in the Department of Molecular Physiology and Biological Physics,** is seeking to fill two **tenure-track faculty positions**. Rank will depend on qualifications. Candidates must have a PhD or MD degree, at least two years of postdoctoral experience, and are expected to be competitive at a national level by recognition through peer-reviewed publications and demonstrated ability to secure competitive national grant support. The Center housed in newly constructed space is based in the Department of Molecular Physiology and Biological Physics in the School of Medicine and also draws faculty from several other Departments.

UVa has a history of outstanding research in the structure and function of membranes, and current strengths include (1) the structural biology of membrane channels, transporters and receptors, (2) signal transduction in membranes, (3) viral and intracellular membrane fusion, (4) trafficking of membrane proteins, (5) cell adhesion, and (6) lipid-protein interactions. We especially encourage applicants with expertise that complements and broadens these areas, including translational research more closely related to disease. The positions offer access to state-of-the-art facilities for membrane protein production, structure determination by crystallography, NMR spectroscopy, and electron microscopy, as well as other biophysical techniques. In addition to membrane biology, the Department of Molecular Physiology and Biological Physics also has strengths in cardiovascular physiology, cancer biology, and structural biology in general.

To apply, visit **https://jobs.virginia.edu** and search on **Posting Number 0604829**, complete a Candidate Profile online and attach Curriculum Vitae with publication list, cover letter, a statement of significant research accomplishments and future research plans, and a list of three references with name, email address and phone number. Review of applications will begin **January 25, 2010** and the positions will remain open to applications until filled.

For additional information about the positions, please contact the chair of the search committee, **Dr. Lukas K. Tamm, Director of the Center for Membrane Biology, Department of Molecular Physiology and Biological Physics, University of Virginia Health System, P.O. Box 800886, Charlottesville, VA 22908-0886**. For further information about the application process, please contact **Howard Phipps** at **memsearch@virginia.edu**. We also recommend you send a pdf copy of your application to this email address.

*The University of Virginia is an Equal Opportunity/Affirmative Action Employer.*

UMASS AMHERST

## Associate or Full Professor

The Department of Biochemistry and Molecular Biology of the University of Massachusetts Amherst invites applications from Ph.D.-level scientists for a **tenure-track position at the level of ASSOCIATE or FULL PROFESSOR**. This is one of several positions to be filled on campus as part of an initiative in ***cellular engineering***. We particularly encourage individuals who incorporate systems and computational approaches in their research programs to apply. Moreover, we seek candidates working in areas that complement existing Departmental and campus strengths in cellular biochemistry and biophysics, which include signal transduction, protein trafficking/folding, organelle biogenesis, protein degradation and apoptosis, structure/function of proteins and protein/nucleic acid complexes, gene expression and regulation, and cytoskeletal organization. The successful candidate will have access to students from several interdepartmental graduate programs and will participate actively in the Institute for Cellular Engineering, the home of an NSF IGERT grant for graduate training. The candidate will be expected to teach both at the undergraduate and graduate levels.

The Five College Consortium, comprised of Smith College, Amherst College, Mount Holyoke College, Hampshire College, and the University of Massachusetts Amherst provides a rich academic and intellectual environment. The Department is strongly committed to increasing the diversity of the faculty, student body, and curriculum.

**Applicants should send curriculum vitae, a description of research interests, and names of three people who can provide letters of recommendation to: Prof. Lila Gierasch at cesearch@biochem.umass.edu or Cellular Engineering Search, Biochemistry & Molecular Biology, LGRT 913, 710 N. Pleasant St., University of Massachusetts, Amherst, MA 01003. Appointment is subject to the availability of funds. Review of applications will begin January 15, 2010 and continue until the position is filled.**

*The University of Massachusetts is an Affirmative Action/Equal Opportunity Employer. Women and members of minority groups are encouraged to apply.*

# Max Planck Institute for Plant Breeding Research

Max-Planck-Institut für Züchtungsforschung

**International Max Planck Research School:**

*"The molecular basis of plant development and environmental interactions"*

## 12 Ph. D. Studentships

The Max Planck Institute for Plant Breeding Research and University of Cologne invite applications for Ph.D. fellowships in the International Max Planck Research School (IMPRS) in Cologne, Germany.

The IMPRS is intended for highly motivated students with a strong training in molecular sciences. The constellation of participating institutions provides excellent conditions in the area of plant sciences with expertise in plant genetics, plant biochemistry, structural biology, bioinformatics, cell biology, and molecular microbiology.

The training includes regular seminars, yearly retreats, supervision of a thesis committee of the research school, and soft skill and practical courses on modern laboratory techniques.

The program is taught in English and open to students from all countries holding a Master's degree or a corresponding Diploma degree.

For detailed information about the application process and the Ph.D. program please visit the IMPRS homepage at www.mpiz-koeln.mpg.de/english/studentInformation/index.html.

Deadline for applications is March 31, 2010.

The Max Planck Society is an equal opportunity employer. We strongly encourage female scientists to apply for the program. After registration, the fellowship application should be mailed to:

Max Planck Institute for Plant Breeding Research
IMPRS – Molecular Plant Development
Scientific Coordinator
Carl-von-Linné-Weg 10, 50829 Cologne / Germany

MAX PLANCK GESELLSCHAFT

UMASS AMHERST

## Assistant Professor

The Department of Biochemistry & Molecular Biology invites applications from Ph.D.-level scientists for a **tenure-track position at the level of ASSISTANT PROFESSOR**. We seek candidates working in areas of plant biochemistry and molecular biology that complement existing Departmental and campus strengths in cellular biochemistry, including signal transduction, membrane biology, metabolism, gene expression and regulation, and cytoskeletal organization. The position is one of several on campus to expand an existing cluster focused on **biofuels and renewable energy research.** We are particularly interested in candidates that complement ongoing programs within The Institute of Massachusetts Biofuels Research (TIMBR), an interdisciplinary group of biologists, chemists and engineers focused on renewable energy. The successful candidate will have access to students from several interdepartmental graduate programs and will participate in teaching at both undergraduate and graduate levels.

The Five College Consortium, comprised of Smith College, Amherst College, Mount Holyoke College, Hampshire College, and the University of Massachusetts Amherst, provides a rich academic and intellectual environment. The Department is strongly committed to increasing the diversity of the faculty, student body, and curriculum.

**Applicants should send curriculum vitae, a description of research interests, and three letters of recommendation to: Prof. Jennifer Normanly at pbsearch@biochem.umass.edu or Biofuels/Renewable Energy Search, Biochemistry & Molecular Biology, LGRT 913, 710 N. Pleasant St., University of Massachusetts, Amherst, MA 01003. Review of applications will begin January 15, 2010 and continue until the position is filled.**

*The University of Massachusetts is an Affirmative Action/Equal Opportunity Employer. Women and members of minority groups are encouraged to apply.*

### Center for Advanced Drug Research (CADRE)
### at SRI Shenandoah Valley (SRI SV)
### Biosciences Division
### SRI International

Located in brand new, state-of-the-art laboratories in Virginia's beautiful Shenandoah Valley, CADRE is one of world's few groups focused on the proteomics of host-vector-pathogen interactions to discover new ways to prevent, detect, and treat infectious diseases. The group combines SRI's well-established expertise in drug discovery, preclinical development, and computational biology with proteomics to develop new diagnostics, therapeutics, and vaccines for infectious and neglected diseases and for biodefense.

Research at CADRE is focused on three distinct program areas:

- Proteomic studies of host-vector-pathogen interactions, including insect-borne viruses, respiratory and diarrheal pathogens, and parasitic protozoa.
- Identification of 'critical links' underlying the mechanisms of antibiotic resistance, intracellular toxin transport, and vector competence to enable discovery of novel biomarkers, well-characterized targets, and therapies.
- Mining SRI's and others' databases for biological pathways that play a critical role in disease development.

CADRE moved into its new building in September 2009, and now seeks group leaders, research scientists, post-doctoral fellows, and research assistants for several open positions at both Ph.D. and non-Ph.D. levels. For senior positions, applicants should have a successful track record of generating their own funding through vehicles such as government grants and contracts. Current extramural funding is preferred.

SRI International is an independent, nonprofit research institute headquartered in Menlo Park, California. Founded at Stanford Research Institute, SRI has met the strategic needs of clients and partners for more than 60 years.

For more information please visit **www.sri.com/jobs** and/or email **sv-jobs @sri.com**.

*SRI is an Equal Opportunity Employer.*

### POSTDOCTORAL POSITIONS
### Xenopus Development,
### Stem Cell Research,
### Transgenic Mouse Generation, Genetics
### The Hormel Institute,
### University of Minnesota,
### Austin, MN 55912

Postdoctoral positions are available immediately at The Hormel Institute, a research branch of the University of Minnesota, located in Austin, MN. Successful candidates have the opportunity to work in a variety of research positions in the Cellular and Molecular Biology Group (**Dr. Zigang Dong** and **Dr. Ann M. Bode**) at The Hormel Institute.

Postdoctoral positions are available to study the role of histone, MAPKs and other kinase affecting Xenopus development process. Applicants should have experience with injection into frog embryos and some manipulation of embryonic tissue. Postdoctoral positions are also available for transgenic mouse generation and applicants should have experience in mouse genetics, mouse/human embryonic stem cell culture, and especially, experience in terminal differentiation of ES/iPS cells is preferred.

Postdoctoral position is available requiring experience in genetics, linkage analysis, SNP chips, and human and mouse genome databases, and additional training in molecular biology, mouse models, and gene characterization. Postdoctoral position is also available requiring training in molecular biology, cloning, mouse model development, advanced microscopy methods such as FISH, immunohistochemistry, and histology.

A Ph.D. in genetics, molecular biology, cellular development, biochemistry, pharmacy, biology or related fields is required.

All candidates must apply on-line at the University of Minnesota employment page, **https://employment.umn.edu/applicants/Central?quickFind=76394** In addition, please e-mail your curriculum vitae to: **ambode@hi.umn.edu**.

*The University of Minnesota shall provide equal access to and opportunity in its programs, facilities, and employment without regard to race, color, creed, religion, national origin, gender, age, marital status, disability, public assistance status, veteran status, sexual orientation, gender identity, or gender expression.*

UNLV
UNIVERSITY OF NEVADA LAS VEGAS

## Dean, College of Sciences

The University of Nevada, Las Vegas (UNLV) seeks an innovative and energetic individual for the position of Dean of the College of Sciences. The successful candidate will have the experience and demonstrated skills to enhance the College's national and international reputation as an emerging research entity while maintaining its historic commitment to teaching excellence. For more information visit: **http://sciences.unlv.edu/**

The Dean reports to the Executive Vice President and Provost. Candidates must possess a terminal degree from an accredited college or university in a discipline appropriate to the College, along with a strong record of research productivity and teaching experience meriting a tenured appointment at the rank of Professor in one of the College's academic units. Experience in administration at or above the level of department chair or its equivalent is required.

The Search Committee will accept applications and nominations until the position is filled. Screening of candidates will begin immediately. To guarantee full consideration, applications should be completed by February 8, 2010. Application materials must include a cover letter, curriculum vitae, and names, addresses, and telephone numbers of five professional references which may include supervisory, subordinate, peer or student contacts. The initial review will evaluate applicants based on documented, relevant qualifications and professional work experience. Thus, the cover letter should describe the applicant's qualifications and past accomplishments, with specific reference to program development, resource acquisition, fostering a collaborative environment, and promoting transparency in decision-making. Materials should be addressed to Dr. Karen P. West, Dean of the School of Dental Medicine, Search Committee Chair, and must be submitted online at **https://hrsearch.unlv.edu/**. For assistance with UNLV's on-line applicant portal, please contact Jen Martens at (702) 895-2894 or **hrsearch@unlv.edu**

***UNLV is an Affirmative Action/Equal Opportunity educator and employer committed to excellence through diversity.***

Berkeley
University of California

Energy Biosciences Institute

### Faculty position in microbial, biochemical & metabolic engineering, systems & synthetic biology

The University of California at Berkeley seeks applicants at both the senior and junior levels for a tenured/tenure-track faculty position in the general area of microbial bioengineering. Of particular interest are individuals whose research includes metabolic engineering and/or systems and synthetic biology; however, creative and energetic individuals who show extraordinary promise or accomplishment in related areas will also be considered.

Applicants must have a Ph.D. and evidence of outstanding scholarship within a relevant discipline. We encourage applications from candidates with the communication skills and cross-cultural abilities to maximize effective collaboration with a diverse community of campus and external colleagues.

This position is sponsored by the Energy Biosciences Institute, (http://www.energybiosciencesinstitute.org) which will provide significant resources and collaborative opportunities for individuals to develop a leading-edge program in biofuels research. Both start-up and multi-year research funds will be available from the EBI for the bioenergy components of the individuals' research programs. Candidates hired into these positions would also be free to seek support for research in other areas.

Applications should include a resume, statements of research and teaching interests, selected publications, and the names of three references and be submitted online at http://bioeng.berkeley.edu/career/ebifaculty.php. Online applications are strongly preferred; we will also accept application materials sent by mail to: Department of Bioengineering, 306 Stanley Hall #1762, UC Berkeley, Berkeley, CA 94720.

Applications received through June 1, 2010 will be considered; however the review of applications will commence on February 15, 2010. Candidates will be reviewed on an ongoing basis, and early application is recommended.

*The University of California is an Equal Opportunity, Affirmative Action Employer.*

## Lawrence Berkeley National Laboratory

## Deputy Laboratory Director

**Req Number: 23844**
**Division: Laboratory Directorate**

**In the world of science, Lawrence Berkeley National Laboratory (Berkeley Lab) is synonymous with excellence. Eleven scientists associated with Berkeley Lab have won the Nobel Prize and 55 Nobel Laureates either trained here or had significant collaborations with our Laboratory. Berkeley Lab is an incubator for ideas, innovations and products that help society and explain how the Universe works:**

- **Renewable energy sources such as biofuels and artificial photosynthesis**
- **Energy efficiency at home, at work, and around the world**
- **The ability to observe, probe and assemble materials atom by atom**
- **Climate change research, environmental science and the growing connections between them**
- **The chemistry and physics of matter and force in the Universe from the infinite to the infinitesimal; and more**

Lawrence Berkeley National Lab is looking for a proven Leader to be its next Deputy Lab Director.

Reporting to the Laboratory Director, the Deputy Laboratory Director is the Chief Research Officer responsible for the overall integration of scientific goals and objectives consistent with the Director's vision and the Laboratory's mission. The Deputy Laboratory Director serves as management liaison with the University, the Department of Energy, and other public and private agencies to represent the Laboratory's programs, accomplishments and initiatives. Within the Laboratory and under the direction of the Director, the Deputy Director is responsible for management oversight of divisional interdisciplinary programs and interacts with policy and advisory committees to ensure the highest quality scientific achievement.

**How To Apply**
For complete position description
and to apply directly online, visit
**http://jobs.lbl.gov/details.asp?jid=23844&p=1**
and follow the online instructions
to complete the application process.

*As part of the online application process, please submit a single attachment that includes both your resume or CV and a statement of your research interests. Please be sure to reference where you found out about the position.*

BERKELEY LAB

Berkeley Lab is an affirmative action/equal opportunity employer committed to the development of a diverse workforce.

CBSF

# Center for Biomolecular Structure and Function

## Research Laboratory Manager and Research Assistant Positions

In its continuing commitment to excellence in basic scientific research in structural and chemical biology and molecular biophysics, The University of Texas M. D. Anderson Cancer Center announces the opening of the **Center for Biomolecular Structure and Function (CBSF)**.

The recent faculty recruitments of Maria A. Schumacher, Ph.D., Richard G. Brennan, Ph.D., and John E. Ladbury, Ph.D. – three leading figures in the above fields – provide a new core of expertise and represent a major investment and advancement in the capabilities of M. D. Anderson Cancer Center in this important area of basic science. A key goal of the CBSF is to enhance collaborations between basic scientists and clinical and translational researchers thereby facilitating access to structural, chemical and biophysical approaches towards meeting the research goals of the M. D. Anderson Cancer Center.

The CBSF now seeks to recruit a highly energetic **Research Laboratory Manager** to oversee its scientific endeavors and to supervise its collaborative programs. The successful candidate will have an advanced degree in molecular biology, biochemistry or related field and have proven abilities in prokaryotic and eukaryotic recombinant protein production and purification. Ideally, the candidate will possess experience in some or all of the following instrumental methods: UV, CD and fluorescence spectroscopies; isothermal titration calorimetry; surface plasmon resonance; and dynamic and static light scattering. Excellent communication and computer skills are necessary as the manager will be the interface between structural and chemical biologists and clinical and translational researchers, thereby facilitating the bench-to-bedside efforts of M. D. Anderson. Moreover, the manager will present his or her work and the activities of the CBSF to the diverse research community of M. D. Anderson and the Texas Medical Center to raise awareness of the expanding capabilities and accomplishments of this new center.

In addition to the above post, a **Senior Research Assistant** position and a **Research Assistant II** position are available. BS/BA level applicants with proven experience in recombinant protein expression and purification protocols will be considered. Ideally the candidates will have experience at bacterial, insect and mammalian cell expression methods.

For more information regarding these positions, please visit **www.mdanderson.jobs** (keyword: Science Journal)

**Application deadline: 12 February 2010**

THE UNIVERSITY OF TEXAS
MD ANDERSON CANCER CENTER
*Making Cancer History®*

M. D. Anderson Cancer Center is an equal opportunity employer and does not discriminate on the basis of race, color, national origin, gender, sexual orientation, age, religion, disability or veteran status except where such distinction is required by law. All positions at The University of Texas M. D. Anderson Cancer Center are security sensitive and subject to examination of criminal history record information. The University of Texas M. D. Anderson Cancer Center is a smoke-free and drug-free environment.

## SCHOOL OF MEDICINE
INDIANA UNIVERSITY

**James Whitcomb Riley Hospital for Children**
**Herman B Wells Center for Pediatric Research**

### Hematologic Malignancy and Stem Cell Biology Program Assistant/Associate Professor

The Department of Pediatrics and the Herman B Wells Center for Pediatric Research is recruiting for two faculty positions at the Assistant/Associate Professor level. The research focus for these positions will be on normal hematopoietic and leukemic stem cell biology with emphasis in basic and translational research. Candidates will have a PhD, MD or MD/PhD and must have a strong research background and either current, or potential for, independent funding. Laboratory space will be in the Herman B Wells Center for Pediatric Research (**http://www.wellscenter.iupui.edu/**). New faculty will be provided with generous start-up packages and laboratory space. MD faculty will have protected time for research activities. New faculty will join an active and growing multi-disciplinary hematopoiesis research community with a strong collaborative atmosphere.

The search committee will begin evaluating applications as they are received and applications will continue to be reviewed until the positions are filled. Interested candidates are encouraged to submit curriculum vitae, summary of past accomplishments and future plans, and names and email addresses of three references to:

**Reuben Kapur, PhD**
**Director, Program in Hematologic Malignancies and Stem Cell Biology**
**Wells Center for Pediatric Research**
**Department of Pediatrics**
**Indiana University School of Medicine**
**1044 W. Walnut Street, Room 425**
**Indianapolis, IN 46202**
**rkapur@iupui.edu**

*Indiana University is an EO/AA Educator, Employer and Contractor (M/F/D).*

## FACULTY POSITION
### *Microbial Pathogenesis*

Applications are invited for tenure/tenure-track faculty positions in microbial pathogenesis, with rank commensurate with qualifications. Applicants with an interest in emerging infectious disease pathogens, biodefense and expertise in host-pathogen interactions are particularly encouraged to apply. The successful candidate will have demonstrated research productivity and will be expected to maintain an independent, innovative, funded research program and to participate in graduate and postgraduate training. A competitive start-up package and outstanding core facilities are available, including animal imaging, informatics, and extensive BSL-3 and ABSL-3 containment facilities.

Applicants should submit a curriculum vitae, a statement of research experience, a summary of future plans, and names of three references by March 1, 2010, to: **Dr. David Perlin, e-mail: perlinds@umdnj.edu**. AA/EEO Employer M/F/D/V.

UMDNJ
NEW JERSEY MEDICAL SCHOOL
University of Medicine & Dentistry of New Jersey

## EVMS
Eastern Virginia Medical School

### Scientific Director—Glennan Center for Geriatrics and Palliative Care

EVMS seeks applications for the position of Scientific Director of the Glennan Center for Geriatrics and Palliative Care with a faculty appointment in the Department of Internal Medicine at the level of associate professor or professor. Candidates should have an MD or PhD degree, must have demonstrated excellence in research and possess exceptional leadership qualities. The Director will have the opportunity to lead a prominent center, emphasizing excellence in research and teaching related to aspects of aging and palliative care. EVMS is undergoing a significant expansion in the areas of basic and translational research. There are significant resources available, including excellent laboratory space, an endowed professorship, and other support for the program.

The Glennan Center for Geriatrics and Palliative Care has gained national and international recognition for excellence in immunology, driving and cognition in the context of aging research. The program is ranked in the top 50 in the latest US News and World Report ranking. The Center is also a leader in clinical care, providing innovative services to meet the special health care needs of older adults across a full range of practice settings from independent living to assisted living, long-term care, palliative care, and hospital care. The Center offers a comprehensive program for clinicians and scientists that provide training in geriatrics, palliative care and gerontology for medical students, residents, fellows, other health care professionals and junior faculty members. Excellent collaboration is available with the basic science departments and affiliated Universities in the region.

Eastern Virginia Medical School is located in coastal southeastern Virginia in the nation's 27th largest metropolitan statistical area. The region offers premier waterfront communities, large beaches, excellent golf, tennis, sailing and other recreational opportunities, and top ranked schools.

Please send a letter of interest including current curriculum vitae to the Executive Search Committee by e-mail at **execcomm@evms.edu**.

*AA-EOE.*

COLUMBIA UNIVERSITY MEDICAL CENTER

### Weil-Granat Professorship in Neurodegenerative Disease
### Taub Institute for Research on Alzheimer's Disease and the Aging Brain

We seek an established, clinical-qualified Physician-Scientist to be the inaugural occupant of this chair. Applicant must have a strong record of funded, clinically relevant research in the area of Parkinson's dementia, frontotemporal dementia, or related conditions. He/she should be board-certified in one of Neurology, Neuropathology, Psychiatry, or Internal Medicine. The appointment will be joint with the Department of Neurology and other departments, if appropriate. Applicant should qualify for appointment at the level of associate or full professor with tenure and must be eligible to obtain a license to practice in New York State.

Modern laboratory space, a superb collaborative environment, and substantial start-up funds are available. The Taub Institute has close collaborations with the Parkinson's Disease and the Motor Neuron Disease Centers as well as the basic neurosciences at Columbia.

Applicants should send curriculum vitae and names of three referees to: **Department of Pathology and Cell Biology, Columbia University, 630 West 168th Street, New York, NY 10032.**

To apply online, go to:
**https://academicjobs.columbia.edu/applicants/Central?quickFind=52523**

*Columbia University is an equal opportunity/affirmative action employer.*

UNC CHARLOTTE

## ENDOWED PROFESSORSHIP
## DEPARTMENT OF
## BIOINFORMATICS AND GENOMICS

We invite applications for the Carol Grotnes Belk Distinguished Professorship in the Department of Bioinformatics and Genomics. This research department, housed in the newly dedicated, $35M Bioinformatics Building, has a collaborative and interdisciplinary research focus targeting areas within structural biology, molecular biophysics, plant genomics, metagenomics, and human health. The department seeks candidates who have established outstanding research programs directed toward critical issues in 21st century biology using computational techniques, alone or in combination with experimental approaches. The successful candidate should have a demonstrated interest in fostering collaboration, and a commitment to teaching and mentorship.

Applications must be made electronically at **jobs.uncc.edu** (position #1070) and must include a CV, a list of four references, and statements on research, teaching, and leadership. Applicants are also encouraged to contact the **Search Committee Chair, Dr. Cynthia Gibas (cgibas@uncc.edu)**. All enquiries and applications will be treated as confidential. For additional information, please visit our website at **www.bioinformatics.uncc.edu**.

*UNC Charlotte is an EOE/AA Employer and an NSF ADVANCE Institution.*



THE UNIVERSITY OF KANSAS
CANCER CENTER

### Faculty Positions: Basic, Translational, and Clinical Cancer Research

The University of Kansas Cancer Center is seeking laboratory-based faculty members with a Ph.D., M.D. or DVM and an interest in cancer research. Based on qualifications, the successful candidates will be appointed on the University tenure track at the assistant, associate or full professor. The candidates will be expected to establish and maintain an independently funded research program concentrating on basic, translational and/or clinical cancer research.

An excellent start-up package including space and equipment is available, as well as a competitive salary. Additional attractions are emphasis on cancer research within the university, the consolidation of cancer researchers with similar interests, and the chance to collaborate with an outstanding drug discovery, development and delivery team associated with the top ranked NIH funded School of Pharmacy. The University of Kansas Cancer Center is experiencing significant growth in basic, translational, and clinical research with an increase in the number of faculty and basic and clinical research facilities.

To view the complete position description and apply **on-line only**, go to **http://jobs.kumc.edu** and click on the link in the top left corner titled, "Search Postings", type in number **J0084013**, then select the Search button. The posting title is Assistant/Associate/Professor.

*AA/EOE.*

### Laboratory Head Positions
### Center for Brain Disorders
### Institute of Neuroscience
### Shanghai

The Institute of Neuroscience (**http://www.ion.ac.cn**), Shanghai Institutes for Biological Sciences, Chinese Academy of Sciences, invites applications for laboratory head positions in the newly founded Center for Brain Disorders. We are seeking outstanding scientists who are interested in studying mechanisms of brain diseases and in developing animal models for studying brain diseases, with an emphasis on non-human primate models.

Candidates must have a Ph.D or equivalent training, with significant post-doctoral research accomplishments. Appointments may be made at the level of Investigator or Senior Investigator, equivalent to tenure-track assistant/associate professor or tenured professor in the US research universities, respectively. The laboratory heads are expected to develop an active research program and to supervise graduate students and post-doctoral fellows. Excellent start-up fund, annual operating fund, competitive salary, and housing benefits will be provided.

Interested individuals should send C.V., a brief research plan, three letters of references, via e-mail to Yan Wang (**yw@ion.ac.cn**). Applicants will be considered within one month after the receipt of the application.

## Assistant/Associate Professor, Biology (2)

The Biology Department at York College of The City University of New York invites applications for two tenure-track positions at the Assistant/Associate Professor level to begin September 1, 2010: **Evolutionary biology**, emphasizing molecular phylogenies and bioinformatics (code 1877), and **Developmental biology** (code 1861).

Qualifications include a Ph.D., post-doctoral experience and a commitment to undergraduate teaching. Successful candidates are expected to teach lecture and laboratory courses in the area of expertise as well as general biology courses, and to establish an active research program supported by external funding.

To view the complete position descriptions, go to **CUNY.edu**, click on **Careers at CUNY**, and then select the **Additional Job Postings** link. For departmental information, see **www.york.cuny.edu/academics/departments/biology**.

York College/CUNY is an EEO/AA/IRCA/ADA Employer.

YORK COLLEGE IS CUNY

## The Montreal Neurological Institute of McGill University
## Faculty Position in Brain Imaging

The Montreal Neurological Institute (MNI) of McGill University is conducting an international search for a magnetoencephalography (MEG) Scientist to lead the MEG program within the McConnell Brain Imaging Centre (BIC). The MNI is a broad-based neuroscience research institute integrated with the Montreal Neurological Hospital and is part of one of the largest and most diverse neuroscience communities in North America. The BIC (www2.bic.mni.mcgill.ca) is a large multi-disciplinary neuro-imaging research centre with 15 faculty members, 40+ affiliated faculty members, 25 technical staff members and approximately 100 graduate students and postdoctoral fellows. BIC research-dedicated facilities include state-of-the-art human MRI/fMRI and PET scanners, animal MRI and PET, cyclotron and radiochemistry labs, and large scale computing facilities. The BIC is now expanding to include an MEG program based upon secured equipment and construction funding provided by the Canada Foundation for Innovation and private donors.

We seek applications for a tenure track faculty position as an MEG scientist. Applicants should have a PhD, MD, or the equivalent, and advanced training and experience with MEG methods, instrumentation and neuroscience applications. They should also have an established track record in obtaining research funding, teaching and working in a collaborative multi-disciplinary environment. The new recruit will be expected to establish and lead the MEG laboratory and to develop a successful research program of basic and clinical neuroscience.

We offer highly attractive salary and start-up packages and an exceedingly high quality of life in Montreal, one of North America's greatest and most lively cities.

Applications should consist of a PDF file containing a letter outlining current and future research interests, CV, and the names and addresses of three references. Completed PDF files should be addressed to Dr. Robert Dunn, Associate Director Scientific Affairs at megsearch.mni@mcgill.ca and must be received by February 28, 2010. Applications will be evaluated as they are received. More information can be found at www.mni.mcgill.ca.

All qualified applicants are encouraged to apply; however, Canadians and permanent residents will be given priority. McGill University is committed to equity in employment and diversity. It welcomes applications from indigenous peoples, visible minorities, ethnic minorities, persons with disabilities, women, persons of minority sexual orientations and gender identities and others who may contribute to further diversification.

## PRIZES

COLUMBIA UNIVERSITY
IN THE CITY OF NEW YORK

# THE 2010 LOUISA GROSS HORWITZ PRIZE FOR BIOLOGY OR BIOCHEMISTRY

The Louisa Gross Horwitz Prize was established under the will of the late S. Gross Horwitz through a bequest to Columbia University and is named to honor the donor's mother. Louisa Gross Horwitz was the daughter of Dr. Samuel David Gross (1805-1889), a prominent surgeon of Philadelphia and author of the outstanding Systems of Surgery who served as President of the American Medical Association.

Each year since its inception in 1967, the Louisa Gross Horwitz Prize has been awarded by Columbia University for outstanding basic research in the fields of biology or biochemistry. The purpose of this award is to honor a scientific investigator or group of investigators whose contributions to knowledge in either of these fields are deemed worthy of special recognition.

The Prize consists of an honorarium and a citation which are awarded at a special presentation event. Unless otherwise recommended by the Prize Committee, the Prize is awarded annually. Dr. Victor Ambros University of Massachusetts Medical School, Worcester, MA, and Dr. Gary Ruvkun, Harvard Medical School, Boston, MA, were the 2009 awardees.

### QUALIFICATIONS FOR THE AWARD

The Prize Committee recognizes no geographical limitations. The Prize may be awarded to an individual or a group. When the Prize is awarded to a group, the honorarium will be divided among the recipients, but each member will receive a citation. Preference will be given to work done in the recent past.

***Nominations must be submitted electronically at: http://www.cumc.columbia.edu/horwitz/***

**Nominations should include:**

1) A summary, preferably less than 500 words, of the research on which this nomination is based.
2) A summary, preferably less than 500 words, of the significance of this research in the fields of biology or biochemistry
3) A brief biographical sketch of the nominee, including positions held and awards received by the nominee
4) A listing of up to ten of the nominee's most significant publications relating to the research noted under item 1.
5) A copy of the nominee's curriculum vitae.

**Deadline date: January 31, 2010**

## Gordon Research Conference

March 7-12, 2010
Ventura Beach Marriott, Ventura, CA

### Antibody Biology and Engineering From Basic Mechanisms to Antibody-Based Therapeutics

Chairs: **E. Sally Ward** (University of Texas Southwestern Medical Center) and **Davinder Gill** (Pfizer)
Vice-chair: **Derry Roopenian** (The Jackson Laboratory)

This international conference will emphasize both the basic biology of B cells and the exploitation of antibodies for therapeutic purposes. Conference sessions are:

B Cell Biology
Antibody Repertoires and Diversification Mechanisms
Molecular Recognition by Antibodies and FcγRs
Functional Effects of FcγRs and Complement
FcRn and IgG Dynamics
Imaging of Antibodies and Antibody-Related Processes
B Cell Tolerance
Antibody Fragments and Novel Protein Scaffolds
Therapeutic Antibodies

For GRC information and to register, visit:
**http://www.grc.org/programs.aspx?year=2010&program=antibody**

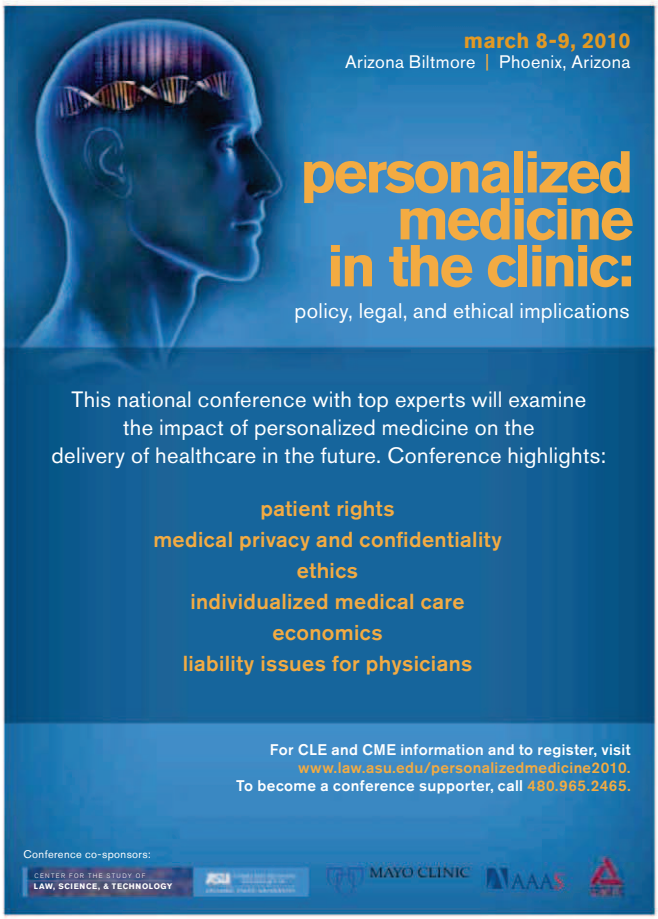

## POSITIONS OPEN

### INVERTEBRATE BIOLOGY
**Harvard University Department of Organismic and Evolutionary Biology and Museum of Comparative Zoology**

The Department of Organismic and Evolutionary Biology (OEB) at Harvard University invites applications for an entry-level, tenure-track **FACULTY POSITION** in the field of marine biology, emphasizing the evolution, systematics, ecology, physiology, and/or environmental biology of any clade(s) of invertebrate animals. We seek an outstanding scientist who will establish an empirical research program and teach two courses a year at the undergraduate and graduate levels. In addition to a faculty appointment in OEB, this person will receive a curatorial appointment in the Museum of Comparative Zoology (MCZ) and will share oversight responsibilities for MCZ's invertebrate collections. The appointment is expected to begin as early as 1 July 2010.

Applicants should submit the following as PDF files: curriculum vitae, statements of research and teaching interests, three to five representative publications, and the names and contact information of three persons from whom you have requested letters of recommendation. Letters of nomination from third parties are also welcome. Send all materials via **website: http://www.lsdiv.harvard.edu/oeb/inverts_search/**. Review of applications and nominations will begin 15 February 2010.

Further information about OEB and MCZ is available at their **websites: http://www.oeb.harvard.edu; http://www.mcz.harvard.edu/**.

*Harvard University is an Affirmative Action/Equal Opportunity Employer. Applications from or information about women and minority candidates is encouraged.*

### POSTDOCTORAL FELLOWSHIP

The Lillehei Heart Institute is a premier institute at the University of Minnesota, Minneapolis with state-of-the-art technologies and core facilities focused on the molecular regulation of myogenesis, stem cell and regenerative biology. We are accepting applications for highly motivated Postdoctoral Fellows to work on NIH-funded research pertaining to the role of transcription factor mediated networks to direct the fate of stem and iPS cells to a mesodermal fate (i.e., cardiac, endothelial, skeletal muscle). Ph.D. and expertise with molecular biological–biochemistry techniques, the use of transgenesis and knockout technologies will be required for this position. Interested applicants should apply online to: **Daniel J. Garry, M.D., Ph.D., Director of Lillehie Heart Institute, University of Minnesota** at **website: http://employment.umn.edu** (reference **job search #161786**) and include curriculum vitae, statement of interest, and names of three references.

*The University of Minnesota is an Affirmative Action/Equal Opportunity Employer.*

CAL POLY

**COMMUNITY ECOLOGIST, tenure-track position.** The Biological Sciences Department at California Polytechnic State University, San Luis Obispo is seeking a full-time, academic year Community Ecologist beginning September 2010. For details, qualifications, and application instructions (online faculty application required), visit **website: http://www.calpolyjobs.org** and refer to **requisition #101985.** Review begin date: February 8, 2010. *Equal Opportunity Employer.*

## POSITIONS OPEN

THE UNIVERSITY OF ARIZONA

**ASSISTANT PROFESSOR OF BIOCHEMISTRY.** The Department of Chemistry and Biochemistry of the University of Arizona, in conjunction with UA's Department of Medicine, seeks applications from Ph.D. scientists for a tenure-track position in any area of modern biochemistry. The newly merged Department of Chemistry and Biochemistry was awarded in excess of $19 million in federal funding in 2008-2009 and includes 45-plus faculty with broad research interests in the biological and chemical sciences. The laboratory space associated with the position is located in the new Medical Research Building that houses interdisciplinary basic biomedical research groups from several colleges, including the Arizona Diabetes Program. The successful candidate will be offered a competitive startup package and will participate in teaching at the undergraduate, graduate, and/or medical student levels. To apply, please submit a letter of application, curriculum vitae, and statements of research and teaching interests online at **website: http://www.uacareertrack.com** (**position #43764**). Three letters of recommendation should be sent to: **Prof. Roger Miesfeld, Biochemistry Faculty Search, c/o Beth Vinson, Department of Chemistry and Biochemistry, P.O. Box 210041, Tucson, AZ 85721.** Review of applications begins in early February 2010.

*The University of Arizona is an Equal Employment Opportunity/Affirmative Action Employer, Minorities/Women/Persons with Disabilities/Veterans. Women and minorities are especially encouraged to apply. The Immigration Reform and Control Act requires you to have proof of authorization to work in the U.S.A.*



## POSITIONS OPEN

THE UNIVERSITY OF MISSISSIPPI MEDICAL CENTER

### POSTDOCTORAL FELLOW POSITIONS
**Kidney and Cardiovascular Disease**

The Department of Pharmacology at the University of Mississippi Medical Center seeks to recruit two Postdoctoral Research Fellows interested in: (1) the role of eicosanoids and TGF-β in the pathogenesis of hypertension and chronic kidney disease and (2) the genetic basis of the myogenic response and the role of impaired blood flow regulation in the development of renal and cerebral vascular disease. Available techniques include micropuncture and tubular perfusion, laser Doppler flowmetry, liquid chromatography/mass spectrometry, in vivo and in vitro fluorescent imaging, patch clamp, radiotelemetry, and molecular genetics. Candidates with a Ph.D. or equivalent and expertise in kidney disease, vascular biology, or patch clamp techniques are encouraged to apply. The Department of Pharmacology in conjunction with the Cardiovascular Center at the University of Mississippi Medical Center offers an outstanding training environment with active research programs in the areas of hypertension, obesity, diabetes, and cardiovascular disease.

Interested candidates should submit their curriculum vitae to:

**Richard J. Roman**
**Department of Pharmacology**
**University of Mississippi Medical Center**
**2500 North State Street**
**Jackson, MS 39215-4505**
**Telephone: 601-984-1602**
**Fax: 601-984-1637**

*Equal Opportunity Employer, Minorities/Females/Persons with Disabilities/Veterans.*

The Division of Gastroenterology at the University of Pennsylvania is seeking a well-qualified **POSTDOCTORAL RESEARCH** (Ph.D., M.D., or M.D.-Ph.D.) candidate to join a laboratory in the genetics of colon cancer or pancreatic cancer. Must have experience in advanced molecular and cell biology, genetic mouse models, and be eligible for applying to NIH grants.

Please send cover letter and curriculum vitae to:

**Anil K. Rustgi, M.D.**
**T. Grier Miller Professor of Medicine and Genetics**
**University of Pennsylvania**
**600 Clinical Research Building**
**415 Curie Boulevard**
**Philadelphia, PA 19104-6140**

*The University of Pennsylvania is an Equal Opportunity Affirmative Action Employer.*



## MARKETPLACE

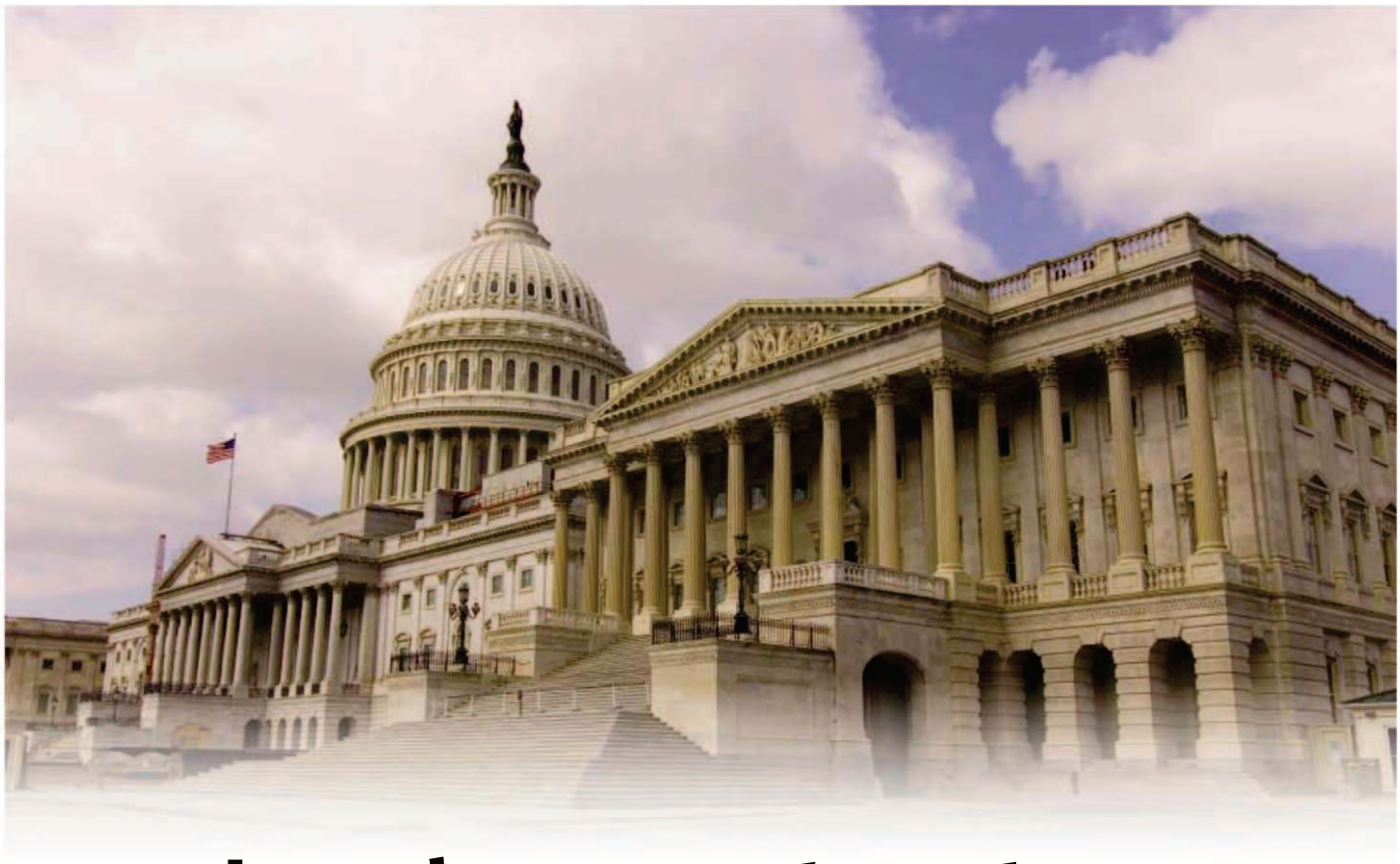

# Learn how current events are impacting your work.

***Science*Insider, the new policy blog from the journal *Science*,** is your source for breaking news and instant analysis from the nexus of politics and science.

Produced by an international team of science journalists, *Science*Insider offers hard-hitting coverage on a range of issues including climate change, bioterrorism, research funding, and more.

Before research happens at the bench, science policy is formulated in the halls of government. Make sure you understand how current events are impacting your work. Read *Science*Insider today.

**www.ScienceInsider.org**

ScienceInsider

**Breaking news and analysis from the world of science policy**

Science

AAAS